



HAL
open science

**Final report of the EURISOL Design Study (2005-2009)
A Design Study for a European
Isotope-Separation-On-Line Radioactive Ion Beam
Facility**

J. Cornell, Y. Blumenfeld, G. Fortuna

► **To cite this version:**

J. Cornell, Y. Blumenfeld, G. Fortuna. Final report of the EURISOL Design Study (2005-2009) A Design Study for a European Isotope-Separation-On-Line Radioactive Ion Beam Facility. 2009, pp.1-220. in2p3-00462950

HAL Id: in2p3-00462950

<https://in2p3.hal.science/in2p3-00462950v1>

Submitted on 10 Mar 2010

HAL is a multi-disciplinary open access archive for the deposit and dissemination of scientific research documents, whether they are published or not. The documents may come from teaching and research institutions in France or abroad, or from public or private research centers.

L'archive ouverte pluridisciplinaire **HAL**, est destinée au dépôt et à la diffusion de documents scientifiques de niveau recherche, publiés ou non, émanant des établissements d'enseignement et de recherche français ou étrangers, des laboratoires publics ou privés.

Final Report
of the

The logo for EURISOL Design Study features the word "EURISOL" in large, bold, multi-colored capital letters (E: red, U: orange, R: yellow, I: green, S: blue, O: light blue, L: dark blue). To the left of the letters is a stylized grey and white graphic of a beam or particle path. Below "EURISOL" is the phrase "Design Study" in a blue, italicized, sans-serif font.

EURISOL
Design Study

(2005-2009)

**A DESIGN STUDY FOR A
EUROPEAN ISOTOPE-SEPARATION-ON-LINE
RADIOACTIVE ION BEAM FACILITY**

November 2009

**Final Report of the
EURISOL Design Study
(2005–2009)**

A DESIGN STUDY FOR A
EUROPEAN ISOTOPE-SEPARATION-ON-LINE
RADIOACTIVE ION BEAM FACILITY

Co-ordinated by
Yorick Blumenfeld and Graziano Fortuna

A report to the European Commission

EUROPEAN COMMISSION CONTRACT No. 515768 RIDS

Edited by John C. Cornell

Published by GANIL
B.P. 55027, 14076 Caen cedex 5, France
September, 2009

Foreword

This report summarises the work done during the 4½ years of the EURISOL Design Study, which was co-funded by the European Commission under the 6th Framework Programme: “Structuring the European Research Area”. Technically, the project was a Research Infrastructure Action, and the contract was for a Design Study implemented as a “Specific Support Action”.

The full title of the EURISOL Design Study was “European Isotope Separation On-Line Radioactive Beam Facility”. It followed on from the EURISOL Feasibility Study which was led by Jean Vervier during the 5th Framework Programme.

Twenty “Participant” institutions signed a Consortium Agreement, and engaged to contribute manpower and resources to the Design Study, with some expenses being eligible for reimbursement by the European Commission. The total amount of this reimbursement was 9.16 million euros. Another 21 institutions around the globe joined the Design Study as “Contributors”, making resources, expertise and manpower, and in some instances beam time, available to the Study.

We express our thanks to all Participants and Contributors for their unstinting support for the Design Study. Without the cooperation of all these institutions, their directors, scientific and technical staff, post-docs and students, it would not have been possible for the project to succeed as it has done.

The commitment, hard work and leadership skills of the task leaders, who constituted the Coordination Board, were the driving forces of the study. We thank the members of the Steering Committee, representing their respective Participant institutes for their commitment and support. Thanks are also due to the International Advisory Panel who took an intense interest in the project and gave invaluable advice to both the Steering Committee and the Management Board. We also extend our thanks to the Site Investigation Panel who performed a difficult task with enthusiasm.

Finally, we extend our personal thanks to our colleagues who have served on the Management Support Team, with whom it has been a pleasure to work and who have made things much easier in the coordination and day-to-day running of the Design Study.

Yorick Blumenfeld, Peter Butler, Graziano Fortuna & Mats Lindroos

EURISOL Design Study Management Board

Participant Institutions



GANIL:

Grand Accélérateur National d'Ions Lourds, Caen, France



CNRS/IN2P3:

Centre National de la Recherche Scientifique/ Institut National de Physique Nucléaire et de Physique des Particules, France



INFN:

Istituto Nazionale di Fisica Nucleare, Italy



CERN:

European Organization for Nuclear Research, Geneva, Switzerland



UCL:

Université Catholique de Louvain, Centre de Recherches du Cyclotron, Louvain-la-Neuve, Belgium



CEA:

Commissariat à l'Energie Atomique (Direction des Sciences de la Matière), Paris, France



NIPNE:

"Horia Hulubei" National Institute for Physics and Nuclear Engineering, Bucharest-Magurele, Romania



JYU:

University of Jyväskylä, Jyväskylä, Finland



LMU:

Ludwig Maximilians Universität München, München, Germany



FZJ:

Forschungszentrum Jülich GmbH, Jülich, Germany



FI:

Institute of Physics, Vilnius, Lithuania



UW:

Warsaw University, Warsaw, Poland



SAV:

Institute of Physics - Slovak Academy of Sciences, Bratislava, Slovakia



U-Liverpool:

The University of Liverpool, Liverpool, United Kingdom



GSI:

Gesellschaft für Schwerionenforschung m.b.H. Darmstadt, Germany

Participant Institutions (continued)



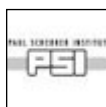
USDC:

Universidade de Santiago de Compostela, Santiago de Compostela



STFC:

Science and Technology Facilities Council, United Kingdom



PSI:

Paul Scherrer Institute, Villigen, Switzerland



IPUL:

Institute of Physics, University of Latvia, Salaspils, Latvia



SU-MSL:

Stockholm University–Manne Siegbahn Laboratory, Stockholm, Sweden

The institutions listed above were contractors to the EURISOL consortium. Those listed below were contributing institutions, but received no direct funding from the European Commission

Contributor Institutions



U-FRANKFURT:

Johann Wolfgang Goethe-Universität, Frankfurt, Germany



BINP:

Budker Institute of Nuclear Physics of Novosibirsk, Novosibirsk, Russia



VNIITF:

Russian Federal Nuclear Center - Zababakhin Institute of Technical Physics, Snezhinsk, Russia



PNPI:

Petersburg Nuclear Physics Institute, Gatchina, Russia



ORNL:

Oak Ridge National Laboratory, Oak Ridge, Tennessee, USA



ANL:

Argonne National Laboratory, Argonne, Illinois, USA



KAERI:

Korea Atomic Energy Research Institute, Daejeon, South Korea

Contributor Institutions (continued)



JAERI:
Japan Atomic Energy Research Institute, Kashiwa, Japan



TRIUMF:
Tri-University Meson Facility, Vancouver, Canada



SOREQ:
Soreq Nuclear Research Centre, Yavne, Israel



U-MAINZ:
Johannes Gutenberg Universität Mainz, Mainz, Germany



KVI:
Kernfysisch Versneller Instituut Groningen, Groningen, The Netherlands



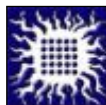
U-SURREY:
The University of Surrey, Guildford, United Kingdom



U-YORK:
The University of York, Heslington, United Kingdom



U-PAISLEY:
University of Paisley, Paisley, United Kingdom



VINCA:
VINCA Institute of Nuclear Sciences, Laboratory of Physics, Belgrade



U-UPPSALA:
Uppsala University, Uppsala, Sweden



NSCL:
National Superconducting Cyclotron Laboratory, Michigan State University, East Lansing, Michigan, USA



FNAL:
Fermi National Accelerator Laboratory, Batavia, Illinois, USA



HUG:
Hospital University of Geneva, Geneva, Switzerland



ITN:
Nuclear Technology Institute, Lisbon, Portugal

Management Board

Yorick Blumenfeld (*IPNO/CERN*) – *EURISOL DS Project Leader* [2007–2009]

Peter Butler (*Liverpool University*)

Graziano Fortuna (*INFN*) – *EURISOL DS Project Leader* [2005–2006]

Mats Lindroos (*CERN*)

Management Support Team

Alberto Andrichetto (*INFN*) [2005–2006]

Rosella Battistella (*INFN*) – *Administrative and legal issues*

Sandrine Bon (*IPNO*) [2007]

John Cornell (*GANIL*) – *Technical Coordinator*

Michele Gulmini (*INFN*) – *Database* [2008–2009]

Céline Hovaguimian (*IPNO*) [2006]

Michele Comunian (*INFN*) [2005–2006]

Domenico Lazzarato (*INFN*) – *Website* [2007–2009]

Jacques Lettry (*CERN*) – *Target Consultant* [2008–2009]

International Advisory Panel

Sytze Brandenburg (*KVI, The Netherlands*)

Witek Nazarewicz (*ORNL/U. Tennessee, United States of America*)

Paul Schmor (*TRIUMF, Canada*) – *Chairman*

Site Investigation Panel [2008]

Alan Shotter (*U. Edinburgh, United Kingdom*) – *Chairman*

Giacomo Cuttone (*INFN-LNS, Italy*)

Don Geesaman (*ANL, United States of America*)

Alex Mueller (*IN2P3, France*)

Steve Myers (*CERN, Switzerland*).

Coordination Board

Task 1: Management of EURISOL Design Study	Graziano Fortuna (<i>INFN</i>) [2005–2006] Yorick Blumenfeld (<i>IPNO/CERN</i>) [2007–2009]
Task 2: Multi-MW Target Station	Helge Ravn (<i>CERN</i>) [2005] Yacine Kadi (<i>CERN</i>) [2005–2009]
Task 3: Direct Target	Jacques Lettry (<i>CERN</i>) [2005] Thierry Stora (<i>CERN</i>) [2005–2009]
Task 4: Fission Target	Luigi Tecchio (<i>INFN-LNL</i>)
Task 5: Safety & radioprotection	Danas Ridikas (<i>CEA</i>) [2005–2007] Jean-Christophe David (<i>CEA-IRFU</i>) [2008–2009]
Task 6: Heavy-Ion Accelerator Design	Marie-Hélène Moscatello (<i>GANIL</i>)
Task 7: Proton Accelerator Design	Alberto Facco (<i>INFN-LNL</i>)
Task 8: Superconducting Cavity Development	Sébastien Bousson (<i>IPNO</i>)
Task 9: Beam Preparation	Ari Jokinen (<i>JYU</i>)
Task 10: Physics & Instrumentation	Robert Page (<i>U. Liverpool</i>)
Task 11: Beam Intensity Calculations	Karl-Heinz Schmidt (<i>GSI</i>) [2005–2007] Aleksandra Kelić (<i>GSI</i>) [2008–2009]
Task 12: Beta-Beam Aspects	Michael Benedikt (<i>CERN</i>)

Ex officio observers (by invitation):

Vittorio Paladino (*INFN Naples, representing the BENE network*)

Roland Garoby (*CERN, representing the HIPPI network*)

Steering Committee Members

Representatives of Participant Institutions:

Nicolas Alamanos (*CEA, France*)
Juha Äystö (*JYU, Finland*)
Jose Benlliure (*USDC, Spain*)
Emil Běták (*IP-SKS, Slovakia*)
Heinz Brücher (*FZJ, Germany*)
Enrico Chiaveri (*CERN, Switzerland*) [2005]
Janis Freibergs (*IPUL, Latvia*)
Heinz Gäggl (*PSI, Switzerland*)
Sydney Galès (*GANIL, France*) [2006–2009]
Dominique Goutte (*GANIL, France*) [2005]
Dominique Guillemaud-Mueller (*IN2P3, France*)
Gilbert Guignard (*CERN, Switzerland*) [2005–2007]
Dieter Habs (*LMU, Germany*) [2005–2006]
Jerzy Jastrebski (*UW, Poland*)
Anders Källberg (*SU-MSL, Sweden*)
Philippe Lebrun (*CERN, Switzerland*) [2008–2009]
Marc Loiselet (*UCL, Belgium*)
Paul Nolan (*U. Liverpool, United Kingdom*)
Arturas Plukis (*FI, Lithuania*)
Gabriele Puglierin (*INFN, Italy*)
John Simpson (*STFC, United Kingdom*)
Klaus Sümmerer (*GSI, Germany*)
Peter Thirolf (*LMU, Germany*) [2006–2009]
Dave Warner (*CCLRC, United Kingdom*) [2005]
Nicolae Zamfir (*NIPNE, Romania*)

Ex officio observers (by invitation):

Roy Aleksan (*ESGARD Project Leader*) [2005–2009]
Brian Fulton (*NuPECC Chairman*) [2006–2007]
Alex Mueller (*EURONS Project Leader*) [2005–2008]
Muhsin Harakeh (*NuPECC Chairman*) [2005]
Gunter Rosner (*NuPECC Chairman*) [2008–2009]

Preface

This report summarises the work of the EURISOL Design Study and represents an enormous amount of work, carried out by many people over 4½ years. However, in order to reduce the size of the printed document, we have limited the number of pages per topic. The resultant document thus gives a somewhat restricted description of what has been achieved, and the limitation on what could be included will inevitably have led to some omissions, for which we apologise. Fuller descriptions and additional information can be found in the Addenda which are provided on the CD which accompanies this report.

John Cornell

*Editor & Technical Coordinator
EURISOL Design Study*

Contents

	Page
Foreword	iii
List of Participant and Contributor Institutions	iv
Management Board and Panels.....	vii
Coordination Board.....	vii
Steering Committee.....	ix
Executive Summary	1
1. Introduction and Objectives	11
2. The Driver Accelerator	15
3. The 100-kW Direct Targets	27
4. The Multi-MW Liquid-Metal Target.....	43
5. The Fission Targets.....	61
6. Beam Preparation.....	75
7. The Post-Accelerators	89
8. Superconducting Cavity Development	107
9. Calculated Yields of Exotic Ions	123
10. Physics & Instrumentation.....	139
11. Radiation Safety.....	149
12. Layout of the Facility.....	161
13. Site Investigation Panel Report.....	169
14. Beta-Beam Aspects.....	175
15. Cost Estimation	193
16. International Advisory Panel Report	197
17. The Future of EURISOL.....	201
18. Conclusions.....	203
19. Publications.....	205

Executive Summary

Introduction

The Design Study for EURISOL – a European isotope-separation-on-line (ISOL) facility – is aimed at the construction of an accelerator-based ISOL system for producing exotic radioactive ion beams (RIBs) with intensities several orders of magnitude greater than those available today. EURISOL is intended to be complementary to FAIR – the Facility for Antiproton and Ion Research, currently being built in Germany. Ion beams at FAIR will be based on in-flight separation of isotopes, using heavy-ion beams, and will therefore produce a range of radioisotopes different from those produced using the ISOL method. With high-power beams of protons producing higher yields for a different range of exotic isotopes, EURISOL will provide a unique facility for European scientists.

The EURISOL Design Study follows on the earlier Feasibility Study co-financed by the European Commission under its Fifth Framework Programme (FP5) from 2000 to 2004. At that time, several other ISOL projects were proposed, such as SPIRAL2 at GANIL, HIE-ISOLDE at CERN and SPES at LNL, Legnaro, which are now regarded as “intermediate” or “precursor” facilities, since they will provide improved beam intensities, albeit much lower than those proposed at EURISOL.

The present Design Study was launched in 2005, again with EC support (under FP6) and again with GANIL as Coordinating Institution. Twenty institutions formed a consortium of Partners, with another 21 Collaborators (without EC funding), including institutions in other continents.

The work of the Design Study was divided between 12 work packages called “Tasks”, as follows:

- Task 1: Management
- Task 2: Multi-MW target station
- Task 3: Direct (100-kW) target
- Task 4: Fission target
- Task 5: Safety & radioprotection
- Task 6: Heavy-ion accelerator
- Task 7: Proton accelerator
- Task 8: Superconducting cavity development
- Task 9: Beam Preparation
- Task 10: Physics and instrumentation
- Task 11: Beam intensity calculations
- Task 12: Beta-beam aspects.

The last of these arose from the realisation that the high-yield RIB facility proposed would also be suitable for producing the neutrino-emitting isotopes required for the so-called “beta-beam” concept.

The driver accelerator

An international collaboration between the INFN-LNL (in Italy) and the CEA and IN2P3 (in France), with valuable contributions from SOREQ (in Israel) and TRIUMF (in Canada), has produced the design of a superconducting linac for proton, deuteron and $^3\text{He}^{2+}$ beams that fulfils the EURISOL DS driver linac specifications. This accelerator is based on three different types of superconducting resonator (viz. half-wave, spoke and elliptical cavities) with 6 different optimum velocities. The maximum beam energy for H^- is above 1 GeV, and the maximum beam current is 5 mA. The injector section includes a 1.5·4 MeV RFQ and two ion sources. H^- is accelerated instead of protons, to allow CW beam splitting at high energy by means of a novel technique with low beam losses. Up to 4 beams (one of 4 MW and three of 100 kW each) can be delivered simultaneously by the EURISOL driver to RIB production targets. Beams of 2-GeV, 100- μA ^3He ions, and 270-MeV, 4-mA deuterons can also be produced.

The beam splitting is achieved by using a primary H^- beam (up to 5 MW), and neutralizing part of it (up to 100 kW) by Lorenz stripping in a very short 3-dipole magnet chicane. The un-neutralized H^- ions are then diverted to a different beam line by means of a (weak) dipole magnet. When the two beams are sufficiently separated, the neutral beam is transformed into a proton beam by means of a stripper foil. From here on, the H^- and H^+ beams can be transported independently. The splitting operation can be repeated by adding more splitting sections, thus providing a number of CW beams. The beauty of this system, developed within the Design Study, is that the amount of stripped beam is continuously variable (from zero), and has little impact on the intense H^- beam.

The linac design is based on proven technology that includes components developed in the EURISOL Design Study framework. Its beam dynamical design has been studied section by section with macroparticle beam simulations, and has been validated with error studies with large statistics and high sensitivity. The beam-loss distribution along the linac, in the presence of realistic construction errors, has been calculated with large statistics as well. We have demonstrated that the linac complies with the EURISOL driver specifications.

The targets

The multi-MW target of EURISOL is the most unique feature of the facility. It has been designed for a 4-MW beam of protons using a liquid-metal “converter” target to transform the proton beam to a neutron flux. The neutrons will, after suitable moderation, hit the surrounding fission targets, which are inserted through the massive shielding and positioned close to the converter. The ions are ionized in the target, preferable with a selective ion source such as a resonant-ionization laser ion source (RILIS), and extracted to the beam preparation stage.

Initially, three types of liquid-metal multi-MW converter targets were studied: (a) the horizontal “jet” target proposed during the earlier Feasibility Study, (b) a “coaxial guided-flow” converter, and (c) a converter based on a vertical liquid-metal “curtain”. The horizontal jet itself was abandoned, as the technical difficulties involved in containing it without a strong solenoid field were considered to be too great. The “coaxial guided-flow” spallation-source type of target was selected as the baseline target, to be prototyped and studied in detail, while further prototyping was also done on the “windowless” vertical curtain target, which uses advanced flow guides to create a homogenous vertical curtain of liquid metal. (All these targets could use either mercury or a Pb-Bi eutectic, but mercury was chosen for prototyping since it does not require heating to remain liquid.)

The compact neutron spallation source target was studied in great detail. The mercury flow was studied through detailed computer simulations, together with the beam heating of the window and the mechanical stresses caused by this heating. Monte-Carlo simulations were performed to determine the neutron flux, the escaping charged particles and also waste production. Similar simulations were performed for the vertical curtain target, but in less detail.

A literature study was performed to investigate how to purify irradiated mercury and the feasibility of extracting commercially valuable isotopes from it. A first study was done – based on discussions with experts – on how purification could be implemented for the volumes required for an operational facility. A small-scale laboratory experiment was performed with a sample of irradiated mercury. A method for the solidification of radioactive mercury for long-term storage was also proposed.

Prototypes of each of the two liquid-metal targets were constructed and tested at the renovated mercury loop – also part of the target task – at the mercury laboratory in IPUL outside Riga in Latvia. The tests showed that the targets could be operated at nominal flow and pressure parameters. A new system for cavitation detection using a laser vibrometer was also tested and its efficiency proven. However, final tests of these targets with a proton beam were not part on the Design Study.

A study of the liquid-mercury loop with all its auxiliaries including the beam dump was made and an integration study of the complete target station was carried out. Animated visualization sequences were produced for the full target station system, to provide input for the next steps of design. Detailed estimated for radiation protection parameters in the target station buildings were made using Monte-Carlo simulation tools.

Two types of uranium-carbide fission target were proposed. The first idea had 8 uranium carbide targets surrounding the mercury converter, all enclosed within one outer graphite moderator, but this was finally discarded as being poorly adapted to efficient target replacement and maintenance. The second configuration has six individual UC target-and-moderator units inserted close to the converter. This version – inspired by the ISOL project in Munich at the high-flux reactor (MAFF), and a similar project at ILL in Grenoble (PIAFE) – was selected for detailed study. An engineering study of all parts of the target units was made, including detailed mechanical studies of the local moderator, the ion source, the cooling required, the beam transport system to carry the ions out of the shielding, the neutral radioactive gas traps, the system of interconnections needed to allow target replacement and

the mechanical system for changing target units. The position – and the resulting yield – in each of the six inserted fission-target units was optimized and estimated using Monte-Carlo simulation tools. The heat produced in the target units was calculated. Using advanced thermo-mechanical design tools, a model was proposed which keeps the target units homogeneously hot, but below melting points, and which can transport the heat away. A new type of high-density UC compound was also tested on-line. Measurements were performed of diffusion properties and the stability of the compound at high temperature over long periods. A massive version of the target was designed and first tests were performed with it.

For the direct targets (which are irradiated directly with the proton beam from the driver), out of more than 100 possible ion-source and target-material combinations, four were selected for prototyping and tests: a carbide target, an oxide target, a liquid-metal target and a dual-transfer-line target. Each test yielded important input for the design of the future EURISOL direct target. For example, sub-micron SiC used in the carbide target tests proved to be stable at high temperatures, yielding record yields of some short-lived isotopes; the dual-transfer-line test units demonstrated the feasibility of using multiple target units with a single ion source without any significant loss of efficiency; the oxide target tested at TRIUMF at high beam power confirmed that the design effort spent on how to manage heat transfer from such a unit was well invested; and the liquid-metal loop tests showed that a new approach with a diffusion cell to manage splashes can work for such a target. Numerous other benefits and lessons from the design work and tests can be listed, demonstrating that the ISOL technology with direct irradiation of the target units can be used with high efficiency at the high beam power available at EURISOL. The direct-target task was also the only EURISOL task to result in a patent – for sub-micron structured SiC stable at high temperatures. High-dose irradiation tests were done for many different target materials at a test rig at PSI. The irradiated target materials were analysed in hot cells, yielding important information of target material stability for high dose rates. An engineering design of the target station was performed in collaboration with the safety task.

The direct target task also studied targets to produce ${}^6\text{He}$ and ${}^{18}\text{Ne}$ for the proposed beta-beam project. The ${}^6\text{He}$ production units include a solid “converter” target surrounded with BeO in which the helium is produced. Detailed simulation for the converter was performed and a new form of highly porous BeO was tested on-line at ISOLDE. The ${}^6\text{He}$ production seems feasible. Theoretical work based on cross section measurements and the dual-transfer-line target test shows that it is much harder to reach the required nominal production rate of ${}^{18}\text{Ne}$. An alternative method based on a direct reaction in an oxide target with a ${}^3\text{He}$ beam impinging on the target has been tested and is deemed feasible for reasonable estimates of the target size, heat deposition etc.

In conclusion, the target tasks represent the heart of the EURISOL facility and the work performed by these tasks during the Design Study has exceeded initial expectations. Feasible concepts for all parts of the target systems have been proposed and the studies performed give confidence that EURISOL can be realized.

Beta-beam aspects

The objective of the beta-beam task was to produce a first Conceptual Design Report for a beta-beam facility at CERN which would use the existing PS and SPS accelerators for the injection of ions at a Lorenz gamma-value of 100 into a new decay ring. The detector for this facility was assumed to be localized in the Frejus tunnel on the French-Italian border, some 130 km from CERN.

Initially, the machine cycle of the facility was optimized and a loss study was performed based on data from the CNGS operation at CERN. This work demonstrated the feasibility of the concepts for ${}^6\text{He}$ but also highlighted the problem of reaching the nominal performance for ${}^{18}\text{Ne}$, as mentioned above. An alternative approach to boost these yields using a low-energy accumulation ring was also studied.

A detailed design for a rapid-cycling synchrotron (RCS) – to be used before the CERN PS machine – has been completed. This includes lattice studies with accompanying beam dynamics, injection studies, initial studies for magnets and other elements and a very detailed radiation protection study. A full design was made of the decay ring, with lattice studies, transverse and longitudinal beam dynamics, intra-beam scattering estimations, transverse and longitudinal collimation studies, injection studies and

work on the insertions needed for both injection and the decayed-particle beam dump at the end of the straight sections. A dynamic-vacuum study of all machines in the injector complex has been done together with collimation studies for the existing PS machine, demonstrating that the present vacuum technology is sufficient and that the dose received by the PS magnets is reasonable. Using a combination of particle-matter-interaction Monte-Carlo simulation tools and particle-tracking codes, a study of collimation and magnet protection in the decay ring was performed.

This work was complemented by a study of open mid-plane superconducting dipoles, rather than large-aperture superconducting magnets for the decay ring. A study of all RF parameters in the injection chain and a detailed study – including tests in the CERN PS – of an innovative longitudinal accumulation scheme for the decay ring have been done. An initial study for the high-beam-load RF system for the decay ring was also done. The feasibility of using the new PS2 synchrotron, which is proposed to replace the PS for the beta-beam has been analysed.

The beta-beam task has thoroughly studied the beta-beam concept at a Lorenz gamma-value of 100 using the existing CERN PS and SPS machines. The study has demonstrated the feasibility of this beta-beam configuration opening the path to a full technical design of this configuration.

The post-accelerators

The main EURISOL post-accelerator is essentially a high-energy, heavy-ion machine, its nominal design being based on $^{132}\text{Sn}^{25+}$ accelerated up to 150 A MeV. An additional low-energy accelerator, will provide beams with energies from 1 to 5 A MeV, and will essentially be a clone of the low-energy part of the main machine. A very low-energy (1-MeV) accelerator, required for astrophysics, is regarded as part of the instrumentation, and was not studied.

The design for the whole post-accelerator is now very solid, in the sense that it is based on existing types of cavities and accelerators. Various beam tests performed have confirmed the assumptions made, in particular where charge breeder emittances are concerned. The beam dynamical calculations for the whole linac show that the proposed accelerator is very safe (i.e. with minimal beam losses), even if multi-charge transport still needs some software development.

Beam tests with two different RFQs have been satisfactory as well: the normal-conducting (NC) IH-RFQ in Frankfurt is still undergoing tests, and more precise measurements are in progress. However, the final choice for the NC-RFQ solution favours a 4-rod type RFQ, because it has several advantages, such as simpler frequency tuning to compensate for manufacturing errors and thermal frequency drift during operation. Nevertheless, an example the superconducting (SC) RFQ has been in operation for more than two years at LNL, Legnaro, and the results are very encouraging. Thus, at this stage of development, both RFQ solutions appear equally feasible. The final choice will have to be made nearer to construction time, depending on the long-term operational reliability of the NC-RFQ, and the technical proposed solution proposed for the SC-RFQ on a high-voltage platform.

For RIB diagnostics, we have developed double-sided strip detectors based on synthetic polycrystalline diamond produced via chemical vapour deposition. First results of in-beam tests have proved to be very promising, and this development will continue in the frame of intermediate projects like SPIRAL2 and HIE-ISOLDE.

A prototype of an innovative high-frequency chopper capable of selecting 1 bunch of ions out of 10, has been constructed, but still requires some more development before it can be tested with the SPIRAL2 beam, when this becomes available. This device, based on travelling-wave “meander” electrodes in a magnetic dipole field, is a key component, and its development will be pursued in the frame of SPIRAL2 project. The tests of the whole system have still to be completed under vacuum, and the last step will be to test it with the SPIRAL2 beam in future.

Very low beam losses were taken into account for the evaluation of shielding wall thickness, etc., but nevertheless the importance of contamination remains an open question, and should probably be investigated in more detail in future. Intermediate projects like SPIRAL2 or HIE-ISOLDE will help to give more precise information about this problem, and will let us know if, and where, robot manipulators will be necessary for maintenance during post-accelerator operation.

Superconducting cavity development

The EURISOL driver linac is based on different superconducting structures: half-wave resonators, “spoke” cavities and elliptical cavities, each of them of two different β (with $\beta = v/c$, the reduced particle velocity). For the driver, it was decided that the work should focus on the superconducting accelerating structures for the intermediate-energy part of the driver (from ~10 MeV to ~140 MeV). The reason for this choice is that at the starting time of the project, these structures were in a less advanced development stage as compared to the high-energy accelerating cavities, already developed and operated in other projects (such as the SNS, for instance).

Development of a reliable accelerating structure requires the optimization of an accelerating cavity and careful design of all the cavity ancillary systems, such as the cold-tuning system (CTS) for in-situ control of the cavity resonant frequency, and the power coupler (supplying the RF power to the cavity from the external RF source). We addressed all these issues for two different superconducting cavity types: half-wave resonators and spoke resonators. For each of them, a prototype was designed, fabricated and tested together with the associated cold-tuning system and power coupler. For the superconducting “spoke” structure, a test cryomodule was also designed and fabricated, and a final test of a fully-equipped spoke cavity in this cryomodule was done.

The tasks tackled successfully included:

- prototyping and testing of half-wave resonators at 352 MHz ($\beta = 0.31$ and 0.17) and at 176 MHz ($\beta = 0.09$ and 0.16), including the CTS;
- prototyping and testing of single-spoke resonators ($\beta = 0.35$ and 0.15), including the CTS;
- designing and prototyping of triple-spoke cavity resonators at 352 MHz;
- development of 352-MHz solid-state MOSFET RF amplifiers: one of 5 kW, and two of 10 kW;
- prototyping and testing of the RF power couplers;
- designing and testing of a spoke-cavity in its cryomodule.

Our aim, within the EURISOL Design Study was the design, construction and testing of several key components of the EURISOL accelerators. Important prototyping work was performed on half-wave resonators and spoke resonators in order to assess their capabilities for efficiently accelerating intense hadron beams. The performance obtained with both these accelerating structures, together with their ancillary systems, proved that this technology has now reached in an advanced stage, and that that these systems can be considered as a viable part of the reference solution for the EURISOL accelerators.

Beam preparation

The aim of the Beam Preparation Task was to develop techniques of ion-beam cooling and bunching, mass-purification and charge breeding, before injection into the post-accelerator, as the linear accelerator offers no mass selectivity. Another important part of this task was to construct a prototype for a high-intensity pulsed 60-GHz ECR ion source, for rapid ionisation of He and Ne atoms necessary for the beta-beam project. This task also took on the design of the low-energy beam switchyard and the ion-beam merger for the multi-MW target.

At ISOLDE at CERN, an RFQ cooler (ISCOOL) has been designed and constructed. An acceptable efficiency was achieved following the installation of a quadrupole triplet, and good results have been obtained for transmission in both DC and pulsed mode. Now installed on one of the ISOLDE on-line mass separators, the device has demonstrated excellent on-line efficiency, and the radioactive ion beams have been transmitted routinely through the device. Its excellent performance for transmission and space-charge capacities has now been confirmed for numerous beams. It has been used in pulsing mode together with REXTRAP for testing a mass-separation technique at REX-ISOLDE. Ultimately, ISCOOL will allow the injection of low-emittance beams into a high-resolution separator, for which the design has been established and detailed calculations carried out.

A prototype next-generation RFQ cooler, more suitable for the proposed high-intensity EURISOL beams, has been built at Orsay. Several tests of this device have been carried out relating to injection and to operation in a high-pressure environment. A major achievement was the injection and trapping of a microampere beam into the cooler with good transmission. The first emittance measurements of transmitted beams have also been made.

In parallel, work has progressed on the “Phoenix” ECR based at ISOLDE. Tests have been carried out to determine the chemical sensitivity of ion injection into the ECR. ECRIS efficiencies – of a few percent – were observed, and other parameters were also measured at ISOLDE for radioactive atomic and molecular ion beams. Tests of the pulsed mode were successfully carried out using noble gases, but beam purity and application to light masses are problematic with this type of ion source.

At JYFL, a novel ARC-ECRIS concept has been developed and a prototype built. Further simulations have been performed and are still in progress to fully characterize this concept and its feasibility as beam merging device and/or as a radiation-hard ion source for future facilities such as EURISOL.

The tests of the advanced charge-breeding techniques at the REX-EBIS at ISOLDE have also progressed well, attaining a 2% efficiency for $A/q = 4$ ions. Several advances have been made in the operation of REX-EBIS, particularly the demonstration of slow extraction and the breeding of heavy ions (with $A \sim 200$). Major advances have been made in obtaining beam purity in the demonstration of isobaric separation using REXTRAP prior to charge breeding in REXEBIS.

Measurements of the charge states of ions have also been carried out at the INFN-Bari EBIS (BRIC) set-up at Legnaro in Italy. Good progress has also been made with the Frankfurt MAXEBIS, installed at GSI. It has been tested with injected argon ions, and the injection and breeding efficiency as well as the beam emittance have been measured. Other measurements of the dependence of efficiency and emittance upon electron beam current for the highest available current density have been carried using the RHIC test EBIS at BNL, Brookhaven.

The first steps of the 60-GHz ECR programme have been taken, and good progress was made in setting up external collaborations and gaining additional funding for this project. The construction and magnetic field testing of the 18- and 28-GHz prototype source, using high-field superconducting and permanent magnets, are in progress, and preparations are well in hand for migration to the 60-GHz prototype source. Meanwhile systematic studies of the pre-glow charge-breeding pulsed efficiency have been made using a lower field configuration.

Calculated yields of exotic ions

Reliable beam intensity estimates are crucial to assess the scientific potential and competitiveness of a radioactive ion beam facility such as EURISOL. Cross section measurements, benchmarking of codes and estimates of the efficiency of various elements of the facility were combined to produce an intensity database for EURISOL. In addition this task proved instrumental in determining the main characteristics of the driver and post-accelerator.

Protons of 1 GeV can induce fission and spallation reactions. A knowledge of their cross sections at 1 GeV and lower energies is necessary for accurate yield determination and this was obtained from data from GSI and dedicated experiments at JYFL. Sophisticated models such as ABLA-PROFI and FIPRODY were benchmarked with these results. A database of radioactive beam intensities at EURISOL is now available to the community. In addition measurements were performed to assess the possibility of using intermediate-energy radioactive ions produced at EURISOL to create very neutron-rich nuclei, with encouraging results.

Cross section calculations for deuterons and ^3He ions as projectiles led to the incorporation of additional capabilities into the design of the driver accelerator. The addition of a 2-GeV ^3He beam will fill gaps in nuclide production due to the limited choice of ISOL target materials, in particular for many neutron-deficient isotopes, and will also increase the production of light, neutron-rich nuclides. Deuterons at 300 MeV will be useful for the production of certain fission fragments and heavy ions with $A/Q = 2$ for light, neutron-deficient elements.

A specificity of EURISOL is the opportunity to fragment very intense radioactive beams such as ^{132}Sn , which can be produced at more than 10^{12} particles per second. A dedicated experiment was performed at GSI to measure the cross sections for such a reaction, which were then compared to the predictions of different codes. It turns out that this “two-step fragmentation” scheme will be one of the highlights of EURISOL, leading to beams of n-rich nuclei which have never been observed up to now, such as ^{125}Pd or ^{120}Ru , with intensities above 10^4 pps, taking into account extraction, ionisation and beam-preparation efficiencies. The “magic” nucleus ^{125}Ru with $N=82$ will be produced at approximately 1 count per second! Obtaining such yields of very exotic species necessitates post-acceleration to an energy of 150 A MeV for ^{132}Sn .

Physics & instrumentation

The main goals of the Physics and Instrumentation task group were to propose key experiments in different fields and to determine the requirements for the innovative instrumentation necessary to perform these experiments.

Working groups were established to address the key experiments and instrumentation in each scientific research area that will be carried out at EURISOL. A workshop held at the ECT* centre in Trento presented ideas for EURISOL experiments, which formed the basis for the specimen experiments that were presented and discussed at subsequent meetings. Another important aspect was to provide input and guidance to the EURISOL team, driven by the requirements of the EURISOL physics research community, in particular the requirements for the post-accelerator parameters.

The work then focussed on the simulations of the selected apparatus for key experiments in several areas:

- neutron detector schemes for direct and break-up reaction studies,
- integrated charged-particle and gamma-ray detection for direct reaction studies,
- recoil separators for superheavy element studies,
- low-energy beta-beam studies.

This work included the analysis of data from current experiments. A report on the in-beam validations of some of the design concepts and the simulation tools for the main experimental programmes at the EURISOL facility was published, and the details of the design and costing of major instruments have also been completed. A report summarizing the group’s work on low-energy beta beams has also been prepared.

Finally, the Physics and Instrumentation task group played a leading role in setting up the EURISOL User Group, which has an elected Executive Committee and has already held a number of meetings. This User Group will continue to exist after the end of the Design Study, and will continue to organize topical meetings with the aim of updating the physics case for EURISOL

Safety & Radioprotection

EURISOL will produce unprecedented amounts of radioactive nuclei for an accelerator-based installation, and therefore safety and radioprotection concerns are of paramount importance and particularly challenging.

The main thrust of the task was the estimation of the radiation and activation in all parts of the facility in order to propose shielding and protection guidelines which must be taken into account in the design of the elements and in the global layout of the facility, and which will contribute a sizeable amount to the overall cost. Benchmarking of the available codes led to the choice of FLUKA and MCNPX2 as basis for the simulation work. Necessary shielding thicknesses to protect persons, soil and ground-water have been determined for the major parts of the facility, viz. the driver accelerator, the direct and multi-MW targets, the post-accelerator and experimental areas. The driver and targets – and probably also the post-accelerator – will be located underground to minimize the volume of concrete needed to contain the radioactivity. The most challenging element is the multi-MW target area, which will be shielded by a six-metre thickness of concrete to attenuate radiation sufficiently in the beam handling area.

In another important activity, a software tool – the “EURISOL Desktop Assistant Toolkit” (EDAT) – was developed using expertise from the nuclear power industry, which will assist in the management of safety and radioprotection at EURISOL and other high-power RIB facilities. A preliminary survey of safety and radioprotection legislation in different countries which might host EURISOL was also carried out, in order to identify possible major obstacles to its installation. A preliminary risk assessment study was carried out, listing and classifying the major risks to the operation of the facility, and proposing mitigating actions.

Hardware studies were carried out on two fronts. A prototype cryotrap system was built and tested and proven to be an efficient tool to minimize the migration of unwanted radioactivity within the beam transport system. Decommissioning of the facility will require solidification of the whole Hg volume. Several possible inorganic compounds and metal alloys were studied and HgS was chosen for final disposal. A specimen embedded in a cement matrix was also produced. Such a decommissioning procedure was deemed feasible and reliable, but is estimated to be very costly.

Management aspects

The Design Study was managed by a Project Leader, aided by a 3-member Management Board and a small Management Team comprising a Technical Coordinator, a secretarial and administrative assistant and a web-master. The Management Board reported to the Steering Committee, composed of one representative from each Participant Institution. A Coordination Board, consisting of the Management plus the 12 Task Leaders, met very regularly to discuss progress and to direct the work of the Design Study. When thought necessary, the Management appointed panels of 2 or 3 experts in a particular field to discuss problems which had arisen and to propose solutions.

Each year, a 3-day Town Meeting was held, at which the progress was reported in detail to the community. In addition, an International Advisory Panel comprising experts from TRIUMF, ANL, and KVI was appointed to review the progress each year, and to report to the Steering Committee and to the Management Board. This Panel was found to be invaluable in guiding the Design Study towards its goals, and led to the setting up of the EURISOL User Group. A Site Investigation Panel of experts was also appointed, and reported towards the end of the study.

Cost estimation

A cost estimate was done in the closing stages of the Design Study, resulting in a Total Estimated Cost of 1.3 billion euros. This includes labour and installation, but excludes scientific instrumentation, and does not include any contingency factor. However, since no architectural or structural engineering studies of the proposed buildings were possible within the ambit of the Design Study, these costs must be regarded as rough estimates only. This is a preliminary costing exercise, and much will depend on the site chosen for the facility, particularly with respect to existing infrastructure, where applicable.

Site investigation Panel

The Panel was tasked with investigating a number of examples of sites which could host the EURISOL facility, but these are not the only possible candidates, nor did this imply that these sites will be available. The report concluded that Europe has several sites that are extremely well-suited for hosting EURISOL and which have a great deal of existing value in facilities, equipment, expertise and experience.

International Advisory Panel

In their final report to the Steering Committee, the IAP acknowledged that much had been achieved by the Design Study, but also expressed some concerns. Considering the limited resources available for continuation of the EURISOL project beyond the Design Study, the IAP suggested that further studies should concentrate on a limited number of topics that are critical for the feasibility of the EURISOL concept:

- the coaxial mercury target, preferably in collaboration with ESS. An effort should be made to continue work on the windowless target because of the perspectives for EURISOL performance improvement it holds;

- the MAFF-type fission target in combination with different ion sources, focussing on laser ionisation schemes. The emphasis of this work should be on the technological aspects rather than on the further optimization of the target material;
- system integration of the spallation target and the fission target + ion source;
- beam purification and charge breeding;
- radiation safety of the multi-MW production target and the post-accelerator.

Chapter 1: Introduction & Objectives

The idea behind EURISOL – a European isotope-separation-on-line (ISOL) facility – is to work towards the construction of an accelerator-based ISOL system for producing exotic radioactive ion beams (RIBs) with intensities several orders of magnitude greater than those available today. When this idea was first mooted, studies had also started towards constructing the Facility for Antiproton and Ion Research (FAIR) in Germany, and proposals were also made for the Rare Isotope Accelerator (RIA) in the USA. Since FAIR was based on in-flight separation of isotopes, using heavy ion beams, the range and yields of radioisotopes would be different from those produced using the ISOL method. EURISOL would therefore be complementary to FAIR, and would provide a high-power facility for European scientists.

The EURISOL Feasibility Study

The first step towards EURISOL was a Feasibility Study [1], a collaboration of European laboratories with GANIL as the coordinating institution, co-financed by the European Commission under its Fifth Framework Programme (FP5) from 2000–2003. At the same time, several other ISOL projects were proposed, such as SPIRAL2 at GANIL, HIE-ISOLDE at CERN and SPES at LNL, Legnaro, which are now regarded as “intermediate” or “precursor” facilities, since they will provide improved beam intensities, albeit much lower than those proposed at EURISOL. Similar efforts are under way in ISAC-II at TRIUMF in CANADA. An alternative ISOL method was proposed in a facility called MAFF at Munich, based on using neutrons from a reactor, but this project has now been cancelled.

During the EURISOL Feasibility Study, it became clear that a 1-GeV proton beam would be very suitable for RIB production, and that it had certain advantages over heavier-ion beams since the beam energy would be distributed over a greater depth in the target material, ameliorating the problem of target cooling. Beam intensities of up to 4 MW were considered to be feasible, and indeed necessary to produce the goal of over 10^{15} fissions per second in the target. For such a scheme, it was clear that a liquid-metal target, such as mercury or a Pb-Bi eutectic, would be needed to remove the heat load from the target. The original concept involved a high-speed Hg “jet”, coaxial with the proton beam, and surrounded by a cylinder of uranium carbide. The protons would give rise to a high flux of spallation neutrons in the Hg “converter” target, which would then cause fission in the uranium, thus producing a range of isotopes, radioactive and otherwise.

For production of elements not available from the fission of uranium, work was also done investigating targets able to accept 100-kW beams of protons, using specific target materials to produce selected radioactive isotopes.

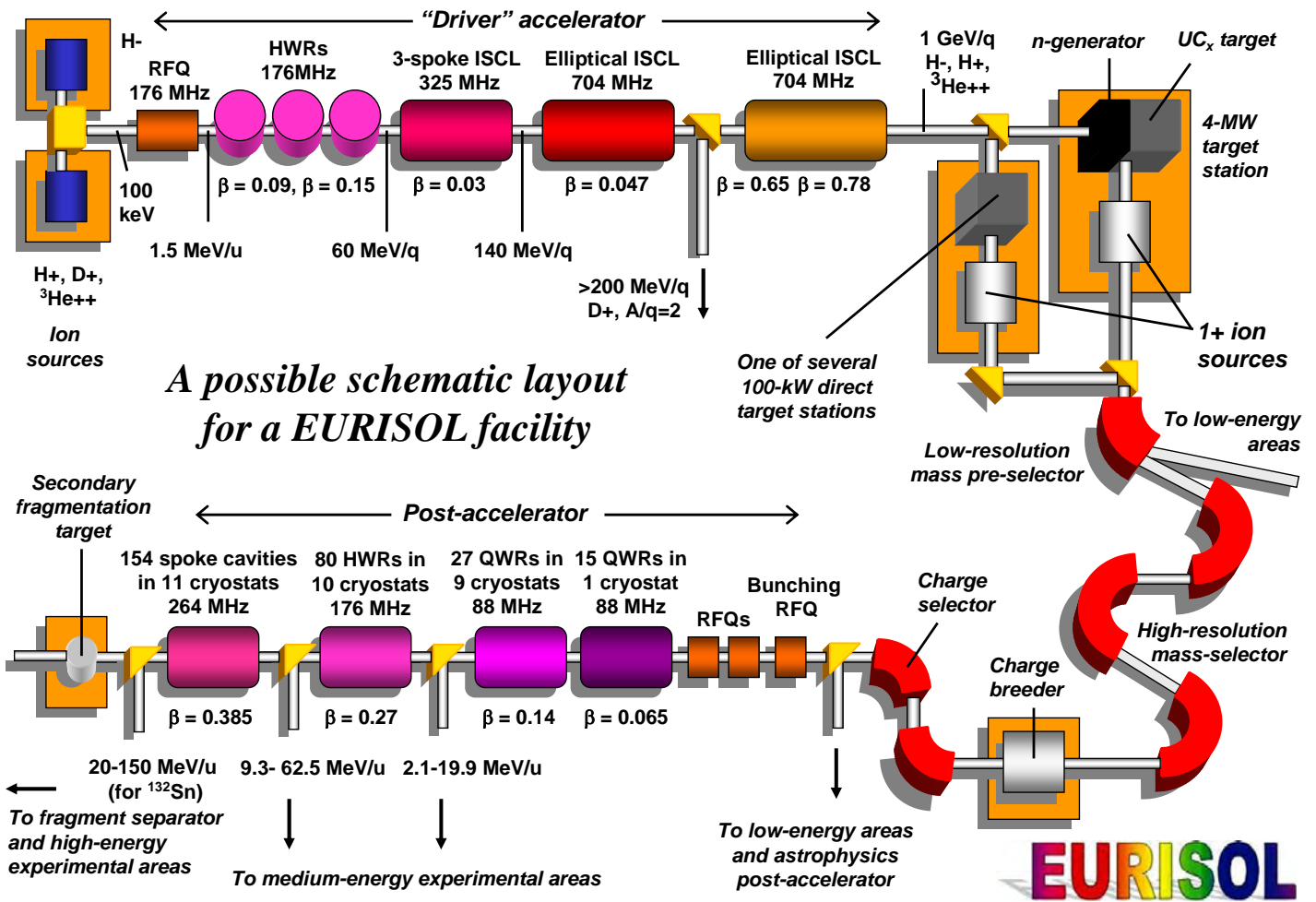
The EURISOL Design Study

At this stage it was realised that further study was needed, and the present Design Study was launched in 2005, again with EC support, this time under FP6. Twenty institutions formed a consortium of Partners, with another 21 Collaborators (without EC funding) including institutions in other continents. Meanwhile, the US proposal was reduced in scope, and this has recently been accepted by the DoE under the name of Facility for Rare Isotope Beams (FRIB), to be located at Michigan State University.

The work of the Design Study was divided between 12 work packages called “Tasks”, as follows:

- Task 1: Management
- Task 2: Multi-MW target station
- Task 3: Direct (100-kW) target
- Task 4: Fission target
- Task 5: Safety & radioprotection
- Task 6: Heavy-ion accelerator
- Task 7: Proton accelerator
- Task 8: Superconducting cavity development
- Task 9: Beam preparation
- Task 10: Physics and instrumentation
- Task 11: Beam intensity calculations
- Task 12: Beta-beam aspects.

The last of these arose from the realisation that the high-yield RIB facility proposed would also be suitable for producing the neutrino-emitting isotopes required for the so-called “beta-beam” concept.



A schematic diagram of the envisaged EURISOL facility.

High-power targets

Early in the EURISOL Design Study, it was realised that a fission target in the form of a single, large uranium cylinder would not work, since the effusion and diffusion times from such a large volume would preclude the survival of short-lived nuclei produced in the inner parts of this material. This gave rise to a re-evaluation of the fission target geometry, and a subsequent “MAFF-like” proposal in which 6 small fission targets are located around the liquid-metal converter target, each with an adjacent ion source. The implication of this is that each fission-target/ion-source assembly, together with its beam transport system, would have to be inserted in a tube through the 7-metre steel and concrete shielding needed around the spallation target. This system has been elaborated in some detail.

Much work has been done on the liquid-metal converter target, with the baseline proposal being a long, coaxial, cylindrical target, in which the liquid metal flows in one direction in an outer concentric cylinder towards a thin window, where it turns through 180° and then contra-flows down the central cylindrical target volume. The neutronics, heat-flow, liquid-metal loop, maintenance and safety aspects have all been studied in great detail. Mercury was used in prototypes during the Design Study (as used in the SNS): however, a Pb-Bi eutectic (as tested at PSI) can also be envisaged.

An alternative spallation target has also been proposed, in which the liquid-metal is made to fall as a “curtain” with the proton beam traversing the length of the curtain. This could have advantages in that the 6 fission targets could be placed with 3 on each side, closer to the source of spallation neutrons.

Another innovative aspect of the proposed facility is the idea of accelerating beams of ^{132}Sn , for example, which is already a neutron-rich radioisotope, and then fragmenting this beam to produce a

whole spectrum of neutron-rich radioisotopes, much farther from stability than can be reached today. The intent is to produce some 10^{13} ions per second of ^{132}Sn , re-accelerated to an energy of 150-*A* MeV. Many extremely exotic ion species can be produced in this way, and extensive yield calculations have been done: for example, the expected intensity for ^{125}Pd , which was only discovered in 2007 at the new RIKEN facility, is 2.4×10^6 particles/sec, while for ^{120}Ru it is 1.5×10^5 pps.

Challenges

It is also clear that in order to achieve the very high yields expected from the multi-MW target, the extracted RIBs from the 6 fission-target/ion-source assemblies need to be merged. This is still a challenge, and may be met using an innovative ion-source called ARC-ECRIS, which provides access for multiple beam-lines because of its open-sided coil structure.

Other challenges facing the team included the splitting of the 1-GeV proton beam to provide variable intensities of beams from zero up to 100 kW to any of 3 direct targets, without interrupting the high-intensity beam. An innovative beam-splitting method based on magnetic Lorentz stripping has been proposed for this.

Superconducting technology has now come of age, and the proposed solutions for both driver and post-accelerator use superconducting linear accelerator cavities, while either superconducting or warm RFQ structures can be envisaged. Cryostats and several different types of superconducting cavities have been designed and prototyped, but the aim has always been to make use of tried-and-tested technology for the accelerators, wherever possible, to minimise risks with the high-power or radioactive ion beams. On the other hand, reliable solid-state power supplies (up to 10 kW) based on MOSFET technology for the accelerating cavities have also been prototyped during the Design Study.

The overarching challenge for such a high-power facility, producing RIBs with never-before-used intensities, is to ensure that the operation is safe and radiation contained, to make provision for remote-handling facilities for routine operation and maintenance, and to cope with any abnormal situations and breakdowns. Only if such risks are properly analysed and evaluated, with suitable mitigating infrastructure in place, can such a facility expect to be permitted to operate.

Clearly a more detailed Engineering Study will be required before the facility can be constructed. However, many of the problems have been addressed very successfully, while those which have arisen during the Design Study and remain open questions should be the subject of focussed R&D in the coming years.

Reference

1. *“The EURISOL Report – A Feasibility Study for a European Isotope-Separation-On-Line Radioactive Ion Beam Facility”*, ed. J. Cornell, published by GANIL, December 2003.

Chapter 2: The Driver Accelerator

2.1 Introduction

The design of the driver accelerator for the EURISOL RIB facility was carried out by a task group led by INFN-LNL, with the participation of CEA (Saclay) and IPN (Orsay), and with contributions from SOREQ NRC (Yavne, Israel) and TRIUMF (Vancouver, Canada). The work commenced using the specifications given in the earlier EURISOL Feasibility Study [1], i.e. a 1-GeV, 5-mA fully superconducting proton linac with heavy-ion capabilities given by a second linac injector. However, investigations of expected yields [2] showed that the modification of the driver to allow a 2-GeV, ^3He beam would be a better investment than the construction of the second, very large, machine for acceleration of a wide range of heavy ions. In addition, the possibilities given by intense deuteron beams at energies considerably higher than those presently available were pointed out by the EURISOL community and this became a further specification. The layout of the driver had thus to be revised and modified from the previous one, to meet the new requirements, i.e.:

- a final beam energy of 1 GeV for the proton beam;
- an average beam current of 5 mA for the main multi-MW ‘2-step’ production mode (using a spallation target), and 0.1 mA for the 100-kW ‘direct’ production mode;
- a duty cycle of 100% (CW beam), retaining the possibility of pulsing the beam for setting-up;
- the possibility of accelerating deuterons to less than 300 MeV and a $^3\text{He}^{2+}$ beam up to 2 GeV.

The work of the group was organized into 7 sub-tasks. The first two (*Proton source and LEPT tests*, and *RFQ and MEPT*) were related to the old proton driver design, although the new specifications meant that these items were no longer on the critical path. The work was nevertheless continued and completed. The third and fourth sub-tasks (*Low- and Medium- β Linac*, and *High- β Linac*) were dedicated to the layout and beam dynamics design of the core of the machine, the superconducting linac. Sub-task 5 (*Ion Injector*), originally intended only for the ion injector linac of the old design, became the design of the main injector after the new specifications were introduced, and a way to combine the proton and ion lines was then required. Sub-task 6 (*High Energy Beam Transport*) was dedicated to the design of the beam extraction and beam transport lines to the RIB production targets. This work, which was originally expected only to consist of standard beam optical calculations, eventually led to the introduction of the new concept of high-power, CW proton beam splitting, allowing the EURISOL project to include the possibility of parallel delivery of continuous proton beams to different targets starting from one main beam [3]. This achievement required a modification of the injector section to replace the proton beam with an H^- beam. The seventh and last sub-task (*Beam Loss Calculation*) consisted of the end-to-end beam dynamics study of the driver, after the introduction of realistic errors in the nominal field distributions (caused by misalignment, ripple, power supply instabilities, etc.), and a statistical calculation of the beam-loss distribution along the linac. This was a necessary step in order to verify the conformity to specifications and the shielding requirements of the whole accelerator. This conclusive check showed that the final driver design matches the EURISOL needs.

In this work, care was taken to choose components with reliable performance, rather than very challenging ones, in order to ensure the possibility of constructing the facility in a predictable time. Where necessary, we have also used components specifically developed for this project by the EURISOL Superconducting Cavity Development group [4–6].

2.2 EURISOL driver layout

The EURISOL “driver” is a superconducting (SC) linac that includes 5 different sections: injector, low- β section, medium- β section, high- β section and high-energy beam transport section (HEBT), which includes a CW beam-splitter. The lengths of the injector and of the superconducting part are 9 m and 241 m, respectively, while the 4-way beam splitting section is about 55 m long. About 20 more metres are required to transport the high-power beam to the multi-megawatt target. An additional

extraction sector is located at the beginning of the high- β section, giving the possibility of building an intermediate-energy beam line (e.g. for 270-MeV deuterons) in the future. Deuterons can also be transported inside the linac right to the end of the machine. The low- β cryostats are planned to work at 4.5K, while the high- β ones should be operated at 2K with superfluid helium. The spoke-cavity cryostats could work efficiently in both cases. According to the SNS experience, however, the linac could also be operated (although with a somehow lower efficiency) with all cryostats at 4.2K.

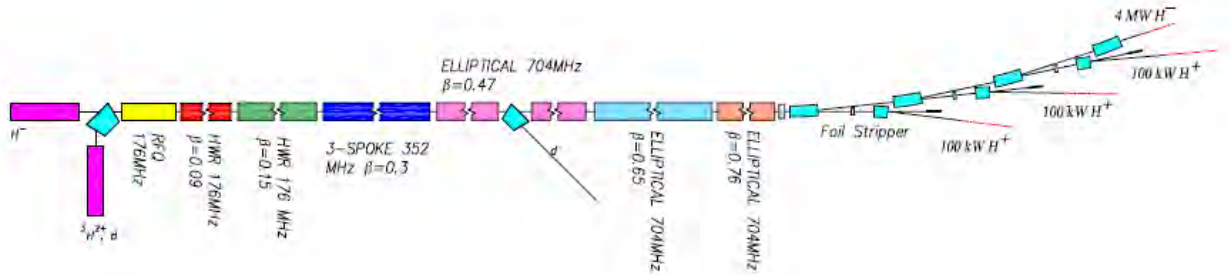


Fig. 1: EURISOL Driver schematic layout (not to scale) showing the different sections.

2.2.1 Injector

The injector design has many similarities to the SARAF injector in Israel, with modifications required by the different beam types. Two ion sources are used. The first one is a TRIUMF-type multicusp H^- source, located in the straight injection line. The second one, located in the 90° branch to allow A/q selection, is an ECR source for production of deuterons (5 mA) and doubly-charged ^3He ions (0.1 mA). The limiting beam parameters at the source outputs are listed in table 1.

Table 1: Beam specifications at the inputs to the low-energy beam transport lines.

Beam	H^-	$^3\text{He}^{++}$	D^+
E (keV/nucleon)	20	20	20
I (mA)	6	0.2	6
ϵ_x, ϵ_y (π mm.mrad rms norm.)	0.125	0.125	0.1

Two focusing solenoids are located in each branch between the source and the dipole. A common beam line, including two more solenoids, connects the dipole magnet to the RFQ. An adjustable aperture to control the beam intensity and to cut tails is located just downstream of the bending magnet. Movable slits, wire scanners and a Faraday cup to provide measurements of the beam profile, emittance and current are installed between these solenoids. A beam stopper, a diaphragm and an electron suppressor is mounted at the end of the low-energy beam transport line (LEBT), in front of the RFQ.

The 176-MHz RFQ resembles the SARAF one [7] in its electrodes profiles; it is 3.8 m long and it must be able to operate in CW mode. Its mechanical design might be either of the 4-rod type (like the SARAF one) or even of the 4-vane type (like the IFMIF 175-MHz RFQ) [8] which is expected to be easier to cool for CW operation. The EURISOL RFQ must allow acceleration up to $1.5A$ MeV, requiring a maximum power of about 300 kW for the deuteron beam. Little emittance growth and relatively small size and cost are its main characteristics, at the price of a none-too-spectacular transmission (92% accelerated beam for H^- ions and 95% for deuterons and ^3He -ions). However, this appears to be fully acceptable for our application. The particles transmitted but not accelerated by the RFQ (about 3%) are lost in the MEBT which is used to match the RFQ beam to the superconducting linac in order to prevent halo formation.

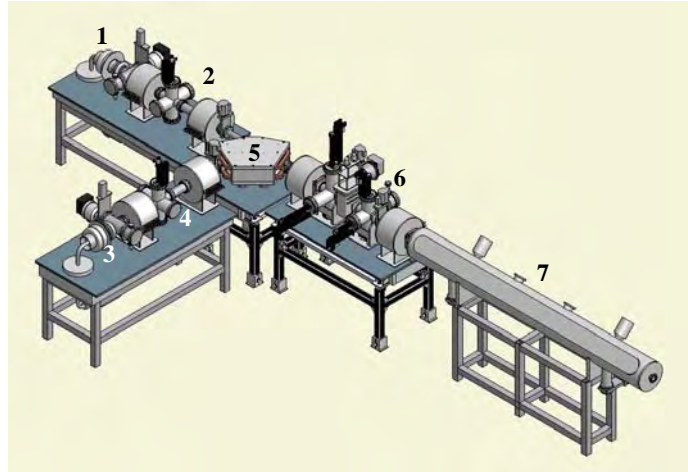


Fig. 2: The EURISOL ion injector station, showing (1) multicusp H^- source, (2) H^- beam line, (3) D^+ & ${}^3\text{He}^{++}$ ECR source, (4) D^+ & ${}^3\text{He}^{++}$ beam line, (5) analysing dipole magnet, (6) diagnostic line, and (7) RFQ.

2.2.2 Low- β section

The low- β section consists of a MEBT and 9 cryostats, containing eight 176-MHz, half-wave resonators (HWRs) each.

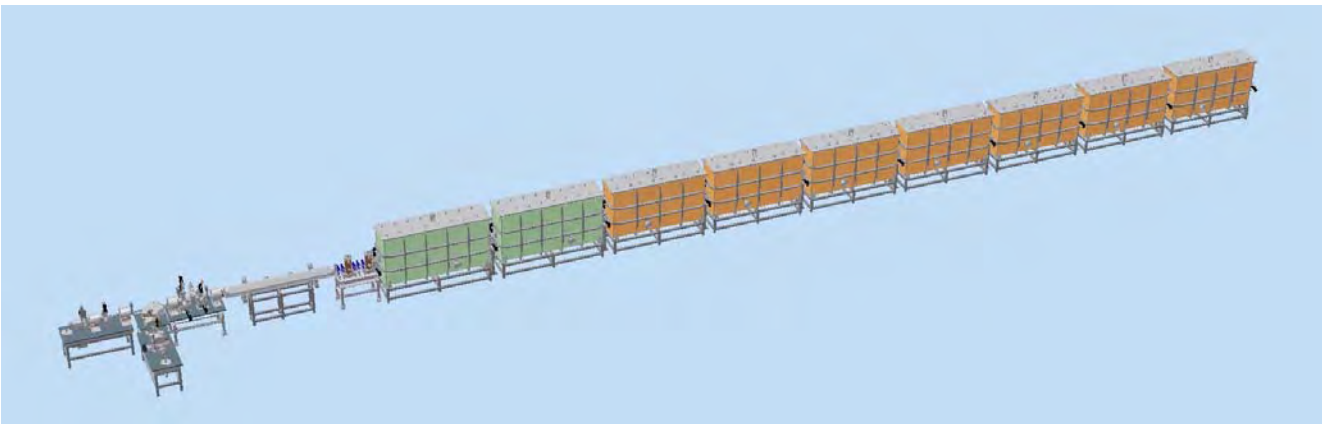


Fig. 3: The EURISOL driver front-end, showing the injectors and the low- β section.

The MEBT has the function of matching the various beams to the superconducting linac in different configurations. It includes 5 short quadrupole magnets and 2 normal-conducting buncher resonators of the quarter-wave type (QWR), with $\beta_0=0.056$ (the RFQ output beam velocity). A diagnostics box is available at the end of the section. Another function of the MEBT is to stop the transmitted but not accelerated particles from the RFQ. These particles hit the MEBT walls in different positions, due to the dependence of the quadrupole focusing strength on beam velocity. A water-cooled, 5-mm radius diaphragm just before the first cryostats allows for final cleaning of the beam of the outermost particles, limiting halo formation and emittance growth in the subsequent linac sections. The resonators required in the superconducting section are of two types, with $\beta_0=0.09$ and $\beta_0=0.16$, working at the conservative gradients of 4.7 and 5.2 MV/m, respectively. Prototypes of these cavities have been developed in the EURISOL framework, but the SARAF resonators and those of IFMIF might also be adapted to this linac.

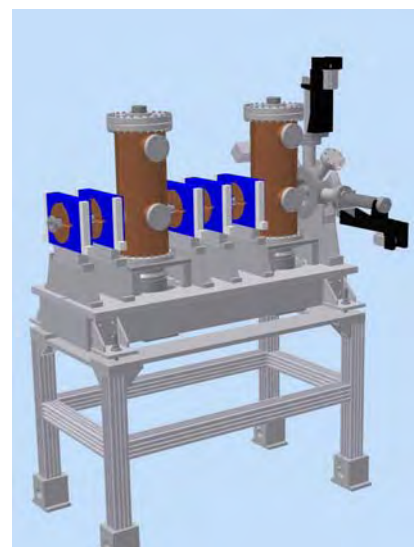


Fig. 4: The MEBT section.

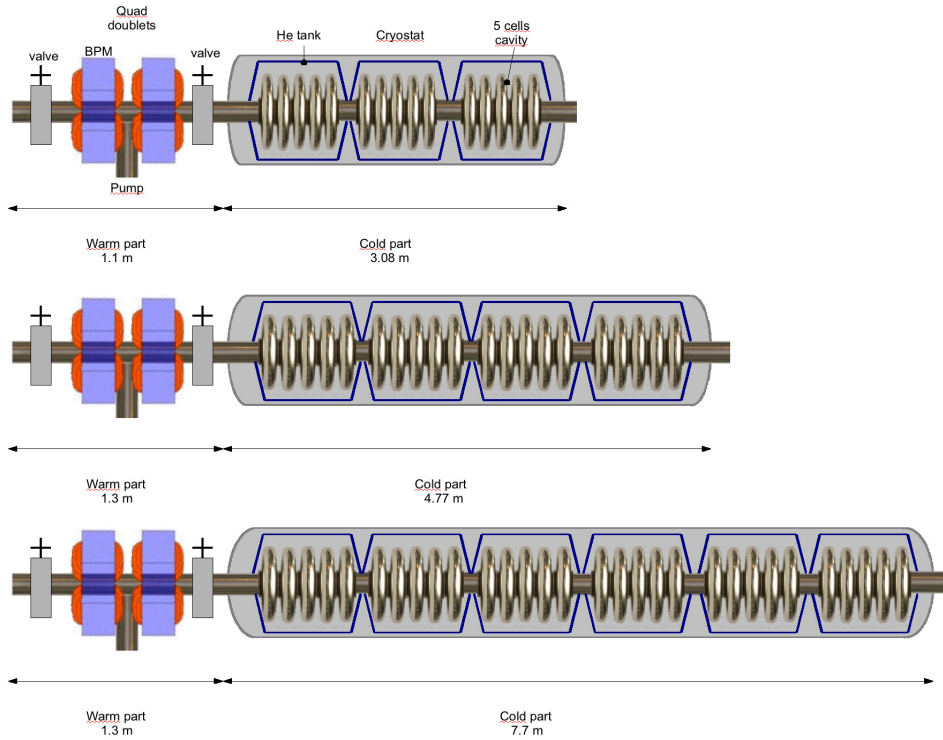


Fig. 7: Schematic drawing of the three different lattice periods of the SC linac.

2.2.5 High Energy Beam Transport section

A unique peculiarity of the EURISOL driver is its possibility of delivering parallel CW proton beams to different targets with low losses [9]. This is achieved by using a primary H^- beam (up to 5 MW), neutralizing part of it (up to 100 kW) by magnetic stripping, and then displacing the un-neutralized H^- ions to a different beam line by means of a dipole magnet. When the two beams are sufficiently separated, the neutral one is then transformed into a proton beam by means of a stripper foil. From here on, the H^- and H^+ beams can be transported independently. The 100-kW limit of the extracted beam is dictated by the present RIB direct target technology. The beam losses, mainly due to the stripper foil efficiency, can be limited to a few tens of watts and collected by a small beam dump. The splitting operation can be repeated by adding more splitting sections, providing multiple CW beams.

A critical component of the system is the special magnetic neutralizer, a simple and unconventional chicane made of 3 short dipoles that can provide partial neutralization without affecting the primary beam emittance and without producing unwanted H^+ ions. Since the neutralization rate is determined by the magnetic field intensity, it is possible to raise the field (and thus the secondary beam current) slowly, to avoid thermal shocks in the direct targets.

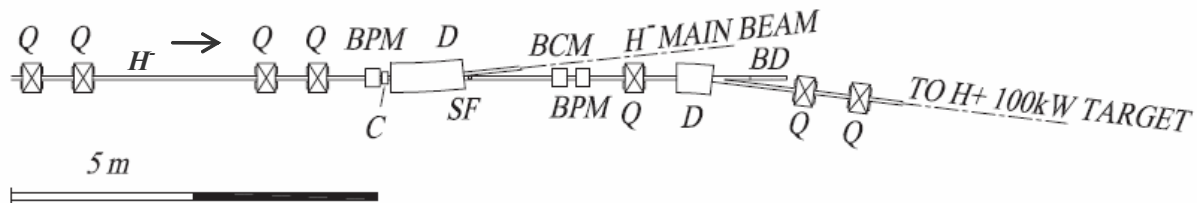


Fig. 8: One unit of the CW beam splitter. The main H^- beam (from the left) is partially neutralized in a small magnetic chicane (C). In the first bending magnet (D), the main H^- beam is guided to the next splitter section, while the H^0 particles move straight to the stripper foil (SF), to be stripped into H^+ and then transported to the target. Q=quadrupole magnet, BD=beam dump, BCM=beam current monitor, BPM=beam profile monitor.

The final HEBT layout includes one main line bringing a 4-MW, 1-GeV H^- beam to the high-power neutron converter, three lines leading to the 100-kW direct targets for 1-GeV protons and 2-GeV ${}^3\text{He}^{++}$ ions, and one more line for a 270-MeV-deuteron beam. This layout can easily be adapted for different positioning of the RIB production targets, while maintaining the same beam-splitting scheme.

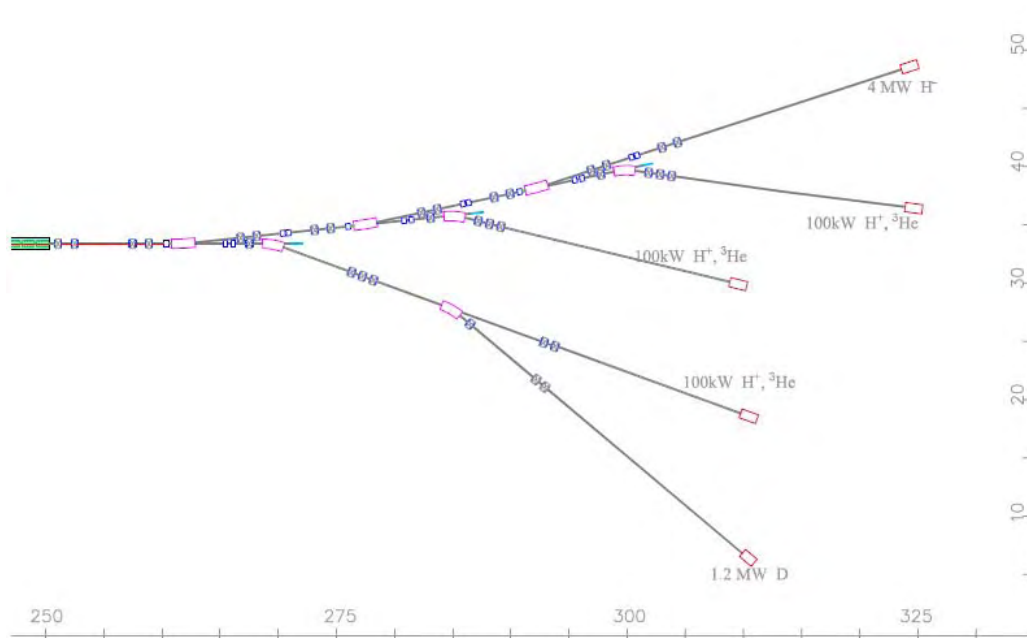


Fig. 9: The HEBT layout, showing the upper “backbone” line and the 4 extraction lines

2.3 Beam dynamics

The linac beam dynamics was studied using the TRACEWIN code developed at CEA Saclay [10]. The transport of all the beams (H^- , D^+ and ${}^3\text{He}^{++}$) was simulated from the exit of the ion source to the target with macroparticles. All the cavities and the solenoids have been simulated with their computed electro-magnetic field maps.

We chose to use conservative specifications for the linac components (i.e. cavity gradients and magnet fields) in order to achieve a reliable design without depending on future technological breakthroughs. In order to satisfy the requirements of small emittance growth and halo formation, the design uses the following philosophy:

- keeping the average phase advance per meter (average beam confinement) as smooth as possible;
- keeping the focusing lattice scheme as continuous as possible;
- matching the rms beam parameters at the transitions;
- avoiding zero-current phase-advance per lattice higher than 90° ;
- avoiding the same transverse and longitudinal phase advances in order to stay away from emittance exchanges when the space charge is important;
- keeping the tune depression as high as possible;
- avoiding insufficient bunching, and variation from cell to cell of the average beam aspect ratio.

We kept the transverse and longitudinal phase advance per period below 90° along the linac, and carefully tried to avoid parametric resonances. The continuity of the phase advance per metre has also

been an important criterion in order to simplify the matching at transitions. This point is especially relevant to transporting different beam currents in a common linac. The frequency jump from 352 to 704 MHz was managed by smoothly varying the phase advance per period in order to avoid a longitudinal bottleneck just before the high-energy section. Beam losses could be confined to the region below 1.5 MeV, i.e. before entering the superconducting linac.

A special effort was required for transporting the 5-mA H^- beam in the low- β section, where cryostats with different structure introduce discontinuities in the lattice. To suppress the x - y mixing caused by solenoids, their axial field was set with the required strength but opposite sign at every consecutive element, thus restoring the original phase space orientation every 2nd solenoid. With this expedient, the final layout could allow transport with satisfactory acceptance and emittance growth for all beams.

For extraction of the deuteron beam accelerated up to 270 MeV in the $\beta=0.47$ section, two schemes have been studied: the first is the transport through the two last high- β sections, with detuned and unpowered cavities (for which the optimum velocity is too high for the deuteron beam), and extraction at the HEBT; a second option is to add a focusing period at the end of the first section and replace the cryostat by a dipole to extract the beam and transfer it to a dedicated experiment. This last option may help to minimize deuteron losses in the whole machine but could require a very long transfer line to the target. Thus, the first option was chosen as the reference one. Nevertheless, the additional period with a drift instead of a cryostat was included in the layout, in order to allow future addition of a new, intermediate-energy beam extraction line.

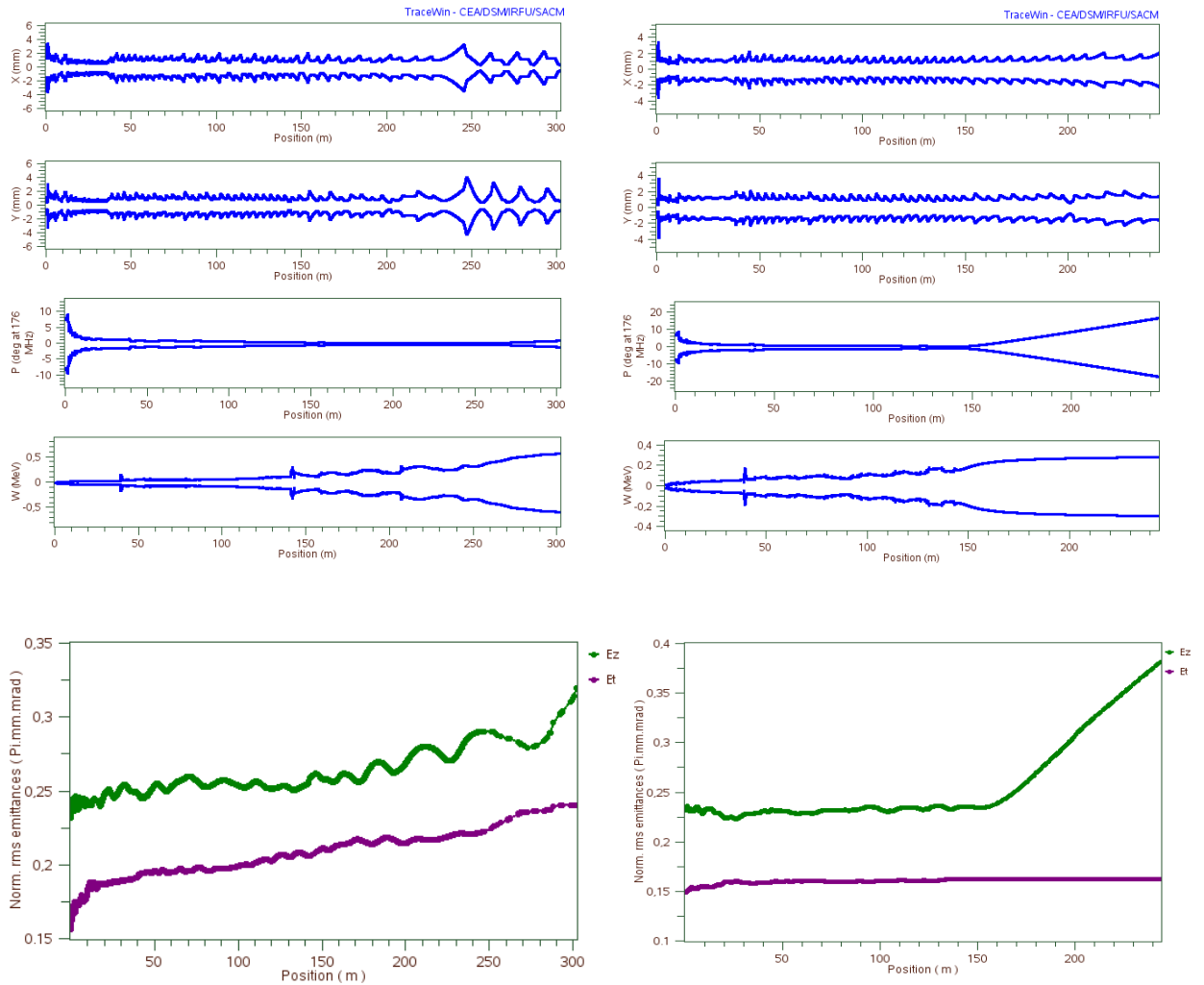


Fig. 10: Beam envelopes (top) and normalized rms emittance evolutions (bottom) for the proton beams (left) and deuterons (right).

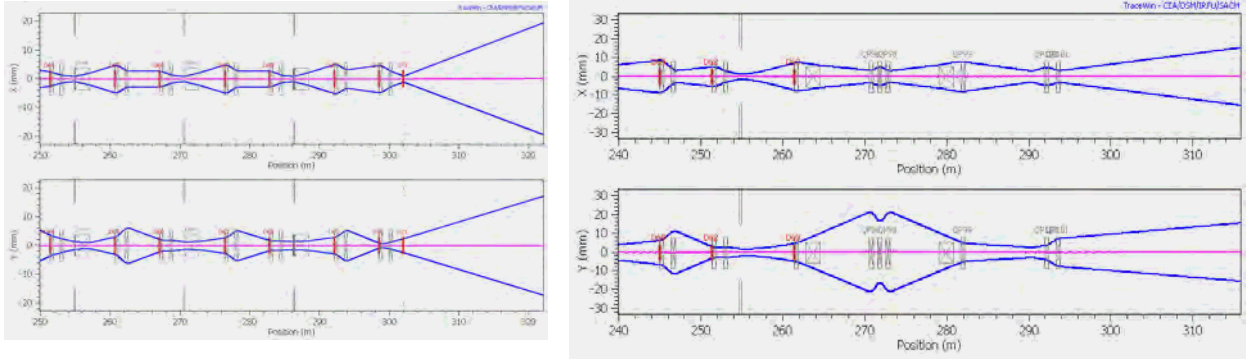


Fig. 11(Left:) H^- multiparticle envelope along the 4-MW “backbone” line with the 3 beam-splitters. (Right:) deuteron multiparticle envelope in the 1.2-MW line.

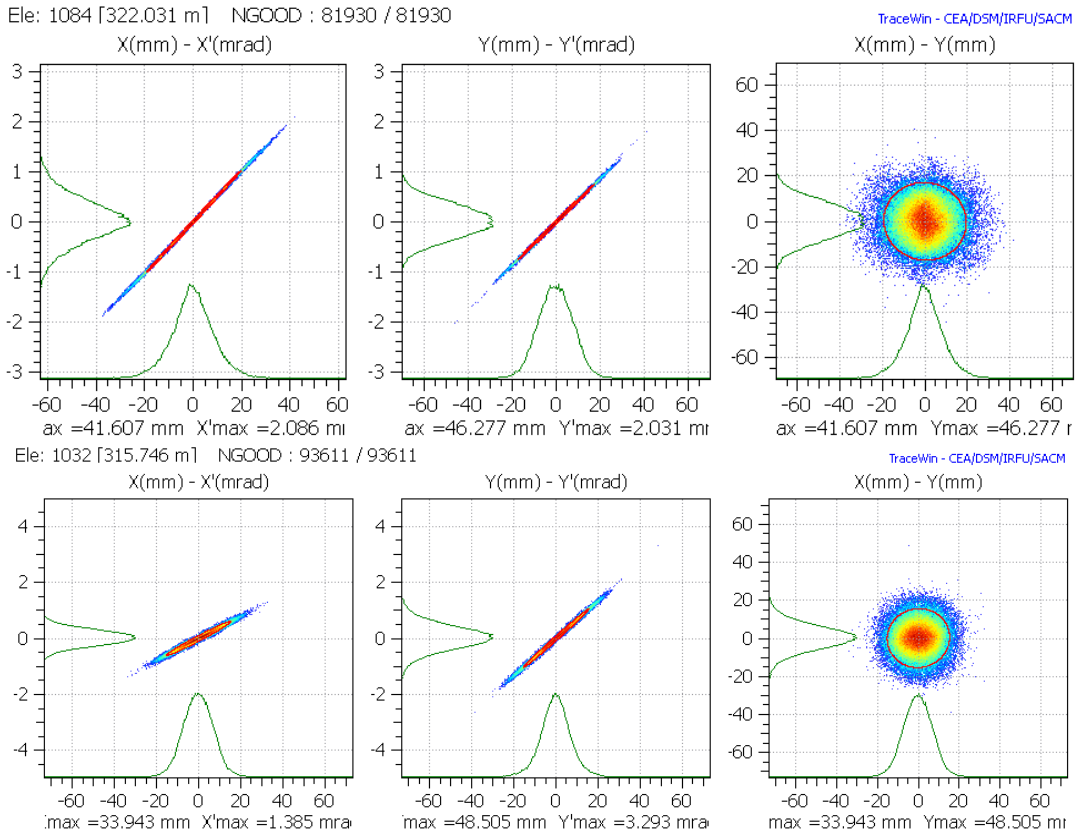


Fig. 12: Transverse phase spaces and beam cross-section at the RIB production target for H^- (top) and D^+ .

2.4 Beam loss calculations

In order to define tolerances for the linac construction and to test the robustness of the achieved architecture, the effect of imperfect elements on the reference design was evaluated. To manage such errors (misalignments, field instabilities due to ripple, etc.) a strategy based on correctors and diagnostics was established [11] taking into account that the diagnostics are also imperfect (with misalignments, measurement errors, etc.) To achieve realistic simulation of a high-intensity linac, it is necessary to perform start-to-end transport calculations to be able to estimate the impact of halo produced at low energy on the beam losses in the high-energy part of the accelerator. Macroparticles are used to estimate the beam distribution and to record the losses on the beam pipe. The discrete recorded losses at different locations in the linac allow us to build a Cumulative Distribution Function (CDF) to determine the probability of depositing more than a certain fraction of the beam.

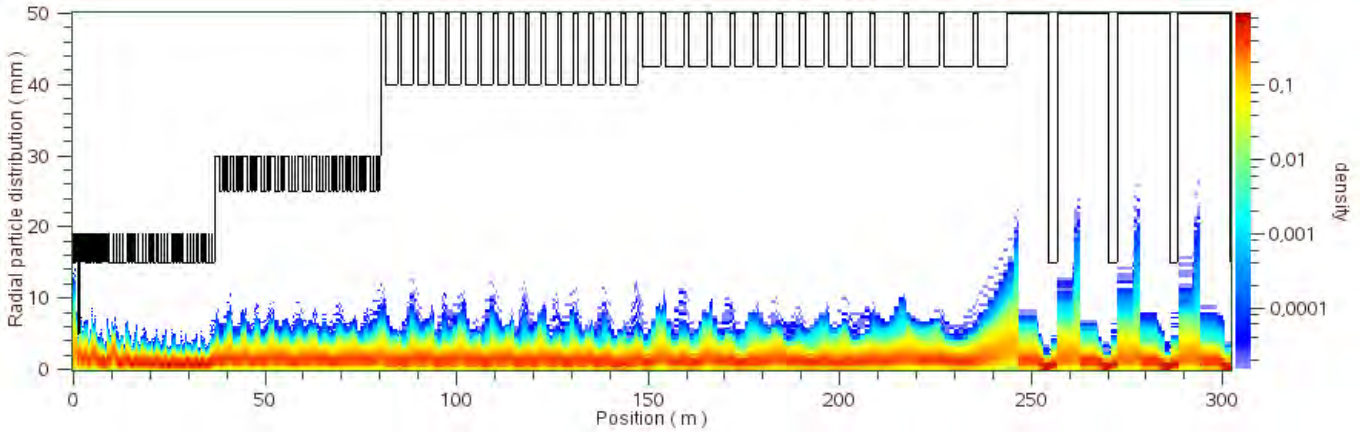


Fig. 13: The radial distribution of protons in the transverse plane along the EURISOL driver.

The Extreme Value Theory [12] provides a firm theoretical foundation to compute the average probability of the occurrence of beam losses in the range of a few watts up to a few tens of watts in the EURISOL driver. Confidence intervals (error bars) associated to this evaluation are calculated. The procedure uses large-scale simulations of linacs combining different sets of errors. The correction scheme manages the transverse beam centre.

2.4.1 The reference design and the calculation framework

For each run, a 10,000,000-macroparticle Gaussian distribution cut at 6σ for each plane is used at the input of the MEBT line. This allows us to reach a resolution of 0.5 W at the exit of the linac for the proton case and close to 0.1 W for the deuterons. The simulation takes into account a 3D domain and neighbouring bunches. Several elements are simulated using field maps, i.e. the solenoids and all the resonators. Preliminary studies have shown that the simulation of the other elements can be performed using the classical hard-edge formalism (quadrupoles and dipoles). To manage the necessary huge number of runs for the Monte-Carlo study, it has been implemented in TraceWin, a software package that permits one to pilot a heterogeneous collection of PCs or to use the numerous computation nodes of a cluster.

The rms emittance evolutions are illustrated in figure 10. No significant emittance growth in the accelerator for the two beams is observed. Only the longitudinal emittance of the deuteron beam increases by a factor close to two, since the beam is transported with all cavities unpowered and detuned after the first high- β sections, to permit the beam transport through the linac to a dedicated transfer line. No consequence is expected for the transport to the target. The envelope behaviour plotted in figure 10 is when all elements are perfect. The beams are “scraped” in the first part in the MEBT which includes a collimator in order to clean the beam before the superconducting part of the machine. It corresponds to a deposited power of a few watts. No loss occurs elsewhere. The acceptable losses in the SC linac are assumed to be lower than 1 watt/m.

Two families of errors have to be allowed for. The corrected errors are applied before the tuning of the linac (cavity and quadrupole misalignments, static field errors) and corrected with steerers coupled with beam position monitors. In the longitudinal plane, the centre is tuned with time-of-flight measurements. The uncorrected errors are applied after the correction procedure and represent the dynamic fluctuations of the RF field, mechanical vibrations from the environment or a residual static error due to imperfect correction. The main threshold for the error amplitudes in the EURISOL driver is set to avoid losses in the superconducting section above 1 W/m, in order to allow hands-on maintenance. The acceptable values for the errors have been chosen after iterating with the engineering teams and the background from previous studies on high-intensity linacs, converging on values that may be reached with the present technology and know-how, in order to avoid any extra cost required for R&D.

In the H^- case, 155 linacs were simulated with 10,000,000 macroparticles per run. Two hot spots were found, corresponding to the collimator in the MEBT and the first dipole in the HEBT line (figure 14).

The deposited power on the collimator corresponds to low-energy ions (1.5 MeV per nucleon) and for this reason we assumed that these are controlled losses. The average power lost at the second hot spot is lower than one watt. Several runs exceeded several tens of watts, which is huge at the energy of 1 GeV. The probability of this event is very low, but it would require re-alignment of the system.

For deuterons, 269 different linacs have been randomly generated and simulated with 10,000,000 macroparticles per run. The average deposited power again obeys the hands-on maintenance rule of being less than one watt/metre (figure 15). It turns out that only longitudinal losses are present in the machines and therefore only the average values are relevant. The effect of both gas and magnetic stripping (for H^-) was found to be negligible.

In conclusion, this application of the Extreme Value Theory to beam-loss estimates in the EURISOL driver linac based on large-scale Monte-Carlo computations allowed us to provide a loss probability for this linac. The start-to-end error studies showed manageable losses with a 6σ Gaussian as input distribution and the use of a collimator in the MEBT. The probability to lose more than one W/m in the driver predicted with the Extreme Value Theory is less than 8% for the proton beam. Such an event will happen on average for few linacs in every hundred linacs built. The losses in the superconducting section are directly linked to the MEBT scraper that has to handle only a few tens of watts at 1.5 MeV per nucleon. For the deuterons, the origin of the losses is longitudinal and corresponds to a peak average deposited power of 0.4 W. These results obtained are according to specifications.

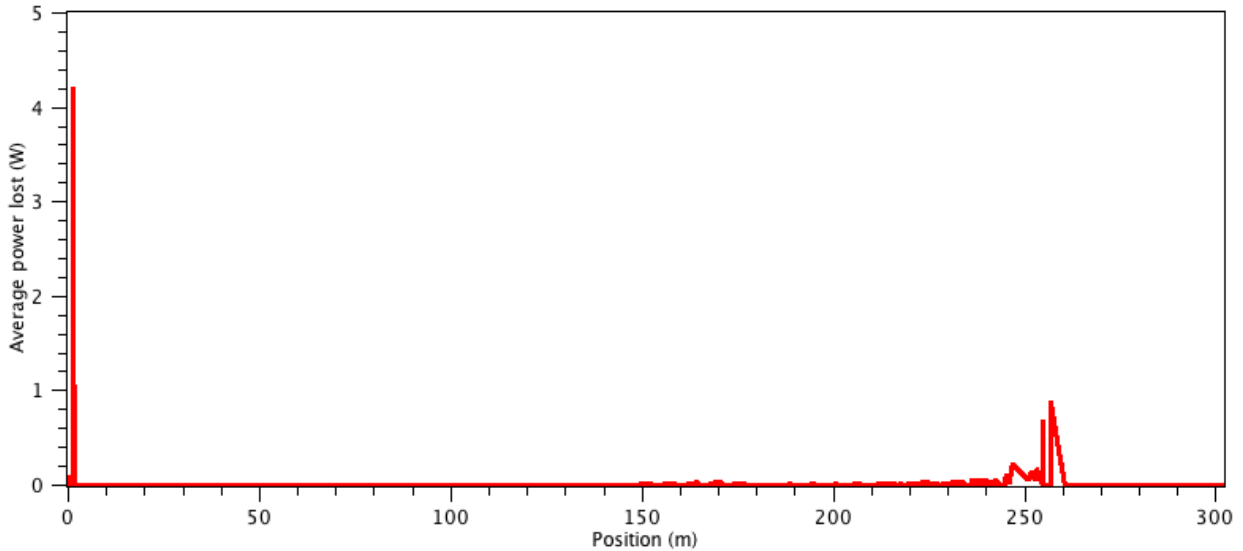


Fig. 14: Average loss distribution along the structure for H^- ions.

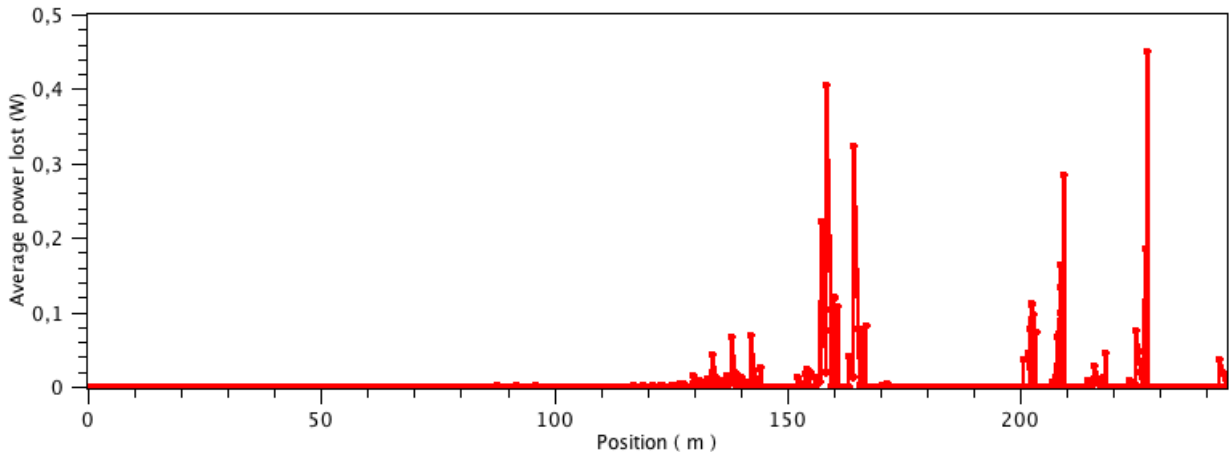


Fig. 15: Average loss distribution along the structure for deuterons.

2.5 Conclusions

This work, performed as an international collaboration between INFN-LNL, CEA Saclay and IN2P3 Orsay, with valuable contributions from SOREQ and TRIUMF, has produced the design of a superconducting linac for proton, deuteron and $^3\text{He}^{2+}$ beams that fulfils the EURISOL DS driver linac specifications. This accelerator is based on three types of superconducting resonators (viz. half-wave, spoke and elliptical cavities) with 6 different optimum velocities. The maximum beam energy for H^- is above 1 GeV, and the maximum beam current is 5 mA. The injector section includes a 1.5·4 MeV RFQ and two ion sources. H^- is used to produce the proton beams, allowing CW beam splitting at high energy by means of a novel technique with low beam losses. Up to 4 proton beams (one of 4 MW, and three of 100 kW each) can be delivered simultaneously by the EURISOL driver to RIB production targets. Beams of 2-GeV, 100- μA ^3He ions, and 270-MeV, 4-mA deuterons can also be produced.

The linac design is based on proven technology that includes components developed in the EURISOL Design Study framework. Its beam dynamical design has been studied section by section with macroparticle beams simulations, and has been validated with error studies with good statistics and high sensitivity. The beam-loss distributions along the linac, in the presence of realistic construction errors, have been calculated with good statistics as well. We have demonstrated that the linac complies with the EURISOL driver specifications.

References

1. “*The EURISOL Report – A Feasibility Study for a European Isotope-Separation-On-Line Radioactive Ion Beam Facility*” – Appendix B, ed. J.C. Cornell, published by GANIL, (2003).
2. K.-H. Schmidt, A. Kelić, S. Lukić, M.V. Ricciardi, and M. Veselsky, Phys. Rev. ST Accelerators and Beams, **10**, 014701 (2007).
3. A. Facco et al., “*Beam dynamics studies on the EURISOL driver accelerator*”, Proc. LINAC08, Vancouver, Canada (2008).
4. A. Facco et al., PRST-AB **9**, 110101 (2006).
5. S. Bousson et al., Proc. of LINAC 06, Knoxville, Tennessee (2006) p. 706.
6. F. Scarpa, D. Zenere and A. Facco, “*Status of the high-power, solid-state RF amplifier development at Laboratori Nazionali di Legnaro*”, Proc. EPAC08, Genoa, Italy (2008).
7. P. Fischer, A. Schempp and J. Haeuser, “*A cw RFQ accelerator for deuterons*”, Proc. PAC’05, May 2005, Knoxville, Tennessee, USA, p.794, and P. Fischer and A. Schempp “*Tuning of a 4-rod cw-mode RFQ accelerator*”, Proc. EPAC06, Edinburgh, Scotland (2006).
8. A. Pisent et al., “*IFMIF-EVEDA RFQ Design*”, Proc. EPAC08, Genoa, Italy (2008) p. 3542.
9. A. Facco, D. Berkovits, R. Paparella and I. Yamane, Phys. Rev. ST Accel. Beams **10**, 091001 (2007).
10. R. Duperrier, N. Pichoff, and D. Uriot, in Proc. Internat. Conf. on Computational Science, Amsterdam (2002).
11. R. Duperrier and D Uriot, “*Deliverable D7: Beam loss calculations*”, EURISOL DS technical note 07-25-2009-0018.
12. P. Embrechts, C. Kluppelberg and T. Mikosch, “*Modelling Extremal Events for Insurance and Finance*”, 2nd ed., Springer-Verlag, Berlin. (1999).

Chapter 3: The 100-kW Direct Targets

3.1 Introduction

EURISOL will operate with three 100-kW direct target stations and another station with a 4-MW liquid-metal “converter” target surrounded by six fission targets. This chapter describes the conceptual design of the 100-kW target station and the target units within it, together with some experimental and simulation data collected during the study. The station layout presented in this document has been designed after a survey of a number of different ISOL facilities presently in operation.

A detailed study has been made of four representative target-and-ion-source units: a refractory foil target, an oxide target, a carbide target, and finally a molten-metal target. Their designs have been validated with numerical tools, with the data collected from new experimental techniques and from in-beam tests. A major part of these activities was thus focused on the development and validation of experimental and numerical tools on the one hand, and on the development and online tests of selected target-and-ion-source prototypes on the other. The prototypes were tested under beam irradiation at CERN-ISOLDE in Geneva, CRC at Louvain-La-Neuve, IPUL in Latvia, PSI in Villigen and at TRIUMF in Vancouver, to validate particular elements of the proposed designs. Finally, the ${}^6\text{He}$ and ${}^{18}\text{Ne}$ production rates were estimated for β -beams, both with the baseline 1-GeV proton beam and with low-energy (10–50 MeV) light-ion beams.

3.2 100-kW target station layout

The three 100-kW target stations are envisaged as operating in a multi-user mode. This is described in more detail in a separate report [1] defining the functional specifications. An important requirement for the target station layout is the ability to change from a used target to the next “conditioned” unit and to set up the beam within a week, while the other stations are in operation, as shown in figure 1.

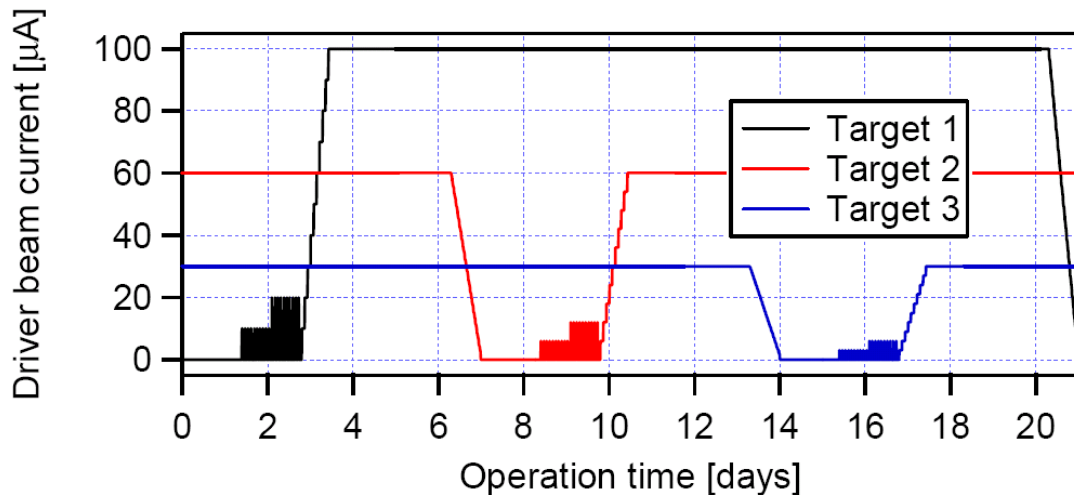


Fig. 1: Example of how the three target stations would operate in parallel, with the following sequence of operation phases: target exchange, stable beam set-up, proton beam scan, isotope yields checks, beam production at nominal intensity, end of beam production, cool-down period [3].

The main constraints are related to radiation hazards and to preventing accidental release of radioactive contamination. Indeed, high levels of radioactivity are expected during operation, as shown by the prompt dose of 10^4 Sv/hr in the irradiation pit when a 100-kW beam strikes a tantalum target. Since target changes will occur every three weeks during operation (and hence one every week

if one considers the three stations), the layout was chosen to be able to perform the frequent exchanges and maintenance of critical beam line elements with minimum down-time of the facility. Both the requirement for the best possible contamination confinement, mitigation of the risk of failure of the targets during operation or exchange procedures, and a reduced facility down-time, led us to adopt the following technical options (illustrated in figure 2):

- An irradiation pit composed of 3 levels: “level -2” for target irradiation; “level -1” for target handling and location of the pre-separator room; “level 0” for the laser ion source rooms and beam delivery to the experimental areas. The target irradiation chamber is located within a “hot cell” type area, with appropriate remote-handling manipulators, nuclear ventilation systems, radiation monitoring and shielding.
- A 3-stage radiological contamination containment level, as required for instance by the French authorities, i.e.:
 - ◆ The 1st barrier is provided by the target vessel, filled with helium.
 - ◆ The 2nd barrier is composed of a metallic leak-tight target irradiation pit filled with air or inert gas at 0.1 mbar. (The reduced gas pressure is used to suppress gas activation, to help keep the target container at -60 kV potential, and to detect possible ruptures and leaks in the 1st containment level with simple and reliable helium gas trace detectors.
 - ◆ The 3rd containment level is provided by the hot-cell enclosure, with air-tight penetrations for the required services, the incoming proton beam and the secondary radioactive ion beam lines. The services (cooling, gas, electricity) are considered to be independent for each of the three stations to avoid interdependencies. However, for cost saving, some might evolve into shared services. The high-voltage service rooms, which need to keep power supplies and cables at 60 kV, are usually located in close proximity to the target front ends, which forms a severe integration constraint.

Preliminary estimates on shielding requirements made with the FLUKA Monte-Carlo simulation code have shown [2] that the dimensioning of the proposed layout will need moderate changes to comply with target station operation as proposed in figure 1; a more in-depth study will be required when EURISOL enters the engineering-oriented study phase.

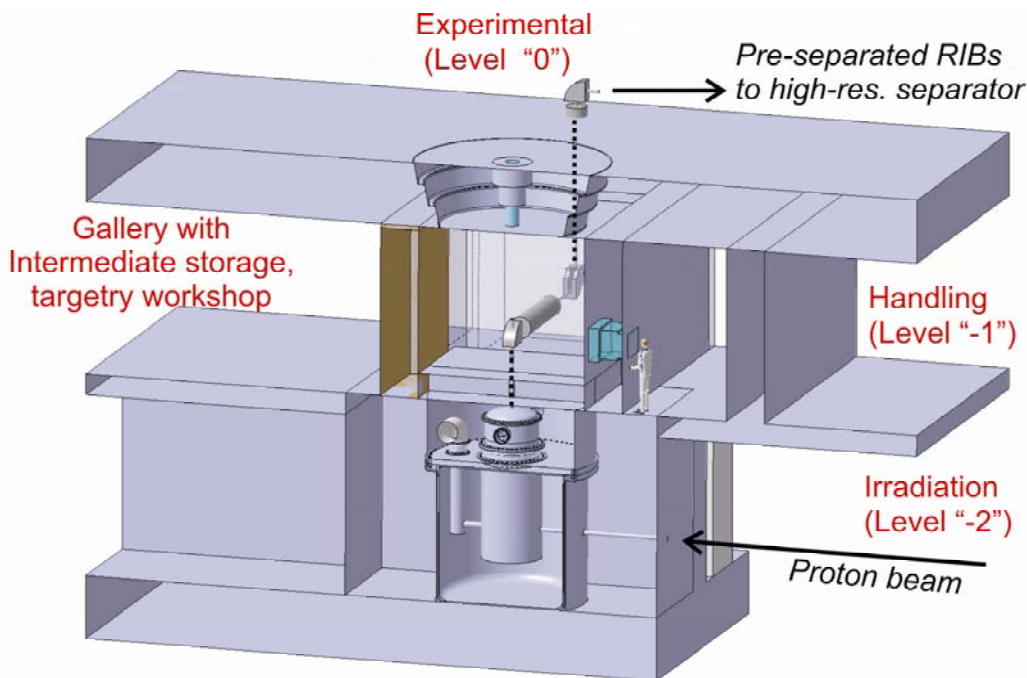


Fig. 2(a): One of the three identical 100-kW target stations for EURISOL.

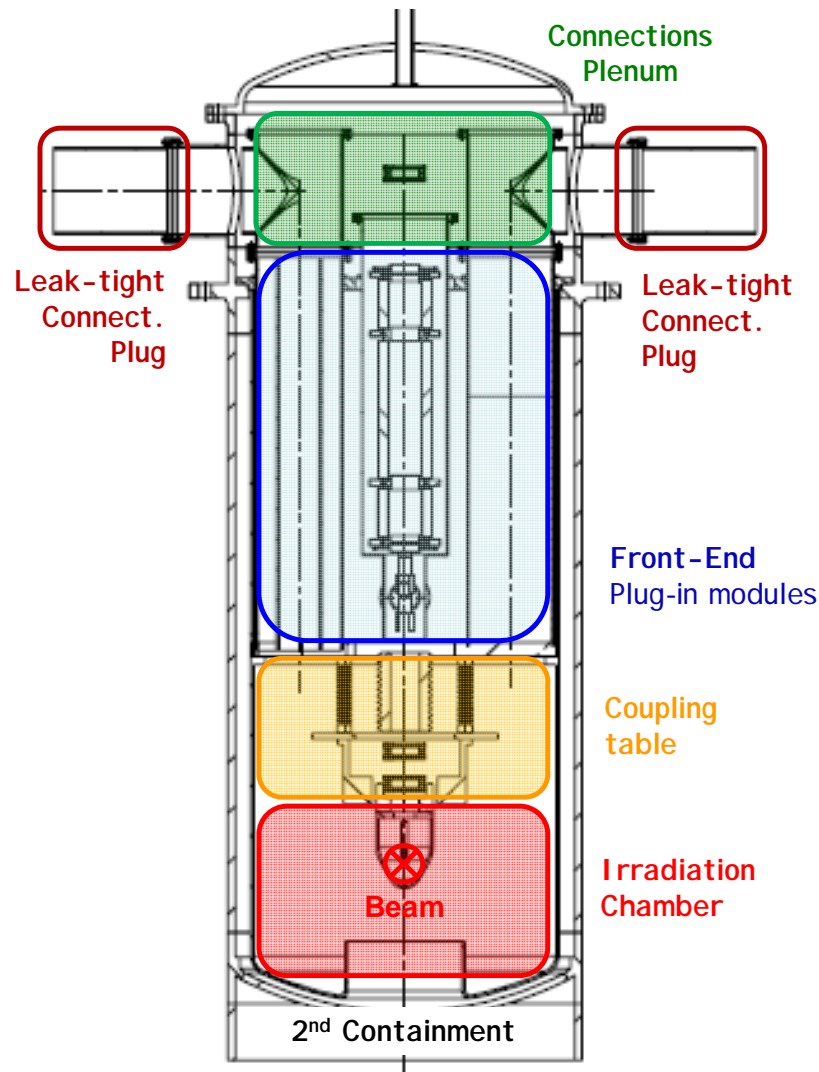


Fig 2(b): Detail of the containment module proposed for the 100-kW target station.

3.3 Design of the 100-kW target-and-ion-source units: challenges and methodology

3.3.1 Challenges and tools

The methodology used during the Design Study was introduced in a feasibility study report [4] (see figure 3). The main challenges related to the development of appropriate target-and-ion-source units deal with heat management issues (to evacuate the heat generated in the target by the interaction of the target elements and the 100-kW, 1-GeV proton beam), the ageing of the structural and target materials while maintaining high beam production rates for 3 weeks, and preserving – or even improving – present target release and ion source efficiencies with the new EURISOL unit concept.

Four representative benchmark target-and-ion-source units were considered, and designs for the more than one hundred different combinations of target materials and types of ion sources presently in operation at ISOL facilities were proposed to accommodate the 100-kW proton beam available at EURISOL.

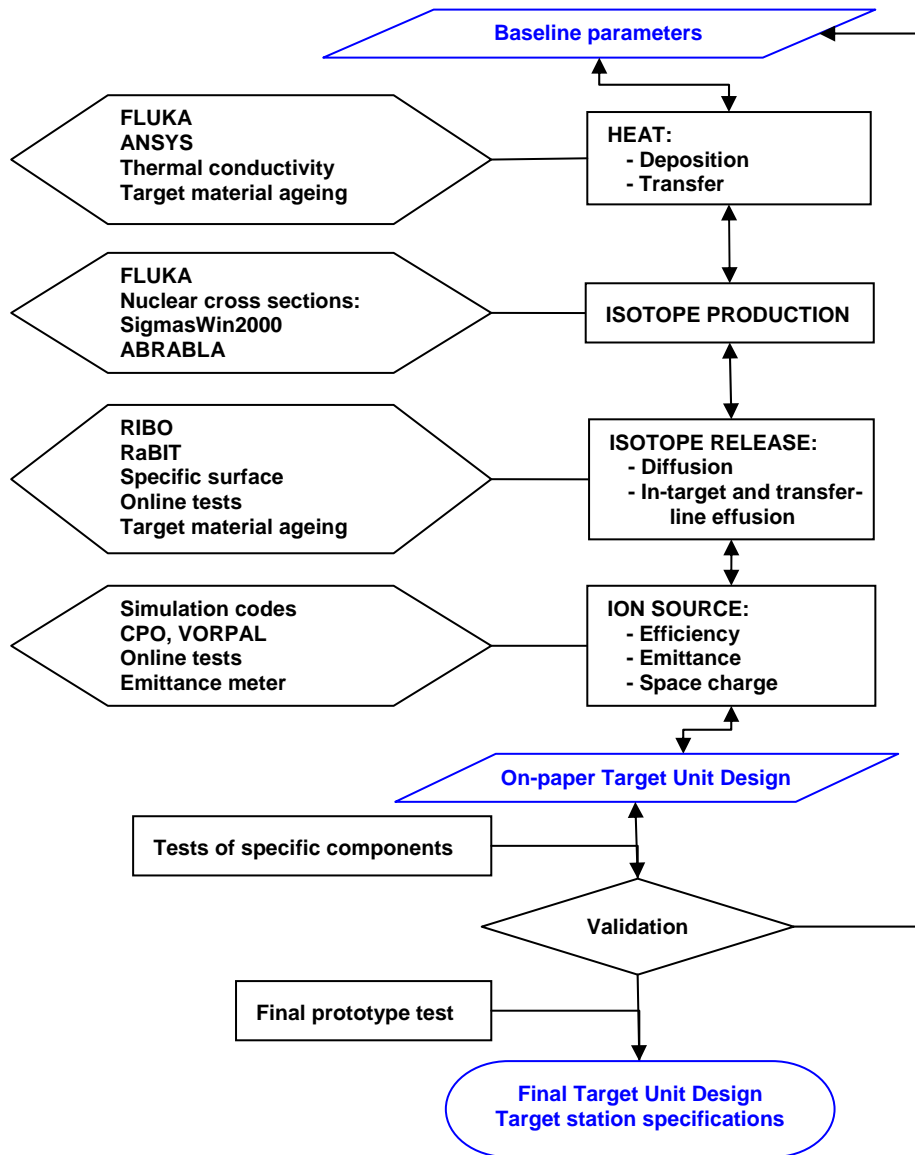


Fig. 3: Methodology used during the Design Study. Details on the methods are available in ref. [4].

3.3.2 Target unit designs

The solid-target and molten-target designs were developed taking into account the following important constraints:

- Using appropriate schemes to evacuate the heat from the deposited power of the primary proton beam.

This was solved by splitting more conventional solid-target units into several subunits linked to a single ion source. This configuration enhances radiative heat exchanges between the subunits and an externally cooled containment vessel. Present-day static molten-metal targets are limited to 1-kW operation owing to the high dE/dX , while offering the advantage of the highest target material densities. Operation at 100 kW can be achieved by evolving the present static-bath configuration into circulating liquid-metal loops equipped with an electromagnetic pump and heat exchanger.

- Dimensions of the target unit to be kept small, to obtain fast isotopes effusion, similar to present conventional configurations.
- Diffusion-limited isotope release-fractions from the targets to be maintained, or even improved.

This has been achieved for the solid targets by using submicron and nanostructured materials with reduced diffusion path lengths. The static molten-metal targets presently used also suffer from long diffusion times [5]. This is improved in the proposed design with a diffusion chamber in which the molten metal is fragmented into droplets or jets when it passes through a grid into a diffusion chamber. The chamber is connected via a temperature-regulated transfer line to an ion source.

The conceptual design of the proposed solid-target units is shown in figure 4(a). For the molten-metal loop, the required ancillaries are identical to those used at the LISOR Pb-Bi loop operated at PSI [6], shown in figure 4(b). It is dimensioned to evacuate the same 30 kW of deposited power. During the design study, a prime focus was the development of the diffusion chamber and dimensioning of the electromagnetic pump, as reported in the following section.

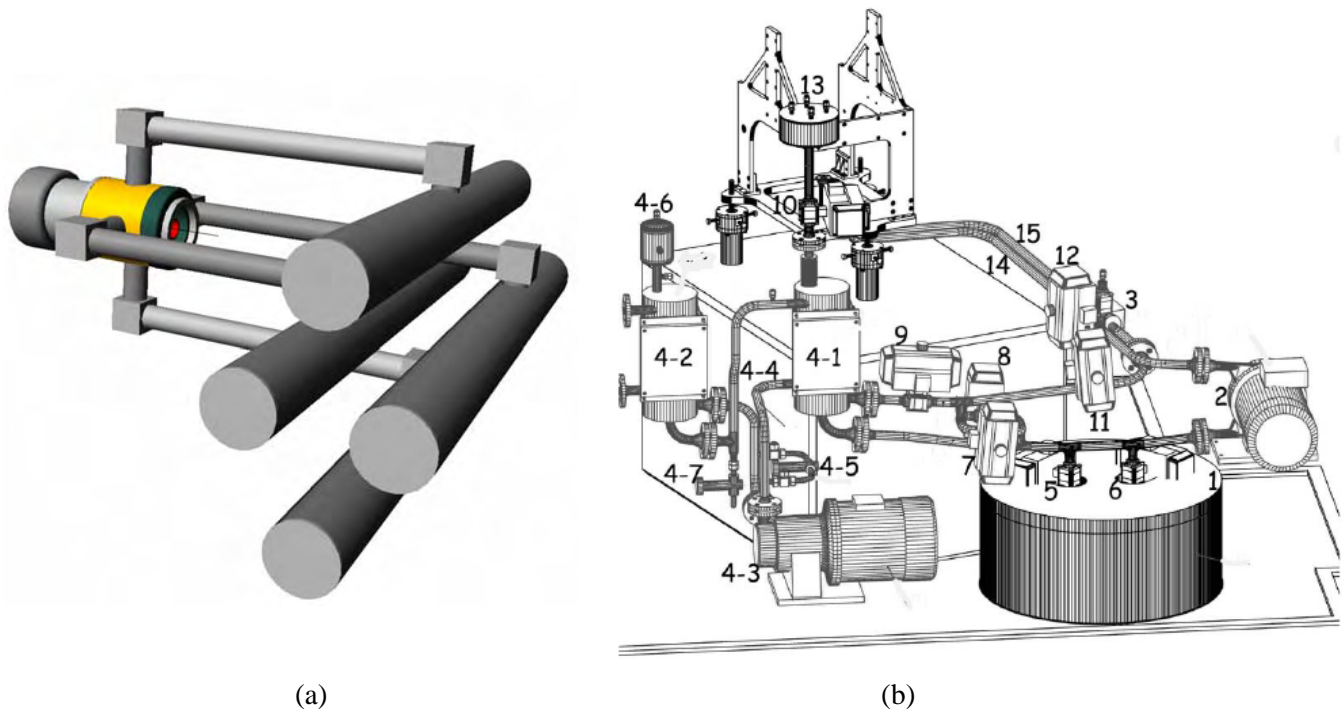


Fig. 4(a): Conceptual design of 100-kW solid target units. (b): Components of the molten Pb-Bi loop LISOR operated at PSI: (1) storage tank, (2) induction pump; (3) electromagnetic flow meter; (4) thermostat with (4-1) and (4-2) PbBi-DIPHYL and DIPHYL-H₂O heat exchangers, (4-3) oil pump, (4-4) Venturi tube, (4-5) bypass, (4-6) oil expansion tank, and (4-7) valves for filling and draining the oil loop; (5)–(12) automatic valves; (13) expansion tank; (14) and (15) inlet and outlet pipes.

3.4 Prototype tests

A number of prototype targets have been developed and tested during the Design Study as integral – and even as the most critical – steps of the methodology introduced in figure 3. This section describes the most important results obtained from the different in-beam tests of the prototypes.

The main parameters of the in-beam tests of the four benchmark 100-kW targets for EURISOL are given in table 1.

Table 1: Table of the nominal parameters for the EURISOL target tests.

Parameter	Symbol	Units	Ta	SiC	Al ₂ O ₃	Pb
Beam particles	Z_{beam}	-	Protons			
Beam particle energy	E_{beam}	GeV	1			
Beam current/subunit	I_{beam}	μA	100	50	25	100
Beam time structure	-	-	CW			
Gaussian beam geometry	σ_{beam}	mm	7			3–20
Total beam power	P_{beam}	kW	100			
Target element	-	-	Ta	Si (C)	Al (O, Nb)	Pb
Baseline form	-	-	Foil	C/SiC Composite	Nb/Al ₂ O ₃ Composite	Liquid
Reference isotope	-	-	⁸ Li	²¹ Mg	¹⁸ Ne	¹⁷⁷ Hg
Isotope's half life	$T_{1/2}$	S	0.84	0.122	1.67	0.17
Design Temp. range	T_t	K	2000–2500	1800–1900	1500–1800	700–1200
Thermal cond. @ T_t	k	$\text{W m}^{-1}\text{K}^{-1}$	75	15	5 @ 1300K	15
Density	ρ_{th}	g cm^{-3}	16.6 (100%)	3.22	3.96	11.34
Useful density range	-	g cm^{-3}	1–16.6	1–3.22	0.5–3.96	
Layer thickness*	t	μm	20	200	1000	-
Grain (droplet) size	-	μm	-	0.6	3 or 0.4	(200)

* Optimal coating thickness of a target matrix by the given target material.

3.4.1 Molten-metal loop and diffusion chamber offline tests at IPUL

An experimental program [5] was set-up in collaboration between CERN and the Institute of Physics of the University of Latvia (IPUL) to study the feasibility of circulating a molten-Pb loop that could accommodate a 100-kW incoming proton beam, and in particular to determine:

- the dimensioning of the diffusion chamber and the pressure losses within it;
- the type of pump required to operate at high temperature and at the required pressure.

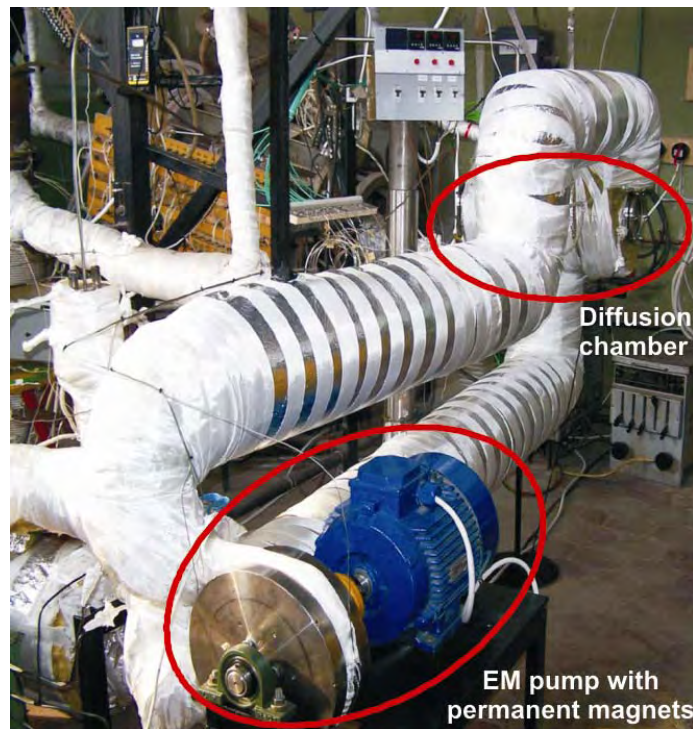


Fig. 5(a): Photograph of the liquid-metal loop setup at IPUL.

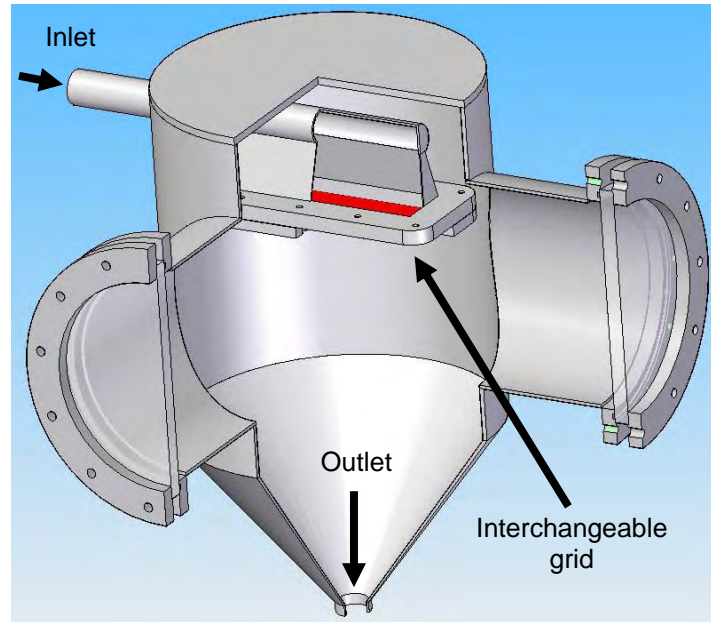


Fig. 5(b): Schematic diagram of the diffusion chamber.

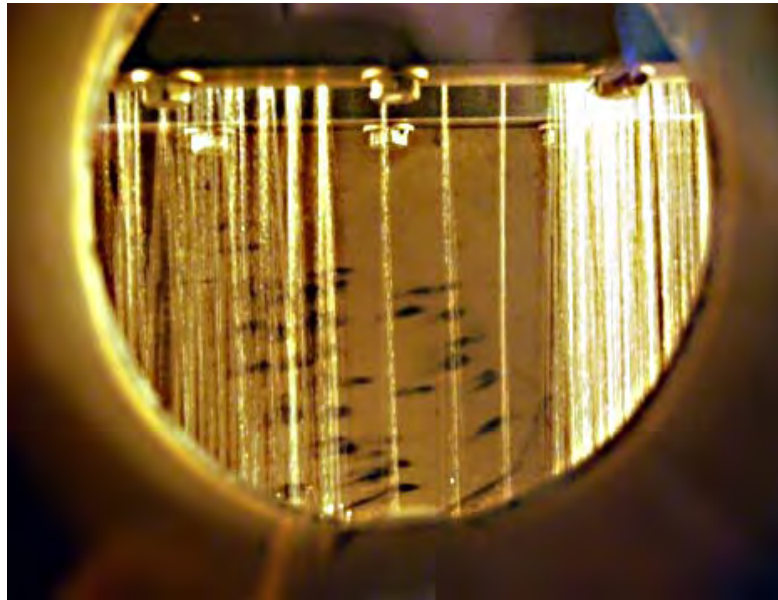


Fig. 5(c) Pb-Bi shower in diffusion chamber at the exit of the interchangeable grid.
(Photo taken through a 10-mm thick Spectrosil quartz window).

Preliminary estimations indicated that for $\Delta T = 100^\circ\text{C}$, $P_{dep} = 31.4 \text{ kW}$, $c_p = 155 \text{ J.kg}^{-1}.\text{K}^{-1}$ and $\rho = 10400 \text{ kg.m}^{-3}$, the required flow rate would be $\sim 0.2 \text{ l.s}^{-1}$. The required circulating loop will be equipped with an electromagnetic pump and heaters all along the pipes. The integration of this loop onto a ‘front end’ for beam production was outside the scope of the present Design Study and should be the subject of a future engineering-oriented study.

The molten Pb-Bi eutectic was preferred over molten Pb, to lower the operation temperature of the test loop. It was operated successfully up to 600°C when equipped with an electromagnetic pump with rotating permanent magnets. See figures 5(a)–5(c). The diffusion chamber was tested with a grid of 164 holes of $500\text{-}\mu\text{m}$ diameter, and also with 1017 holes of $230\text{-}\mu\text{m}$ diameter. This configuration is expected to have important benefits, gained from a reduction of decay losses of short-lived isotopes, as illustrated in figure 6(a). The pressure threshold for the onset of metal flow through the grid decreased with increasing temperature.

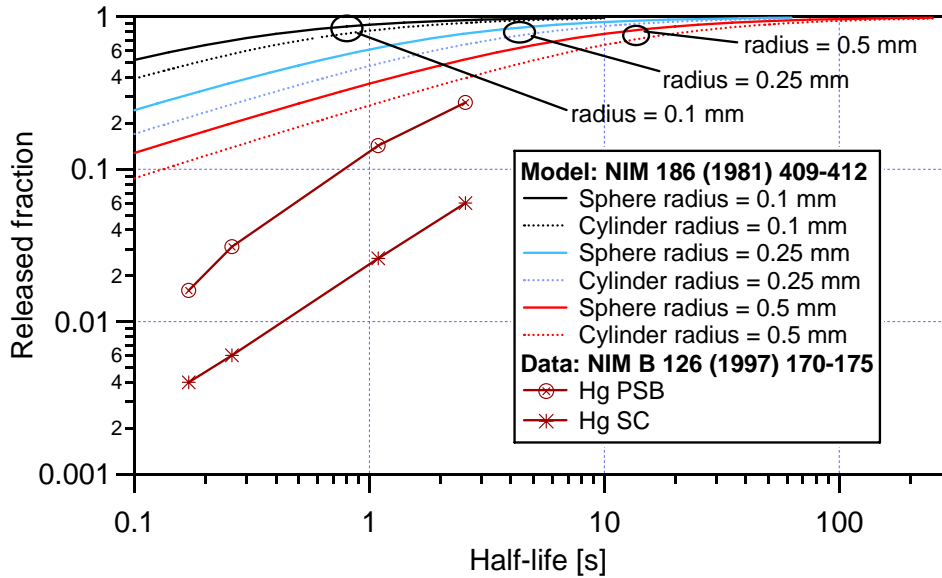


Fig. 6(a): Calculated released fractions of Hg isotopes diffusing out of Pb droplets or jets, plotted versus isotope half-lives for 3 diameters, and compared with data obtained at SC-ISOLDE and PSB-ISOLDE [6].

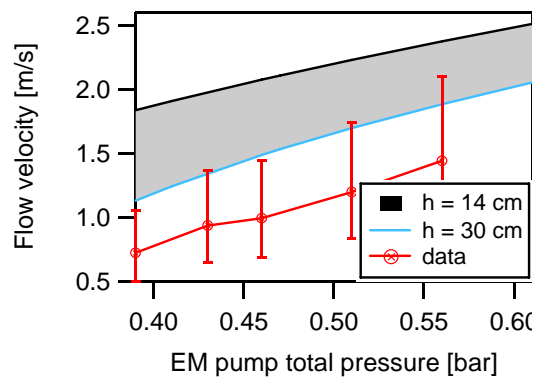


Fig. 6(b): Measured and calculated (for two drop heights) flow velocities out of the diffusion-chamber grid with hole diameter = 230 μm , as a function of EM pump total pressure.

3.4.2 Target prototype irradiations at PSI for EURISOL: “TARPIPE”

The requirement for the average lifetime of EURISOL direct targets is three weeks, a major challenge since they will be exposed to 100-kW proton beams at high temperature. Target sintering, grain growth and radiation damage all affect the lifetime of targets and structural materials at operational ISOL facilities such as ISOLDE at CERN and ISAC at TRIUMF. A study of the impact of radiation damage at high temperatures on the mechanical and release properties of prototype materials was the main objective for the TARPIPE project [7].

The starting materials for oxide and carbide samples came in either powder form or as felts, satin, foam, pellets or nanotubes from various specialized companies. Many of these (mostly powders) were then further processed in-house at CERN. Metal foil samples included Ti, Zr, Nb, Mo, Rh, Hf, Ta, W, Re and Ir with thicknesses varying between 2 and 127 μm . Target materials were grouped with respect to chemical compatibility and maximum irradiation temperature and placed in four different target containers (pipes) to be irradiated one after the other. Two thermocouples per container were used to monitor target temperature during irradiation.

Simulations of energy deposition with FLUKA and heat dissipation with ANSYS Workbench 10.0 were used extensively to design the test jig, dimension the beam dump and determine the maximum beam intensity required for each target container. The control system (cooling water temperature and flow rate, proton beam status and intensity, temperature, vacuum, bunker activity) was implemented with the appropriate interlocks to allow for prolonged periods of unmanned operation (see figure 7).



Fig. 7(a): TARPIPE test jig.

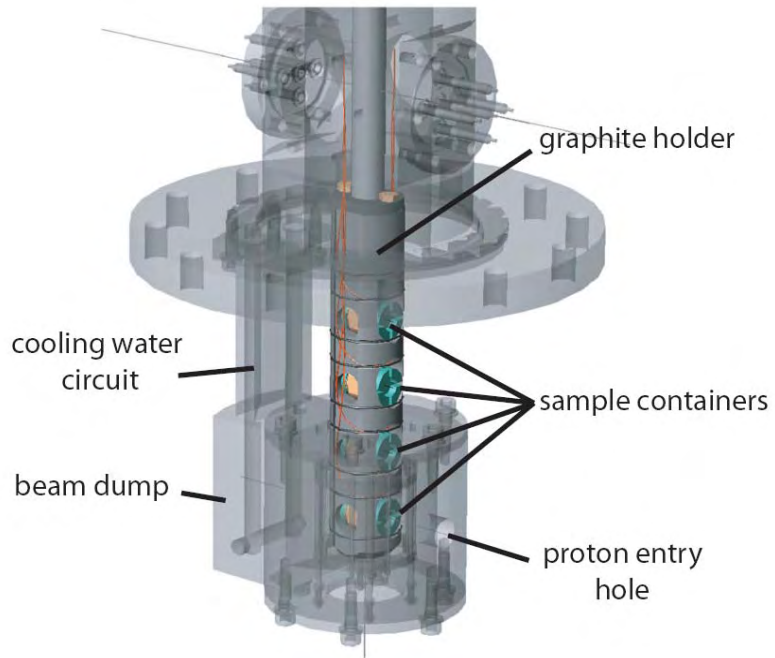


Fig. 7(b): Schematic showing the four sample containers.

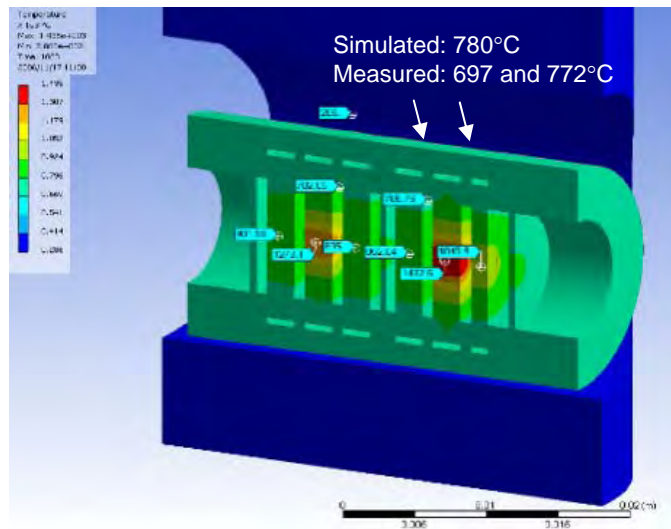


Fig 7(c): Simulated and measures temperatures on a sample container.

Following the irradiation phase (from May 2007 to March 2008), the samples were extracted from their respective containers, separated, placed in storage containers, visually inspected, weighed and their doses on contact and at 10 cm were measured. Gamma spectrometry was performed on a majority of samples and a small subset of these was then investigated by scanning electron microscope (SEM) to reveal their microstructure. Energy-dispersive X-ray spectroscopy (EDX) was also performed for elemental analysis and chemical characterization.

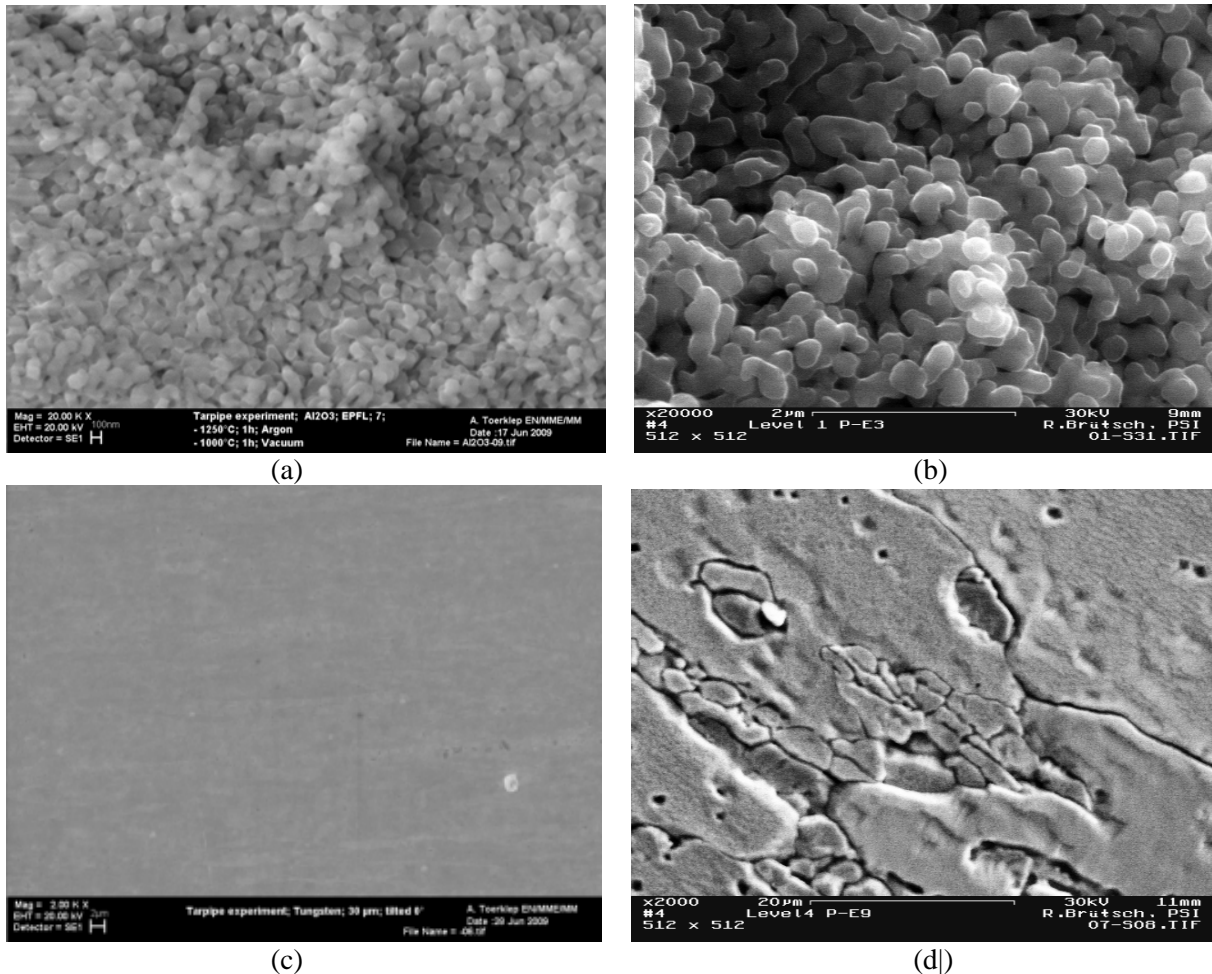


Fig. 8: Scanning electron micrographs of (a) Al_2O_3 before irradiation and (b) after irradiation, (c) a 30-micron tungsten foil before irradiation, and (d) after irradiation.

First results show that for the metal foils studied (Ta, W and Ir) irradiation leads to grain growth from 20–200 μm , preferentially in the rolling direction (see figure 8). Two of the four 2-micron Ta foils featured holes, most likely due to detachment of grains from recrystallisation as the grain size became larger than the foil thickness. Ideally, foil thickness should approach 2 μm to limit decay losses of radioisotopes with very short half-lives down to 10–100 ms. In practice, this appears difficult to implement, although for 6–50 micron Ta foils, detachment of grains was not observed. For the oxide samples studied, Al_2O_3 and Y_2O_3 , sintering was less effective than in metals. For example, for Al_2O_3 , the mean grain size increased by a factor 3, from roughly 100 nm to 300 nm (figure 8). In the carbide sample consisting of a mixture of SiC and carbon nanotubes, no grain growth was observed. Analysis of a selection of other samples will be continuing after the design study, and is expected to provide further valuable results for target and structural materials useful for high-power ISOL targetry.

3.4.3 Bi-valve target tests at CERN-ISOLDE

A target unit made of two target containers and two independent transfer lines merging into a single ion source was developed and tested at CERN-ISOLDE [8]. The goal of these tests was to assess the operation parameters and efficiencies to be expected if several sub-units merge into a single ion source, as proposed in the conceptual design for solid targets (see figure 4).

Each of the two transfer lines were equipped with remotely actuated leak-tight valves. The target material was CaO, connected via water-cooled copper transfer lines to a MK7 FEBIAD ion source for pure Ne and Ar isotope beam production. The purpose of the cold line is to condense out unwanted isobaric contaminants (see figure 9).

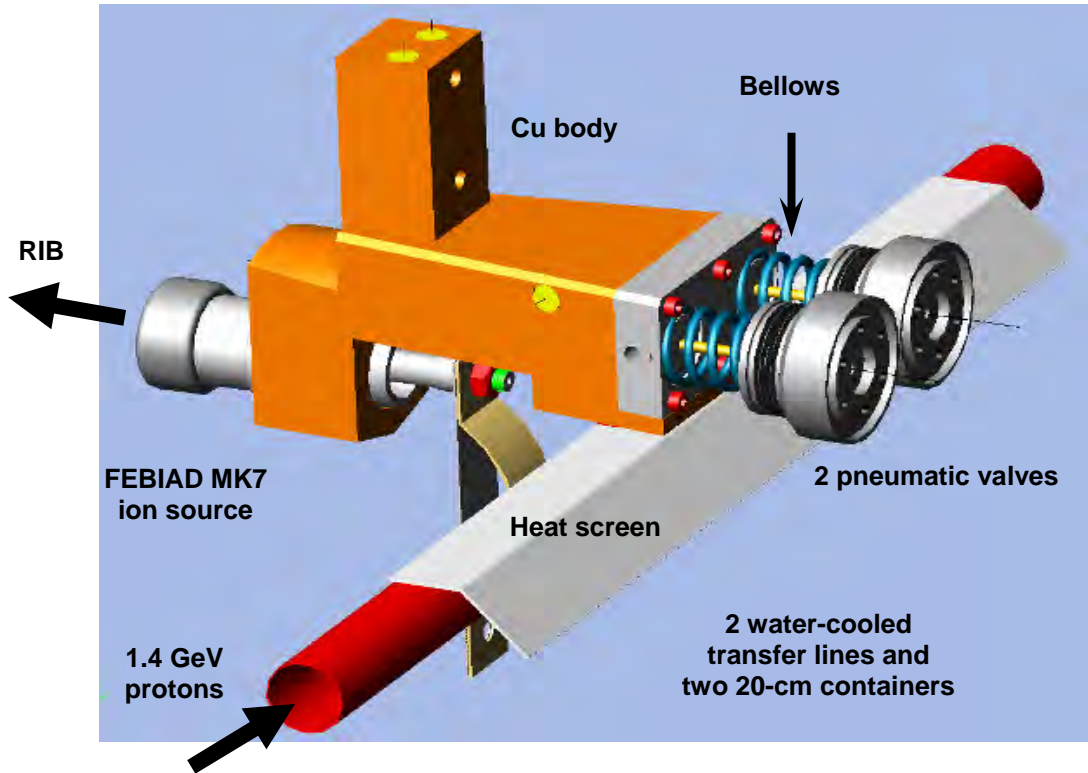


Fig. 9(a): 3D view of the bi-valve target unit.

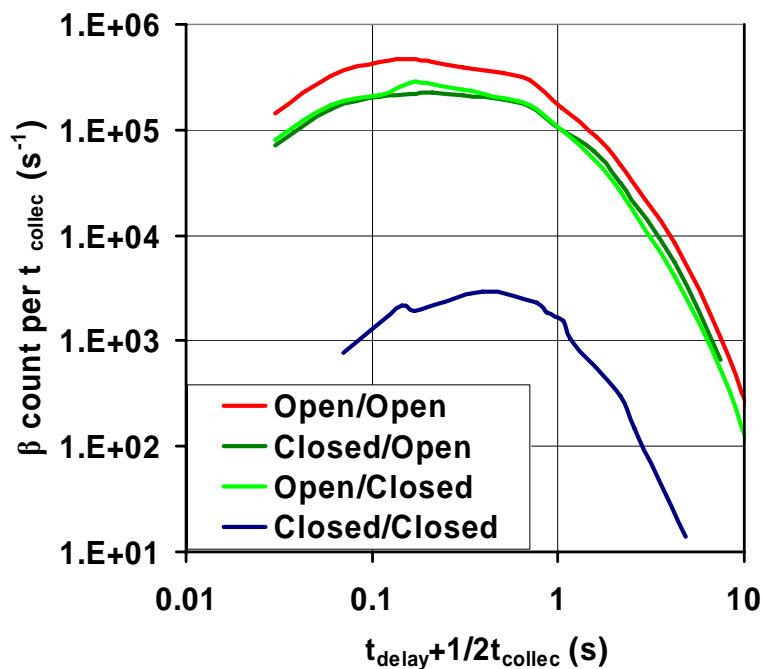


Fig. 9(b): Release curve of ^{35}Ar with different configurations of the two valves.

The main operation parameters and efficiencies are reported for ^{34}Ar and ^{35}Ar in table 2. The yields were consistent with previous figures obtained in standard, single-container ISOLDE units. In the prototype configuration with both lines open, numerical simulations have shown that 2.5% of the isotope fraction produced in one container revisits the 2nd side. Line merging efficiencies were in the range of $83\text{--}95 \pm 10\%$.

Table 2: Main parameters monitored during the tests of the bi-valve prototype at CERN-ISOLDE.

Isotope	Ion source efficiency, temperature T			Symmetry: container 1 container 2	Closed-valve leak rate	Line- merging efficiency
	1 line open [%]	2 lines open [%]	T [°C]			
³⁴ Ar	2.3	2.5	1920	+8%	-	94%
³⁵ Ar				-2%	-	83%
³⁴ Ar	4.9	5.1	2100	+1%	0.3%	95%
³⁵ Ar				+3%	0.3%	87%

3.4.4 Submicron SiC target tests at CERN-ISOLDE

Various SiC target materials were synthesized and their diffusion properties investigated by either ion implantation or proton activation techniques [9]. Subsequent offline isotope release data were collected by gamma spectroscopy after isothermal heating at different temperatures under vacuum. Interesting release properties were obtained for samples characterized by small grain size, of less than 1 micron, and with open porosity of more than 10%. See figure 10.

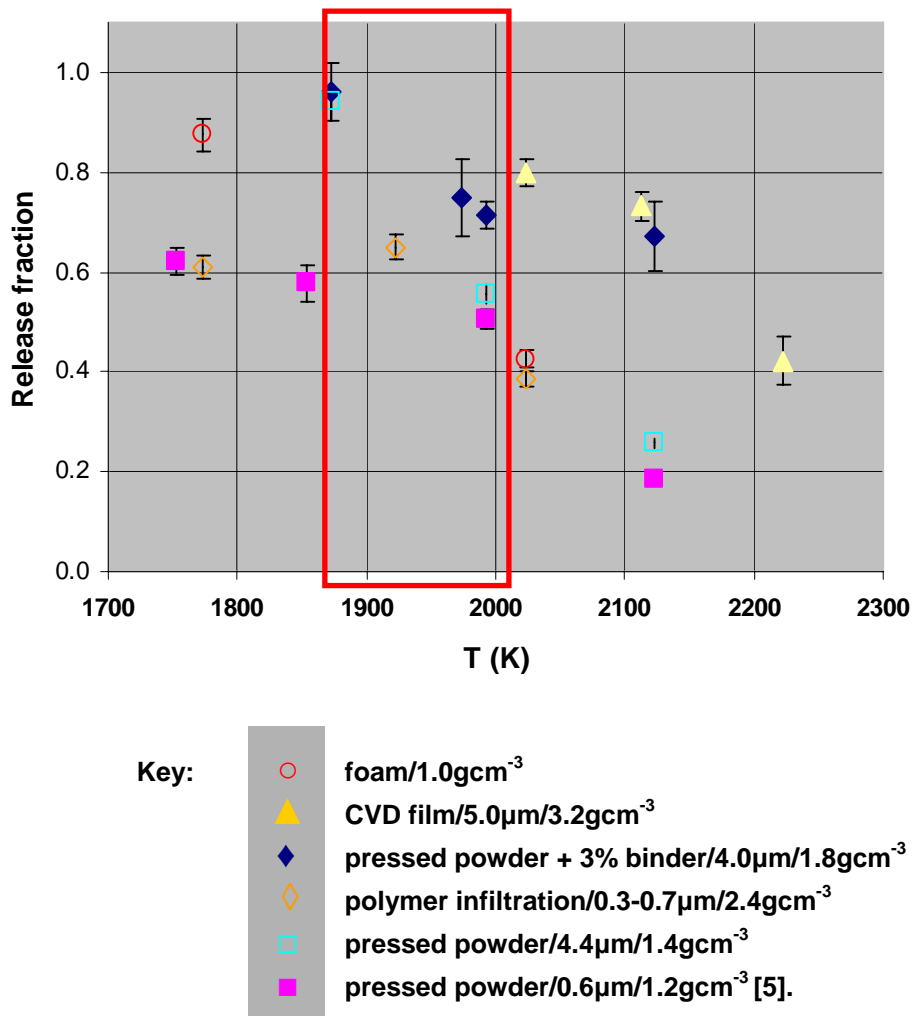


Fig. 10(a): Remaining ²⁴Na radiotracer fraction in irradiated SiC prototype samples, as a function of the heating temperature T during 15 min. The red rectangle indicates the temperature range for online operation.

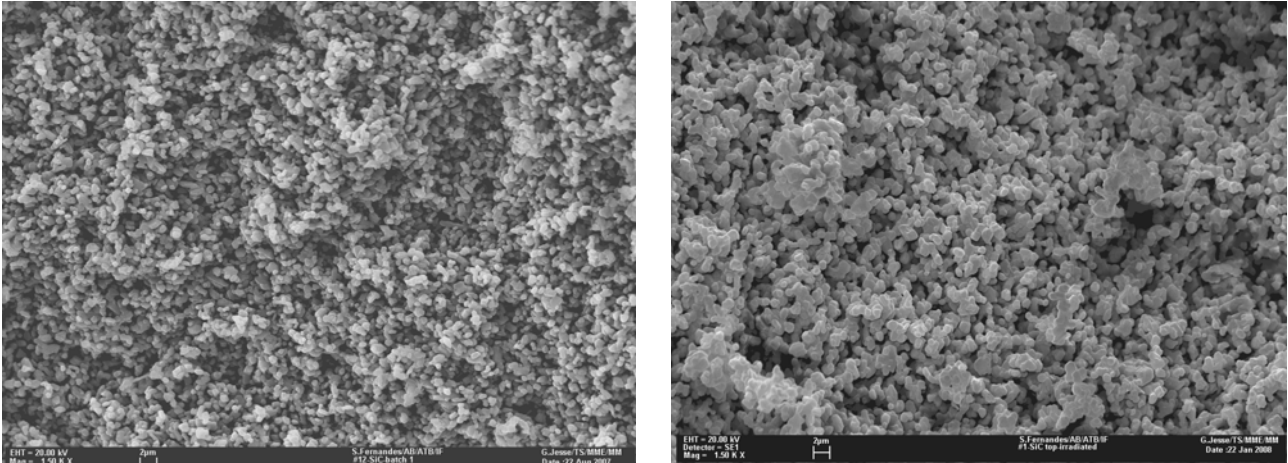


Fig. 10(b): Target microstructure (l.) before and (r.) after proton beam irradiation at ISOLDE.

The best-releasing SiC candidate, with appropriate chemical purity, and available in quantities for a full target container load, was used for beam tests at CERN-ISOLDE. Improvement in yields of short-lived Mg and Na isotopes was obtained with respect to previous SiC target standards. Post-irradiation analysis at CERN confirmed a moderate structural evolution, in accordance with a good performance of the target over time.

3.4.5 High-power oxide target tests at TRIUMF

A high-power oxide target was developed and tested in a collaboration between CERN and TRIUMF [10]. This prototype test was meant to validate the full methodology introduced in figure 3 at realistic beam intensities. The main difference between the proton beam available at TRIUMF and the one envisaged for EURISOL is the proton energy, 0.5 GeV versus 1 GeV, and the maximum Gaussian beam set at $\sigma_{\max} = 2.5$ mm.

Much effort was directed towards the design, engineering and characterization of the target elements and target unit to maximize the dissipation of the heat deposited by the incoming beam power. This optimization greatly depends on the technical orientations chosen during the development of the design, and the quality of the realization. Composite $\text{Al}_2\text{O}_3/\text{Nb}$ -foil target elements were made by reactive brazing at CERN to enhance the low intrinsic thermal conductivity of the oxide material, and to obtain a good thermal contact between the composite material and the target container for maximized heat dissipation [10]. (See figure 11.) These properties were assessed by an electron beam heating set-up to choose amongst the different technical options under consideration. Target performance was monitored online at TRIUMF by following Ne isotope yields, from which released efficiencies were deduced (see figure 12). The prototype operated in a stable mode at a nominal 25- μA proton beam intensity – with a peak at 30 μA – for 9 days, receiving 25% of the total proton intensity envisaged during nominal operation at EURISOL.

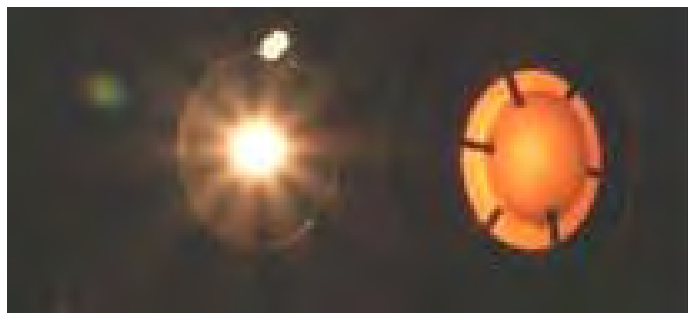


Fig. 11(a): Photograph taken during electron bombardment heating of a composite $\text{Al}_2\text{O}_3/\text{Nb}$ target element.

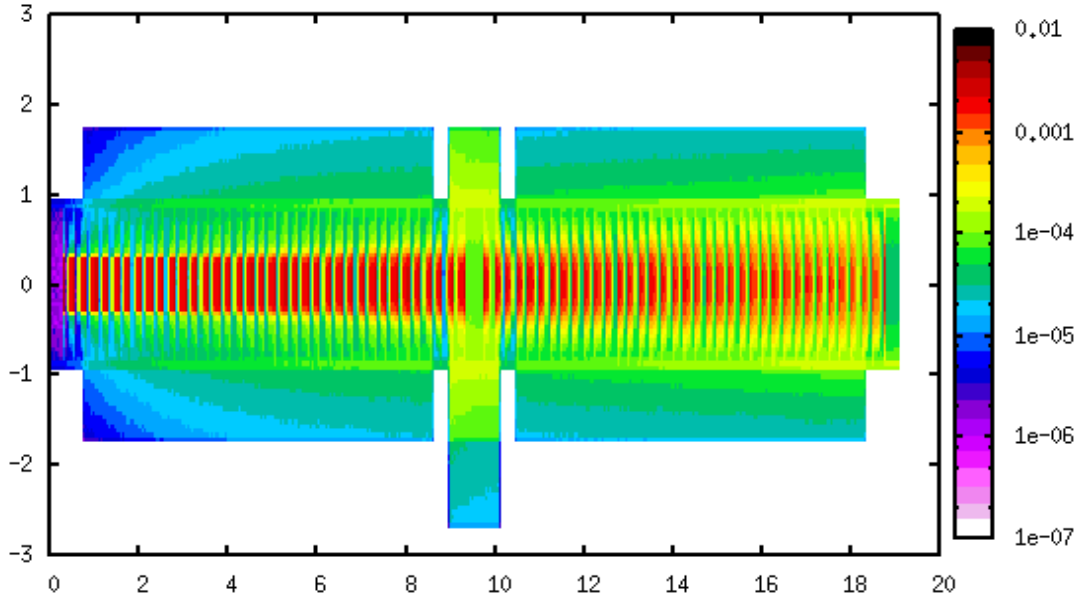


Fig. 11(b): Cross-sectional plot of proton beam heat deposition in the target unit simulated with FLUKA. Radial and longitudinal units are in cm, and heat deposition in GeV/proton/cm³.

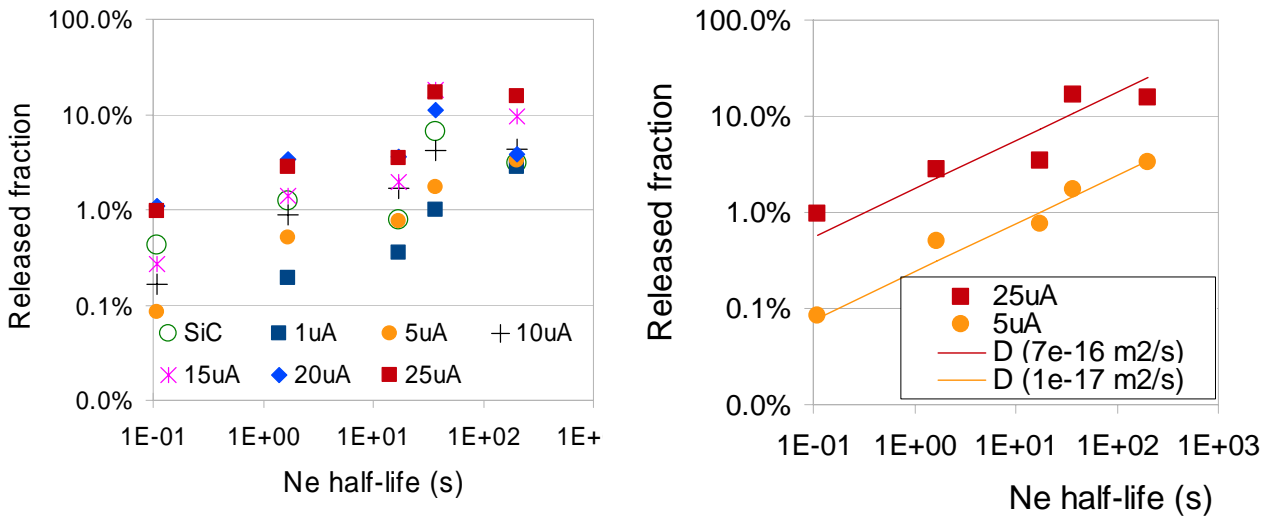


Fig. 12 (Left): Ne isotope yields observed during the prototype tests for increasing proton beam currents. Data are reported for the ^{17-19,23,24}Ne series as a function of $t_{1/2}$. Data for a reference SiC target are also shown for comparison. (Right): Released isotope fractions at 5- and 25- μ A beam currents. The solid lines are a theoretical fit assuming a diffusion-limited isotope release, with D the only free fitting parameter [10].

3.5 Isotope production for β -beams

⁶He and ¹⁸Ne isotope beam production has been investigated for β -beams. Both the production with 1-GeV protons and an alternative low-energy reaction scheme have been considered. Evaluation of in-target production rates showed that with a 100-kW, 1-GeV proton beam on a 200-g/cm² MgO target, the 3×10^{10} ions/s of ¹⁸Ne produced does not meet the required intensity. For the ⁶He β^- emitter, beam production by the ⁹Be(n, α)⁶He reaction scheme has been investigated. Spallation neutrons are produced with protons on a water-cooled tungsten converter. A preliminary conceptual design of the converter and its surrounding BeO target has been proposed and its geometry optimized, providing 3×10^{13} ions/s of ⁶He for a 1-GeV, 100-kW proton beam and 10^{14} ⁶He/s for a 2-GeV, 200-kW proton beam [11,12]. (See figure 13.) Experimental data were obtained at CERN-ISOLDE on operational

parameters and release efficiencies of BeO targets, which confirm the viability of that production scenario.

For the production of ^{18}Ne , the main low-energy reactions are $^{19}\text{F}(p,2n)^{18}\text{Ne}$ and $^{16}\text{O}(^3\text{He},n)^{18}\text{Ne}$ for which experimental data are scarce. They have been studied at CRC in Louvain-la-Neuve with protons and ^3He beams in the energy ranges 23–52 MeV and 8–22 MeV, respectively. These measurements show that the production yield with the ^3He beam is higher than with the proton beam in these energy ranges and a scheme based on the $^{16}\text{O}(^3\text{He},n)^{18}\text{Ne}$ reaction is a good alternative to the baseline scenario. With a 22-MeV ^3He beam and an MgO target, the production yield calculated from these cross sections is 1.2×10^8 ^{18}Ne ions per μC . This corresponds to a production of 1.2×10^{12} $^{18}\text{Ne}/\text{s}$ with a 1-mA ^3He beam (220 kW). From the evolution of the yield, it is clear that higher ^3He energy will further increase the ^{18}Ne production. For the production of ^6He , a 40-MeV deuteron beam and a neutron converter will produce ^6He following the reaction scheme $^9\text{Be}(n,\alpha)^6\text{He}$. The production rate will be 3×10^{13} $^6\text{He}/\text{s}$ with a beam intensity of 2.5 mA, which corresponds to a beam power of 100 kW.

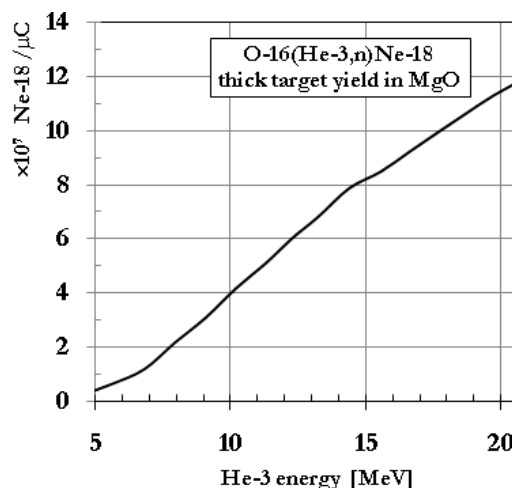
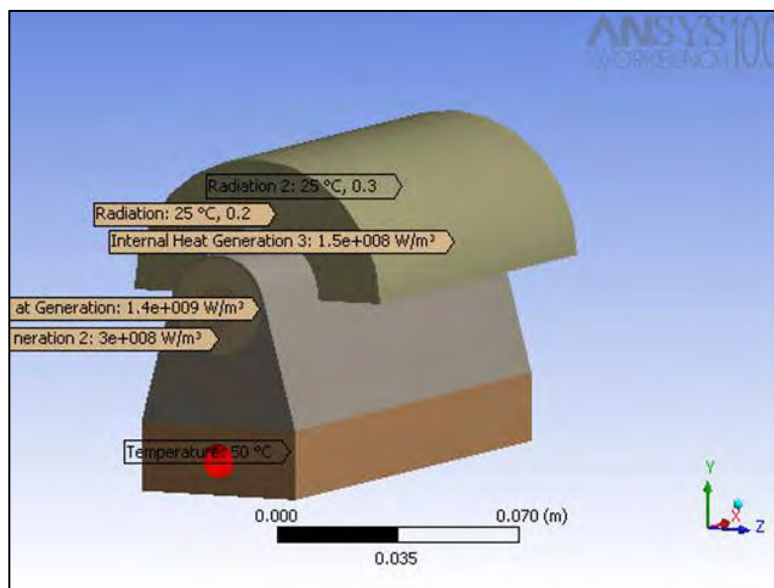


Fig. 13 (Top): 3D view of a solid, water-cooled tungsten converter surrounded by a BeO target for ^6He production. (Below): Production rates of ^{18}Ne in an MgO target deduced from the experimental cross-sections measured at CRC in Louvain-la-Neuve.

References

- [1] L. Bruno, “EURISOL 100-kW target units - Engineering Specification”, CERN EDMS Doc. #752679, <http://edms.cern.ch/document/752679/5>.
- [2] T. Otto, “Shielding of a 100-kW EURISOL Target Station”, CERN EDMS Doc. #909377, <http://edms.cern.ch/document/909377/2>.
- [3] E. Noah et al, “EURISOL Target Stations Operation and Implications for its Proton Driver Beam”, CERN-AB-2006-055, <http://cdsweb.cern.ch/record/971892?ln=en>.
- [4] T. Stora et al, “The EURISOL Facility: Feasibility study for the 100-kW direct targets”, CERN EDMS Doc. #758813, <http://edms.cern.ch/document/758813/2>.
- [5] E. Noah, “Engineering Aspects of 100-kW Liquid-Metal Targets”, CERN EDMS Doc. #844418, <http://edms.cern.ch/document/844418/1>.
- [6] J. Lettry et al., Nucl. Instrum. & Meth. **B 126** (1997) 170.
- [7] E. Noah et al, “TARPIPE deliverable report”, CERN EDMS Doc. #1006506, <http://edms.cern.ch/document/1006506/1>.
- [8] E. Bouquerel et al, “Design and Test of a two-body target unit for 100-kW solid targets”, EURISOL DS technical note 03-25-2008-0009.
- [9] S. Fernandes et al., “Diffusion studies in prospective polycrystalline silicon carbide target materials for radioactive ion beam production at CERN-ISOLDE”, EURISOL DS technical note 03-25-2008-0010.
- [10] S. Fernandes et al, Online tests of a high power Al₂O₃ EURISOL target prototype, CERN EDMS Doc. #1011259, <http://edms.cern.ch/document/1011259/1>.
- [11] T. Stora et al., “W converter - BeO dual target prototype for ⁶He production - a preliminary note”, EURISOL DS technical note 03-25-2006-0003.
- [12] N. Thiollieres et al., “Optimization of ⁶He production using W or Ta converter surrounded by BeO target assembly”, EURISOL DS technical note 03-25-2006-0002.

Chapter 4: The Multi-MW Liquid-Metal Target

4.1 Conceptual layout of the facility

Radioisotopes along the two edges of the so-called “valley of stability” in the chart of the nuclides are of interest for advanced research. These borderline isotopes are ordered into two main groups: isotopes that are proton-rich (compared to the proton-neutron balance in natural isotopes) define the “proton drip-line”, while isotopes carrying an excess of neutrons are grouped along the “neutron drip-line”. The aim of the EURISOL facility is to produce a far higher number of particle collision events than existing facilities, in order to increase the likelihood of finding these unknown isotopes, as well as increasing the yield of isotopes already identified as being of interest but too rarely produced with current state-of-the-art accelerators for any meaningful use.

Proton-rich isotopes result from striking a solid target directly with a proton beam. On the other hand, neutron-rich isotopes are produced indirectly: first a neutron “converter” is used to emit neutrons by spallation, whereby a heavy metal releases neutrons when hit by a proton beam. These neutrons can then be used to fission solid uranium carbide targets which then emit the neutron-rich isotopes.

An initial Design Study funded by the European FP6 research framework program was able to establish the case for the project on a well-founded scientific and technical basis in terms of user cost-benefit analysis, risk identification and mitigation. One major risk item identified early on in the EURISOL program was the multi-megawatt target station. The task of investigating this was assigned to a project group headed by CERN in Geneva and comprising PSI in Switzerland for the liquid-metal “converter” target development, INFN in Italy for the fission targets and IPUL in Latvia for essential liquid-metal technology testing. The essential parameters determined by an initial system analysis by CERN are given in table 1.

Table 1: Essential parameters for the multi-MW ‘converter’ and fission-target system.

Parameter	Symbol	Units	Nval	Range
Converter Target material	Z_{conv}	-	Hg (liquid)	LBE
Secondary Target material	Z_{targ}	-	UC _x , BeO	
Beam particles	Z_{beam}	-	Proton	
Beam particle energy	E_{beam}	GeV	1	≤ 2
Beam current	I_{beam}	mA	4	2 – 5
Beam time structure	-	-	dc	ac 50Hz 1ms pulse
Gaussian beam geometry	σ_{beam}	mm	15	≤ 25 , parabolic
Beam power	P_{beam}	MW	4	≤ 5
Converter length	l_{conv}	cm	45	≤ 85
Converter radius (cylinder)	r_{conv}	cm	15	8 – 20
Hg temperature	T_{conv}	°C	150 (tbc)	$\ll 357$
Hg flow rate	Q_{conv}	ton/s	1 (tbc)	$\ll 3$
Hg speed	V_{conv}	m/s	5 (tbc)	$\ll 15$
Hg pressure drop	ΔP_1	bar	tbc	$\ll 100$
Hg overpressure	ΔP_2	bar	tbc	$\ll 100$
UC _x temperature	T_{targ}	°C	2000	500-2500

It is necessary to integrate the solid targets and liquid converter target into a single facility for ease of access, in order to minimise both construction costs and also the operational effort involved in running the facility. The facility shown in figure 1 achieves the goal of housing all targets in a single complex. At the centre of the facility lies the multi-megawatt target station, in which an accelerated proton beam

strikes a 4-MW mercury converter target surrounded by 6 fission targets. In parallel, to one side, three direct targets can be operating in the 100-kW power range, all of which interface with ancillary systems for target handling, diagnostics, cooling, data retrieval and – most importantly – isotopic separation and treatment.

Target handling for the multi-MW target station is situated on the opposite side to the direct targets to minimise interference between the two distinct types of targets which have different operational modes and requirements. Radioactive ion beam (RIB) lines from the six fission targets near the multi-MW target (green lines in figure 2) are directed to a central node (in blue) where a beam merging device (not shown) will be situated, before further mass-selection is performed.

The proton accelerator must satisfy the needs of several different targets simultaneously. The EURISOL Driver Accelerator team has found a novel method of splitting the beam with minimum losses, described in Chapter 2.

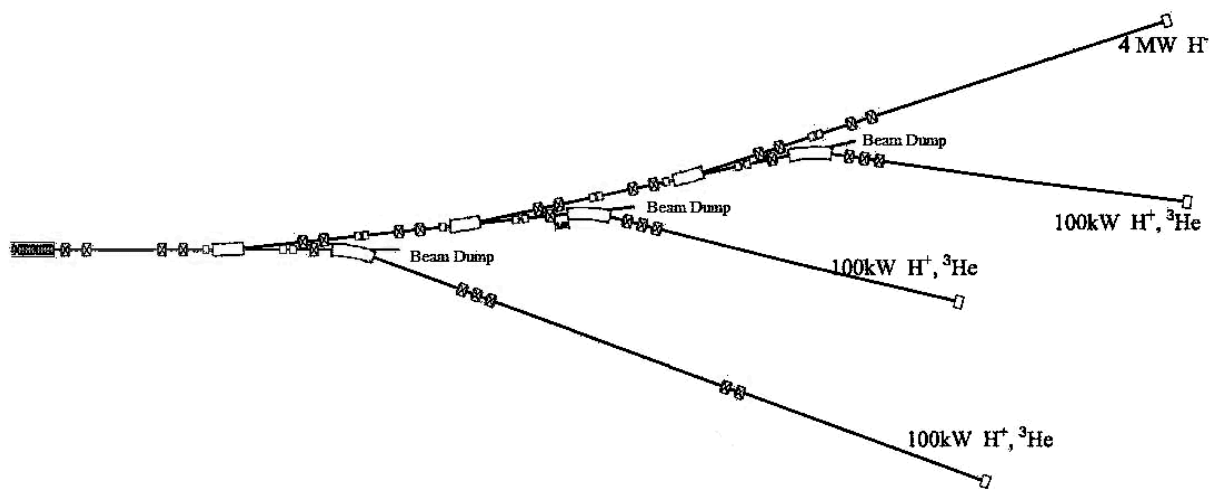
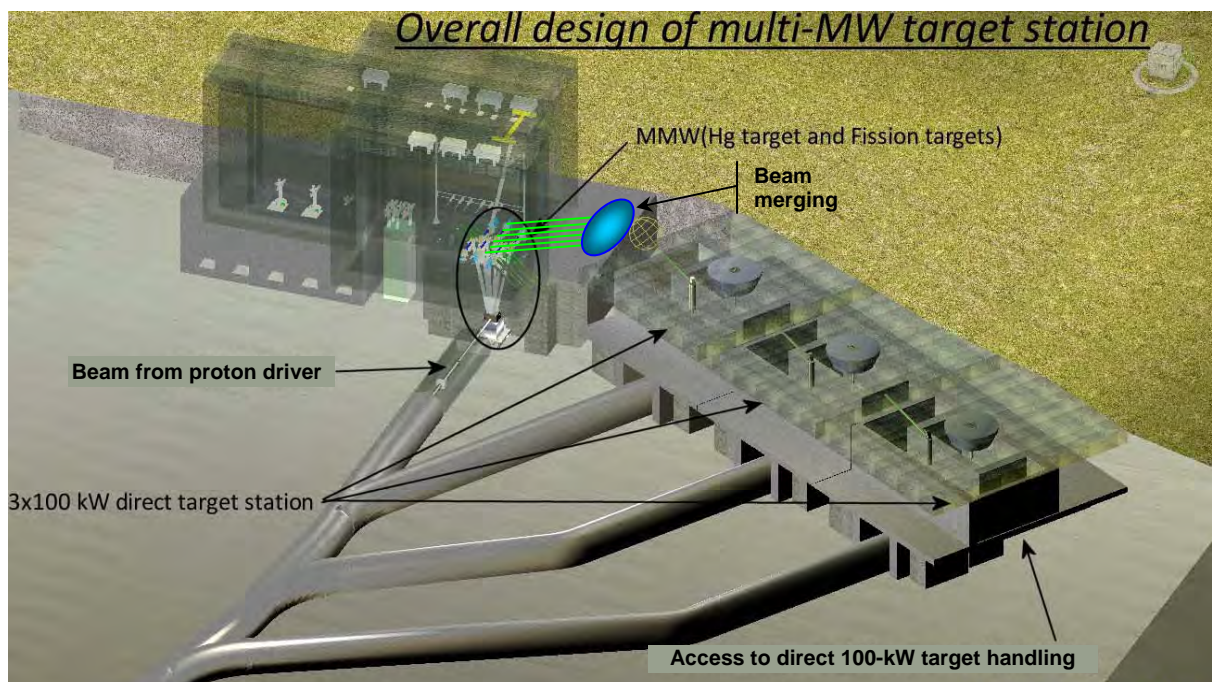


Fig. 1: EURISOL target facility (top) and Lorenz-effect beam splitting system (bottom).

4.2 Design of the neutron “converter” target

Essentially, operation of a liquid-metal target requires a rapid flow of liquid metal at the point of entry of the beam. Heat can thus be evacuated efficiently from the area where the beam hits the target material in order to create neutrons by spallation. Requirements from heat rates in the target are shown in table 2.

Table 2: Operational constraints on the liquid-metal target.

Parameter	symbol	value	unit
Deposited heat in target with margin	Q	3	MW
Thermal cycles short beam trip @ 10%	N_b	10^6	-
Thermal cycles long beam trip @ 100%	N_b	10^4	-
Liquid metal	Hg	13.5	kg/l
Flow rate	φ	172	kg/s
Maximum entrance temperature	T_{in}	60	°C
Maximum exit temperature	T_{out}	180	°C
Pressure drop	ΔP	< 5	bar
Static pressure	P_0	< 5	bar

In a “window” target the point of entry of the beam into the hull containing the liquid metal is called the “beam window”, designed so that where the hull wall is struck by the beam, it is simultaneously cooled by the liquid metal rushing past the inner surface. In a “windowless” target, on the other hand, the beam strikes a free-flowing liquid-metal jet which has no walls to constrain it. Both designs (shown in figure 2) were retained for further investigation in the EURISOL design study; and are henceforth referred to as:

- The coaxial guided stream (CGS) design, where a beam penetrates a cylindrically shaped closed target vessel in which the flow turns 180° at the beam entry point, thus cooling the container wall at the point of entry, also referred to as the beam entry window.
- The vertical transverse film (VTF) design, in which a beam passes a window separating the beam tube from the target, and then strikes a falling curtain of liquid metal, end-on.

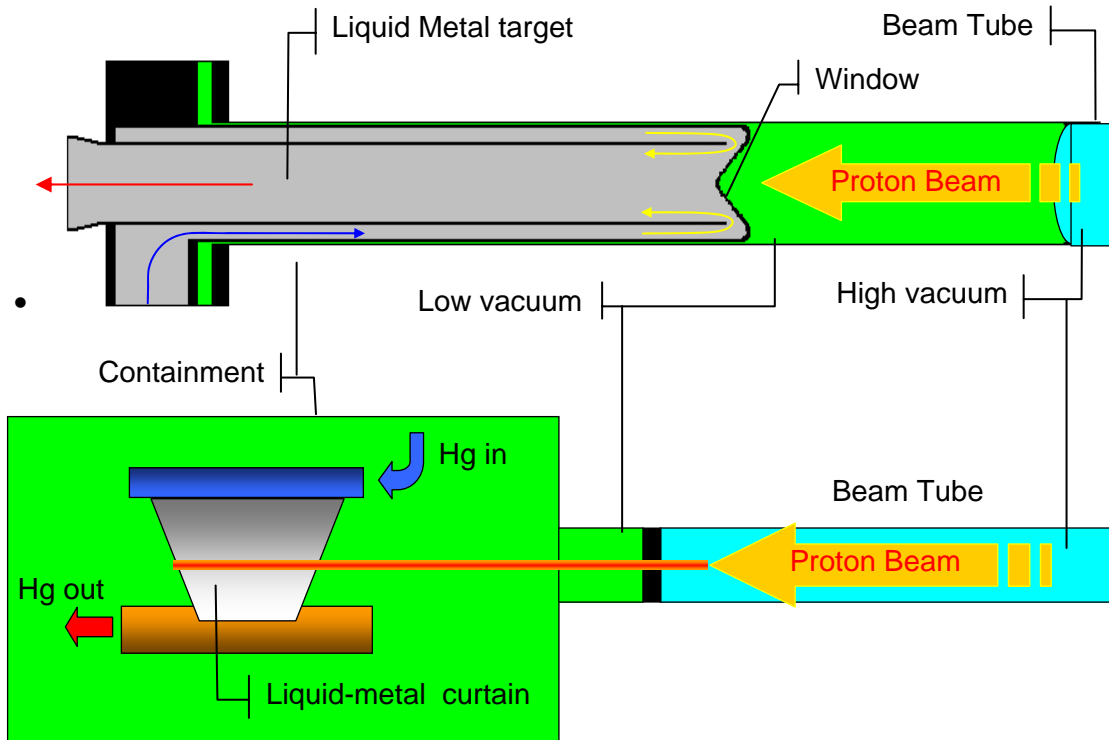


Fig. 2: Two target types: the CGS with a window (top) and the “windowless” VTF target (bottom).

The production of neutrons in a spallation source is a key feature of such targets, and solutions must be found to tackle the ensuing technical challenges. The design of the two targets differs significantly, as shown in figure 3, as they deal with the complex thermo-hydraulic phenomena resulting from the proton heat deposition in a very different way. A balance must be sought between achieving ultimate performance in the realm of pure physics and the necessity to conserve a technologically credible baseline for the design.

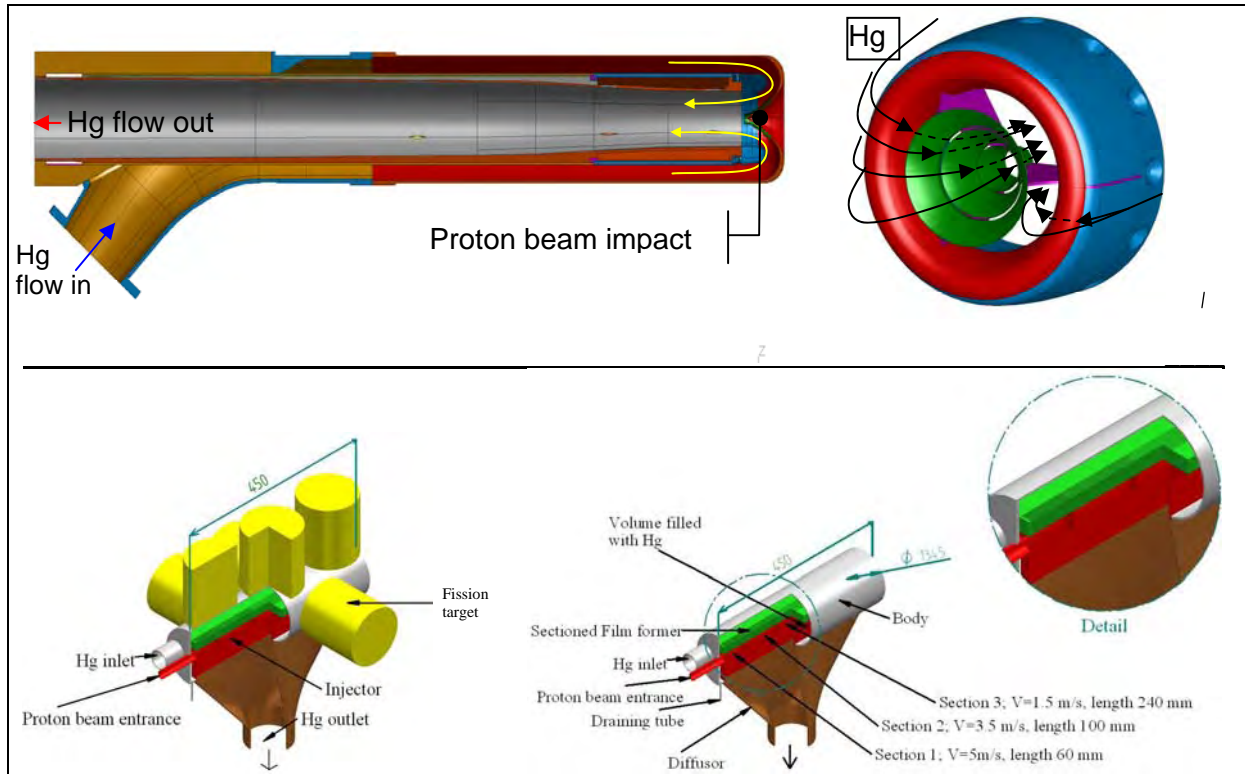


Fig. 3: The PSI design for the CGS target with detail of the flow vanes for reversing the liquid metal (top) and the IPUL concept of the VTF target (bottom).

Firstly, a detailed neutronic study compared the performance of the various possible configurations. The neutronic models of the two retained designs are shown in figure 4, along with the resulting neutron flux, which is also a measure of the likelihood of provoking a fission event in the surrounding uranium carbide fission targets. In reality, the quality of the flux – i.e. its spectrum, which relates to the energy distribution of the neutrons – is also a vital parameter. The comparative neutronic study showed that there would be an advantage in using the vertical-transverse-film (VTF) target, essentially due to the shorter escape route for the neutrons leaving the target and entering into the fission targets. However, because the film target lacked field experience, both options were pursued in parallel in a detailed engineering study.

Subsequent engineering design studies examined matters related to the stability of the liquid-metal flow, safety, structural integrity, impact on maintenance and servicing. These detailed studies culminated in full-scale hydraulic tests of both targets. The tests confirmed many of the predictions made during the engineering phase and also highlighted the fact the CGS target presented a far lower development risk, such that its slightly lower performance in terms of neutronics was felt to be outweighed by the benefits in terms of structural integrity and risk mitigation.

One of the major achievements of the converter target development program was to prove the stability of the CGS target operating under full flow rate; a top speed of 6 m/s was reached in the flowing mercury with no significant level of vibration. Cavitation was found to occur at a higher static pressure than predicted and the overall pressure drop was also slightly higher. However both parameters proved to be manageable and well within the capabilities of the liquid-metal loop.

The VTF target, on the other hand, proved more difficult in terms of managing a stable flow and would need further development. In view of the test results (cf. §4.3 and 4.4) and following a thorough analysis of the two options, the team decided to propose the CGS target as the baseline for the project.

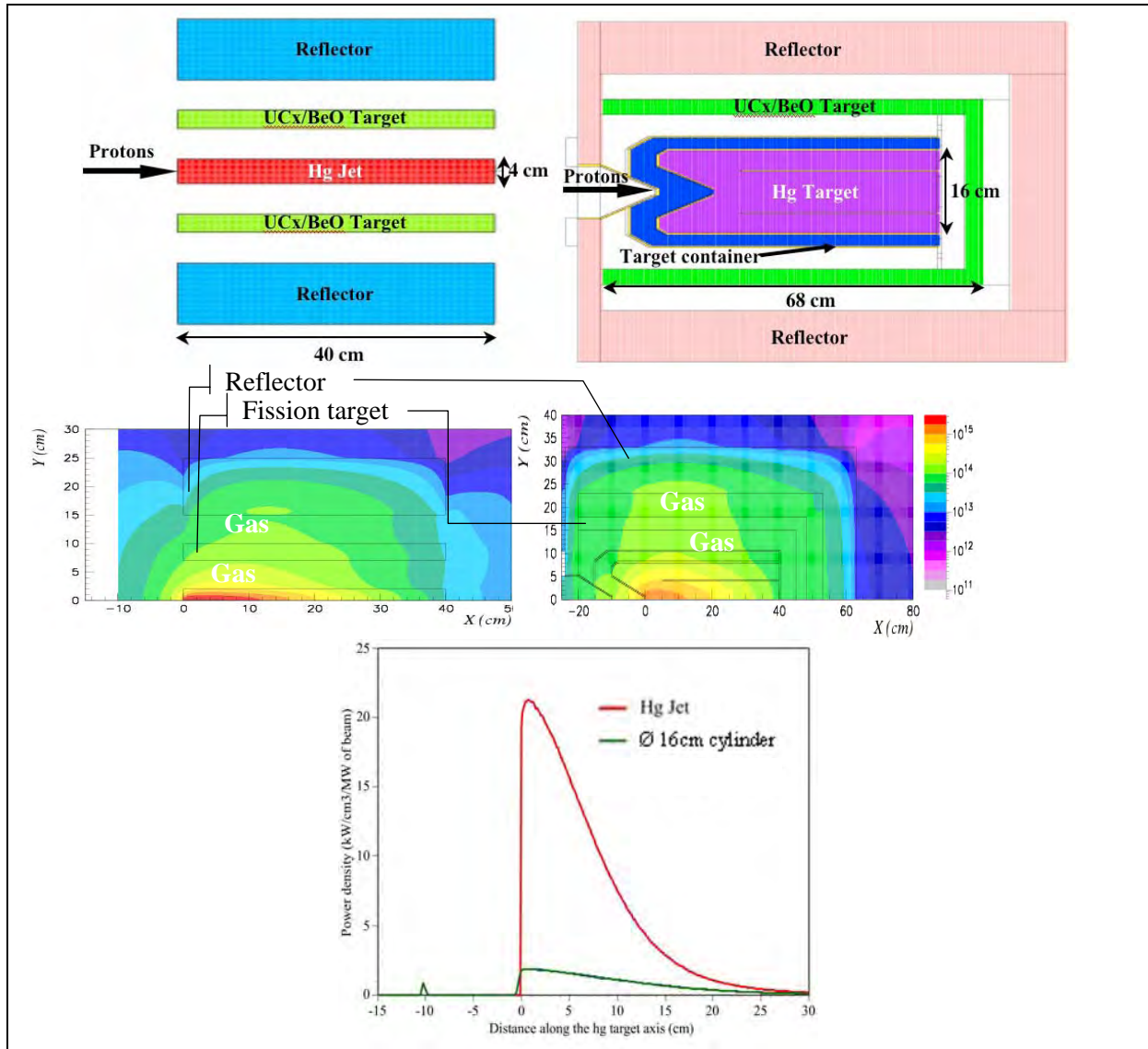


Fig. 4 (Top): Fission target arrangement. (Centre): Neutron flux distribution in $n/cm^2/s/MW$ of beam for the VTF (left) and CGS (right). (Bottom): Heat deposition in the targets.

4.3 Engineering studies and testing of the CGS “converter” target

Experience with the MEGAPIE test led the team at PSI to rely on simulation tools for developing the CGS target. Many novelties were incorporated in the CGS design, including:

- a conical compound-surface shaped beam window with an evolving thickness for improved cooling of the window and resistance to internal pressure.
- a guide-tube with an airfoil section resulting in a hydro-dynamically optimised Venturi for optimising the high-speed flow of mercury.
- flow vanes (optional) located along the wetted surface of the beam window to stabilise the flow at the point of entry of the beam.
- a canted inlet to reduce pressure losses.

The predictions made for the CGS hydraulic test focused much attention on the flow-vanes. A computational fluid dynamics (CFD) calculation, using mathematical models to replicate turbulence, found that without these flow vanes the liquid-metal flow would detach from the window, instantaneously reducing cooling and thereby causing thermal cycling likely to inflict fatigue damage on the window. A comparison of the CFD results with and without flow vanes, shown in the top of figure 5, indicates how a bubble of low-velocity fluid (indicated by an arrow) detaches from the window without flow vanes (right).

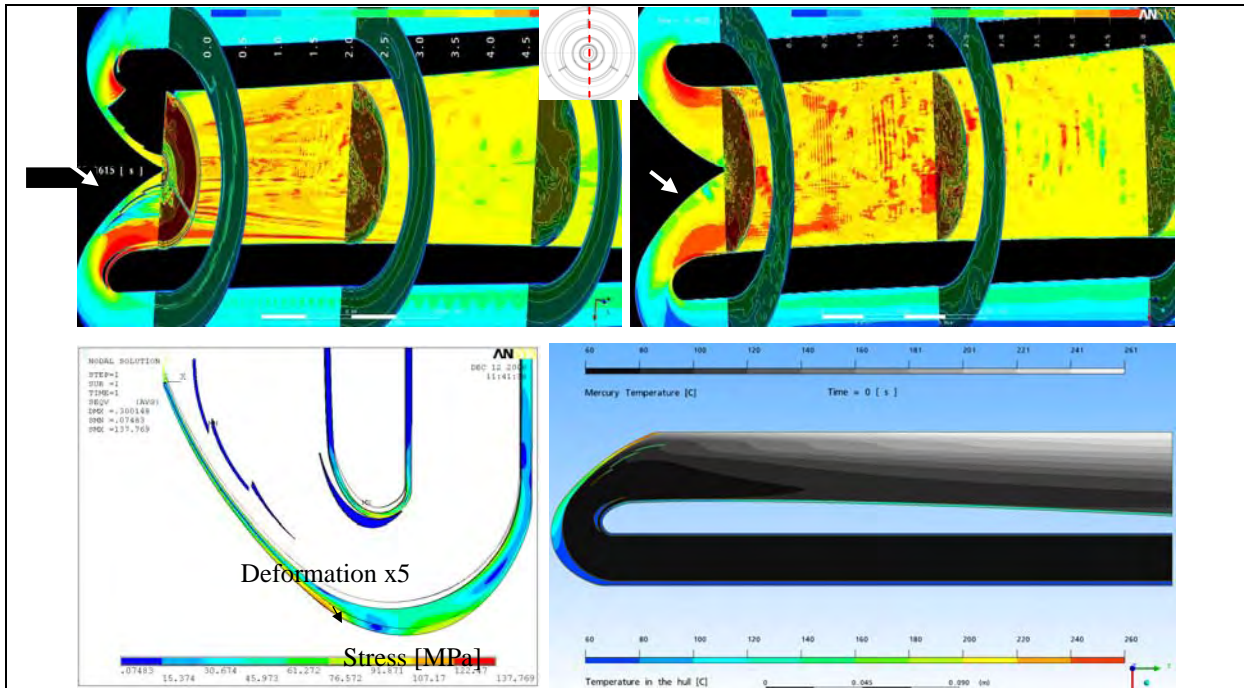


Fig. 5: Velocity magnitude fields with (top left) and without (top right) flow vanes. Stress in window (bottom left), temperature in liquid metal and hull due to the proton beam (bottom right).

The hydraulic test featured a detachable nozzle on the guide tube to allow measurement of the target behaviour both with the flow-vanes and without flow-vanes attached to the fore end of the guide tube. This allowed test predictions to be checked against measurements, but also it proved possible to assess experimentally that the detrimental effect on pressure losses and vibration levels of the flow vanes was well within tolerable limits. The positive effect of the flow vanes on the cooling of the window could not be verified experimentally, as unfortunately funding was not directed towards thermal testing. It would seem essential in a later development that the cooling of the window should be investigated experimentally to ensure that the calculations which predicted improved cooling with the flow vanes are indeed correct. Experience from MEGAPIE leads us to believe that, as long as the velocity in the fluid along the window wall is high, adequate cooling of the window is assured. Hence because the required flow rate was achieved during the test with the flow vanes in place and no severe vibration affected the target as a whole, the project team can affirm that this matter is not likely to be of any concern to future developments. However for reasons of licensing and safety, thermal testing will be mandatory before proceeding with any irradiation test in the future.

A safety analysis performed for the CGS version indicated that temperatures in the mercury under proton beam irradiation would not exceed 260°C (lower right in figure 5) which is 100°C lower than the boiling temperature of mercury at atmospheric pressure. The design static pressure in the loop is 10 bar, hence the margin against boiling of the mercury is even higher: approximately 200°C. In the event of a sudden flow blockage however, an interlock system must switch off the beam in less than ½ second, otherwise the mercury will boil, and mercury vapour pressure will rise, rupturing the hull.

With a Pb-Bi eutectic (LBE), on the other hand, it would take more than 5 seconds for boiling to occur in the event of a flow interruption. The greater time margin would be an argument in favour of using LBE despite its lower neutronic performance.

The beam window of the CGS version was checked for structural strength. The peak stress in the window at the point of entry of the beam reaches 135 MPa (lower left in figure 5), which is well below the design limit of 190 MPa recommended for early design of an irradiated component by the French nuclear safety code RCCMR. In the most unfavourable conditions, such as small-scale instabilities of the flow, temperature in the hull window does not exceed 400°C; at nominal conditions it stays under 300°C, which is well below the recommended limit of 500°C for the T91 stainless steel used in the window. Were LBE to be used as a fluid instead of mercury, the temperature would be approximately 100°C higher, still within tolerable limits.

The predictions for the CGS hydraulic test uncovered some frailties of the design, in particular relating to the flow-vanes. A weld was predicted to fail from fatigue when the turbulence – caused by pressure fluctuations emerging from the CFD calculations – was numerically coupled with a vibration analysis of the structure using the finite-element method (FEM). As shown in figure 6, a sine-sweep of the structural model showed a particular resonance at the root of the connection between the vanes' supports and the circular flow vanes, with a resulting peak dynamic stress of 115 MPa oscillating at 200 Hz and thus accumulating millions of cycles. Clearly this part of the design has to be reinforced in subsequent developments. Movement of the hull was predicted to be minute, less than 50 µm, which would be insufficient to lead to any rupture, be it static or dynamic.

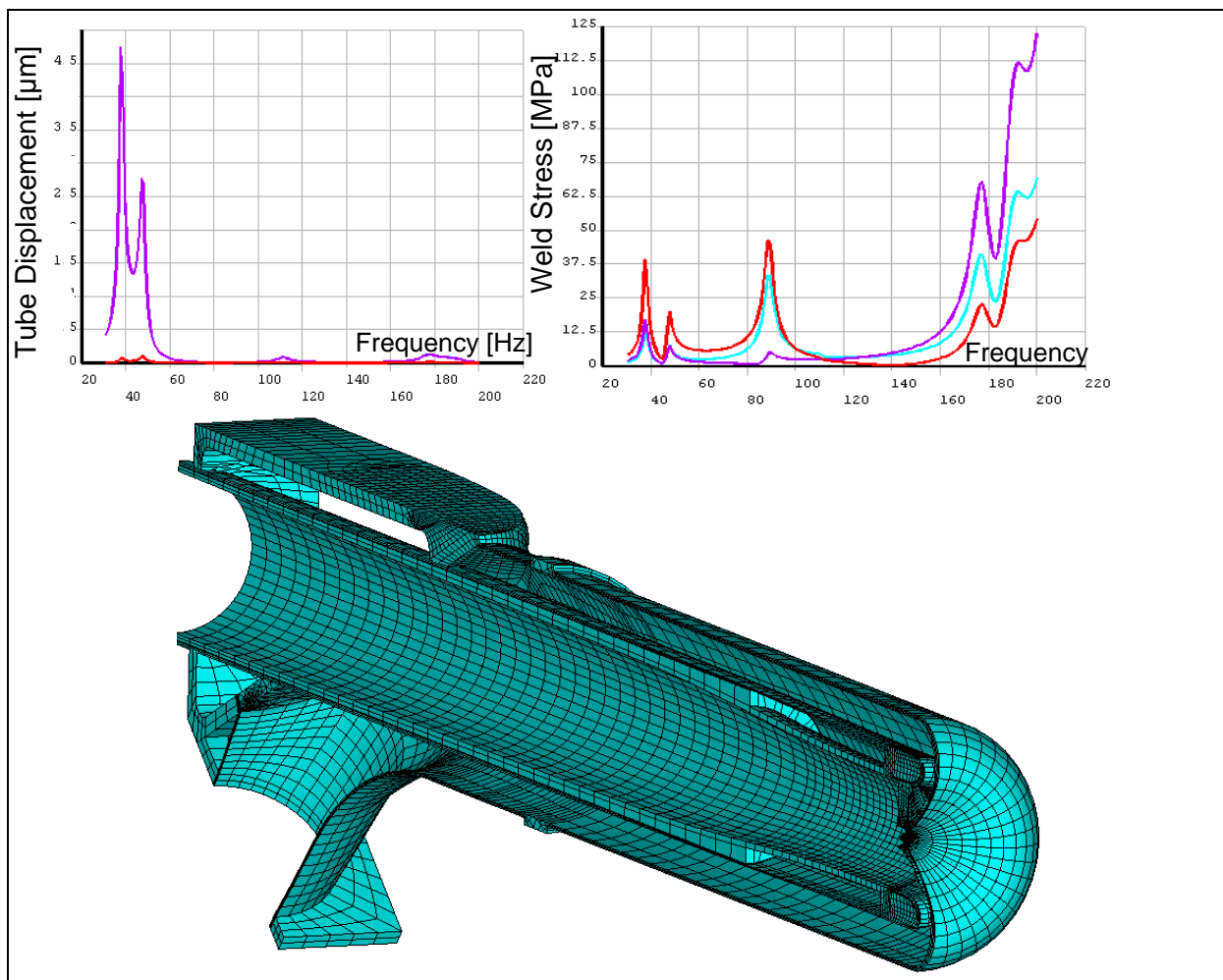


Fig. 6: Structural FEM Model used in calculating the stresses and deformations from the pressure distribution.

The test of the CGS target proceeded apace and confirmed the predictions made above. However, testing conditions were not totally adequate, and careful analysis of the test recordings uncovered a strong fluctuation in the electro-magnetic pump at 100 Hz which led to additional pressure losses in the target and perturbed the pressure fluctuation recording. Nevertheless, filtering was used to eliminate this source of perturbation and a fair correlation of the test results with the predictions was reached.

The target mock-up was connected to the IPUL mercury loop as shown in figure 7 and instrumented throughout, with a variety of sensors, notably:

- pressure-drop measurement across the target,
- pressure fluctuation in the liquid on the inner wall of the window,
- acceleration sensors on the window in horizontal and vertical direction,
- strain measurements of the vertical and horizontal bending motion in the hull,
- thermocouples along the target,
- laser Doppler velocimetry of the thin window wall vibration,
- microphone.

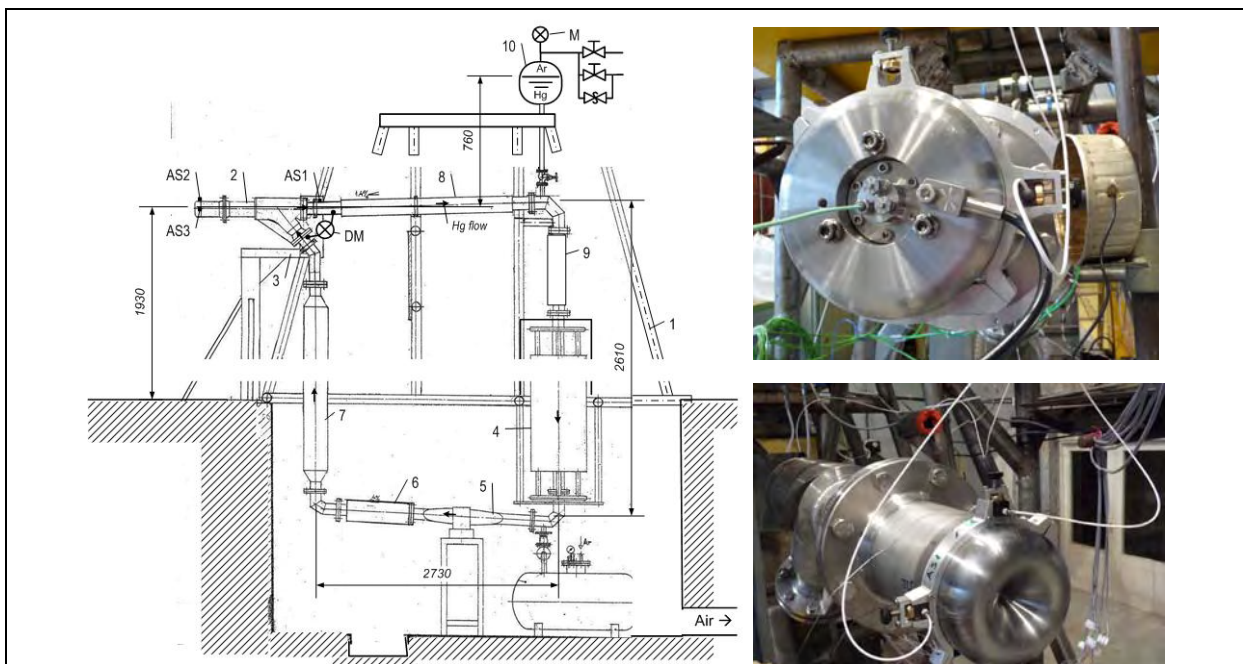


Fig. 7: Hydraulic test set-up in the loop (left) and photographs of the instrumentation (right).

The two right-hand photographs in figure 7 show the pressure transducer pick-up on the inner wall at the window (top) and the accelerometers (bottom). They illustrate how detailed performance of the target was recorded during the test. This was vital to assessing not only the validity of the design choices made, but also the accuracy of the predicted behaviour, as the entire CGS target development was purely reliant on computer-based simulations, with no prior sub-scale component testing.

The pressure drop recorded a higher value than had been predicted; roughly 2 bar at full flow rate. Although this was manageable with the available pump power, the source of the increased pressure drop was investigated thoroughly. It was found to be attributable to a number of small design changes made prior to testing so as to speed up manufacturing, such as using off-the-shelf welded piping rather than a dedicated machined part. This restricted the in-comer annulus section and increased friction

drag. Another high penalty item was discovered in the electro-magnetic pump which was found to possess a very high amplitude of flow rate fluctuation at 100 Hz, producing a kind of “chugging” effect resulting in friction drag. Despite these unfavourable conditions, the target nevertheless achieved full flow rate with little vibration.

Indeed, the strain gauges recorded vibration levels in the hull which correlated well in both frequency content and in magnitude. Figure 8 shows the recorded vibration stress in vertical direction which clearly increases when the flow vanes are present, but only to a magnitude slightly under ½ MPa which matched the calculations. This low level of vibration with flow vanes on the guide tube indicates that the disturbance in the flow caused by the flow vanes is not as detrimental as may have been feared. It would take a thermal test however to confirm experimentally that they do enhance cooling as shown in the calculations. The series of fast Fourier transform graphs in the right-hand column of figure 8 are interesting in that they show a similar pattern in the 0–50 Hz range to the theoretical calculation of the vertical movement of the hull shown in the left-hand graph of figure 6.

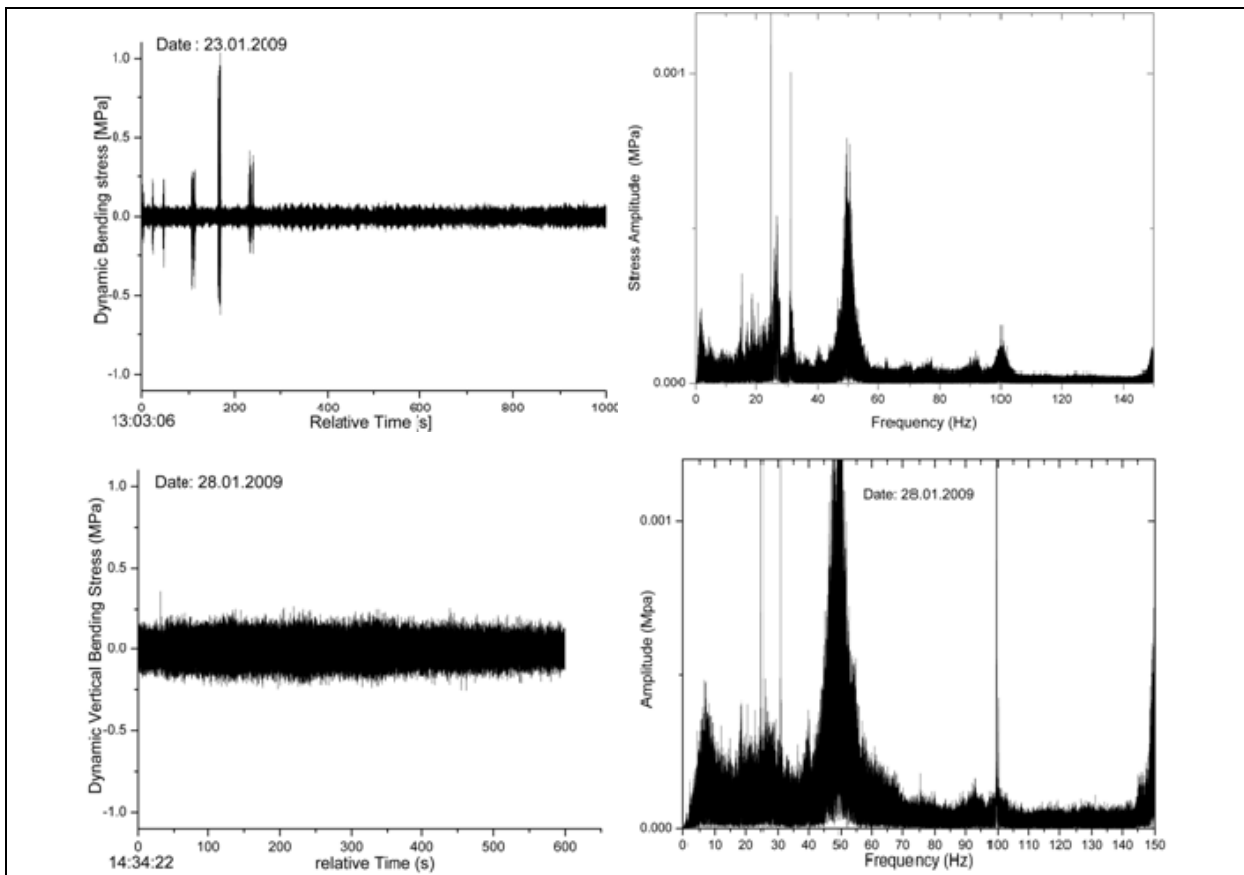


Fig. 8: Vertical bending stress for 8 l/s without (top) and with (bottom) flow vanes. In each case the dynamic signal is represented on the left and the fast Fourier transform thereof on the right

The high-speed pressure transducers along the window picked up pressure fluctuations which were analysed using fast Fourier transform techniques to assess their frequency content. The experimental spectra were checked against prediction made with a CFD turbulence model known as a “large eddy simulation” or LES. This model is known to predict instabilities in fluids such water or air but is untested for liquid metal. First results indicated that the magnitude of the fluctuations compares well with the test. Also the frequency content is in good agreement, once the 100 Hz pulsation from the pump has been filtered out. Comparison above 100 Hz is more debatable, as the perturbation from the pump pulsation is thought to have a higher-order effect in that region. The strong fluctuations at frequencies lower than 100 Hz, which are of primary importance for the structure, were well represented.

The weak support of the flow vanes resulted unfortunately in the rupture of the vane-to-support weld as had been predicted. The sequence leading to the failure was monitored accurately by all the sensors; hence it was validation of the fact that instrumentation in the loop consisting in pressure pick-ups, strain gauges, and even a microphone can give adequate forewarning of any malfunction inside the target. In a further development of the target it would be necessary to increase the strength of these welds and their support, which is quite possible from a manufacturing point of view. The increased drag penalty is expected to be less than 0.1 bar.

The occurrence of cavitation was detected by a variety of the instruments, i.e. the pressure transducers, the microphone and the laser Doppler velocimetry. The design was more susceptible to cavitation than originally thought, possibly an effect of the inconsistencies in manufacturing the target and the electromagnetic pump mentioned above. However the static pressure needed to suppress cavitation at full flow rate was found to be 6 bar, which is quite tolerable in the present design of the target, and may doubtless be improved upon.

The amount of data collected during the test campaign of the EURISOL CGS converter target resulted in the publication of six papers in established scientific journals. The peer review conducted indicates that the proposed design is well able to fulfil all the requirements set for its performance in terms of thermal-hydraulics, structural integrity and neutronics.

4.4 Engineering studies and testing of the VTF “converter” target

Liquid-metal (LM) technology is closely associated with magneto-hydrodynamics (MHD). The Institute of Physics of the University of Latvia (IPUL) is one of the main research centres in the field of MHD technology and has been involved in both theoretical work and applied studies including LM experiments. Mercury is used as an effective modelling material for thermo-hydraulic testing of systems proposed for high-temperature applications using heavy liquid-metals.

The proposed vertical transverse film (VTF) target is shown on the test-stand in figure 9, where it underwent a series of investigations focusing particularly on stability of the flow. The optimised target was the ultimate development in a research program spanning several years at IPUL’s facility, which progressed from small sub-scale testing of components in liquid metal to a full-scale mock-up of the target. This approach is interesting as it differs from that adopted by PSI, which relied on simulations for its development. Both approaches worked satisfactorily and have their respective benefits.



Fig. 9: The VTF target on the test stand at IPUL, seen from below.

There are many advantages to a “windowless” liquid-metal target, as has been recognised by collaboration agreements within the European research framework. In the SINQ facility at PSI the proton beam is bent upwards by special magnets. In principle, the beam could be bent also downwards and aimed at an open liquid-metal surface. A project in this configuration was spearheaded by IPUL in collaboration with the Belgian Nuclear Research Centre (SCK) as part of design and verification experiments for a windowless spallation target for the ADS prototype MYRHA. This application was intended as a small high-performance irradiation facility with fast neutron fluxes up to 10^{13} n/cm²/s.

Within the context of the EURISOL Design Study, the liquid-metal spallation target with a power of several megawatts is a critical component and will require new, advanced technology. With a deposited heat power density of over 10^3 MW/m³, the windowless, free-surface, LM-jet is proposed as a target since it avoids the very serious lifetime-shortening damage caused by the proton beam in a system with a window. In the case of the spallation neutron sources, mercury has been chosen as the most promising high-Z target and coolant material.

In order to develop a windowless target it is necessary to investigate the hydrodynamics of a liquid-metal (Hg) jet. IPUL has become increasingly involved in corresponding investigations. Evaluation of the optimal engineering design of the Hg-loop components, such as the electromagnetic pump, flow meter, piping, diagnostic and control elements, as well as developing and manufacturing an Hg-loop for testing EURISOL target components were IPUL’s main tasks.

During the spring of 2007 IPUL performed several attempts to establish stable, free-falling liquid In/Ga/Sn eutectic film in their experimental facilities. These efforts were part of an IPUL project for the introduction of a novel full-scale Hg liquid-film neutrino spallation target. Several rectangular shaped jet inlets (approx. 10×100 mm) with differently shaped nozzle openings were tested for maximum Hg volume fraction in the jet. Finally, an inlet with multiple rectangular openings for the jet was chosen since it resulted in almost 100% metal in the jet without any gas inclusions. However, the shape of the free-falling unrestrained In/Ga/Sn jet was judged to be unacceptable as the jet evidently shrank during free-fall, with large changes in jet sectional shape.

After much iteration, a final form of the inlet was chosen which featured a segmented nozzle. In this manner it was possible to tailor the local speed to fit the heat deposition. This system is illustrated by the temperature and velocity plots shown in figure 10, where the front part of the film has a top speed of 5 m/s, the middle section stands at 2 m/s, the back part at 1m/s. The resulting peak temperature at 230°C is well within limits and comparable to that of the CGS design. However, unlike the CGS, the mercury in the jet cannot be pressurised as easily, as it falls essentially into a vacuum. The margin against boiling is therefore inherently lower. Nevertheless, the consequences of the mercury boiling are also easier to mitigate as there is enough free space in the target to vent mercury vapour, as long as a beam dump exists at the rear of the target to take up the excess heat from the beam.

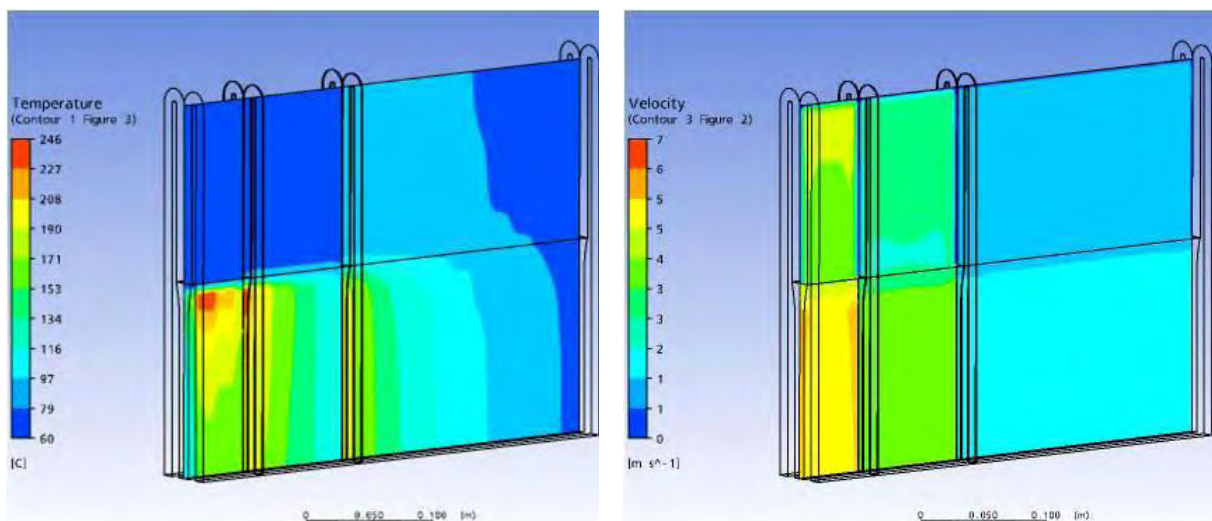


Fig. 10: Film temperature (left) and velocity (right) in the VTF target.

The stability of the film target was investigated experimentally as shown in figure 11. The beam would hit a portion of the film higher than the arrows indicating instability shown in the figure. Hence the design is expected to work within an irradiation test. However, for safety such instabilities would have to be tested at greater length to ensure they do not propagate upwards towards the deposition area where the beam would be located. The pressure drop across the target is thought to be identical to that measured during the CGS test, i.e. 2 bar. A maximum flow speed of 2 m/s was recorded in this test based on flow-meter readings. A later test with a segmented injector managed to reach a peak of 5 m/s in the forward injector again assuming a 2-bar pressure drop.

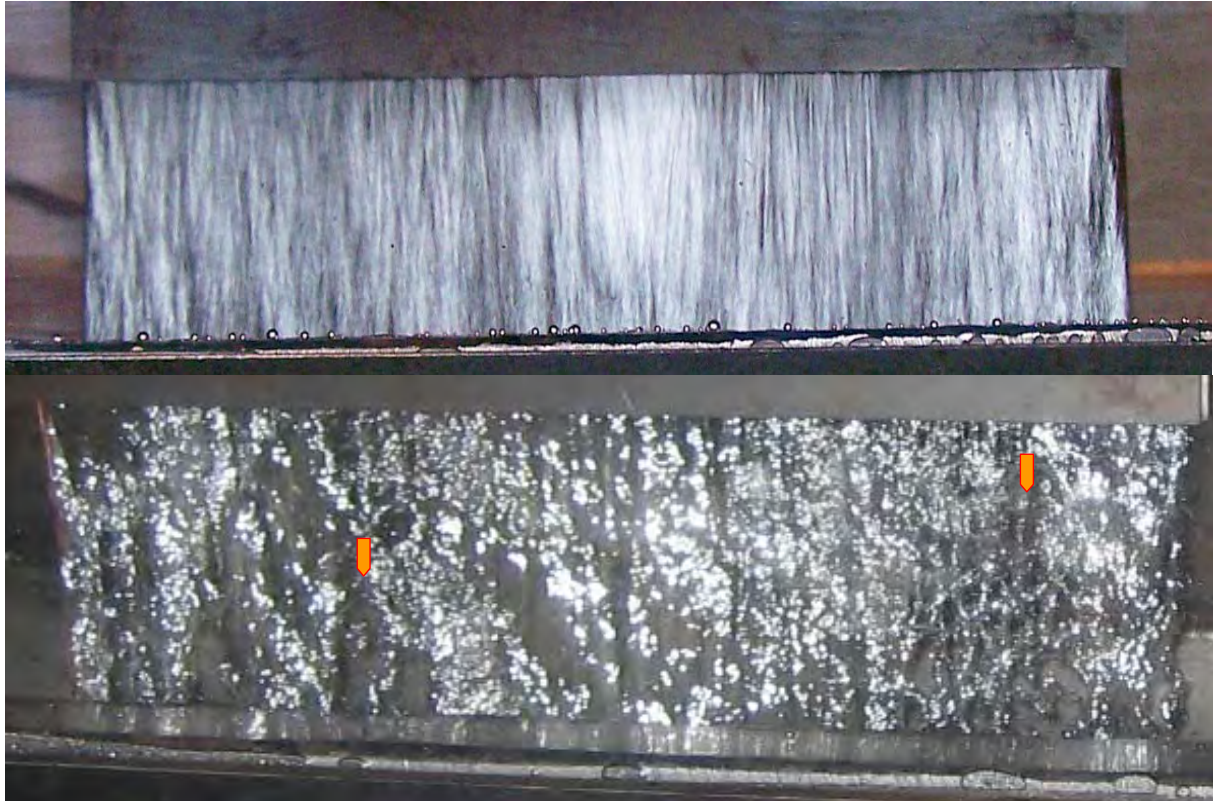


Fig. 11: Photographs of the film target taken at different shutter speeds with arrows indicating instabilities.

The inlet section would have to be optimised in order to ensure sufficient flow at high speed with a reasonable pressure drop. This task would require further developments in instrumentation to monitor flow speeds directly rather than inferring speed from the flow rate, as it is a critical parameter to the survival of the target.

Overall, the proposed transverse film target offers good perspectives as the operating pressure in the mercury loop is only a few bars. The heat distribution in the target mercury from the beam power is easy to adjust by selecting the velocity field appropriately.

The stability of the film flow at speeds higher than a few m/s may need some additional investigations but the step-by-step experimental approach taken to optimise the shape of nozzle holds promise for further optimisation work at the higher speed end of the spectrum.

4.5 Engineering studies for the liquid-metal loop

The proposed EURISOL liquid metal loop is capable of evacuating 2.7 MW of the 4 MW deposited in the neutron spallation target. The loop is designed to cope with the effects of temperature, pressure, irradiation and liquid-metal corrosion, including both steady-state operations and normal transients. The design of the liquid-metal loop at PSI draws on 20 years of experience in the field of cooling spallation targets in SINQ, as well as the 4 months of irradiation of MEGAPIE, the world's first liquid-metal neutron source.

The concept for EURISOL envisages placing the target on a trolley which can be displaced: the trolley supports the target at the front end, fixed to an integral shielding block and behind it the liquid-metal loop. The decision to keep the loop attached to the target and shielding at all times is dictated by safety concerns. In case of an emergency, the target and loop remain attached and are retracted into the hot cell together. Indeed the trolley holding the target cannot be retracted from the irradiation facility easily and rapidly if disconnection operations are necessary. In case of a fire on the irradiated side, it is safer to have an integral loop with attached drain tanks which can safely perform emergency shut-down operations within seconds of an accident, continuing to ensure all vital functions such as cooling, isolation, drainage etc, at the same time as the target is being retracted out of harms way. In doing so, the number of valves and bolted interfaces is also kept to a minimum and replaced by welded connections. The proposed design is shown in figure 12. It features notably:

- a target fixed to the 2.3-m front iron shield with staggered shielding blocks,
- a trolley with mounted shielding, a drive motor displacing the assembled trolley with bogeys rolling on rails,
- piping with Ω -flex tubes to compensate for thermal expansion,
- a heat exchanger comprising 232 internal U-tubes to accommodate thermal expansion,
- an electro-magnetic pump,
- an isotopes separator,
- chemical standard pneumatic valves, and
- a drain tank.

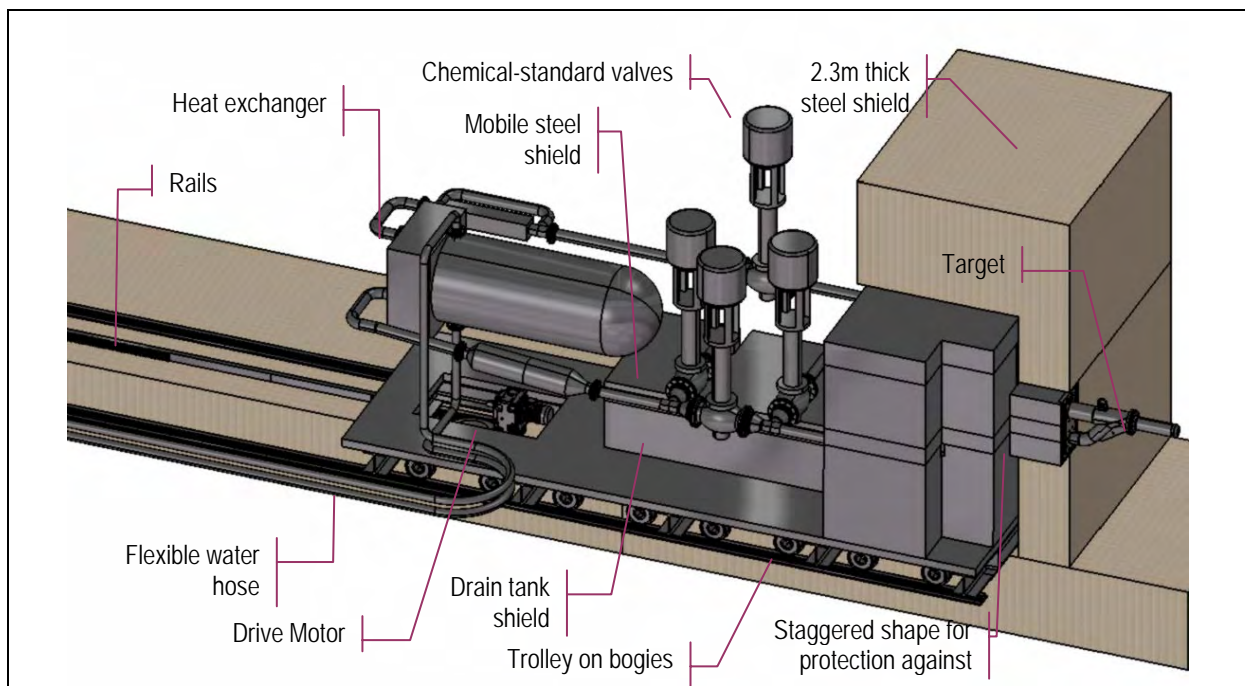


Fig. 12: Cut-away view of the integrated liquid-metal loop with its shielding.

The hydraulic losses at full flow rate of all these components (including the piping), come to less than 4 bar, half of which is ascribed to the target as tested. This is somewhat conservative as it is now recognised that with sufficient preparation the target losses may be halved. The requirements for the pump are therefore the following:

- Pressure head > 4 bar
- Flow rate > 12.6 l/s.

The resulting mechanical power demand is 5 kW, which can easily be delivered by an 80-kW electromagnetic pump at current efficiency levels of at least 6%.

4.6 Radiation and safety

One of the principal challenges lies in the necessity to deal with high flow rates in the loop, whilst at the same time withstanding high doses of irradiation. Although the design of the loop is aimed at the primary function of evacuating heat, some thought has been given to accommodating extraction facilities for the isotopes that are of interest. A typical 20-year lifetime of such an installation places high demands in terms of safety, accessibility and dismantling. The facility aims to maintain a high degree of availability, so that a modular concept is preferred in which the layout facilitates rapid exchange of components. This demand comes at the expense of a less compact design, which does attract some additional cost.

Once integrated into a full model, the target, target loop and shielding could be assessed from the neutronics aspect. The calculations of neutron bombardment shown in figure 13 give a view of the highly localised intensity of the radiation source against which it is necessary to shield the facility. An analysis of the radiation results was completed and corresponding doses in mSv/hr were calculated in various zones of the facility to prove it conforms to the legislation for experimental facilities. The proposed shielding is acceptable.

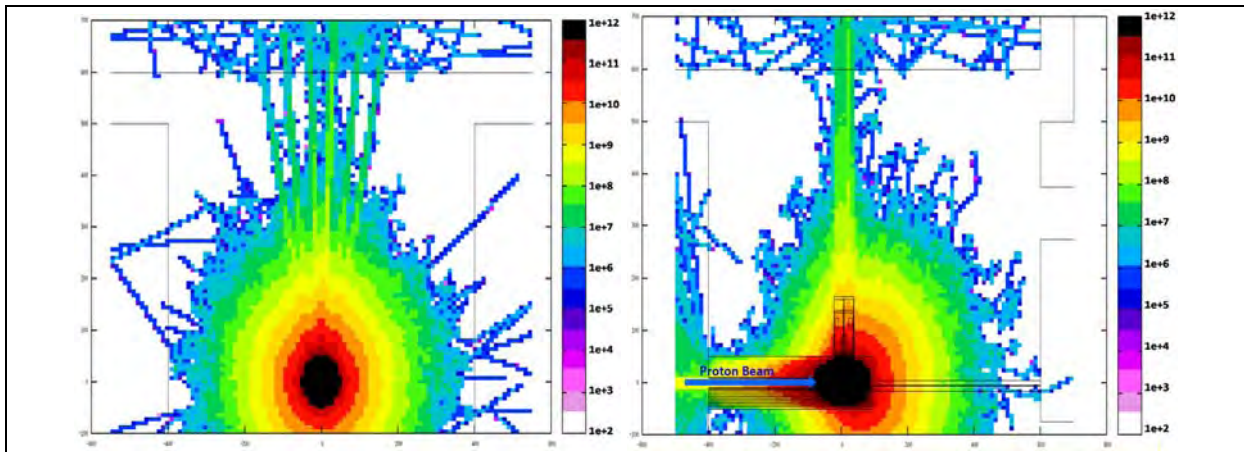


Fig. 13: Neutron flux ($n/cm^2/mA$) exiting the target station in beam direction (left), and side-on (right).

In addition to the direct neutron bombardment from the spallation reaction, spallation also results in the production of gases, soluble and insoluble elements in the liquid-metal loop. The solid and liquid elements are mostly of concern for the design of the filters and also, to an extent, for radioprotection. The choice of mercury as target material poses various challenges for safe operation of such a system that are related to the physical and chemical properties of the target material and the nuclear reaction products produced within the target during a lifetime spanning decades.

Chemical analysis of the production rates in mercury under irradiation was the focus of a dedicated task at PSI which successfully demonstrated at a laboratory scale novel techniques for separating the spallation products from the base liquid metal (cf. figure 14). The goal of this comprehensive work was to gain an insight into the feasibility and usefulness of purifying the mercury in the multi-MW liquid spallation target of a future EURISOL facility. Answering these questions requires taking into consideration matters relating to radioprotection, as well as operational and commercial aspects.

From a radioprotection point of view, a reduction of the radionuclide inventory during operation before final storage, achieved by a purification of mercury, will result in a reduction of the radioactivity during the operational period. First experience from operating mercury spallation sources elsewhere indicates that dose rate reduction could be beneficial for maintenance operations. However, the optimisation of these methods for reducing the dose from radioactivity will require additional R&D efforts.

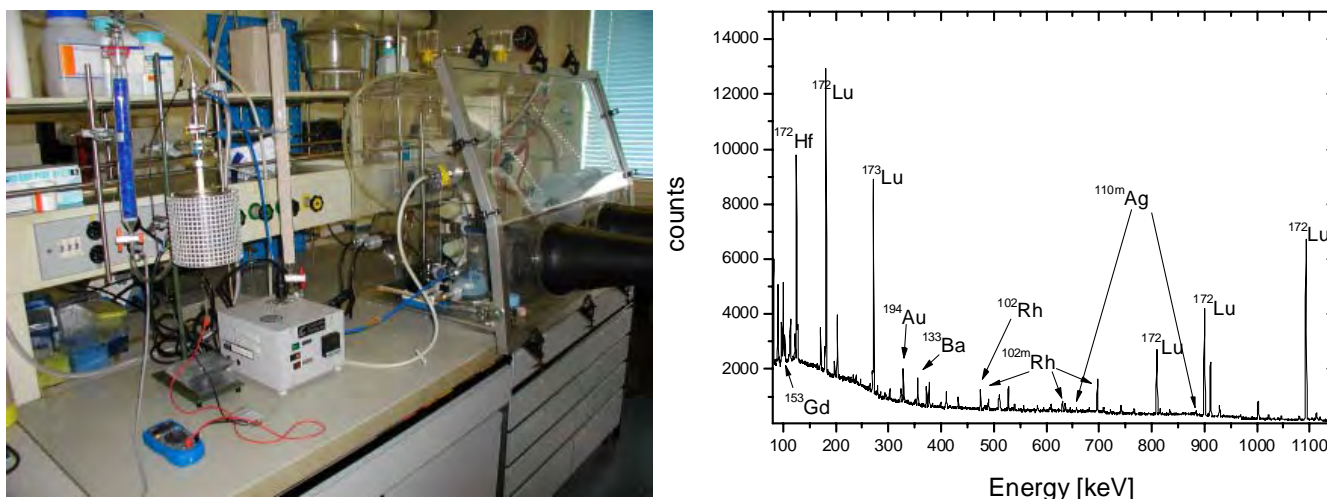


Fig. 14 (Left): Experimental set-up at PSI. (Right): Measured γ -spectrum of the sample irradiated at CERN.

For final storage, on the other hand, any purification of the mercury will not yield substantial advantages because a large amount of the long-term radioactivity is associated with mercury itself, including the long-lived isotope ¹⁹⁴Hg. This radioactivity cannot be separated by chemical means. Conventional operational problems which could be caused by the deposition of impurity materials such as plugging and heat transfer problems will benefit from growing experience gained with liquid-metal spallation target facilities that have started to operate recently.

With respect to nuclide production, the income which might be generated does not seem to compensate for the costs generated by the purification process when conventional purification methods such as distillation are used. The situation can be substantially improved if alternative purification techniques are applied. Additional economic benefits could arise from the development of chemical processing methods that are optimised for the production of several valuable nuclides from the material separated from the spallation system in one multi-stage processing cycle.

4.7 Target integration

As depicted in figure 15, the liquid-metal cooling loop is placed behind a 2.3-m thick mobile steel shield which is associated with the trolley. The target is fixed to the front of the shield and is inserted through the shielding wall, with a tolerance of approximately 1 cm, into the irradiation position in front of the beam tube, where the target is exposed to the 4-MW proton beam.

The converter target is surrounded by a safety hull which acts as a containment in the event of the target window breaking and a mercury leak. The converter target and safety hull are surrounded by the fission targets designed by INFN and which are fully documented in Chapter 5. The entire assembly is located on the other side of the shielding and positioned on the same trolley. The reflector and the biological shielding as well as the safety hull are shown in figure 16.

For accessing the target pipes, the mobile shielding may be removed as the blocks are stacked on top of one another. It is not necessary to remove the mobile shielding to replace the converter target which can be detached from the loop interface by bolts accessible from the front face. Once the target is in position inside the maintenance area a crane may be used to lift it, after it has been detached by the robots using dedicated tooling. Partial disassembly of the target should be favoured as it produces less waste.

All targets are surrounded by considerable shielding which explains the massive nature of much of the building shown in figure 1; this is intended to provide enough protection from the considerable level of radiation emitted in the converter target. Indeed the target emits a neutron flux some 10^{14} n/cm²/s at its surface which is similar to that inside a nuclear reactor. The decay products in the liquid metal also emit considerable γ -radiation. Calculations show that up to 7 metres of concrete shielding are needed.

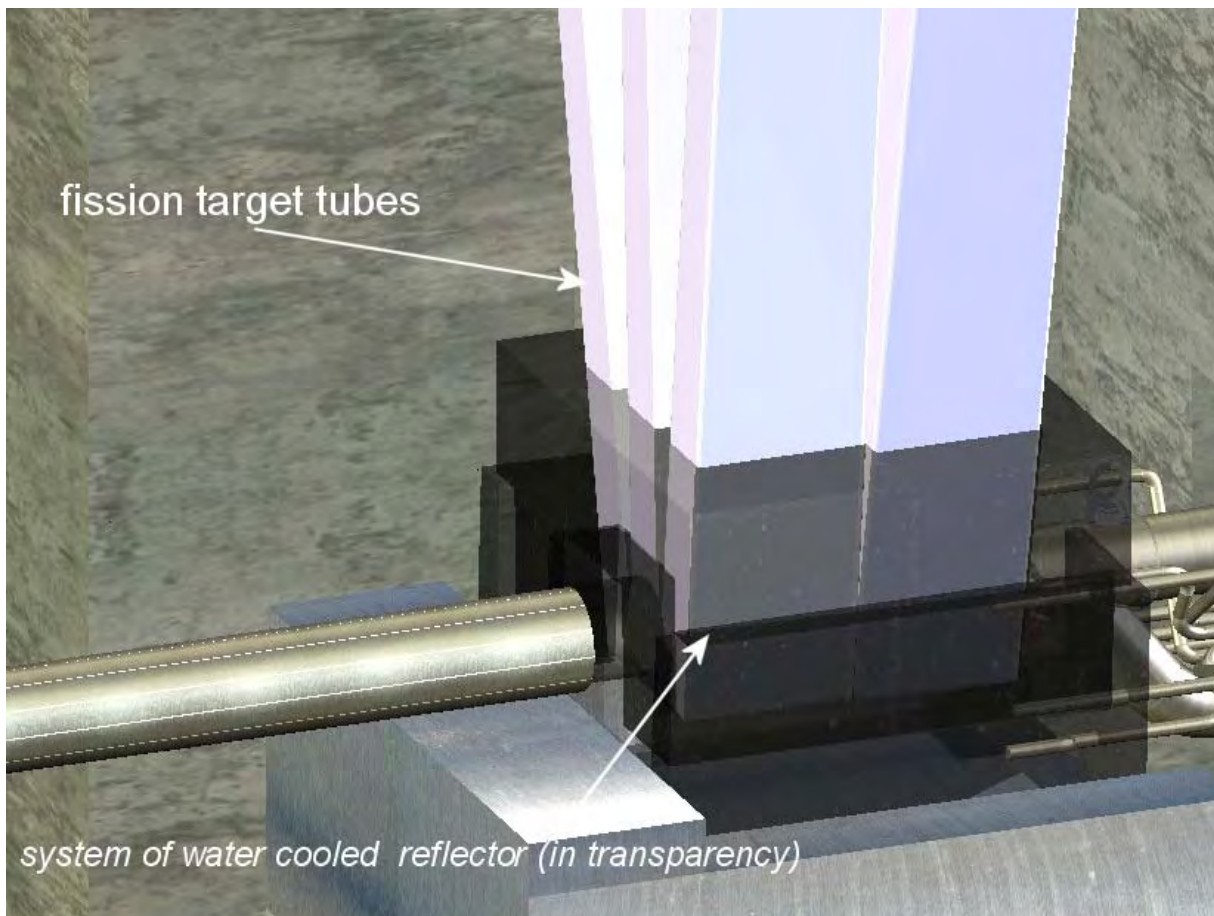
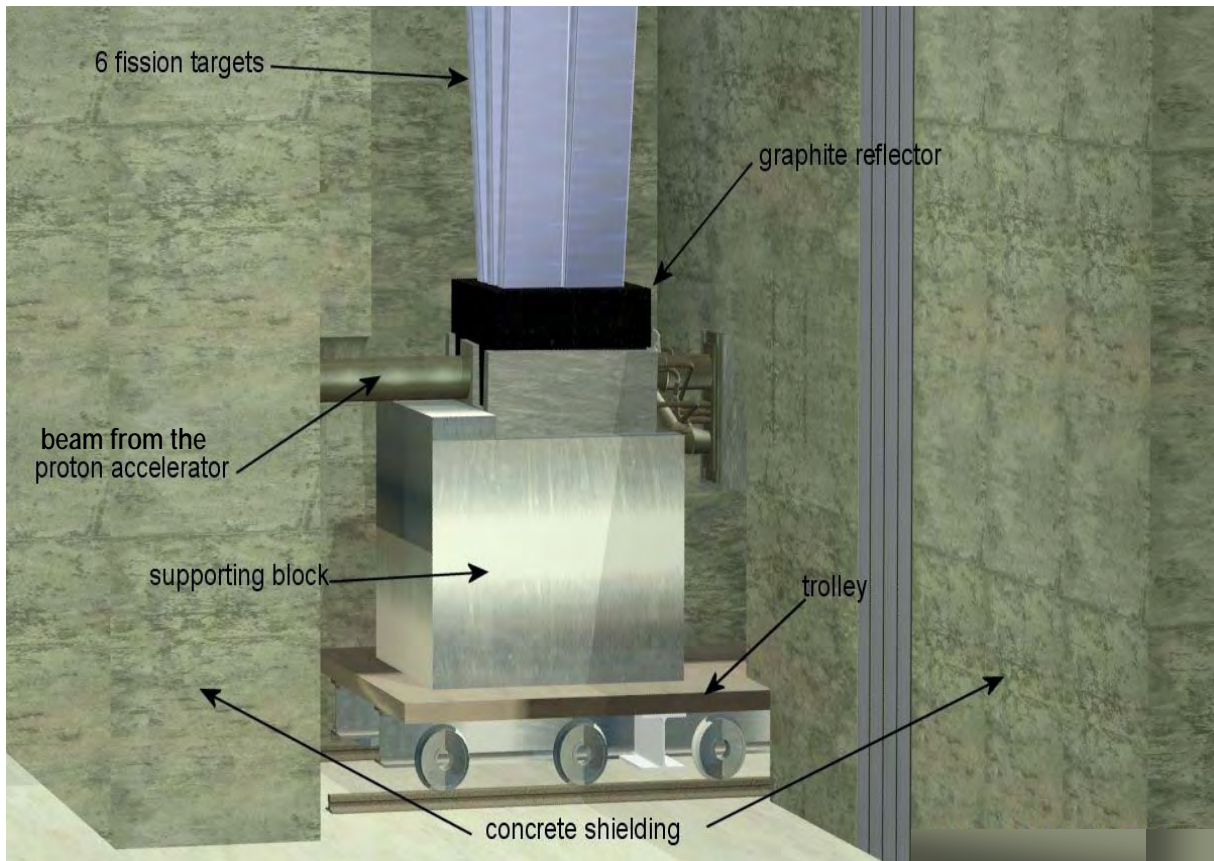


Fig. 1 (Top): The fission target assembly. (Below): Detail of the graphite reflector (shown here as transparent).

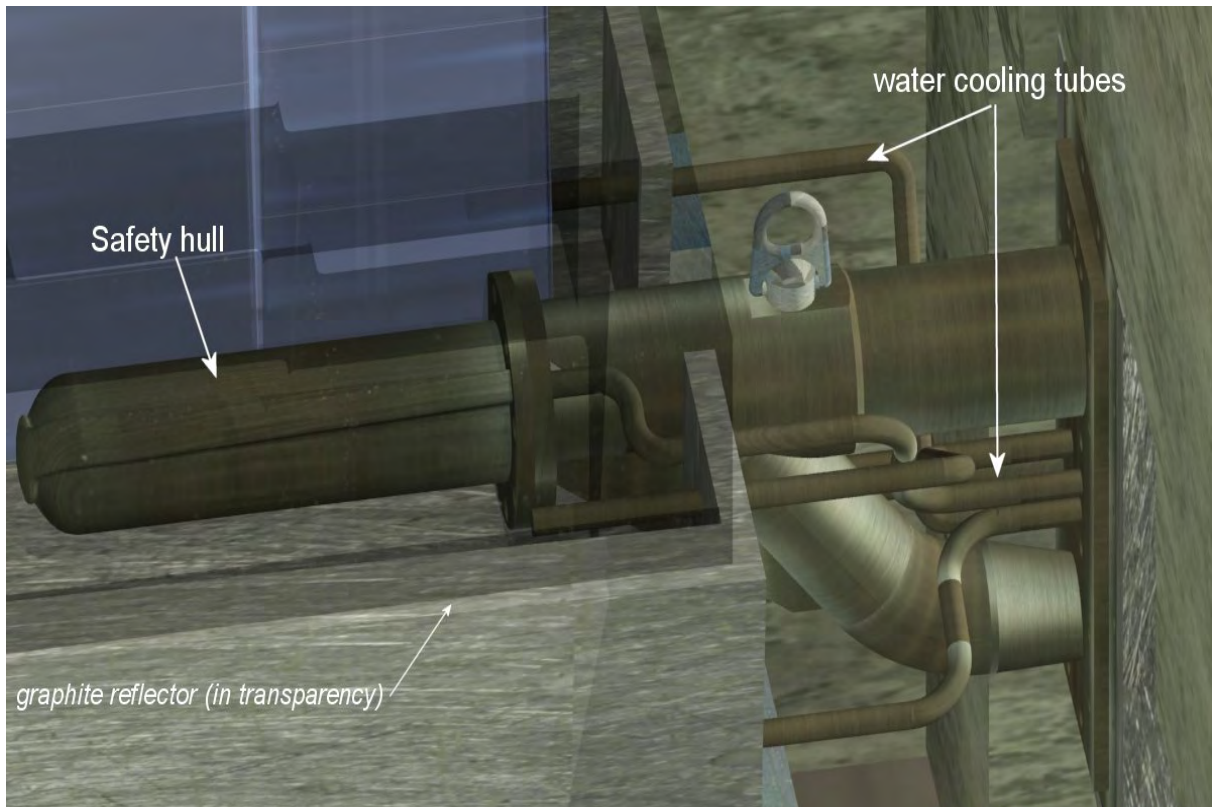


Fig. 16: The safety hull enclosing the liquid-metal target assembly, with the graphite reflector (shown here as transparent).

The facility is divided up into different shielded zones with appropriate restrictions placed upon the movement of personnel and material. Dedicated remote-handling devices and safety barriers aid in the minimisation of the contamination hazard and allow strict enforcement of the ALARA principle throughout the facility.

4.8 Conclusions

The multi-megawatt target group brought together specialists from three major institutes, viz. CERN, IPUL and PSI, whose fields of competence complemented each other in matters related to liquid-metal target development. Such technology is at the heart of advances in high-power targetry, and essential to achieving a valid design for the neutron converter target which was identified as a potential stumbling block early on in the EURISOL proposal.

Two designs have been successfully developed for the converter target and validated by a series of engineering tests. The designs have been reviewed and checked for thermal compatibility, hydraulic performance and structural integrity proving that the designs are able to fulfil the requirements set for the converter target. The engineering teams developed the “coaxially guided stream” target at PSI and the “vertical transverse film” target at IPUL, adopting two very different approaches for their respective development; the former relying on computer-aided tools, whereas the latter made extensive use of liquid-metal testing facilities available on site. Both approaches were successful and complemented each other usefully. For final testing, both designs were set up at the IPUL mercury laboratory facility and tested in representative conditions.

The integration of the converter target, liquid-metal loop and associated fission targets into a facility which can provide safe and easy access to researchers, whilst guaranteeing optimal extraction of the radionuclides was achieved by the design team at CERN. The experience of CERN in working with the FLUKA neutronics code was also valuable in ensuring that the goals set for the production of isotopes could be met. By being able to draw on the experience of the developers of the code, it was possible to put forward a convincing argument that the complex aspects of hadron physics were aptly covered by a team with an extensive and recognised experience in this field.

The production of complex and diverse isotopes by coupling a neutron converter target with fission targets has thus been demonstrated from the practical engineering side as well as the more theoretical neutronics aspect. The possibility of selling some of these radio-nuclides on the pharmaceutical market is a distinct possibility from the radio-chemical analysis conducted. However economic rationale alone will not drive the agenda for such a facility. It should be emphasised that the EURISOL project offers new possibilities for research into innovative medical treatments with radionuclides which have hitherto not been available in any quantity, as well as addressing more fundamental questions in basic science.

Chapter 5: The Fission Targets

5.1 General layout

In the production of radioactive ion beams (RIBs), an increase in the incident beam intensity on target does not necessarily lead to an increase in the RIB intensity [1]. In order to profit from the production potential of a 1-GeV proton beam of MW power, the concept of using a so-called “neutron converter” has been chosen. Here, the power of the primary proton beam is dissipated in and removed from a primary, cooled, liquid-metal “converter” target (e.g. Hg or a Pb-Bi eutectic) and the resultant neutron flux produces fission isotopes in an adjacent thick ISOL fission target, without destruction of the latter by overheating. The multi-MW liquid-metal converter target is described in the preceding chapter.

One of the main tasks of this project is the design of the fission targets which surround the converter target (figure 1). The converter and fission targets are both designed in a modular way, so that individual parts can be rapidly replaced and serviced by means of remote handling.

The EURISOL Design Study fission targets are derived from the concept proposed by the PIAFE (*Projet d’Ionisation et d’Accélération de Faisceaux Exotiques*) [2] and MAFF (*Munich Accelerator for Fission Fragments*) [3] projects. Each target, filled with ^{235}U or other actinide is inserted through a channel created in the shielding and located close to the neutron source at the position of maximum neutron flux (figure 2) [4]. The target modules can be inserted, replaced and serviced by means of remote handling. The shielding around the neutron-spallation source is a combination of iron and concrete with a total thickness of about 6 metres. The neutron flux (shown in figure 3) is reflected and thermalised in order to optimize ^{235}U fission, while for other fissionable target materials, like ^{238}U or ^{232}Th , a hard neutron spectrum is required. Up to six near-vertical channels are envisaged, each containing a MAFF-like production system. Loading and unloading all beam elements, including the fission targets, is accomplished within a mobile transport tube. The assembly is then moved into a hot-cell where remote handling of the components can be performed under visual control.

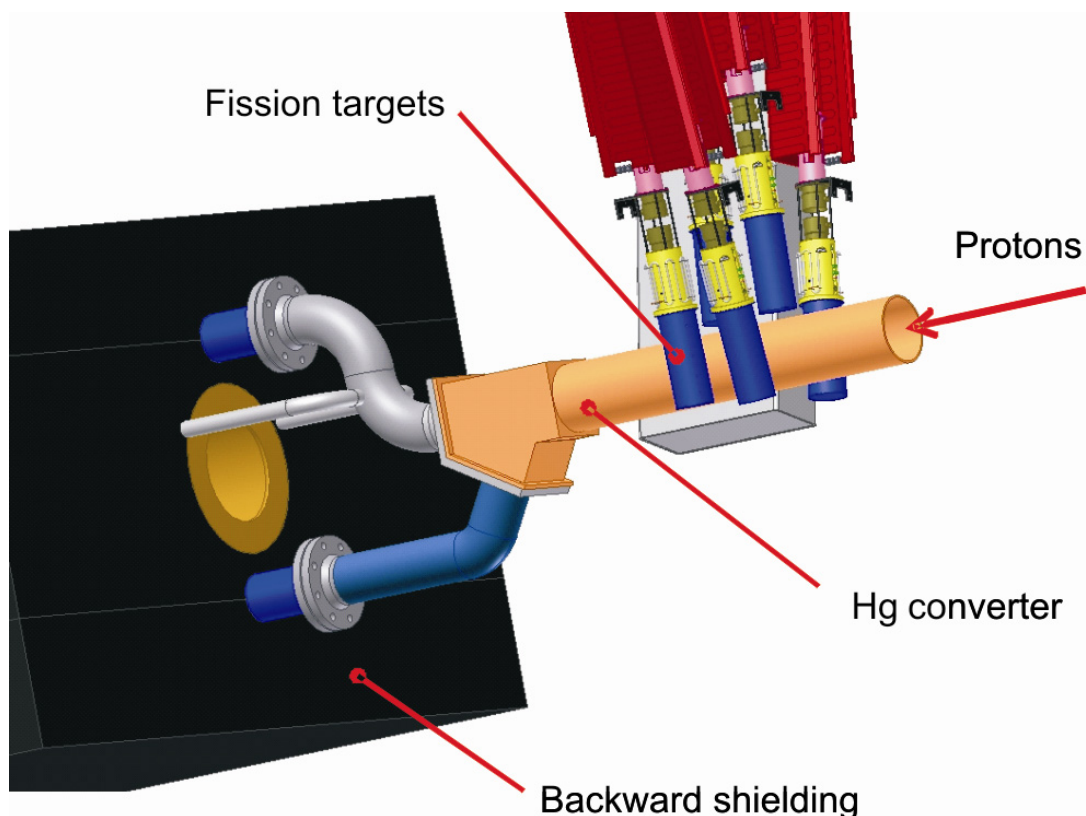


Fig. 1: The positions of the six fission targets around the Hg “converter” target.

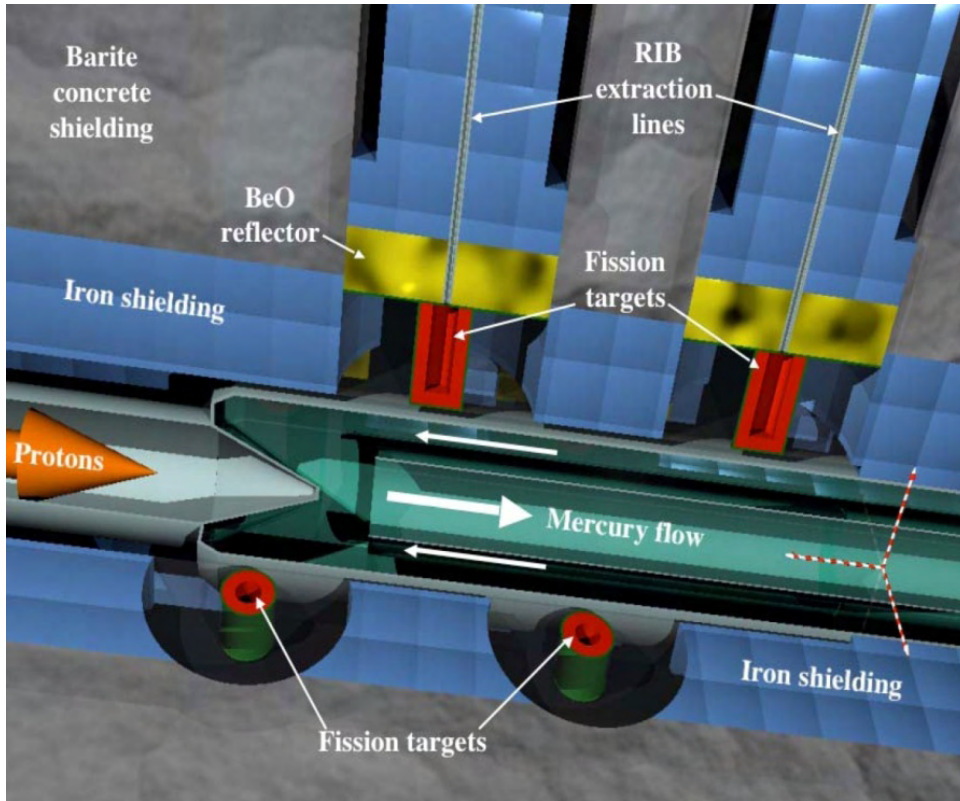


Fig. 2: Conceptual set-up of the converter and target integration.

In the operational position, all components are inside a double-walled vacuum tube embedded in the concrete shielding. A cooling water system is required to evacuate the 30 kW of fission heat from the expected 10^{15} fissions per second. In view of the radiation levels, vacuum pumps have to be placed behind the shielding. In order to capture the gases continuously emanating from the fission target during operation, cryopanel are distributed inside the vacuum tube. This system not only improves the vacuum but also traps and confines the radioactivity from gaseous elements.

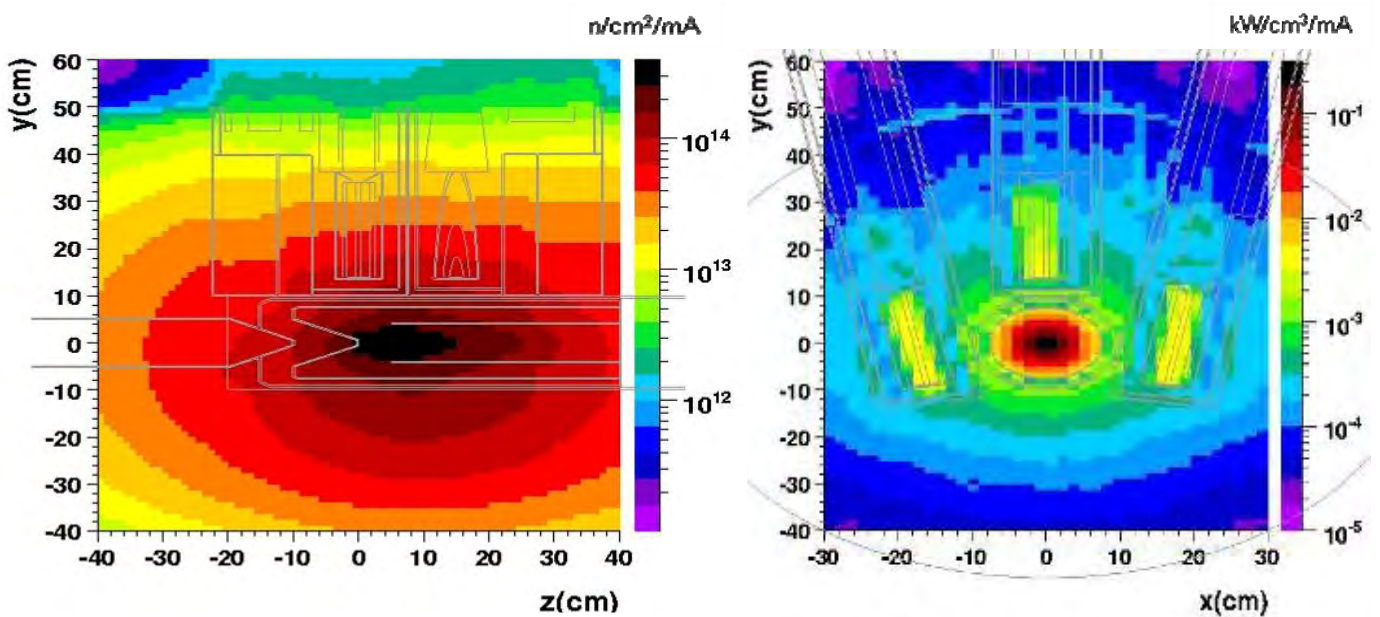


Fig. 3: Neutron fluence (left) and total power density (right) on the inclined targets.

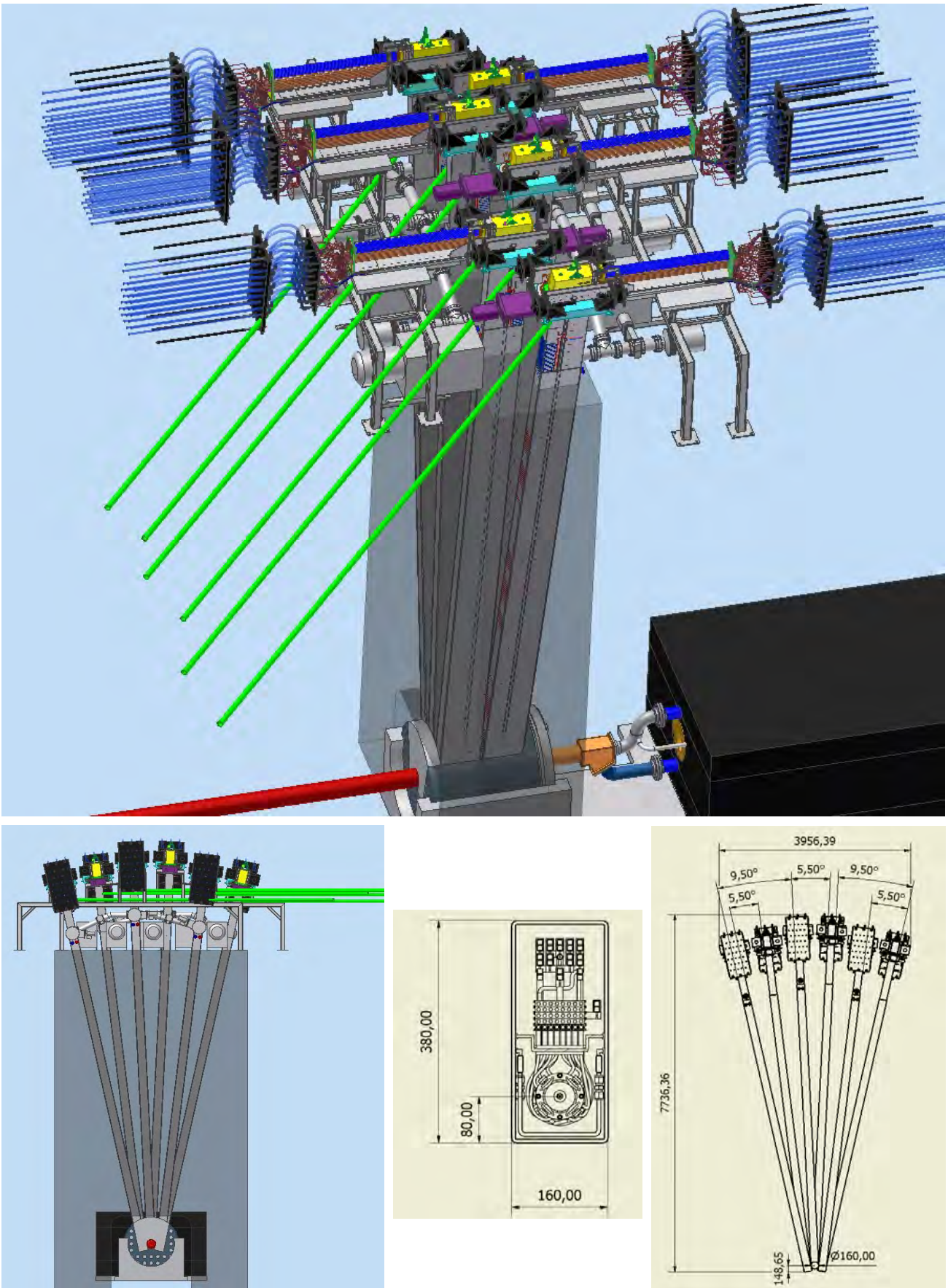


Fig. 4: The targets are inserted from above through the thick shielding around the converter via rectangular, inclined vacuum tubes – shown in section at lower centre.

By installing each fission target asymmetrically in a rectangular vacuum tube as shown in figure 4, the distance between the fission targets can be significantly decreased without decreasing the space available for services. The main limitation remains the fact that the fission target is operated at high voltage while the stainless steel water-cooled vacuum tube is grounded. In the present design the distance between them is about 4 cm, for an external width of 16 cm, equal to the converter target diameter. In this respect, the vacuum quality around the fission target is essential, and cryopanel have therefore been installed as close as possible to the fission target.

To avoid any increase of the distance between targets, and to allow for gate valves and mechanical couplings at the upper end, the vacuum tubes have to be tilted. As shown in figure 4, a maximum inclination angle of less than 12° increases the distance between the tubes to about 80 cm at the top, while at the bottom end the slight changes in target position do not change the overlap with the axially symmetric spallation neutron flux. The second important advantage of vacuum tube inclination is that it allows all six radioactive ion beams to be extracted in the same direction. The horizontal (green) tubes shown in the figure represent the six beam lines leading to a beam-preparation area.

Calculation with the FLUKA Monte-Carlo code, using a geometrical model which included many of the design details, revealed that a fission rate of $\sim 10^{15}$ fissions/second/mA can be obtained. The maximum incident beam power will be 4 mA, but a total fission rate larger than 10^{15} fissions/second cannot be withstood by the fission target, owing to thermal limitations. Therefore many of the design parameters can be relaxed slightly, without compromising the main design goal.

5.2 The fission target

The flexible approach resulting from the multiple fissile targets inspired by the MAFF and PIAFE projects allows neutron spectra from thermal to hard to be produced with a variety of suitable actinides. The isotope production rates have been investigated and the various options yield up to orders of magnitude differences in specific cross sections (due to the difference of thermal-neutron-induced ^{235}U fission versus hard-neutron-induced ^{238}U fission). The individual target units have been designed to handle 10^{15} fission/s for a ^{235}U target in a thermal-neutron flux. A reduction of the fission rate by one order of magnitude is expected for other actinide targets used with hard neutrons.

The release time for the isotopes is driven by diffusion and effusion. The decay losses will depend of the chosen actinide, its isotopic distribution, stoichiometry, mass and geometry. Because similar actinide masses and target volume are involved, the typical release parameters (and decay losses) were found to be close to those of standard targets. Several structures and compositions for fission material have been investigated in collaboration with a number of European institutions [5]. Different fission target materials were examined: MKLN (special graphite), POCO foam (graphite foam) and high-density UC pellets. In the first two cases, the fissile material is highly enriched ^{235}U uranium dispersed in a graphite matrix with an apparent density of about 2 g/cm^3 . For the high-density UC pellets, the fissile material consists mainly of ^{238}U enriched with ^{235}U and a density of 12 g/cm^3 . One common feature is that each target is enriched with 15 g of ^{235}U . The proposed target geometry (figure 5) consists of 86 disks of graphite matrix 1 mm thick and loaded with enriched uranium. In between the UC_x disks, 1.3-mm thick ‘Grafoil’ disks are used so as to retain a high thermal conductivity, for better heat dissipation. All the disks have a 35-mm external diameter and an 8-mm inner hole to allow effusion of fission products towards the singly-ionising ion sources. The disks are pressed together inside a 2-mm graphite container and then enclosed inside a 1-mm tantalum container of 200-mm length. For safety reasons a second, external, molybdenum container is also provided. The fission target has been designed to operate at 100 kV.

Under normal operation, fission produces about 30 kW in the target, raising the temperature to more than 2000°C : this is the temperature required to obtain fast release of fission products. In cases where the fission rate is lower – e.g. due to lower intensity of primary beam or due to target burn-up – the working temperature has to be attained through external heating. The heating is achieved by bombardment with electrons emitted by a filament. The target has to be at a slightly higher positive voltage compared to the filament and the external container at lower voltage. Currents of several hundred amperes would be needed to compensate for the full fission power of 30 kW, if necessary.

This filament can be used also as a diagnostic device: in case of deformation of the target container (either external or internal) contact with the filament will be made, generating a short-circuit.

The lifetime of the fission target/ion-source (TIS) is expected to be 3 months. The burn-up for the 15 g of ^{235}U at a fission rate of 10^{15} fissions/sec will be about 30% during a 3-month period. Tests with a massive high-density uranium carbide target kept at high temperature for a long period showed no modification of release properties [5]. The calculated neutron fluences over 3 months of operation at maximal power are below the acceptable limits for radiation hardness of all the materials involved.

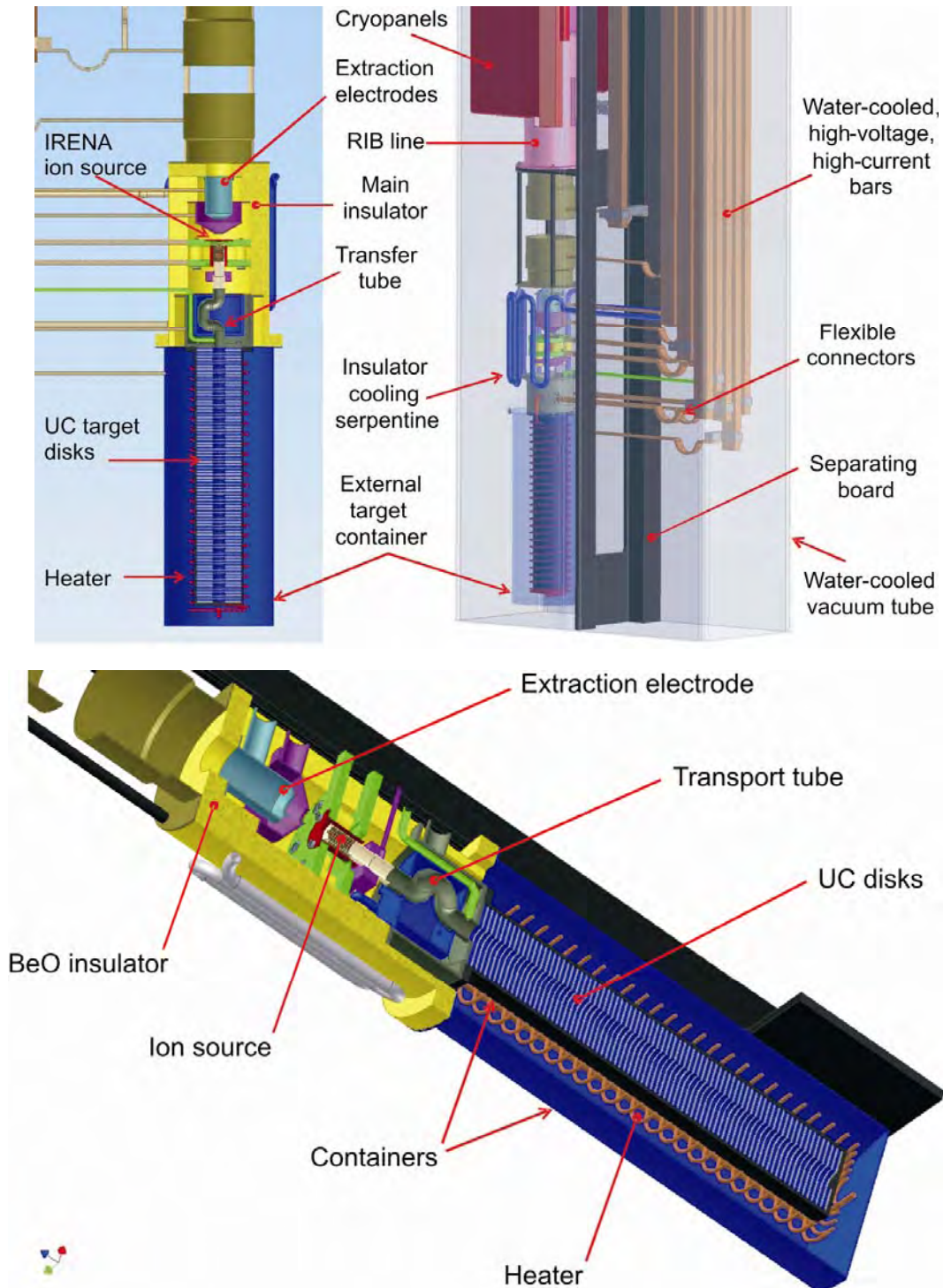


Fig. 5: (Top-left) Cross-sectional view of the fission target/ion-source assembly. (Top-right) View of the same assembly with the vacuum tube and main insulator not shown. (Below) Layout of the fission target.

5.3 Ion sources

Different kinds of ion sources (e.g. laser, plasma, ECR ion sources, etc.) are planned, which can be installed close to the target to ionise the selected fission products to a 1+ charge state. These ion sources will have to deal with intensities of streams of both radioactive and stable elements which are 3 orders of magnitude higher than today's systems.

Ionisation of fission products has to be done in an ion source closely coupled to the fission target. The very high neutron fluxes, and the important gas load due to high fission rate and vaporisation of massive UC_x target materials, limit the number of ion sources to be used. Currently 3 types of ion sources are considered [6]: the surface ioniser, the laser ion source and the FEBIAD source.

The surface-ionisation ion source is the easiest to integrate but limited to alkali, alkaline-earth and rare-earth elements.

The laser ion source is expected to cover 80% of the EURISOL facility's needs. It has the advantage of selectivity, proven capability for working under a high gas load and all the sensitive components are far from the high neutron flux. On the other hand its efficiency is in many cases only 5–10%. However, efficient operation for the multi-MW target station has still to be investigated. Indeed the proposed target thickness is an order of magnitude larger, and the goal intensities for radioactive beams up to three orders of magnitude higher, than in existing installations.

The radioactive-ion laser ion source (RILIS) set-up is well described in reference [4], and a sketch of the layout is given in figure 6. For high-current operation, the on-line RILIS at ISOLDE-CERN shows no evidence of efficiency drop up to an extracted beam of 100 nA, and this is not an upper limit. Furthermore, even in the case of yields over 10^{15} fissions/s, pure radioactive beam intensity should remain significantly below $1 \mu A$ with a RILIS, owing to the selective ionisation. However, the total extracted beam can reach much higher intensities by the production of unwanted ions. In particular, the production of alkali ions by surface ionisation can easily lead to serious beam contamination. Such contamination is all the more severe as Rb and Cs isotopes are abundantly produced by fission. Studies of ionisation cavity material have been initiated to minimise surface ionisation, and development of processes to trap the alkalis is continuing.

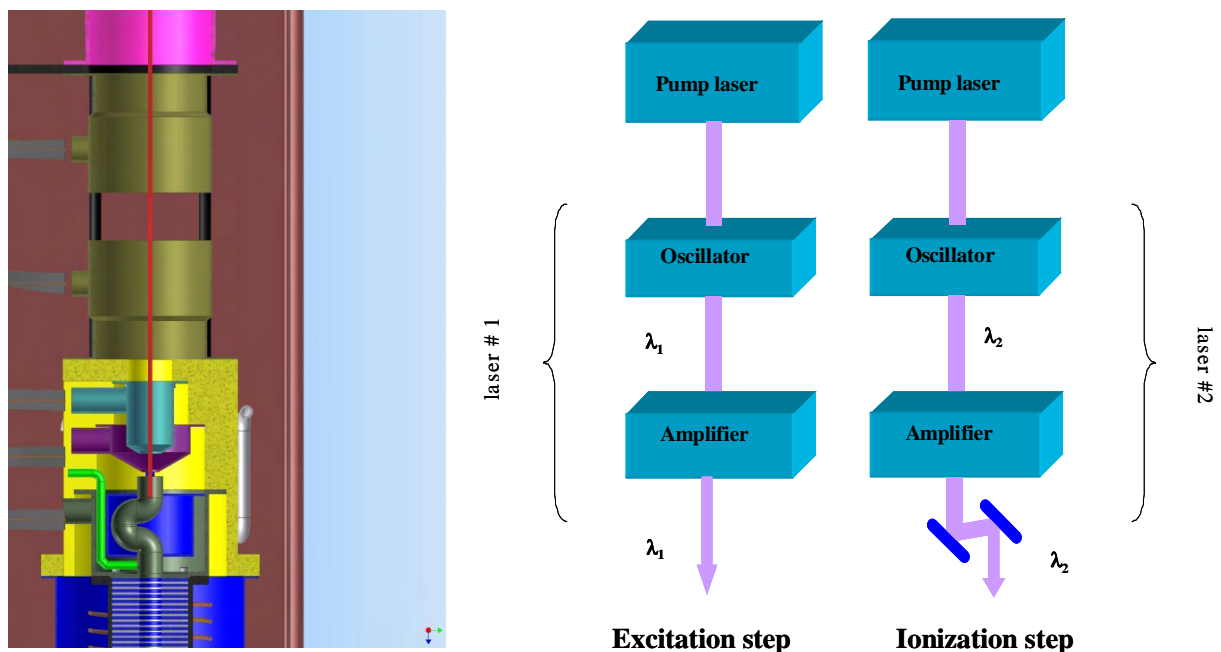


Fig. 6: Layout for the laser ion source and the basic laser scheme of a RILIS with 2 wavelengths, for excitation and ionisation, respectively.

The FEBIAD type ion sources have high efficiency but no selectivity. The use of a cooled transfer tube for trapping the non-gaseous elements can be very useful. IRENA is a FEBIAD ion source developed at IPN-Orsay [7]. The curved transfer tube passes through a small volume where helium gas is circulated for cooling. The tube is directly connected to the anode. The cathode (in red in figure 5) is heated and polarised at a few hundred volts lower than the anode potential, repelling the electrons. Heating of the cathode requires currents of the order of hundreds of amperes. The IRENA ion source components are made of tantalum. Similarly to the target, the required current and high-voltage power are brought close to the ion source by copper bars, each cooled by an internal water loop. Electrical connection between the copper bars and TIS components is done by the means of flexible tantalum connectors with large cross section. An additional pipe (green in figure 5) is used to inject a controlled gas flow into the ion source for tuning purposes.

5.4 Beam extraction and transport

The first extraction electrode is placed a few millimetres away from the ion source. In order to preserve alignment, the ion source and first extraction electrode(s) are mounted on the same large insulator. This same insulator supports the target, its heater and external target container as well. Beryllium oxide is considered to be a suitable material for this insulator, since it is able to resist neutron fluences up to 10^{22} n/cm². This limit is 10 times larger than the fluence calculated at the insulator position, for a period of three months of operation.

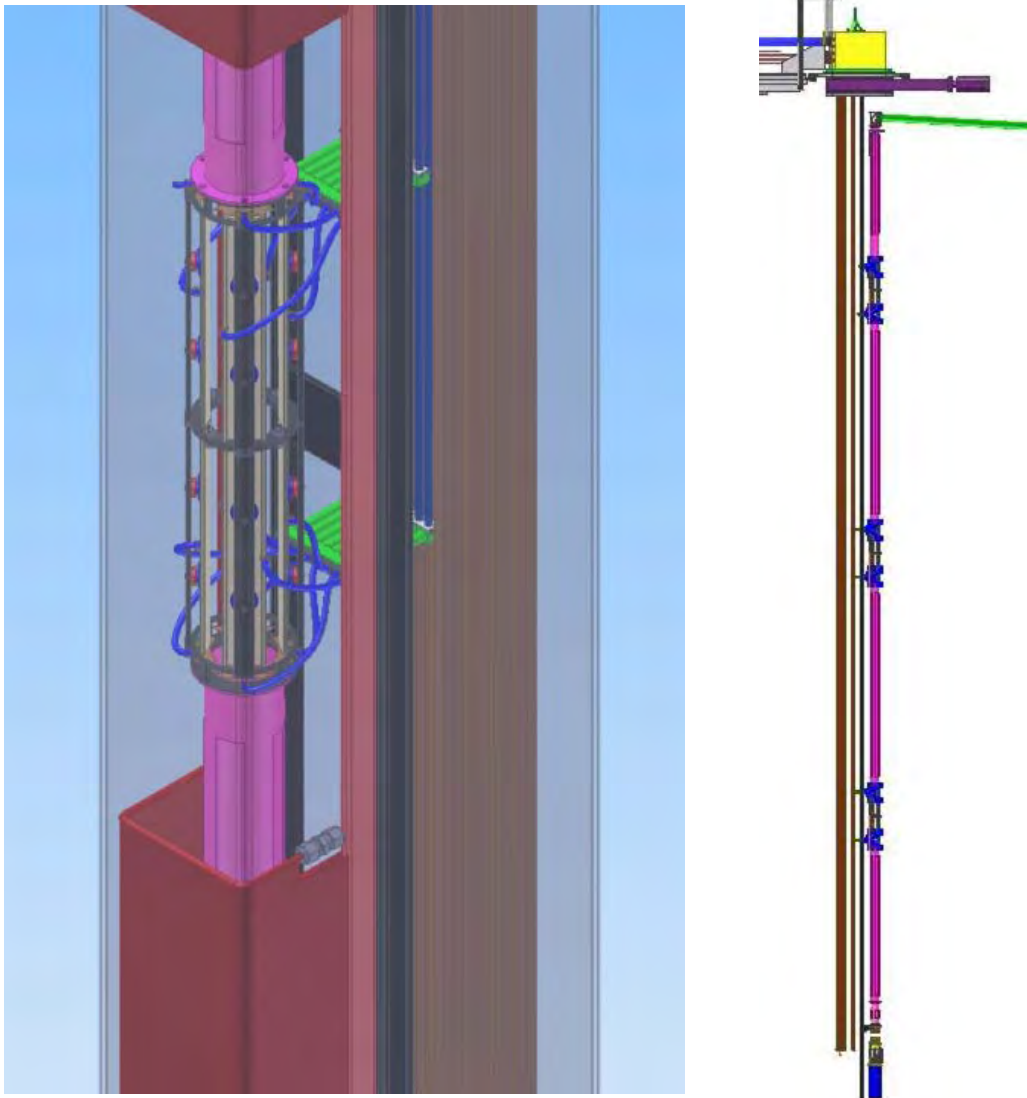


Fig. 7: (Left) One of the electrostatic quadrupole doublets (grey) placed along the RIB line (magenta). (Right) The position of the three quadrupole doublets and the $\sim 90^\circ$ electrostatic deviation.

This insulator is in contact with both hot target and cathode, and therefore has to be cooled. This need brings the water very close to the fission target with the consequent risk of a water leak onto the hot uranium target. Since the cooling serpentine is on the external side of the insulator, any such a leak will first allow water to make contact with external target container, delaying the contact with uranium. Vaporization will take place in the large volume of the vacuum tube, suddenly degrading the vacuum level and consequently the primary beam will be stopped. The water is used also for the cooling of cooper bars feeding and polarizing the TIS components. The rectangular shape of the vacuum tube has the advantage of allowing a separating panel between these bars and the radioactive beam line, which will also act as a screen for the fission target in case a water leak occurs at the level of these bars.

As shown in figure 5, Einzel lenses are employed after the extraction electrodes. To transport the beam through some 6 metres, other focusing elements are required. In the current design, three electrostatic quadrupole doublets are installed along each near-vertical RIB line (see figure 7). To control beam centring, fixed insulated collimators (each split into 4 quadrants) are placed at the entrance and exit of each doublet. To read the current on these slits and for powering the quadrupole elements, many additional HV and current bars are required (in blue on figure 7). Because the current in these beam transport elements is low and they are already far from the maximum neutron flux, cooling is not considered necessary for them. It should be mentioned that the RIB pipe (magenta in figure 7) has only a screening role against the electromagnetic fields that may be induced by the high-voltage line (bars) parallel to the beam axis. Apart from this, the line is open to the vacuum in the tube.

At the upper end, the RIB is rotated into the horizontal direction by an electrostatic deviation as shown schematically in figure 4. Because the beam lines before deviation are not strictly vertical, the bend angle is close to 90° , but each of the six RIB lines has a slightly different angle.

All these RIB transport elements have a limited lifetime and have to be exchanged, or may require cleaning or realignment. In order to do this they will be transported into the hot-cell, together with the TIS. On the horizontal line, other beam focusing elements have to be installed (not included in the present design) in order to transport the beam to the RIB preparation area (where the separators, switchyards, charge breeder and/or the merger of the six beams are located). These additional elements cannot be moved to the hot-cell together with TIS, and their maintenance has to be done using other procedures, with remote handling, etc. Beam preparation is described in Chapter 6.

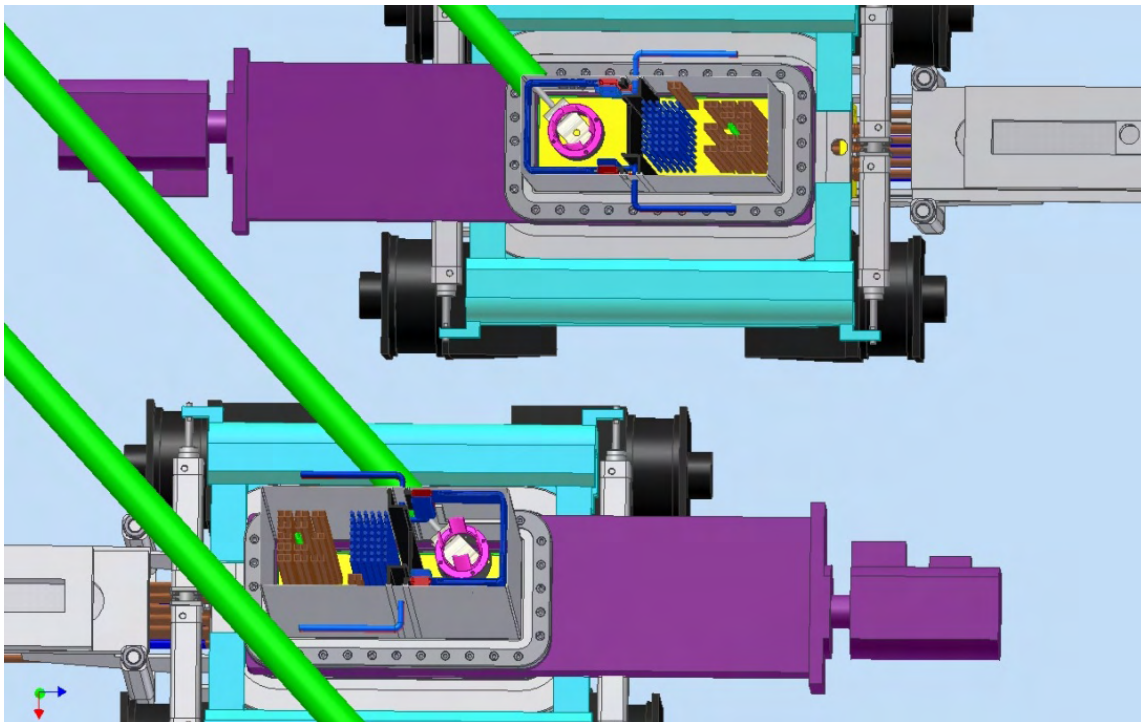


Fig. 8: View of the assembly in figure 3, seen from below, with a slice in the horizontal plane, through one pair of rectangular vacuum tubes (grey).

A slice through a horizontal plane of the assembly in figure 3, viewed from below, gives the image shown in figure 8. Here only one pair of adjacent vacuum tubes is shown, the other two pairs having similar relative geometry. The extraction of all 6 horizontal RIB lines (green tubes in the two figures) in the same direction simplifies the beam transport toward the RIB preparation area. The direction of extraction is given by the constraint that the radioactive beams may not cross regions where the current bars are located. The best direction seems to be at 45° with respect to the incident proton beam direction. Then all other elements such as vacuum pipes, gate valves, etc. are placed so as to allow the passage of the RIB lines.

5.5 Vacuum system

To obtain a high vacuum in the target channels, each of them is connected to a turbomolecular vacuum pump and its fore-pump. Additional shielding may be required to reduce the dose absorbed by these pumps. In case of failure of one of pump, an adjacent pump can be used by the two neighbouring tubes by remotely opening the relevant gate valves (normally closed). The output of the vacuum pumps has to be collected in a storage tank because it will contain volatile radioactive isotopes.

Target outgassing during operation – due to the high fission rate and high temperatures – requires a high pumping speed to assure good vacuum. Being placed so far from the targets (about 7 m), the pumping speed of the vacuum pumps at the level of the fission targets is very low. Large cryopanel are installed in the vacuum tubes providing a large pumping speed. Figure 9 shows the position of the cryopanel along the vertical RIB axis, between the quadrupole elements. Placing cryopanel closer to the target is limited by the power deposited by the high neutron and gamma fluxes, as well as the power radiated by the hot target [8]. The upper cryopanel (blue in figure 9) uses liquid helium to trap the inert gases that do not condense on the cryopanel using liquid nitrogen (red in figure 9).

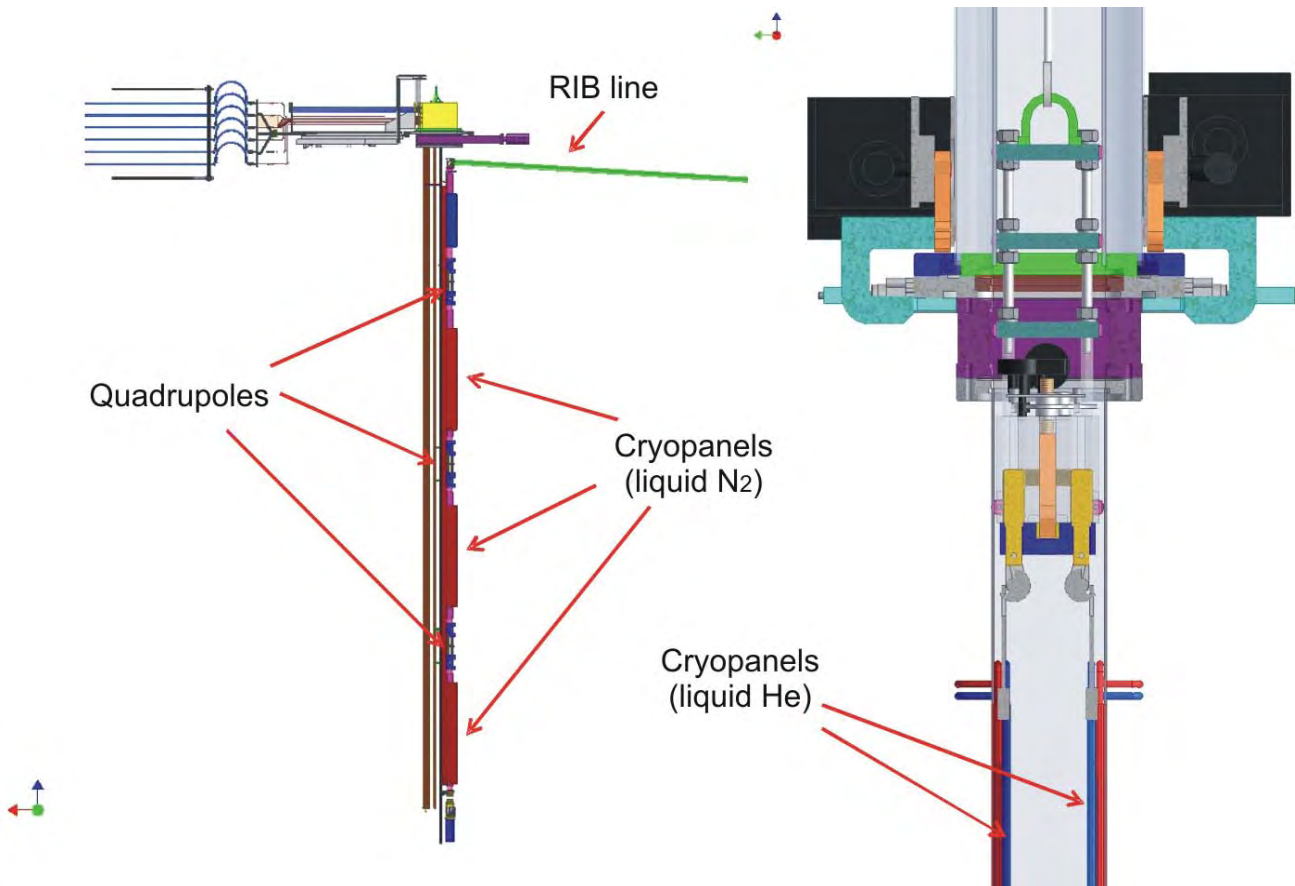


Fig. 9: (Left) Cryopanel installed inside vacuum tubes along the RIB line. (Right) The use of a hook to extract the cryopanel, only if needed, after removal of the target/ion-source assembly from its working position.

The cryopanel has an important role for trapping radioactive elements close to the emission point, i.e. the fission target. The longer they are kept cold, the more radioactive elements will decay there, diminishing the radioactivity level in the vacuum pumps and storage tanks. Because of this, in the current design it is assumed that, after each period of operation, the TIS will be moved to the hot-cell without the cryopanel, which may thus remain cold. In case of failures of cryopanel, an independent system is provided to extract the cryopanel (see figure 9) for repair and exchange in the hot-cell.

When the target is in its working position, the vacuum tube is sealed by the flange of a connection box. An elastomer O-ring can be employed, and changed inside the hot-cell. On the other hand, the gate-valve fixed to the vacuum tube will require a metal seal. The connection between a mobile tube at the upper end of the fixed tube has to be vacuum-tight in order to avoid contamination of handling area. A system of remotely-controlled clamps, shown in figures 10, will press the flange of the mobile tube against the flange of the fixed tube. The mobile tube will also have to be equipped with a pumping system including a small gas-storage tank: after mechanical connection has been made, and before pulling out the fission target, the air between the two gate-valves will have to be pumped out.

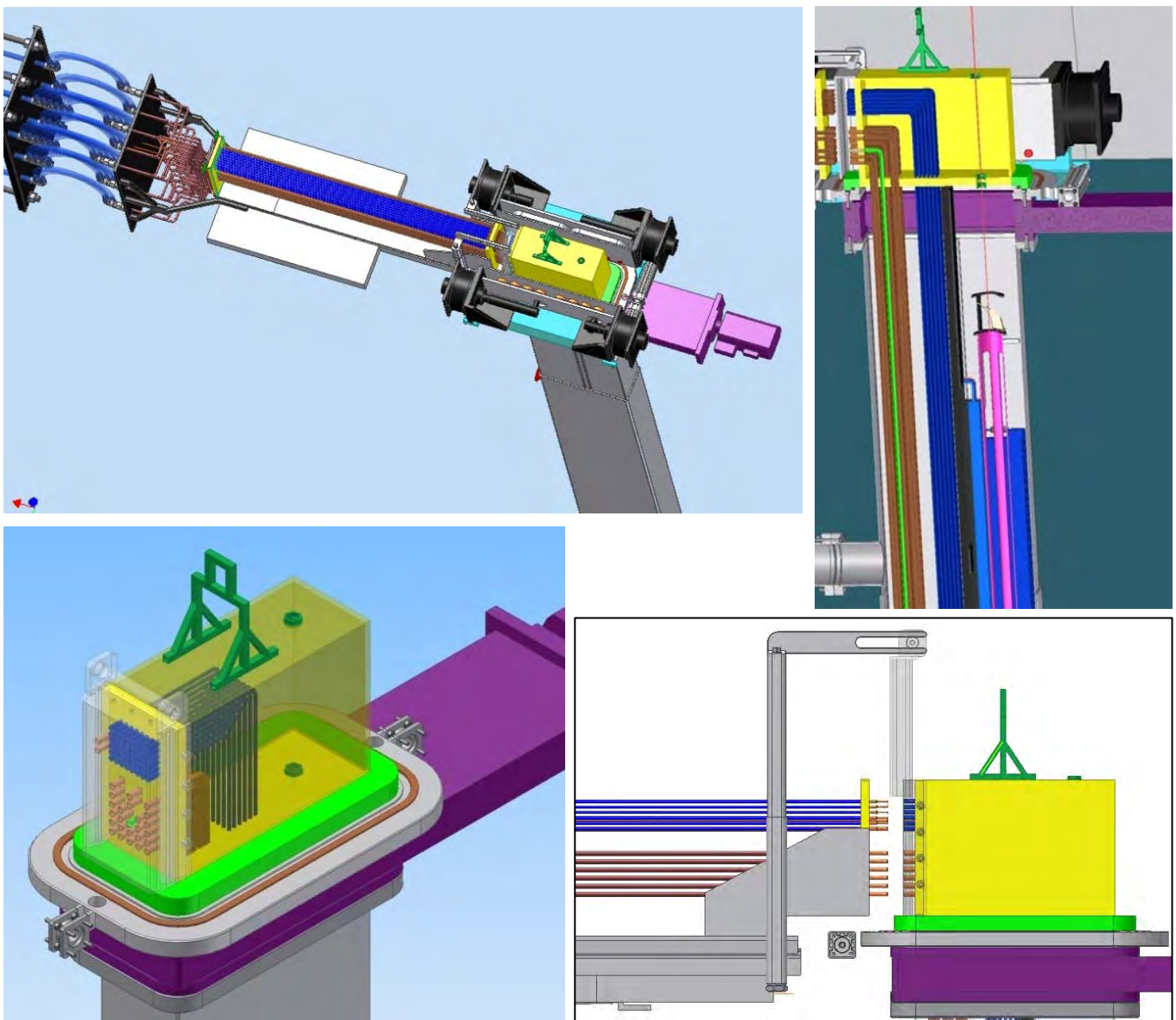


Fig 10: The connector-box has a flange and remotely-operated clamps to seal the rectangular target channels tightly. The electrical and gas feedthroughs are on the bottom face, and the automatic socket-connectors are on a lateral face.

5.6 Remote handling and target disposal

For target/ion-source exchange, after disconnection of the automatic connectors, a mobile tube is connected on top of the target channel. A hook is lowered inside the mobile tube (see figure 11) to catch the U-shaped loop on top of connector box and to pull the TIS into the mobile tube, together with many other components, including the connector-box. The inside of the mobile tube, as well as the inside of the hot-cell and the surface of the connection box will, of course, be contaminated. When the assembly is removed, this contamination can spread into the handling area. It is therefore extremely important to minimise its contamination by various means. One precaution is to cover the socket connectors, on which contamination could more easily accumulate, with a gate – as shown in figure 10, bottom right. The gate has 3 rather small holes on its upper face in order to allow fast air evacuation when pumping for vacuum, but to limit the contaminated air flow over the connectors when the box is in a hot-cell or inside the mobile tube under inert gas atmosphere. Before lowering the fission target inside hot-cell, the inert gas can be injected into the mobile tube through a small-diameter pipe inserted into one of the 3 holes, creating a dynamic barrier for connector contamination.

Several hot-cells will be needed. One of them will be used for TIS exchange. The mobile tube carrying the TIS has to be coupled above the hot-cell and then the TIS lowered onto it. At the upper entrance to the hot-cell will be a duplicate of the mechanical coupling system on the target channel. Additionally, a rotation system inside the hot-cell will give access to any side of the TIS during handling with telemanipulators. In figure 12, the entrance systems above the hot-cell are shown. After being dismantled inside the hot-cell, the TIS will then be enclosed in a transport container and remotely transferred to a nearby temporary storage area. The pumping system coupled to the hot-cell entrance is used to create a vacuum inside the mobile assembly before it is disconnected, with a new TIS inside it. Thus, except inside the hot-cell, the fission targets are handled only in vacuum.

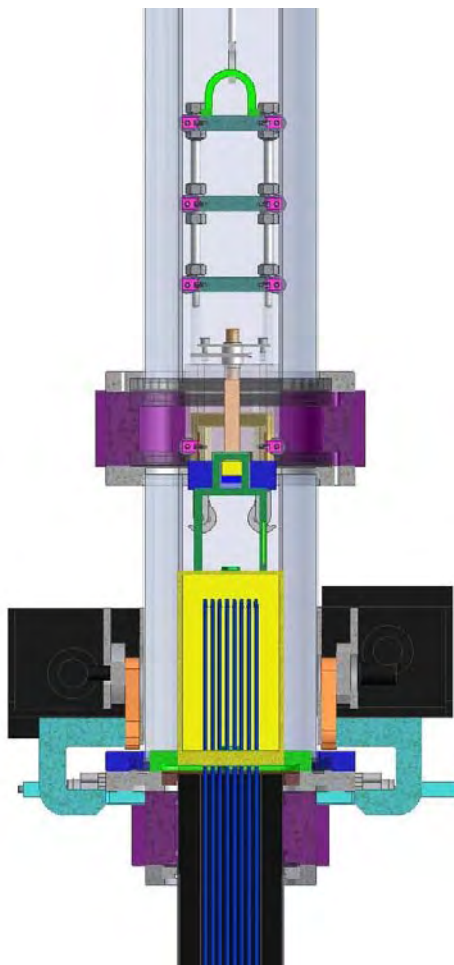


Fig. 11: Cross-sectional view of the mobile tube installed on a target channel.

In order to exchange other components such as quadrupoles or the O-ring on the flange of the connection box after a used TIS is removed, the remaining assembly has to be lowered further, so as to bring the desired component in front of the hot-cell window. These operations require a pit under the hot-cell, as shown in the upper part of figure 13. In fact, it is proposed that there should be two hot-cells equipped with the special vacuum-tight entrance: one of normal size ($\sim 2\text{-}3\text{ m}^3$) where the TIS can only be exchanged – to be used when no other operations are required – and a longer one where the exchange or maintenance of any component can be done.



Fig. 12: Vacuum-tight vertical entrances to the hot-cells.

Two more hot-cells are considered necessary for conditioning of spent targets, ready for transportation off-site or simply for safer temporary storage on-site. These two hot-cells do not need vertical vacuum-tight access. In figure 13 the layout of the four hot-cells and the temporary storage bunkers is shown. A system of rails will allow remote-controlled transportation of activated components.

After exchange, the new target has to be tested before mounting it in the final working position. To this end, a testing vacuum tube is located near the hot-cells. The testing tube is equipped with all the necessary systems: vacuum, automatic connection system, laser beam, etc. such that the target can be heated and conditioned, while ion sources and RIB extraction and transport elements can be fully tested. Additionally, beam diagnostics are mounted at the upper end to control the intensity, position and focusing of the extracted ion beams.

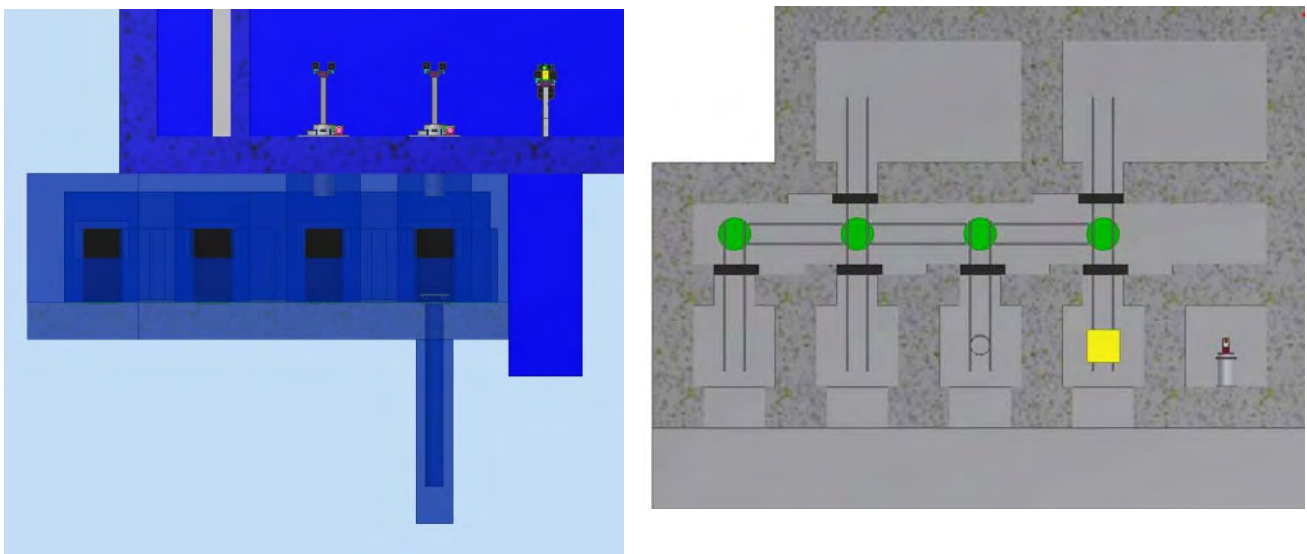


Fig. 13: Layout of hot-cell and temporary storage areas in section (left) and in plan view (right).

5.7 Production yields

Individual nuclide production yields in two-step reactions have been determined using the FLUKA code applied to the geometry depicted in figure 14.

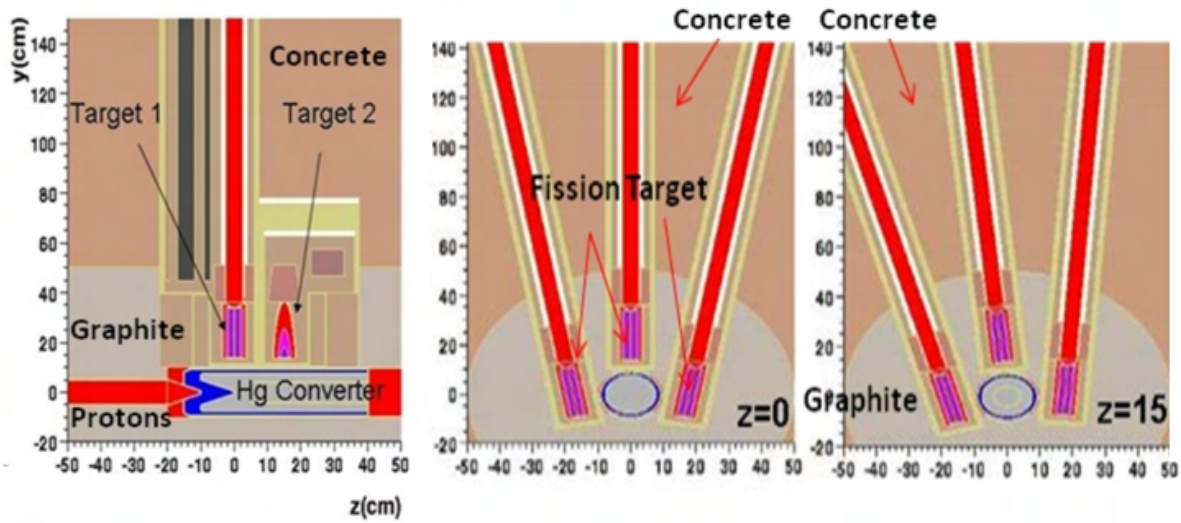


Fig. 14: Geometry used in FLUKA simulations. Left: vertical cross-section in the proton beam direction. Right: vertical cross-sections perpendicular to the beam, at $z=0$ and $z=15$ cm, respectively.

The distribution of nuclides produced by fissions is concentrated in a relatively narrow area of the nuclide chart. Four isotopes of interest recommended by the NuPECC board were analysed: Ni, Ga, Kr and Sn. Detailed fission rates were determined from simulations as a function of the neutron energy and the integrated spectrum to give a thorough characterisation for the ^{235}U case. Using graphite as external reflector, more than twice the number of fissions on target can be obtained with respect to the configuration with no reflector. The highest rate is 6×10^{14} fissions/mA in each target (i.e. 2.4×10^{15} fissions/second at full power). A graphical representation of fission density using graphite as reflector can be seen in figure 15.

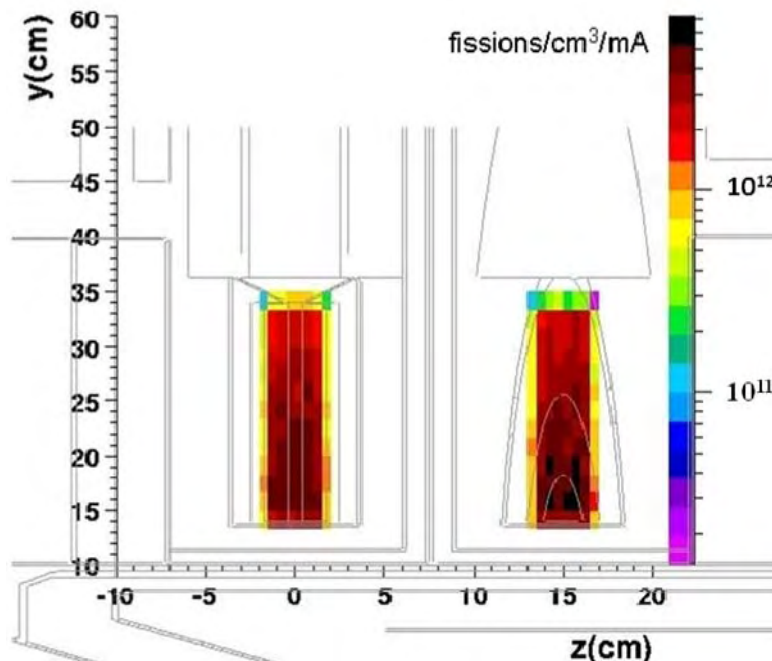


Fig. 15: Graphical representation of the fission density for the two groups of targets.

Table 1 shows the results of calculations for various nuclides of interest. The calculations of the intensity predictions are based on the experimental yields measured at IRIS (in Gatchina) [5] and ISOLDE (at CERN) [9] and the target parameters listed above.

Table 1: In-target production yields for the representative nuclides and the intensities delivered at the extraction from the ion source.

Nuclide	In-target [atom/s]	Release eff. [%]	Ionisation eff. [%]	Intensity [ions/s]
Ni - 74	2.2×10^9	20	7.8*	3.5×10^7
Ga - 81	1.0×10^{11}	10	21*	3.8×10^9
Kr - 90	4.8×10^{13}	90	80**	3.5×10^{13}
Sn - 132	7.2×10^{12}	70	9*	4.5×10^{11}

* RILIS

** ECR ion sources

In this table, the in-target production rates (atoms/s) calculated by FLUKA are shown. The release efficiencies are deduced from the measurement at IRIS-Gatchina and from RIBO [10] calculations presented in Refs. [11, 12]. The ionisation efficiencies are taken from literature for 1+ ion sources. The last column shows the calculated intensities (ions/s) delivered at extraction from the ion source with charge state 1+.

References

1. D. Ridikas, W. Mittig and N. Alamanos, "RNB production with a powerful proton accelerator", report DAPNIA-SPHN-2000-59, CEA Saclay (2000).
2. "Radioactive beam production using a uranium fission source placed in the ILL high flux reactor", Technical report ISN 97-52, July 1997.
3. H.J. Maier et al., Nucl. Instrum. & Meth, **A 438** (1999) 185.
4. O. Alyakrinskiy et al., "Improving design of EURISOL fission target adopting MAFF concept", EURISOL-DS technical report 04-25-2009-0016.
5. A.E. Barzakh et al., "Report on the R&D of uranium carbide targets by the PLOG collaboration at PNPI-Gatchina", EURISOL DS technical report 04-25-2007-0005.
6. C. Lau, "Ion sources: RILIS and others", presented at EURISOL DS Joint Meeting JM-22.
7. M. Cheikh Mhamed et al., Rev. Sci. Instrum. **79** 02B911 (2008).
8. J. Bermudez et al., "Fission Target Design and Integration of Neutron Converter", EURISOL-DS technical report 04-25-2009-0015.
9. J. Lettry, "Review of Ion-Source Developments for Radioactive Ion-Beams Facilities", Proc. Particle Accelerator Conference, New York, 1999.
10. M. Santana Leitner, "A Monte Carlo code to optimize the production of radioactive ion beams by the ISOL technique", PhD. Thesis, UPC-ETSEIB / CERN.
11. M. Barbui, "A MAFF concept fission target for EURISOL-DS: fission yields and release calculations", presented at EURISOL DS Town Meeting TM-03.
12. M. Barbui, "Release time calculations for different geometries of the EURISOL multi-MW target in the MAFF configuration", presented at EURISOL DS Joint Meeting JM-19.

Chapter 6: Beam Preparation

6.1 Introduction

When the radioactive ion beam has been produced, it must still undergo a process of refinement before it can be directed towards experimental areas or to a post-accelerator. The ionised beam may contain a number of contaminants, depending on the type of target material, the kind of ion source used, and the beam transport system. Isobaric contamination is particularly important, and may require a very high resolution spectrometer to resolve and discard unwanted isobars. Other contaminants such as common elements like oxygen, carbon, nitrogen may be present in abundance, masking smaller quantities of rare isotopes. Other aspects of beam preparation are beam cooling, to reduce the emittance, charge breeding – needed to reach higher energies in an accelerator – and matching to the post-accelerator requirements. These aspects are treated below.

6.2 The EURISOL ion-beam cooler

The EURISOL facility is designed to provide radioactive ion beams at intensities that are orders of magnitude beyond those currently available. Inevitably, the production of these more intense beams will result in a concomitant rise in contamination, which must be eliminated before the nuclei of interest can be studied. Simultaneous efforts will therefore be necessary in the field of beam purification, in order to exploit these intensity increases fully. Purification techniques such as laser ionization need to be supplemented by the more universal and robust method of high-resolution magnetic-sector mass separation. However, high resolving power is obtained at a high cost in efficiency due to its (inverse) dependence on beam emittance. Therefore, a reduction in the emittance of EURISOL beams will be necessary so as not to lose the rare nuclides of interest. In order to reduce beam emittance, the beam must be cooled – again, with high efficiency. The technique of buffer-gas cooling in linear radiofrequency traps has emerged as an efficient and universal tool for the production of beams with superior emittance. The developmental challenge in the EURISOL context is for an RFQ buncher capable of accepting beams reaching the microampere range. A schematic illustration of the role of ion cooling in the scheme of EURISOL is shown in figure 1.

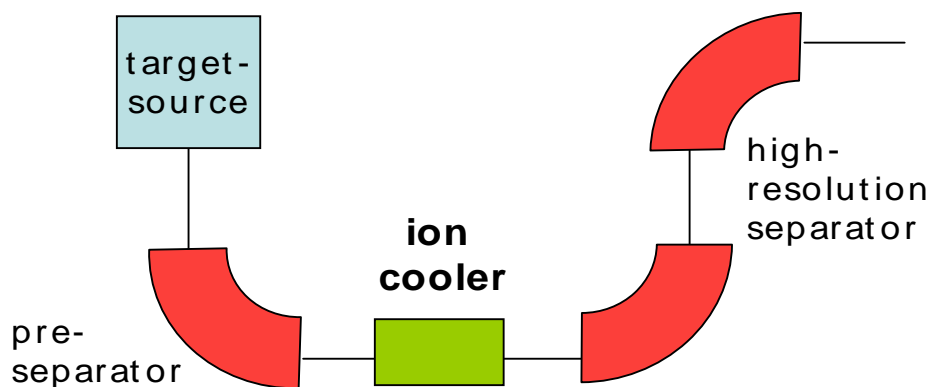


Fig. 1: Schematic layout of the proposed EURISOL beam purification system.

The early stages of the project were mostly concerned with establishing the detailed performance (and limitations) of the state-of-the-art cooler/bunchers in operation at that time. There was the COLETTE continuous-mode cooler being developed at CERN-ISOLDE [1] which helped to advance the general-purpose ion buncher at ISOLDE, called ISCOOL [2]. The injected beam intensity for these devices was established to be in the nanoampere regime, falling far short of what would be necessary for EURISOL.

Early in the project a design was developed for the next-generation cooler that could handle micro-ampere beams. Mechanically, the new design (shown in figure 2) was very similar to earlier coolers, the difference being mostly in the strong confining fields necessary for the higher intensities. This concept was elaborated for achieving higher RF voltages at higher RF frequencies. The details are contained in the preliminary report on high-intensity beam coolers [3], in which the fundamental principles of trapping and cooling were introduced.

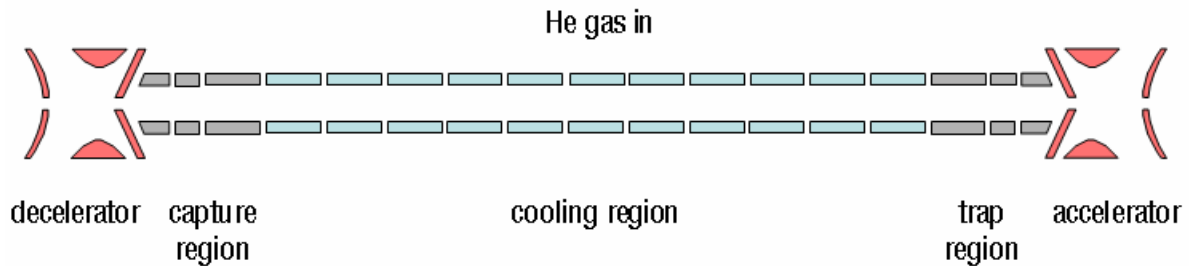


Fig. 2: Schematic layout of the EURISOL beam cooler.

Within the EURISOL project a sub-network was established, including all of the groups developing such devices around the world. We initiated a “wiki” page in the on-line Wikipedia on the subject: http://en.wikipedia.org/w/index.php?title=RFQ_Beam_Coolers, the home page of which is shown below in figure 3. We had hoped that some public exposure would result as well, but to our chagrin, the Wikipedia editors flagged it as “confusing or unclear”. At least we know the entry was not ignored! The details of the entry are described in reference [3].

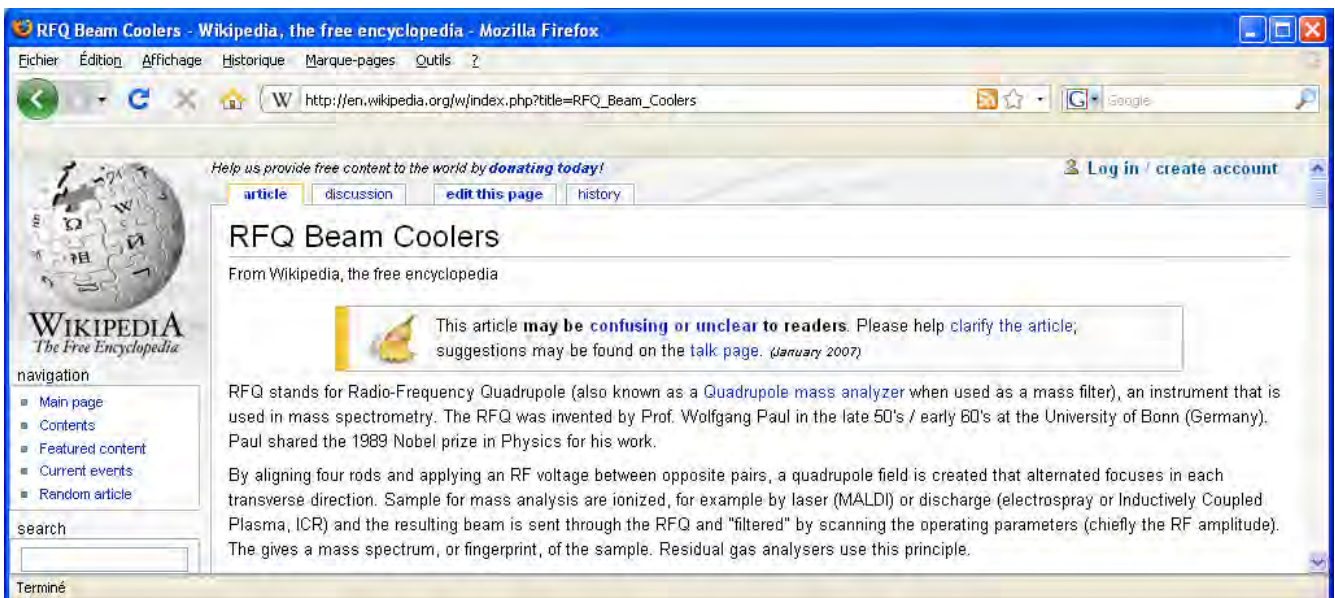


Fig. 3: The Wikipedia RFQ beam cooler page, created and updated in the course of the EURISOL project.

Beam optics simulations and technical drawings occupied the second and early third years of the EURISOL project. While an example of an injected ion simulation is given here (see figure 4, overleaf), the details were also presented in reference [3]. Some of the technical drawings are shown in figure 5.

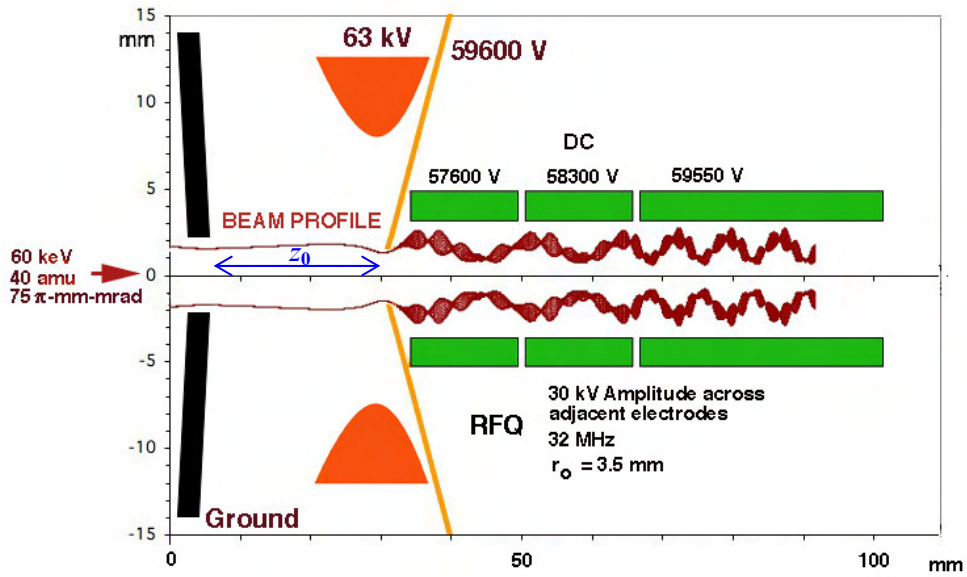


Fig. 4: The beam profile that results from injecting a beam that is slightly larger in diameter than that of figure 3 into a decelerator that has a z_0 of 25 mm.

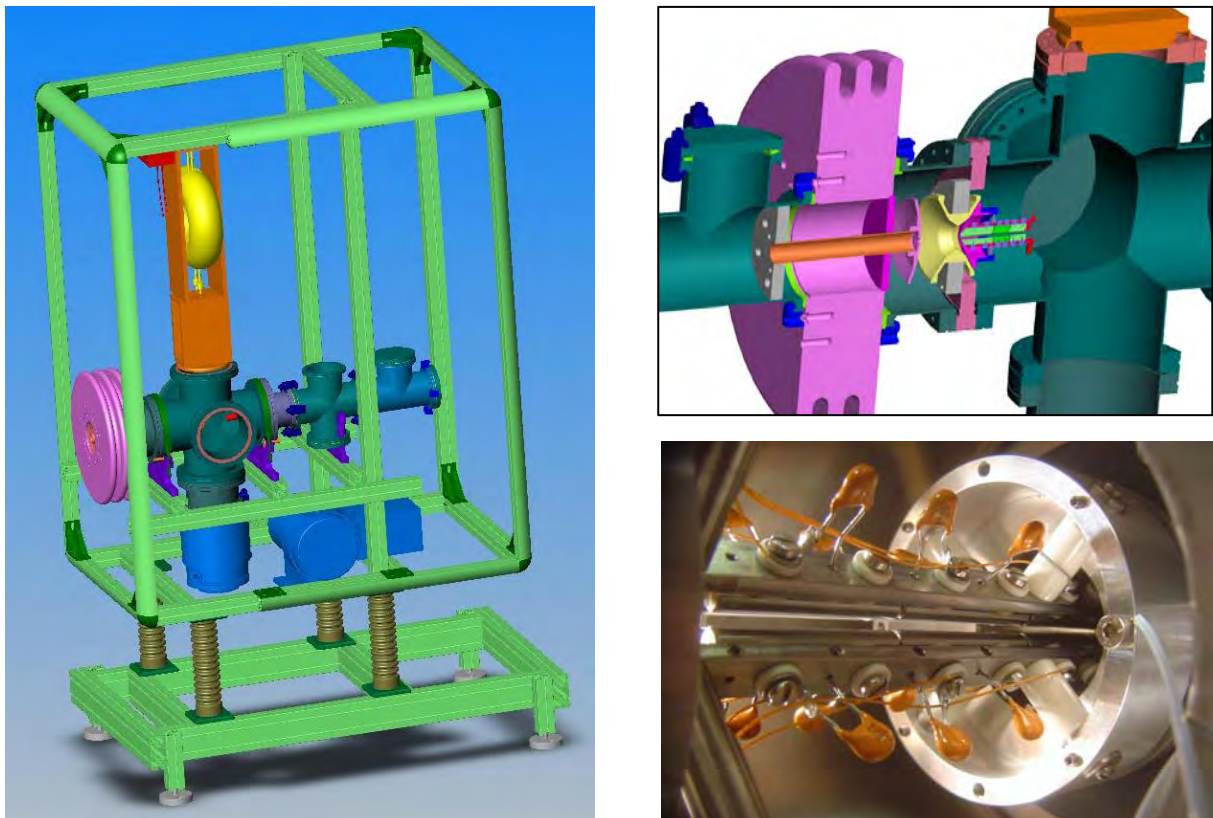


Fig. 5 (Left): CAD drawing of the high-current beam cooler platform. (Top right): detail showing the deceleration and injection electrodes, followed by four sets of radiofrequency quadrupole segments. (Bottom right): photograph of the RFQ electrodes mounted in the chamber.

The first prototype was built during the third year of the project. A photograph of the injection segment is shown in figure 5, together with technical drawings. In parallel, an RF test bench was set

up in order to produce as much high-voltage RF as possible. The first tests of the cooler using a high-intensity beam were performed with the mass-separator SIDONIE at CSNSM in Orsay. A photograph of the connecting line from the separator to the high-voltage buncher cage is shown in figure 6.



Fig. 6: Photograph of the high-voltage cage (right) that houses the high-current cooler assembly. Also visible (left) is the connecting beam line to the SIDONIE mass-separator at CSNSM in Orsay.

The fourth year of EURISOL saw intensive testing and evolution of the prototype cooler. The full-length version was also completed and tested with SIDONIE beam. A photograph of this version is shown in figure 7

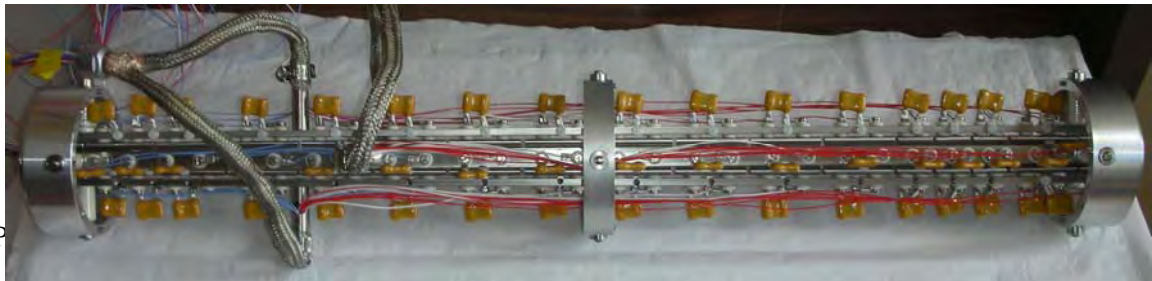


Figure 7: Photograph of the full-length high-current cooler assembly, with connections.

Finally, at the end of four years work, an important milestone was achieved: the injection and trapping of a one-microampere beam into the cooler. The transmission curve (as a function of the operating parameter, proportional to the RF voltage) is shown in figure 8. Note that the inset shows a schematic figure of the injection and trapping electrodes.

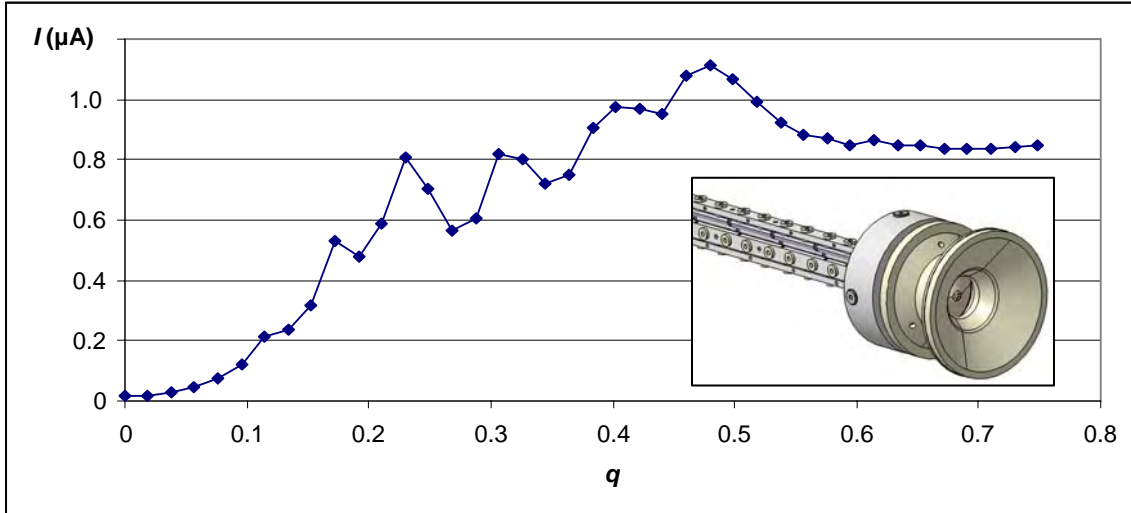


Fig. 8: Transmitted (trapped) beam through the EURISOL cooler. This is the first time that a one-microampere beam has been trapped by such a device. (Inset: the injection optics.)

This work has since been published [4]. Further results on the emittance of cooled beams through this device were also obtained (see figure 9), and are available in a report on the advanced development of the high-current ion cooler/buncher [5].

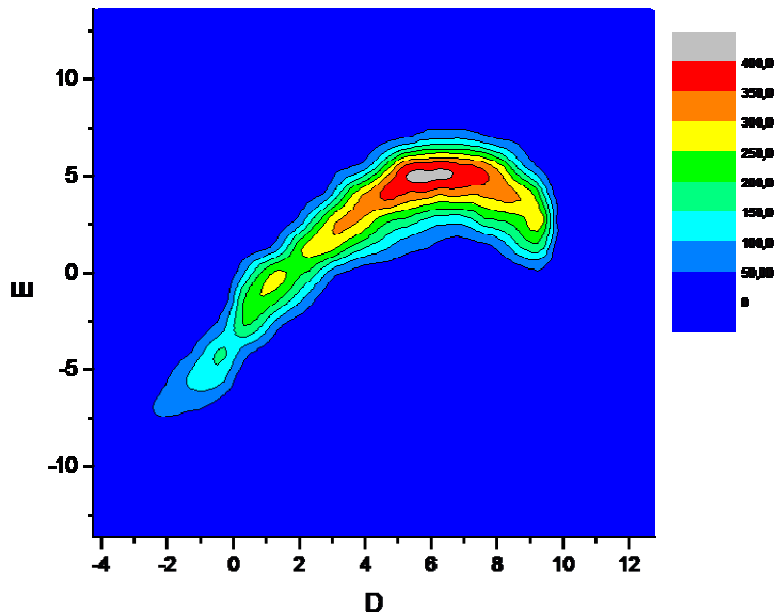


Fig. 9: Measured emittance of a trapped and cooled beam from the EURISOL high-intensity cooler-buncher. E is divergence (in milliradians) and D is position (in millimetres).

6.3 EURISOL high-resolution separator

The high-resolution separator for EURISOL comprises four identical magnets with shaped poles giving suitable multipole fields to obtain required mass resolving power. Each individual magnet has radius of 1 m and a bending angle of 135 degrees. The magnet poles are shaped to create a magnetic field with higher multipoles, and includes circular pole ends, so that separate correction elements are not needed. A schematic presentation is given in figure 9.

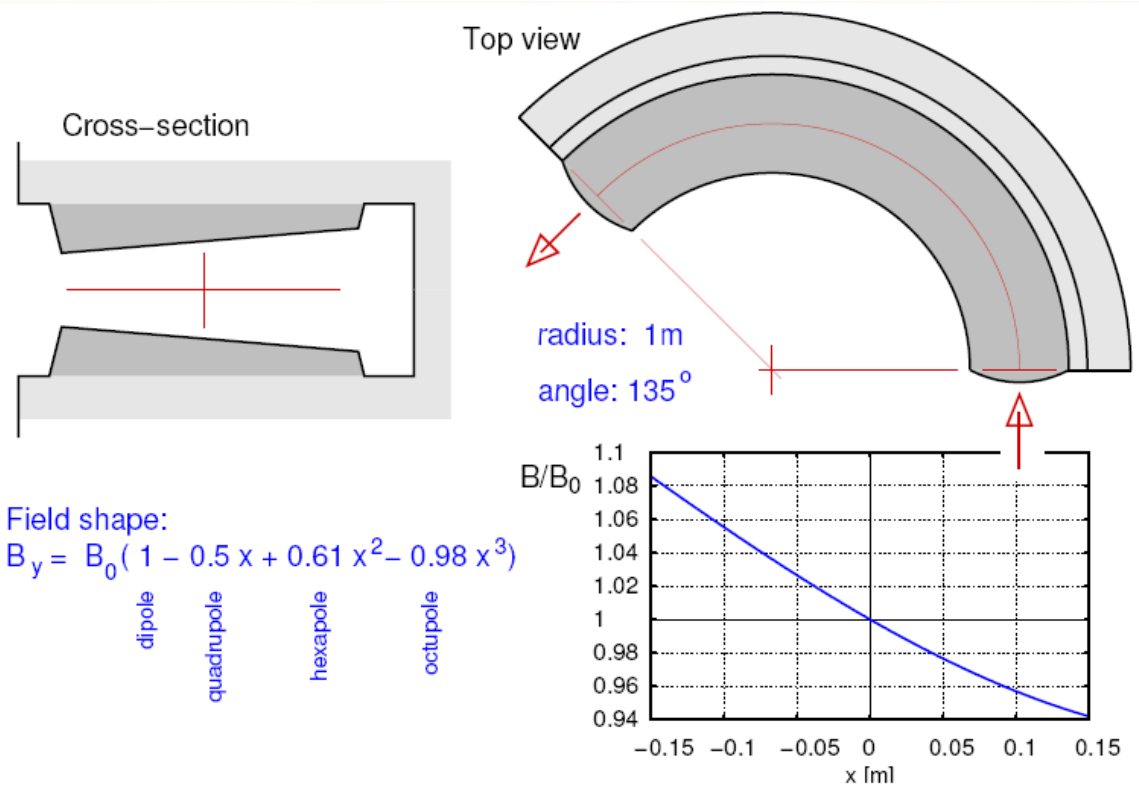


Fig. 9 (Left): A cross-section of the magnetic poles. (Right): Resulting field shape includes multipole corrections.

With four identical magnets, as shown schematically in figure 10, the theoretical mass resolution reaches a value of 64000 if one assumes an emittance of 3π mm.mrad at injection. Examples of ion optical trajectories can be found in appendices to the EURISOL Design Study Report .

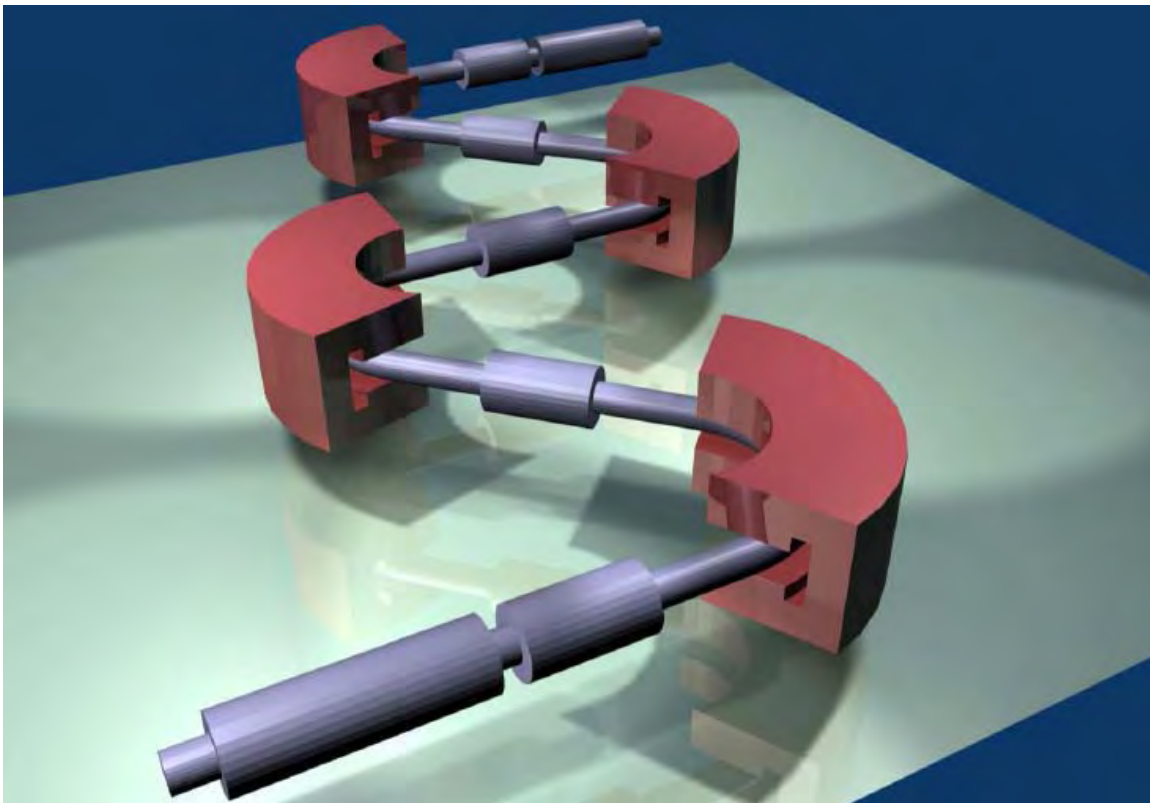


Fig. 10: Schematic picture of the EURISOL high-resolution separator with four identical magnets.

6.4 Charge Breeding at EURISOL

Charge breeding of intense radioactive isotopes produced at EURISOL is a challenge. One of the most difficult problems is to adapt with extremely large range of intensities available. The most intense radioactive beams challenge the space charge capability of charge-breeding devices, while the rarest beams are difficult to charge-breed and separate from the rest-gas ionization. To cope with extremes, we propose that two charge-breeding solutions should be adopted, i.e. an electron-cyclotron-resonance ion source (ECRIS), and an electron-beam ion source (EBIS). These two types of devices have been extensively tested for charge breeding at ISOLDE-CERN. The comparison of these devices is given below in table 1.

Table 1: A comparison of charge-breeding devices.

Device	REXEBS + REXTRAP	PHOENIX (ECRIS) Booster
Mode	Pulsed	CW
Efficiency	20 → 4%	12 → 2% Broader charge-state distribution
τ	13 ms – 500 ms, depending on A	100 ms – 300 ms
A/q	2 – 4.5	4 – 8
A	No real limitation	Injection difficult for $A < 20$
Mode	Pulsed or partially CW	Continuous or pulsed
I_{\max}	A few nA	>10 μ A
Acceptance	11 mm-mrad (95% geometrical) for 60 keV (estimated)	>55 mm.mrad at 18 keV (90)
Beam emittance	15-20 mm.mrad (95% geometrical) for 20 q keV (measured)	10 mm.mrad at 19.5 q keV (90%)
Background	Beside residual gas peaks: <0.1 pA	Usually >2 nA
Reliability	Fragile cathode – needs different gun design; overall system complex.	Robust and simple – only ΔV tuning, but reproducible settings

Based on the expertise with existing devices and using scaling laws and extrapolations from simulations we have decided to propose two charge breeding options: an ECR breeder for high-intensity beams and an EBIS for rare beams. More information on charge breeding is given in the final report on charge-breeding [6], which can be downloaded from the EURISOL DS web-site

6.5 Beam merging device

The EURISOL multi-MW spallation target (Hg), combined with uranium carbide (UC_x) fission targets and adjacent 1+ ion sources, is designed to produce six ion beams of fission products with an energy of 60 keV. Achieving significant gain in terms of post-accelerated beam intensity, compared to lower power (100-kW) target stations, requires efficient (i.e. better than 20% merging efficiency) and fast merging (in a time of the order of ms) of these six 1+ beams carrying up to 10^{15} ions/s. However, a technical solution for beam merging has not been demonstrated conclusively. It has been suggested that a concept called ARC-ECRIS [7,8] could be utilized for the purpose and, for the moment, it seems to be the only viable option. The requirements for the beam merging device and the status of the ARC-ECRIS development are discussed below.

The 1+ ion beams produced in the multi-MW target station have to be mass-separated prior to injection into the merging device. This is realized with dipole magnets located in the high-radiation area adjacent to the fission targets. Inherently high radiation levels also set requirements for the technology of the merging device:

- (i) The structure of the device has to be relatively simple, to permit robotic maintenance.
- (ii) Materials used for the merging device must be radiation hard. In particular, the use of high grade permanent magnets becomes unfeasible due to demagnetization induced by radiation.
- (iii) Materials in direct contact with the ions in the merging device must tolerate high temperatures to prevent adsorption of the atoms of interest on the surfaces in direct contact with the ions (plasma).

The merging process resembles charge breeding in which a single $1+$ ion beam is captured in the ion source plasma for further ionization to $n+$ and subsequent extraction. Thus, the proposed beam merging device (ARC-ECRIS) is based on the operation principle of an ECR charge-breeder ion source with capture efficiency of 50–60 % for gaseous and 20–30 % for metallic species. As the beam merging device has to be operated in continuous mode, technology based on an electron-beam ion sources (EBIS) can be ruled out.

The main difference between the ARC-ECRIS and conventional ECR ion sources is the design of the magnetic field. In conventional ECR ion sources, the magnetic field is a superposition of a “magnetic bottle” generated with solenoids and a hexapole field generated with either permanent magnets (in room-temperature ion sources) or superconducting coils. This structure, called a minimum-B field, provides strong confinement in both axial and radial directions and allows one to reach high charge states. In the ARC-ECRIS the minimum-B structure is achieved with only a single coil, bent as shown in figure 11. The most pronounced difference compared to conventional ECR ion sources is the lack of permanent magnets, which makes the concept resilient to radiation. In addition, the simplicity of the structure leaves room for injection and extraction and allows robotic maintenance.

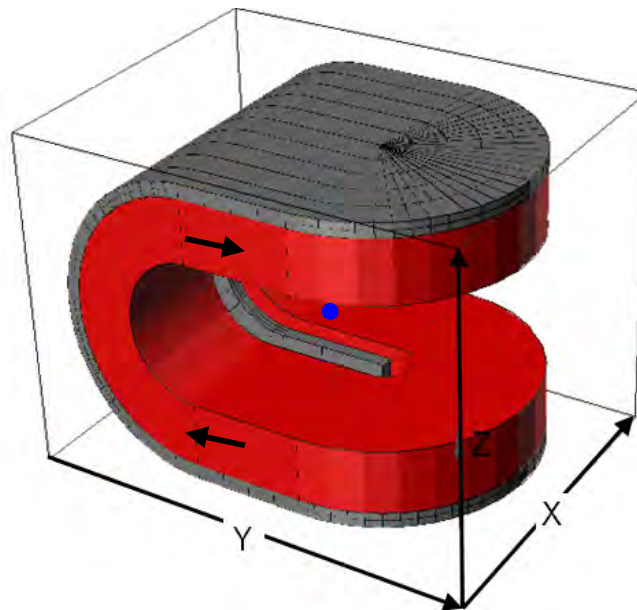


Fig. 11: Schematic of the ARC-ECRIS. The direction of current in the coil is indicated by arrows. An iron yoke with a pole extending into the coil opening covers the coil and shapes the magnetic field. The origin of the coordinate system is in the centre of the geometry indicated by a blue dot.

The magnetic field structure of an ARC-ECRIS, optimized for beam merging, was studied for the EURISOL Design Study with extensive computer simulations. The device has been designed to work at a 14-GHz microwave frequency, with resonance field of 0.5 T, this being the standard for 2nd generation ECR ion sources. The calculated magnetic field of the ARC-ECRIS for beam merging is shown in figure 12. The simulation was performed with OPERA3D. Extraction is located on the positive y -axis at $x = z = 0$, as indicated by the leaking plasma flux in figure 13.

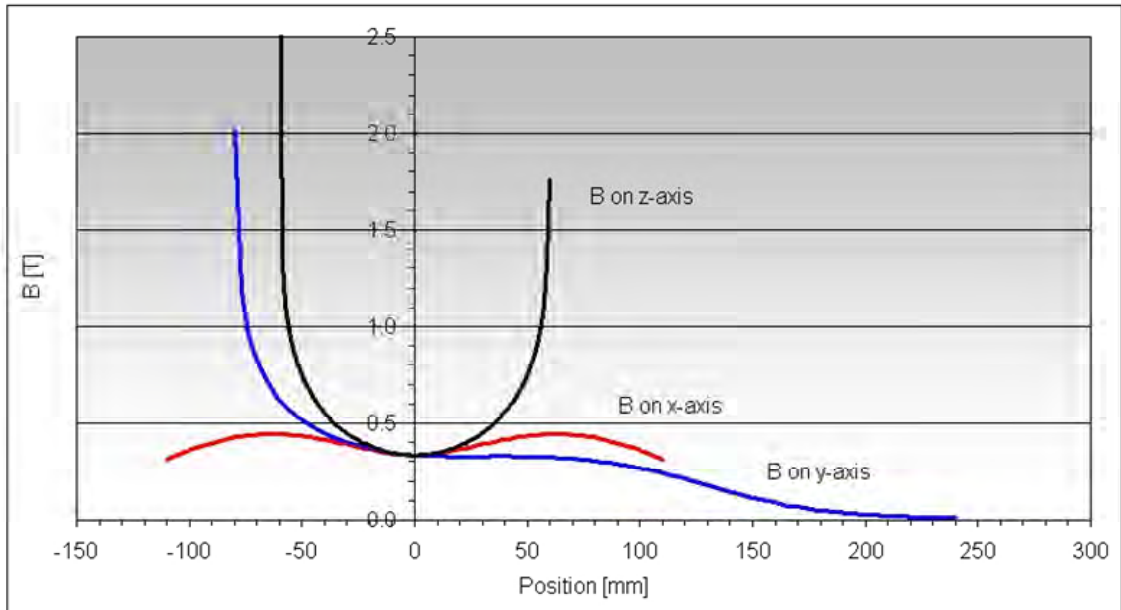


Fig. 12. Simulated magnetic field of the ARC-ECRIS.

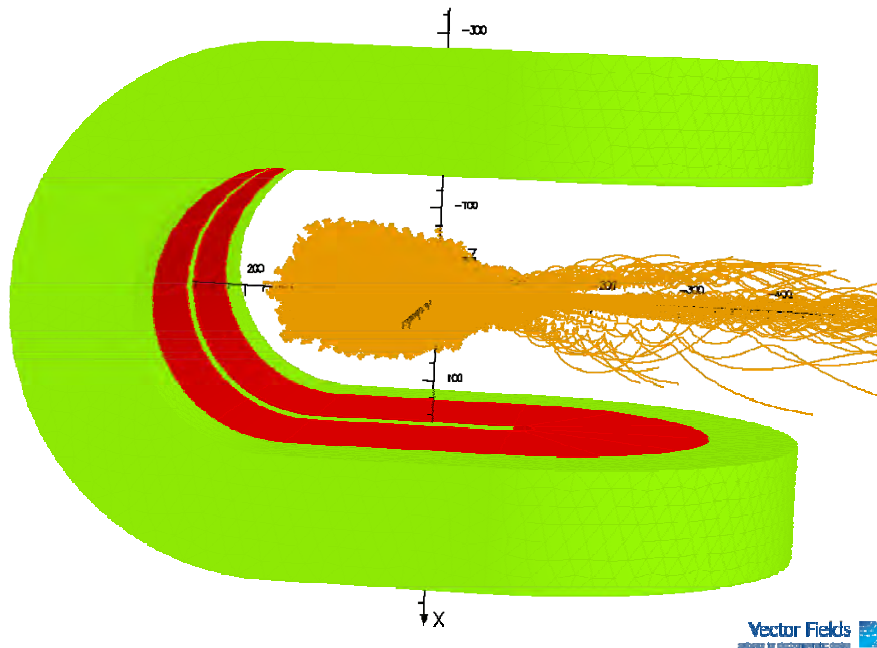


Fig. 13. Simulated electron (plasma) flux from an ARC-ECRIS. Extraction is towards the right.

The injection of the $1+$ ion beams takes place on the $z=0$ plane where all the six beams (almost parallel at this point) are focused in a single spot and decelerated from 60 keV to almost thermal energies. The setup is presented schematically in figure 14. The plasma electrode of the extraction system housing the extraction aperture is designed to be movable in order to experimentally maximize the extraction of merged $1+$ ion beam – a technique which is applied in conventional ECR ion sources. In addition, the design can be further optimized by adding a cylindrical coil around the extraction system in order to affect the magnetic field locally, which would allow one to increase the difference between the injection and extraction mirror ratios.

Preliminary results from the simulations suggest that the extraction properties (emittance and beam shape) from an ARC-ECRIS could be better than those of a conventional magnetic geometry [9,10]. In the simulations the magnetic field strength of the ARC-ECRIS at extraction was higher than is needed for the beam merging application, which results in higher emittance value (as emittance scales with B).

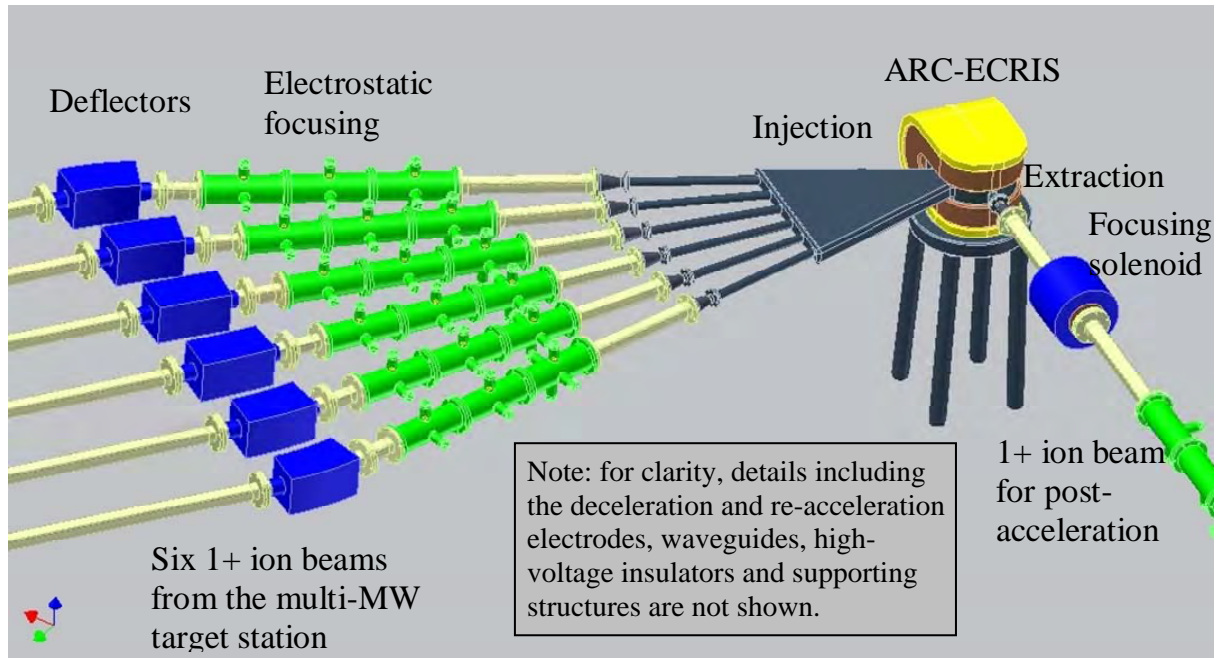


Fig. 14. Schematic diagram of the beam merging setup

The status of the ARC-ECRIS development work at the end of EURISOL Design Study can be summarized as follows: the first prototype (with two coils) was designed, constructed and tested at the University of Jyväskylä Physics Department in 2006. This prototype demonstrated plasma confinement and beam extraction. Owing to the low extraction mirror ratio, the charge-state distribution was concentrated at low charge states. The project was continued by designing a superconducting version of ARC-ECRIS and finally by suggesting the use of the technology as a beam merging device for EURISOL. However, to demonstrate conclusively that this is a technical solution for merging of the 1+ ion beams of fission products produced by the multi-MW spallation target station, it will be mandatory to construct and test a second-generation prototype of an ARC-ECRIS.

6.6 The EURISOL beta-beam ion-source development

The beta beam project aims to use the β -decay of radioactive ions to produce neutrino beams. The experimental study of pulsed-mode operation of the PHOENIX-V2 ECRIS at 28 GHz has clearly demonstrated that increasing the repetition rate of the HF power injection at frequencies higher than 1 Hz causes a transient current peak to occur at the very beginning of the plasma discharge. This was named the “pre-glow” regime. This phenomenon was studied in preliminary work at LPSC Grenoble, and a 0-dimension theoretical model of ECR gas breakdown in a magnetic trap was proposed by the Institute of Applied Physics in Nizhnyi Novgorod, Russia. The results show the possibility of producing intense pulsed beams about an order of magnitude below the expected intensities for the beta-beam project, and suggested a potential increase of this intensity when using higher microwave frequencies. The authors expect that future study of the pre-glow phenomenon under conditions of 60-GHz microwave ECR heating should demonstrate a FWHM reduction in pre-glow current peak, and an intensity increase leading to the expected intensity level.

LPSC has proposed the development of a high-frequency (60-GHz) pulsed ECR ion source prototype for beam preparation. In order to have efficient ionization, the ion source volume has to be small and, owing to the ECR frequency, the magnetic field has to be high, i.e. 6 T at injection, 3 T at extraction, a closed surface with $|B| = 2.1$ T and a magnetic mirror of 4 T.

The generation of the high magnetic field requires the use of the “helix” technique developed at LNCMI. This requires a copper tube into which a helical slit is cut by electro-erosion (see figure 15(a) below). This technique permits us to obtain a high current density (60 000/ cm²) owing to a high heat-transfer coefficient.

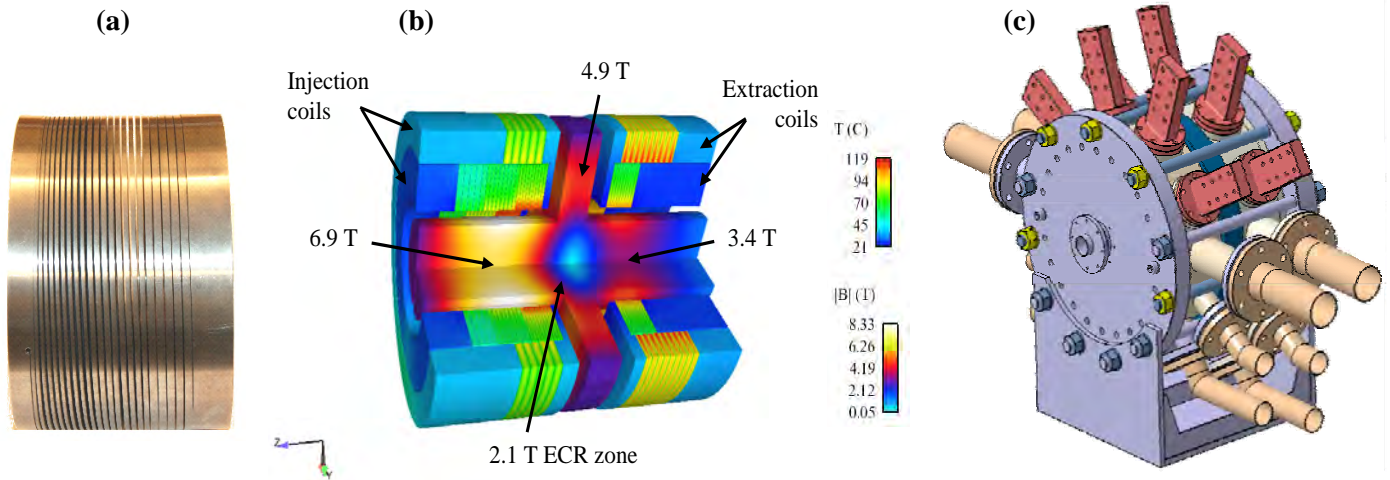


Fig. 15: (a) Aluminum prototype of a helix; (b) 3D calculation of modulus of the magnetic field (in the plasma chamber) and the temperature (in the helices); (c) the 60-GHz ion source design.

As a first approach, a cusp structure has been chosen. 2D and 3D simulations were used to define the geometry of the helices. Calculation has shown that it is necessary to use two concentric, radially-cooled, helices at the extraction side and two at injection, using a pitch change for the internal injection coil. As shown in figure 15(b), the results are better than the initial specifications, so more tuning flexibility will be available for the ion source. In this figure the calculation of the temperature in the helices does not take into account the insulators needed to maintain the space between the windings. An aluminum helix prototype (figure 15(a)) of the internal injection coil has been used to validate the calculation of the magnetic structure, at low current density.

Electrical, mechanical and thermal constraints have been taken into account for the CAD design. The two sets of coils repel each other with a force of 300 kN (30 tons). When taking into account the insulator areas, the average coil temperature varies from 80 to 180°C while the peak temperature locally reaches 330°C. The CAD design is complete (figure 15(c)) and the first 60-GHz magnetic structure (helical coils in their tanks, electrical and water cooling environment) is currently being fabricated for test measurements at half of the nominal current value. A request has been made to the EuroMagNET II Research Infrastructure to permit measurement of the magnetic field of the prototype which is under construction. This request has been accepted and the 15-day measurements will take place at LNCMI in the last quarter of 2009.

In parallel with this, the LPSC and the Institute of Applied Physics in Nizhnyi Novgorod have proposed a scientific collaboration to the International Science and Technology Center. This collaboration of IAP, LPSC, LNCMI, CERN, GSI, and the Instituto di Fisica del Plasma has as its purpose the building of a 60-GHz, 100-kW gyrotron and plasma and ion-beam experiments at LNCMI with the LPSC prototype. The total funding is 720 k€, the LPSC providing 225 k€ to the collaboration. This project has now been accepted for funding.

Further information is available in a EURISOL Design Study technical note [6] on the web-page.

6.7 Ion beam preparation: system layout

The proposed layout of the EURISOL beam preparation system is shown schematically in figure 16. The final layout comprises a beam-merging device for the 6 beams from the fission targets around the 4 MW-target, a beam distribution section before two radiofrequency quadrupole (RFQ) ion coolers to allow two extracted beams from two different sources to be manipulated independently. These two sources can in principle be any two of the four sources available (i.e. the three 100-kW target stations and the merged beam from the ARC-ECRIS). Two independent beam preparation and manipulation chains have their own RFQs and high-resolution separators. Two cooled and mass-purified beams can then be used in different ways:

- 1) One of two singly-charged beams can be transferred to the low-energy section (equipped with traps, etc.) or to the nuclear astrophysics section. (A separate, low-energy post-accelerator for astrophysics is envisaged.)
- 2) Either one or both beams can also be transferred to charge breeding devices, which will provide beams to either of the two post-accelerators.

In general, we assume that one of the 100-kW sources will typically be in use at any time, while another is “cooling down” or being serviced after a run, and the third is being prepared for operation.

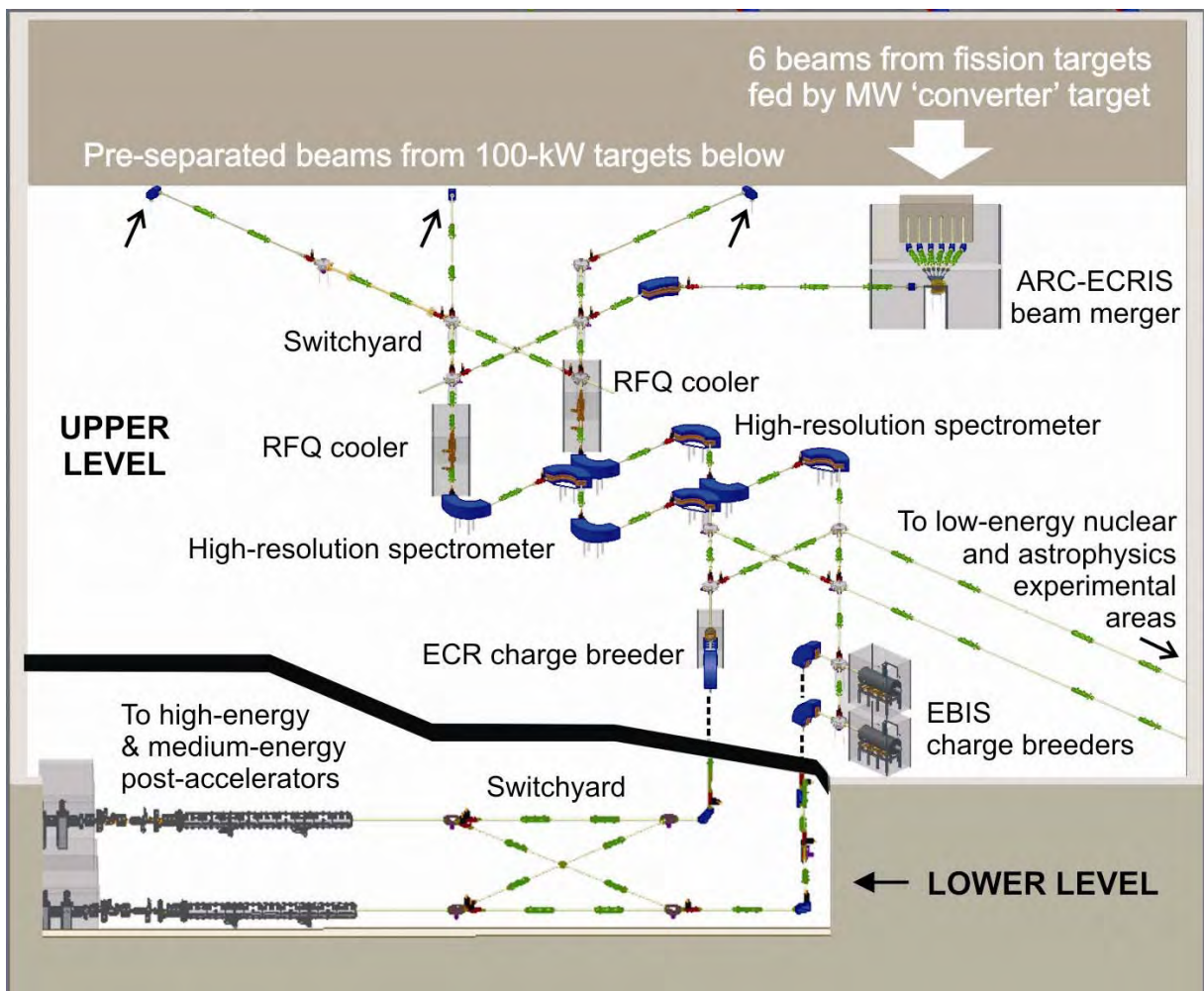


Fig. 16: Schematic layout of the proposed beam preparation area. The heavily shielded target areas are all at a lower level (not shown), together with pre-separators. Normally only one beam from the 100-kW targets will be in use at any one time. Switchyards allow two RIBs from the multi-MW target and/or from the 100-kW target(s) to be independently directed to any of the post-accelerators or experimental areas at any one time.

References

1. D. Lunney et al., “*COLETTE: A linear Paul-trap beam cooler for the on-line mass spectrometer MISTRAL*”, Nucl. Instrum. & Meth. **A 598** (2009) 379.
2. H. Franberg et al., “*Off-line commissioning of the ISOLDE cooler*”, Nucl. Instrum. & Meth. **B 266** (2008) 4502.
3. D. Lunney, “*Preliminary development of a high current ion cooler/buncher*” EURISOL DS technical note 09-25-2007-0002.
4. O. Gianfrancesco et al., “*A radiofrequency quadrupole cooler for high-intensity beams*”, Nucl. Instrum. & Meth. **B 266** (2008) 4483.
5. D. Lunney, “*Advanced development of a high-current ion cooler/buncher*”, EURISOL DS technical note 09-25-2009-0005.
6. T. Lamy et al., “*Bunched efficiency advanced study - 60 GHz*”, EURISOL DS technical note 09-25-2009-0009.
7. P. Suominen, T. Ropponen and H. Koivisto, “*First results with the yin-yang type electron cyclotron resonance ion source*”, Nucl. Instrum. & Meth. **A 578** (2007) 370.
8. P. Suominen and F. Wenander, “*Electron cyclotron resonance ion sources with arc-shaped coils*”, Rev. Sci. Instrum. **79** (2008) 02A305.
9. P. Spädtke, “*Model for the Description of Ion Beam Extraction from ECR Ion Sources*”, Proc. 13th Internat. Conf. on Ion Sources, Gatlinburg, TN, USA, 20–25 September 2009, (to be published in Rev. Sci. Instrum).
10. P. Spädtke et al., “*Low Energy Beam Transport for Ion Beams Created by an ECR*”, Proc. 18th Internat. Workshop on ECR Ion Sources, Chicago, Illinois, USA, 15–18 September, 2008, published by JACOW, available at:
<http://accelconf.web.cern.ch/AccelConf/ecris08/papers/proceedings.pdf> , p. 194.

Chapter 7: The Post-Accelerators

7.1 Introduction

The principal objective of the “Heavy-Ion Accelerator” Task during this contract has been the design of a heavy-ion post-accelerator for radioactive ion beams produced in the EURISOL facility. The following objectives were more precisely defined in the EURISOL contract:

- 1) *A complete design of a linac with emphasis on low beam losses and meeting the user requirements; different types of RFQs to be studied (both room-temperature and superconducting) and a detailed comparison of the various solutions to be reported.*
- 2) *An operational prototype of the room-temperature RFQ cavity and the injection beam line including buncher to be built and compared with superconducting options.*
- 3) *Design and prototypes of innovative diagnostic systems for very low-intensity beams to be developed.*
- 4) *Design and prototype of a new high-frequency chopper, to provide the clean pulse-suppression requested by users, to be implemented.*

We note that there was also an initial requirement from the EURISOL Management Board for the post-accelerator to fit the needs of the “beta-beam” project, but very early in the Design Study it became clear that these needs were not compatible with those of the physics users of post-accelerated radioactive ion beams (RIBs), and this requirement was therefore removed.

The “Heavy-Ion Accelerator” study, coordinated by GANIL, was organised into different subtasks distributed, as far as possible, according to the various laboratories’ competences:

- Subtask 1: Physics requirements, coordinated by **LPC-IN2P3**
- Subtask 2: Beam dynamics, coordinated by **GANIL**
- Subtask 3: Development of a normal-conducting RFQ, coordinated by **LMU** (with **Frankfurt University** as a contributor)
- Subtask 4: Development of a superconducting RFQ, and comparison of the superconducting and normal-conducting solutions, coordinated by **LNL-INFN**
- Subtask 5: Development of RIB diagnostics, coordinated by **LPC-IN2P3**
- Subtask 6: Design and development of a high-frequency chopper, coordinated by **GANIL**.

This report presents a summary of the various studies performed in each sub-task, and the main results obtained which have led to the final post-accelerator solution.

7.2 Physics requirements

Within the context of the design of the heavy-ion post-accelerator for EURISOL and the overall design of the facility, the potential user community was requested to provide input regarding the desired beam characteristics and related machine parameters.

The most significant new requests, with respect to the facility originally envisaged in the FP5 Feasibility Study are:

- an increase of the maximum beam energy to 150 MeV/nucleon;
- beam sharing based on separate target/ion-source/re-accelerator combinations, rather than using the unused charge states of the pilot beam;
- the need to provide beams with energies below 0.7 MeV/nucleon for astrophysics: this could be provided by a small dedicated post-accelerator (classed as an experimental instrument).

These requirements were defined during the different discussion sessions organised at the EURISOL Physics workshop in Trento in January 2006 and also through interactions with individuals during the EURISOL Town Meetings in 2005 and 2006. An additional requirement which emerged later is for a

second post-accelerator to provide beams below 5 MeV/nucleon for long, Coulomb-barrier experiments which would otherwise tie-up the main post-accelerator. This could most easily be provided by building a “clone” of the first part of the main post-accelerator.

Table 1: summary of the user requirements.

Max. energy of $^{132}\text{Sn}^{25+}$	150 MeV/nucleon
Energy tuning step	1 MeV/nucleon
Beam time structure	88.05 MHz (11.4 ns)
Energy definition	$< \pm 0.1 \%$
Time width per beam bunch (FWHM)	0.5 ns
Max. beam intensity	$10^{12} - 10^{13}$ pps
Emittance	$1-2 \pi$ mm.mrad
Pulse repetition rate	10 ns – 1 ms
Stripping station?	No, but a possible option

The heavy-ion post-accelerator design has been organised according to these requirements, in particular the fast-chopper parameters and the pre-buncher design. The beam dynamics studies of the superconducting linac have also aimed at meeting the required beam characteristics. The detailed list of user requirements is described in a report [1] available on the EURISOL web-site.

7.3 General layout and main technical choices

The main EURISOL post-accelerator is essentially a high-energy, heavy-ion machine, its nominal design being based on $^{132}\text{Sn}^{25+}$ accelerated up to 150 MeV/nucleon. Since a low-energy accelerator, providing beams with energies from 1 to 5 MeV/nucleon, fed by a different target-ion source station, has also been requested by the users, it was decided that this could simply be a clone of the first part of the high-energy accelerator, and therefore no specific study was made. However, the beam characteristics at the exit of this low-energy accelerator have in fact been checked.

7.3.1 General layout

The linear post-accelerator is based on a fairly classical scheme for a CW machine, with:

- a pre-buncher, which allows for a 8.8-MHz beam in the experimental areas;
- an RFQ injector, for which two solutions have been studied;
- the medium energy beam transport line (MEBT): this is rather complex, because of the fast chopper to be integrated into the line;
- a superconducting (SC) linac, based on several different cavity families;
- a possibility for using a stripper during acceleration through the SC linac.

The general layout of the EURISOL post-accelerator is presented in figure 1.

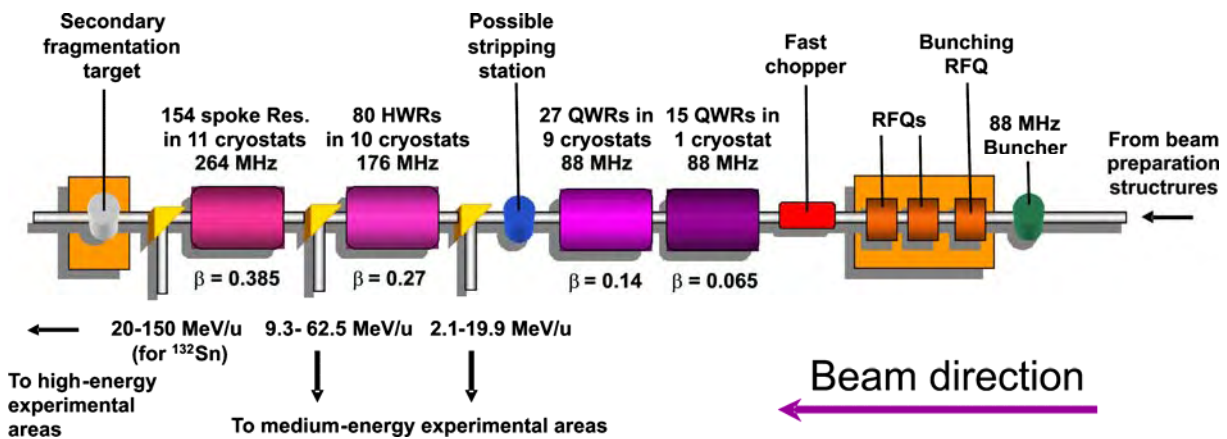


Figure 1: General layout of the EURISOL post-accelerator.

7.3.2 Technical choices

Most of the technical choices made are based on existing operating systems, or devices which are currently under construction. The main reason for this is that acceleration of radioactive beams might lead to significant problems of safety and radioprotection. These beams will be very intense (10^{12} – 10^{13} pps), and some parts of the post-accelerator may therefore have to be maintained or repaired with robots. Under these hypothetical conditions, we feel more confident to base our design on existing equipment, which would only need some mechanical modification to operate in a “nuclear” class of facility. Nevertheless, this modification will not an easy task.

The pre-buncher and the superconducting part of the SC RFQ are identical to those operating at the LNL in Legnaro. The normal-conducting (NC) part of the SC RFQ solution is based on the SPIRAL2 design, currently under construction at GANIL. The NC RFQ solution proposed is similar to that now being commissioned at SARAF in Israel, but with more easily achievable parameters. The medium-energy beam transport (MEBT) line is based on existing systems, except for the fast chopper.

The fast chopper is in fact the main item of equipment which had to be developed, both in the principle of operation and in its design and construction, and further development will continue in the frame of the SPIRAL2 project. For the superconducting linac, the choice of the various cavity families has been made with the same criteria in mind: similar cavities either already exist (e.g. developed for SPIRAL2), or are under development (at IPN Orsay).

If a stripper option is chosen, the rotatable multiple-foil support system used at GANIL can be utilised, but will probably need to be adapted for robotic maintenance. Finally, for beam diagnostics, research has been done on diamond detectors and the first results obtained are very promising (see paragraph 7.8), but further development is still needed and will be actively pursued in the coming years.

7.3.3 Some 3D drawings of the EURISOL post-accelerator

Several 3-dimensional drawings of the whole post-accelerator were made during the last few months of the contract, in order to facilitate the placement of the machine inside the proposed buildings, and two views are presented in figures 2 and 3 below.

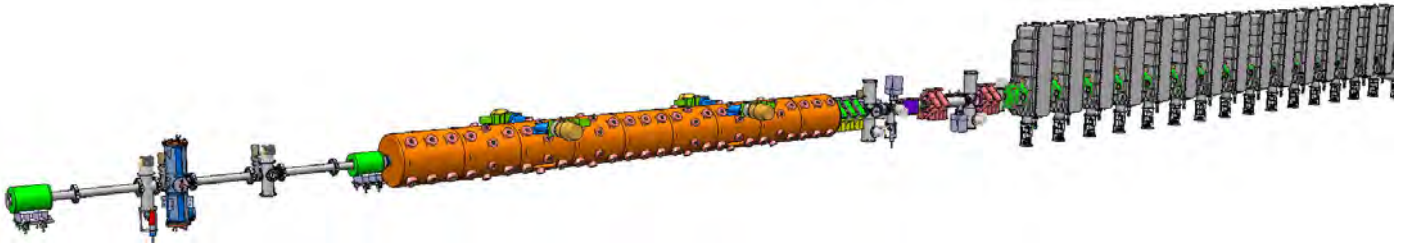


Fig. 2: Low-energy beam line, with pre-buncher and solenoids, RFQ, MEBT, and the first part of the SC linac.

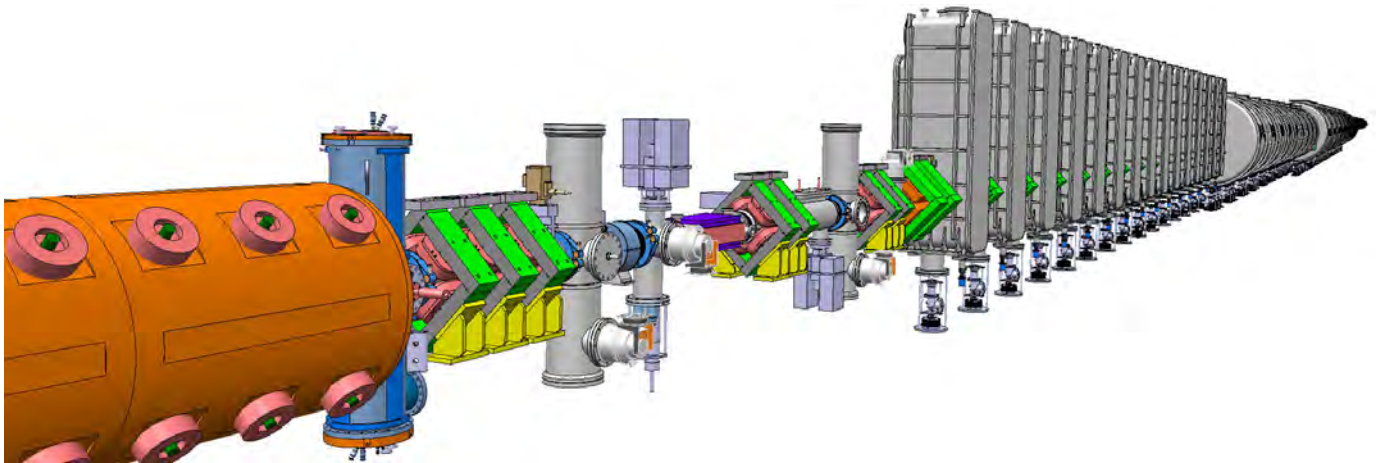


Fig. 3: Overall view of the post-accelerator, from the RFQ onwards.

7.4 RFQ options

7.4.1 Normal-conducting RFQ solution

Construction of the MAFF IH-RFQ and beam tests

Within the funding period of the EURISOL DS, the MAFF (Munich Accelerator for Fission Fragments) IH-type RFQ was built and integrated into a test bench, including a filament-driven volume ion source, an electrostatic injection system (with quadrupoles, horizontal and vertical steerers) and several devices for beam diagnostic (emittance-measurement scanner, Faraday cup, etc.). This work was performed at the Institute of Applied Physics in Frankfurt within the framework of a collaboration with LMU in Munich [2], and was an important aspect of this subtask.

The first beam tests were performed with a helium beam, and after some technical problems were solved, emittance measurements could be carried out in the low-energy beam transport (LEBT) line. For instance, the 90% rms emittance measured in the LEBT is around 0.0137 mm.mrad, which correspond to a suitable beam for the IH-RFQ tests. Measurements were carried out on the IH-RFQ, in order to check the simulated design from the RF viewpoint, and to characterise the IH-RFQ in detail. After some difficulties with the adjustment of the injection system voltage, we decided to place the ion source directly in front of the RFQ, in order to accelerate a proton beam.

This method turned out to be very successful and resulted in a first observation of an accelerated proton beam at approximately 2-kW power consumption, which corresponds to a shunt impedance of 150 k Ω -m. The energy spectrum shown in figure 4 was obtained in the usual way by means of a dipole magnet. The detailed description of the MAFF IH RFQ tests is presented in a report [3], which is available on the EURISOL DS web-site.

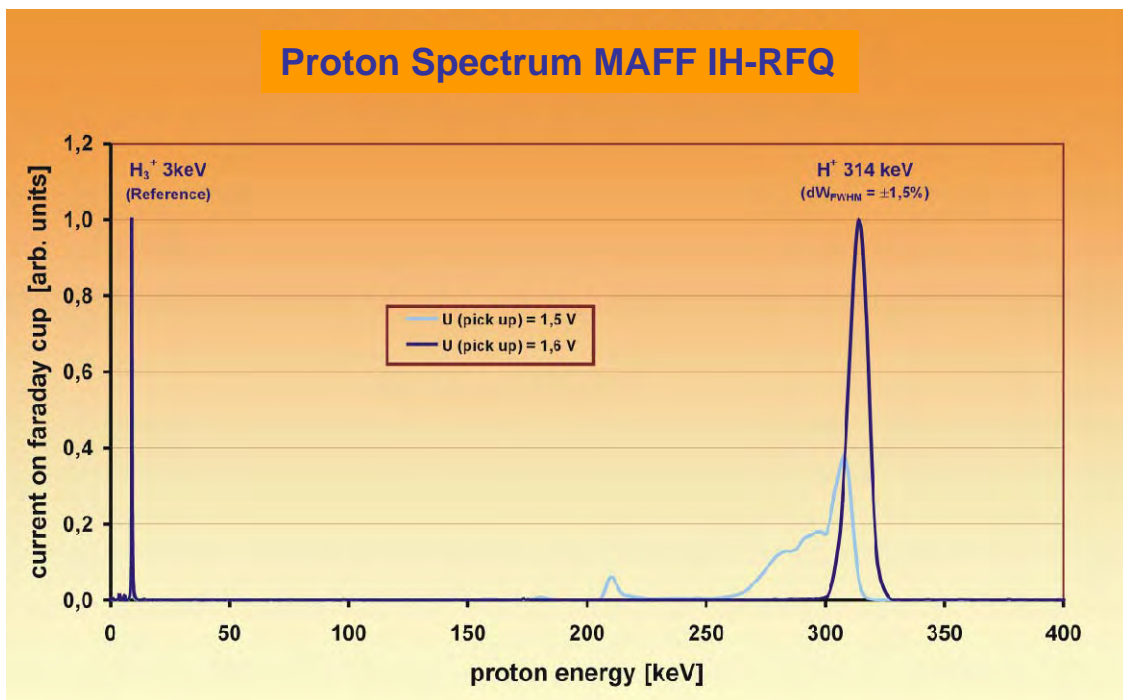


Fig. 4: Energy spectrum of protons accelerated in the MAFF RFQ.

The MAFF IH-RFQ was then prepared for a second set of more sophisticated beam tests. These were performed with a solenoid between the ion source and the RFQ (as shown in figure 5). The transmission through the RFQ for He⁺ was measured to be around 75%, as compared with the theoretical value of 70%.

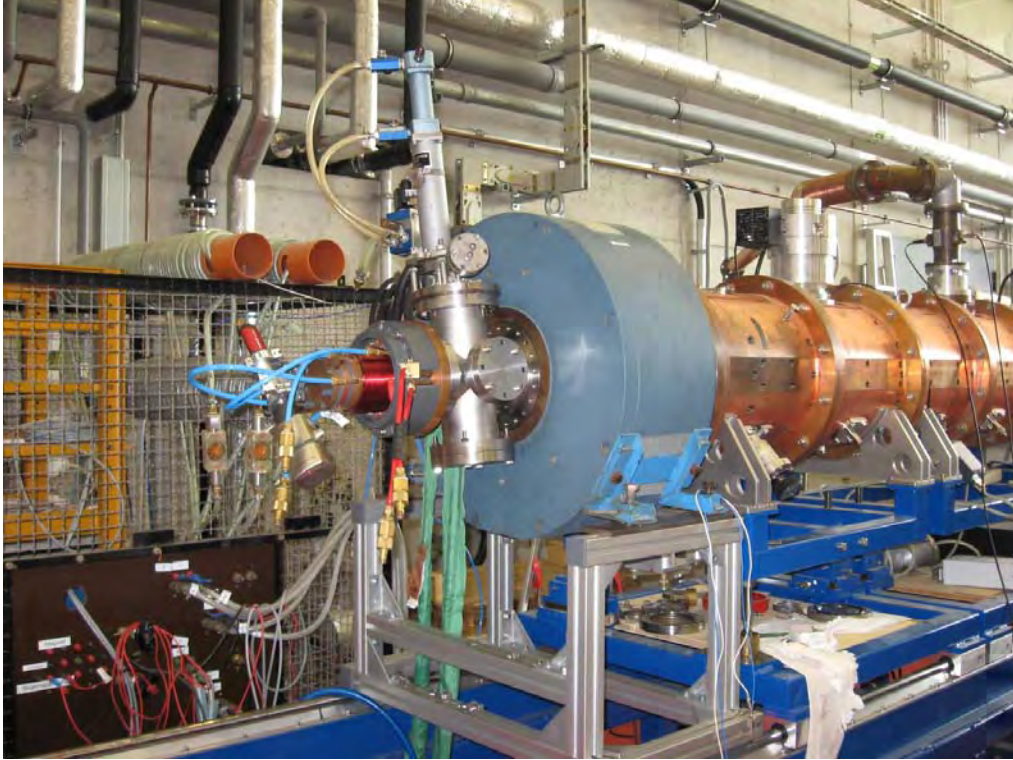


Fig. 5: The experimental setup with a solenoid and a Faraday cup for transmission measurements.

The normal-conducting RFQ design

For the design of the NC RFQ, the best compromise had to be found between the high voltages needed to accelerate high A/q beams, and more moderate voltages to reduce the thermal load on the structure. The electrode voltage was set to 60 kV, and to get from $W_{in} = 5$ keV/u up to $W_{out} = 560$ keV/u, the overall length of the RFQ system at the requested 88 MHz has to be roughly 8 m. In practice, such an RFQ has to be split into two parts forming an RFQ tandem. It was possible to avoid any additional beam line elements between these RFQs, while maintaining very robust and reliable beam dynamics. The transmission of this tandem design is 99.8%, calculated with 10^5 particles. The emittance growth $\Delta\varepsilon$, calculated using an idealized input distribution (i.e. a so-called “4D-water-bag” distribution) with $\varepsilon_{rms,in} = 0.1 \pi$ mm.mrad, is $\Delta\varepsilon = 6\%$. The particle distributions at the exit of each section (RFQ1 and RFQ2) are presented in figure 6.

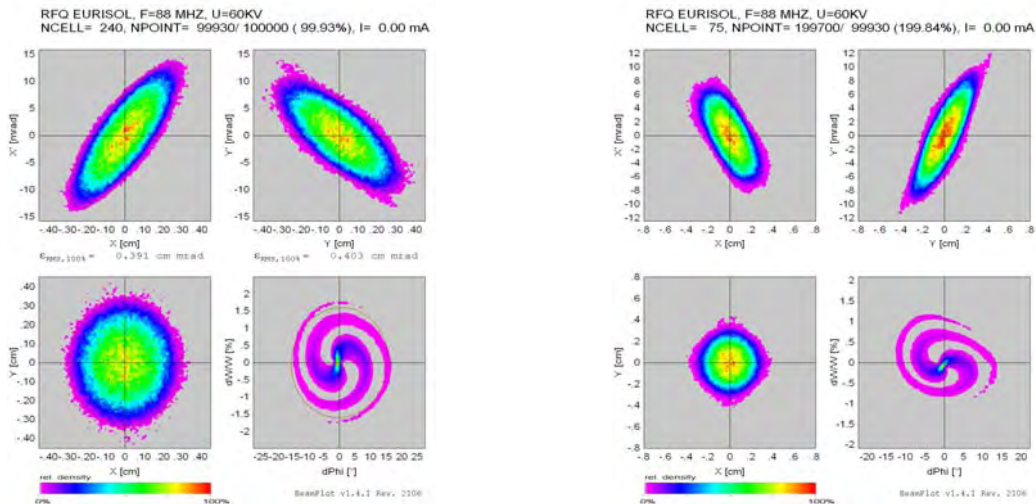


Fig. 6: Output distributions calculated for the exits from RFQ1 and RFQ2, respectively.

After some preliminary RF design work, based on an IH-RFQ structure, we finally chose a 4-rod structure. There has been much recent progress in the field of high-power applications, especially in the field of rare-isotope acceleration (e.g. at SARAF). In comparison, the IH-type structure at 100 MHz, built for the MAFF project, has shown very little advantage – if any – in terms of power consumption. Clear disadvantages are the difficulty of frequency tuning to compensate for manufacturing errors, and thermal frequency drift during operation. Thus some detailed investigations on a 4-rod solution have been carried out and this has allowed us to propose the RF design for the EURISOL NC-RFQ shown in figure 7. An example of a very similar 4-rod RFQ is that at SARAF, for which beam tests are currently in progress. The detailed design of the proposed NC-RFQ is presented in reference [4].

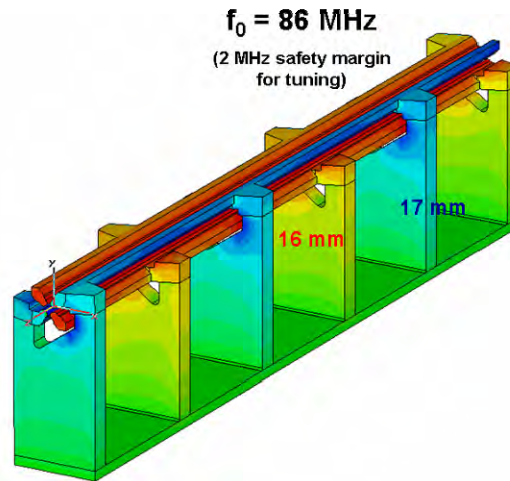


Fig. 7: A simulation for the EURISOL NC-RFQ resonator, created with the MWS program.

7.4.2 Superconducting RFQ solution

Test of the LNL superconducting RFQ

The first goal of this subtask was the testing of the PIAVE superconducting RFQ (SC-RFQ) at INFN-Legnaro (figure 8). This was a key point in the commissioning of the PIAVE injector itself. The reliability of the SC-RFQ option for the EURISOL-DS post-accelerator injector depended crucially on the success of its on-line operation in PIAVE.

In the period January-April 2006, the LNL tandem-ALPI operational programme allotted around 5 days per month for PIAVE+ALPI beam tests. Since then, the SC-RFQ has operated at INFN-Legnaro with remarkable reliability.

Beam tests were first carried out through the low-energy beam transport line (LEBT), then through the SC-RFQs, and later through the entire injector and the ALPI booster to the target and detector arrays. A beam of $^{16}\text{O}^{3+}$ from the ECR ion source on a high-voltage platform was used for the first tests of beam characterization through PIAVE. A current of $\sim 1\text{--}3\ \mu\text{A}$ was typically available from the ion source.

Setting of the relative phase between SC-RFQ1 and SC-RFQ2 was achieved by looking at the final beam energy and transmission. The beam energy at the end of PIAVE was 20.8 MeV, as expected. The beam transmission, which was between 85% and 100% in the cavity-free regions, turned out to be as high as 68% in the 3H-buncher-to-SC-RFQ section (theoretical value 69%).

Transverse emittances were measured using a slit and grid at fixed distances. The vertical emittance with the QWRs turned off (i.e. only SC-RFQ acceleration) is perfectly consistent with LEBT beam measurements, and the 25% increase in vertical emittance, when the QWRs downstream from the SC-RFQs were switched on, is acceptable. For the horizontal measurements, the RFQ-only value is again

in agreement with simulations, while the increase after switching on the QWRs – probably due to beam alignment still being poor – has to be investigated more thoroughly. The beam is in any case well within the transverse acceptance of ALPI. The longitudinal emittance has also been measured in the same position, using a silicon detector intercepting the particles scattered at a 25° angle by a thin gold foil.



Fig. 8: The PLAVE SC-RFQ resonators in their cryostat.

The detailed description of the LNL superconducting RFQ tests is available in a report [5] on the EURISOL web-site.

Revised engineering design

The study of the superconducting solution for the EURISOL post-accelerator injector has been completed according to schedule. In this solution, the envisaged injector uses two RFQs, one normal-conducting (NC-RFQ) and one superconducting (SC-RFQ), both operating in CW mode at 88 MHz, with a matching section between them.

Normal Conducting RFQ

The NC-RFQ – which we call the “bunching” RFQ – has the task of shaping the CW into short bunches at the primary frequency (88 MHz). The design is then optimized in order to have a longitudinal emittance which has to be as low as possible. The length of the structure is related to RF design details and is set to 3 m. The NC-RFQ was designed as a four-vane structure, with the HFSS code. The dissipated power per unit length (~ 7 kW/m) was carefully optimized. This power level allows one to avoid brazing joints between vanes and external tube: they can be bolted on instead. This solution is also proposed for the SPIRAL2 driver, although at a higher power level, and it is thus believed to be very reliable for our requirements.

Superconducting RFQ

The SC-RFQ has been designed to give the maximum energy gain within the limitation of a maximum surface field of 27 MV/m, a value given by applying the best niobium surface-cleaning techniques available to the RFQ structure. As in the NC-RFQ case, a big effort has been made to reduce losses and to keep emittance growth under control.

Since we have not planned to place the SC-RFQ contiguous to the NC-RFQ, owing to the impossibility of complete matching without additional focusing elements, a traditional matching line is required between these RFQs, allowing place for some diagnostics devices. The matching line is able to give a beam with specific transverse Twiss parameters with quadrupole symmetry (no radial

matching section is envisaged for the SC-RFQ) and to focus the beam longitudinally at the SC-RFQ entrance. The SC-RFQ, the geometry of which has conservatively been kept very similar to that of PIAVE at INFN-LNL, was also designed using the HFSS code.

The engineering design requires the use of a titanium stiffening cage, whose role is to increase the frequencies of the structure's mechanical modes as much as possible (beyond 120 Hz), without increasing its size and weight by too much. Slow tuning is provided by mechanical deformation of the end-plates, while fast tuning, compensating for electro-mechanical resonances, is assumed to be provided by VCX systems similar to those adopted at ATLAS (ANL, USA) or PIAVE (INFN-LNL, Italy). The use of a piezo-electric system, possibly superimposed on the slow tuner mechanism, can be envisaged.

Multi-particle simulations (shown in figure 9) for the complete injector reveal no major issues: the output emittances are lower than the superconducting linac acceptance, and the transmission is close to 100%.

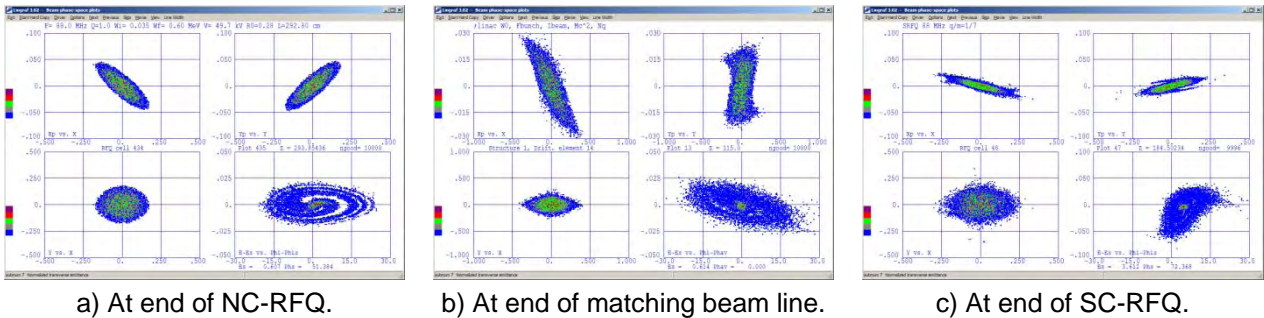


Fig. 9: Particle distribution along the injector for a normalised emittance of 0.1 mm.mrad at input.

The detailed study of the superconducting RFQ solution is available in a report [6].

7.4.3 Comparison of solutions

The two solutions, i.e. a normal-conducting RFQ or a superconducting RFQ, were compared. The main performance parameters (i.e. energy, transmission and emittance of the heavy-ion beam) and an evaluation of the cost of the main components were taken into account for this comparison. The following conclusions were reached:

- (a) Despite a possibly higher degree of complexity, the SC-RFQ option needs no prototyping for the SC-RFQ part, as it is very similar to the one working reliably in PIAVE at INFN-LNL. The NC-RFQ part is a simplified version of the one proposed and being built for SPIRAL2; nevertheless, the tests of the SPIRAL2 RFQ will have to be followed carefully when they take place. For the NC-RFQ option, experience with a CW 4-rod RFQ with high transmission is still limited, as the SARAF 4-rod RFQ is still undergoing tests.
- (b) A reliable comparison of capital and operational costs will require a more careful exercise: at this stage the SC-RFQ option seems 20% cheaper, even if it is not a major issue in the total cost of the accelerator.
- (c) Power at the mains, including that needed for cryogenics in the SC option, is smaller by a factor 2 in the SC case.
- (d) Transverse emittance is comparable, and final transmission is very close to 100% in both cases.
- (e) If the SC-RFQ is positioned on an HV platform (with 30 kV the estimated maximum voltage), it will require liquid helium fed from ground potential. Operational solutions exist, but have not yet been tested experimentally. On the other hand, the far lower power consumption of the SC-RFQ solution (110 versus 190 kVA) is advantageous for the power fed to the 30-kV platform.

Therefore, at this stage of development, both RFQ solutions appear to be very feasible, with the following remarks:

- Proof of the operation of superconducting resonators on a 30-kV platform (SC-RFQ solution) should be demonstrated before the solution can be declared to be fully feasible;
- The reliability of high-power operation of a 4-rod NC-RFQ has only been checked over short periods with the SARAF RFQ, and a real long-term operational period is needed to show that this solution is fully acceptable.

The detailed comparative study is presented in a report [7], available on the EURISOL DS web-site.

7.5 8.8-MHz pre-buncher

An 8.8-MHz buncher appears to be necessary to match the user requirements for some experimental cases, and also when using the fast chopper.

The required 8.8-MHz bunching system should operate in addition to the 88-MHz bunching process which takes place inside the RFQ. The proposed solution is conceptually similar to the triple-harmonic buncher of PIAVE [8], where a cavity houses the first (8.8-MHz) and third (26.4-MHz) harmonics and, after a short drift, another cavity houses the second (17.6-MHz) harmonic. Multiparticle simulations have been performed, and this configuration gives 77% transmission and negligible emittance increase.

For both types of RFQ solution, we have shown that a bunched beam – which provides a higher intensity – leads to good beam dynamics, from the RFQ design and acceptance point of view, and does not affect the beam dynamical design of the following elements: RFQ, MEBT, fast chopper and superconducting linac. For the NC RFQ solution, the simulations have shown that the design is capable of accepting an input distribution with an energy spread up to $\Delta W = \pm 9\%$ without gaining any additional losses. The output distribution remains unchanged. Nevertheless, while the transmission for a CW beam (without pre-buncher) is nearly 100%, that of a bunched beam is only around 77%.

7.6 MEBT and superconducting linac

The medium-energy beam transport line (MEBT) and superconducting linac studies have been performed mainly in a beam dynamics framework, and the main linac parameters were defined according to the user requirements listed in table 1 (see section 7.2).

The study of the MEBT focused mainly on the fast chopper beam dynamics, and in particular on the effect of the superposition of fields (magnetic and electric) on the beam which is transported through the linac. The basic linac configuration, without stripper but with the use of the chopper, has been studied in great detail. The matching between the MEBT and the linac is very good.

The chopper specifications for the design of the prototype and for the dynamics studies were chosen in order to reach a technically feasible solution. The main choice is based on an “inverted” mode of operation, in the sense that a magnetic steering is applied continuously along the fast chopper, and the fast chopper voltage, applied as a travelling wave on a meander-line electrode selects the number of bunches to be sent to the linac. (More detail of the chopper is given in section 7.7.)

The linac is divided into four sections, which correspond to four different cavity families. The first two sections are composed of quarter-wave cavities (QWRs) operating at 88.05 MHz, while the third section contains half-wave cavities (HWRs) and the last, spoke cavities. Between each cryomodule, two quadrupoles provide transverse focusing. In order to provide all final energies for all ions between 5 and 150 MeV/nucleon, an intermediate exit is required at the end of the second family. If necessary for the facility layout and the experimental area arrangement, an additional exit is also possible at the end of section 3, provided that the transition line between families 3 and 4 is redesigned in detail.

All the user requirements are fulfilled with this linac solution, except for the energy-spread in the low-energy linac. At the high-energy end of the linac, the time width is 25 ps FWHM, so the goal of <500 ps should not be a problem; the energy spread is ± 34 keV/nucleon ($\pm 0.02\%$). However, we note that for the low-energy output (5 MeV/nucleon), the energy-spread is 20 keV/nucleon, i.e. $\Delta E/E$ is $\pm 0.2\%$, compared to the requested $\pm 0.1\%$. (This can be improved in the subsequent beam transport line, using a dipole analysing magnet, but only at the expense of some beam loss.)

All the usual error studies have been performed, and indicate no particular problem. The jitter on the target has also been studied in case of instability of the chopper voltage. A jitter of 0.17 mm in the vertical direction on the experimental target is obtained for a (realistic) 2% instability in the chopper voltage, which is acceptable.

The steering effect of the first two cavity families, which are quarter-wave resonators, has been studied, taken into account, and corrected with magnetic steerers. The steering effect, even when corrected, leads to a 20% increase in the vertical beam emittance, which is not a problem.

We recall at this stage that the high-energy heavy-ion linac has been designed to provide re-acceleration without stripping. Nevertheless, the use of a stripper can be interesting, particularly for heavier ions, but only in order to accelerate them to higher energies. The stripping option has therefore been studied within this framework. The stripping section would be located at the end of the second section of the linac. The impact of the stripping foil on the beam emittance (angular straggling), beam energy loss and charge equilibrium have been evaluated, and taken into account to recalculate the beam dynamics in the following part of the linac. The calculated values are:

$$\text{Emittance growth} \sim 70\%; \quad \Delta E/E \sim 0.04 \text{ to } 0.05\%.$$

This emittance growth is quite acceptable, and the final energy dispersion is well within the user requirements, i.e. less than 0.07%, with all errors taken into account.

The main interest of the stripper, as already explained above, is to reach higher energies with heavier ions. Figure 10 shows the final energies that can be obtained when using the stripper, both with ^{132}Sn and ^{238}U beams.

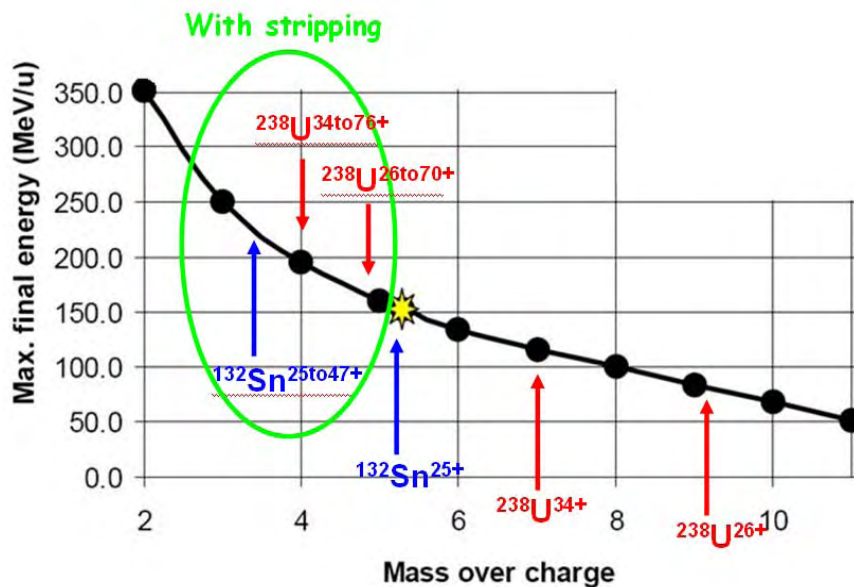


Fig. 10: Final energy versus A/q ratio.

Multi-charge transport

It is possible to transport and accelerate more than one charge state through the system, as has been demonstrated at ANL. This is related directly to the use of a stripper, which then becomes very attractive. Two cases have been studied:

- a) Multi-charge transport without a dipole after the stripper: beam dynamics calculations show good characteristics for the accelerated beam. The case of $^{132}\text{Sn}^{46,47,48+}$ ions accelerated simultaneously has been studied in detail, and the beam emittance at the end of the linac is presented in figure 11.

- b) Multi-charge transport with a dipole after the stripper: this study was not completed, owing to a lack of suitable software to simulate the whole transition line with the dipoles correctly, and to optimise the longitudinal position of each charge state automatically. This point will have to be considered again in future.

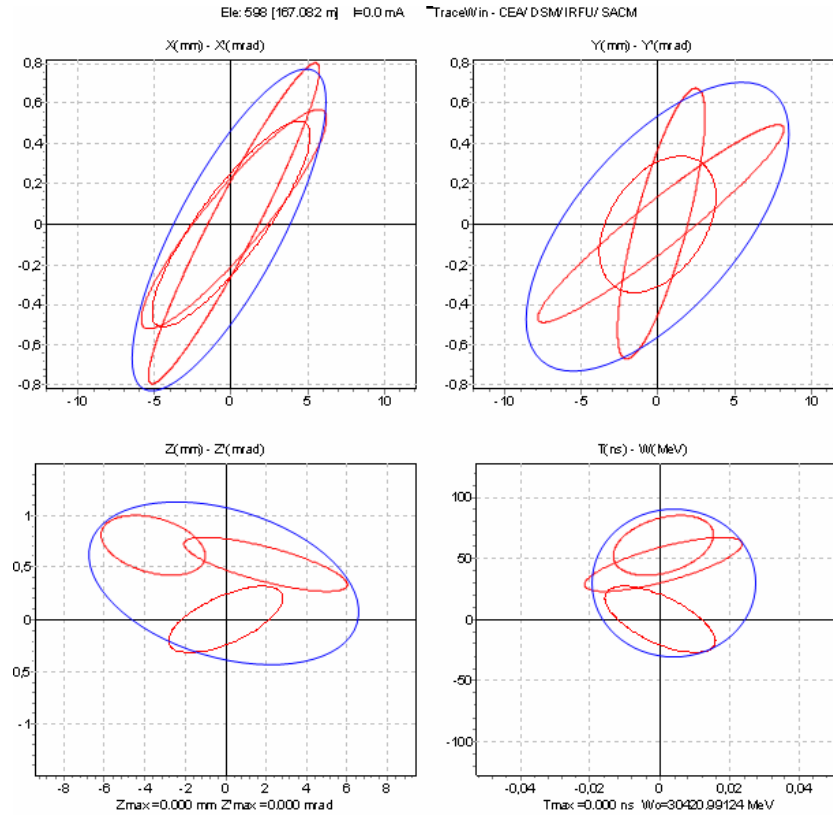


Fig. 11: Emittance at the end of the linac for $^{132}\text{Sn}^{46+, 47+, 48+}$ (without a dipole after the stripping section)

Space-charge effects

The basic design is able to accept the space-charge effect due to a 1 mA beam without difficulty, and can even handle more than 5 mA without beam loss. In all cases, there are no losses, and the emittance stays constant.

Velocity matching

In 2007 it became apparent that the proposed beam-preparation scheme was not compatible with the post-accelerator design, without modification. The beam preparation task group has chosen to extract beams from the ion sources at a constant voltage, to avoid the need for retuning the sources, a solution approved by the EURISOL management board, while, from basic principles, the RFQ used in the post-accelerator accepts a constant velocity beam, whatever the A/q ratio. A solution had then to be found, in order to interface between these approaches. Among the three possibilities considered, that adopted is the positioning of the RFQ on a variable high-voltage platform, to match the beam velocity to the RFQ at injection (figure 12).

Detailed beam dynamics studies have been performed on the $^{132}\text{Sn}^{25+}$ beam, and show that beam emittance and halo increases are less than 2%, along the high-voltage transition, without beam losses. The chopper acceptance in velocity is not an issue, if the maximum platform voltage is less than 30 kV. If necessary, the chopper can be placed on the HV platform as well, which does not cause any problem for the injection into the linac. From a technical point view, there is no major problem for the HV platform: however, the cost can be high, depending on the effective power required on this platform.

A full description of this complete work is available in a report [10] on the EURISOL DS web-site.

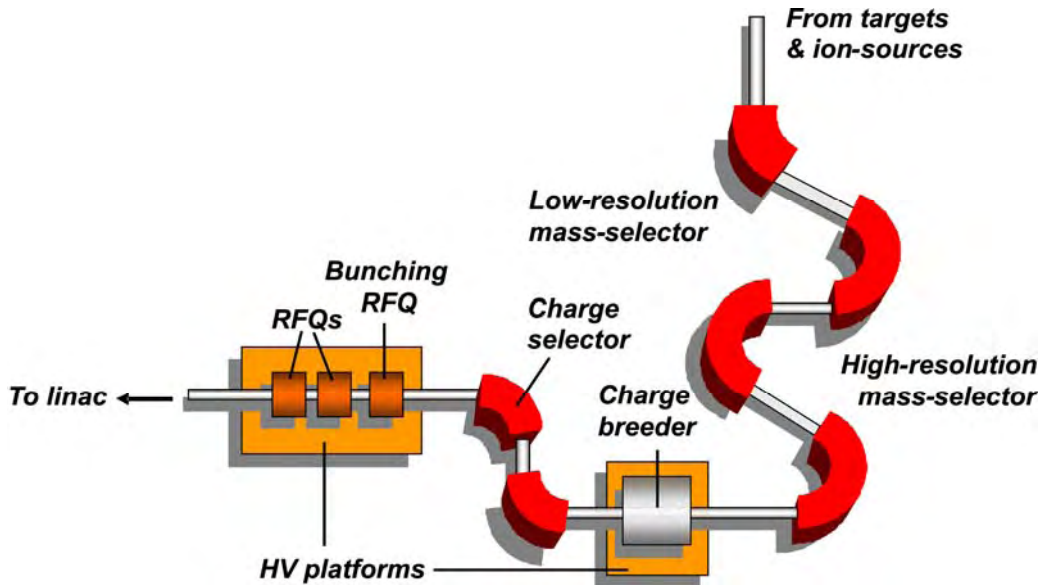


Fig. 12: Schematic view showing matching between the beam preparation section and the RFQ with an HV platform

7.7 Fast beam chopper

The fast chopper parameters have been defined both by user requirements and beam dynamics. At the beginning of the EURISOL DS contract, two possible solutions were investigated: (a) fast switching of capacitive electrodes and (b) travelling wave electrodes driven by pulse generators.

The first solution presents losses which are mainly independent of the duty cycle. Electrodes would have a coverage factor very close to 1 and the system power would be around 4 kW, considering a total capacitance of 70 pF loading a perfect switch. This solution was abandoned as we could not obtain any bids for solid-state switches working at 10 MHz and handling such high power.

In the second solution, the travelling-wave electrode (meander line) has a lower coverage factor (80%) and the power requirement depends on the duty cycle. It would then be unrealistic to chop 9 bunches out of 10 via the pulse: keeping a 3-kV pulse in quasi-CW conditions – even for a high impedance around 100 ohms – would require around 80 kW. The possibility of inverting the duty cycle was then proposed and investigated [11].

Principle of operation

Superimposed electric and magnetic fields are proposed: the DC magnetic field continuously deflects the beam onto a beam stop, leaving the electric field pulse to “un-deflect” only 1 bunch out of 10. This configuration was intensively studied from the beam dynamics point of view and was finally approved. With this proposal, the pulse power requirement has decreased to some 9 kW, which is still high but probably feasible. At this power level, the pulser, connectors, connections to the meander line and thermal dissipation of the electrodes are the main areas of concern.

The flatness of the high-voltage level of the pulse is a major issue if it is not to degrade the beam emittance. A working impedance (Z_c) of 100 ohms has been defined as compromise between RF power (higher Z_c means lower power) and the feasibility of the meander line (higher Z_c means lower transverse line dimension and higher sensitivity to mechanical tolerances).

The initial aim of this subtask was to test the prototype with a SPIRAL2 beam, but this was later modified and limited to a power test of the pulser-electrode system. In fact, the SPIRAL2 beam will now only be delivered in 2 years' time, which is beyond the duration of the EURISOL Design Study.

The completed work involved the design, development, and testing of the various components of the prototype pulser-electrode system.

Technical challenges

The design of the electrode itself was based on a CERN solution for the SPL project, which has been adapted to EURISOL requirements. A ceramic support was preferred for better radiation resistance, thermal conductivity, vacuum properties and because it limits the transverse dimension. Two electrodes were designed: one for the EURISOL nominal value (beta 0.035) and one which is adapted to the SPIRAL2 MEBT line (beta 0.4) where the whole concept will be tested. The latter electrode has been manufactured, ready to be tested with beam when it is available. The detailed study is described in a report [12] available on the EURISOL DS web-site.

The metallic support for the electrode functions both as a heat dissipater and a ground plane for the meander line as this cannot be plated on the back of the ceramic for technological reasons. Almost 7% (600 W) of the pulse power is lost along the meander path, and this has to be cooled by water.

It is not practically possible to braze the ceramic plate to the dissipater, so an alternative solution has been found to improve the poor heat conductivity at the ceramic-to-metal interface [13]. The side-cooling principle has been retained in order to separate RF and heat-dispersal issues. (Every material used between the meander line and the ground plane has to be compatible with RF). The mechanical assembly is now ready for testing under vacuum.

Considering the problems encountered by pulse generators for similar projects, and owing to budget limitations, we decided to order a 1-kW device ready for the test with the SPIRAL2 beam, as a first step toward the more powerful generator required for EURISOL. Two 2.5-kV, 1-MHz pulsers have been ordered from an industrial company (FID Technology), which will be used for these beam tests. The first of these was successfully commissioned in April 2009. The pulse shape fits the requirements (<6 ns transient times and 6 ns flat time) and shows excellent stability and phase jitter (figure 13). The second generator – with reverse polarity – needed for testing the complete system, was then ordered immediately after these first tests.



Fig. 13: (Left) pulser and matching load; (centre) resistances inside the load; (right) pulser and load signals.

System tests

Only low-power tests in air have been performed, with the meander line being matched by a 2-W 100-ohm resistor. Nevertheless they have already revealed some problems which exist in measuring the meander parameters and the pulse shape along the line.

The mechanical support has been designed to implement the side cooling principle discussed in [2] but the cooling still has to be tested (figures 14 & 15). Thus far, we have checked that the indium joint which creates the continuous contact for cooling is deformed by the spring-washer pressure. More detailed results of these tests are presented elsewhere [12].

A vacuum chamber has been designed for the chopper, but more stable pick-ups and a more precise matching network have to be prepared, and then power tests of the whole system can probably be completed later this year, beyond the period of the design study. A preliminary design for integration of the fast chopper into the SPIRAL2 beam line has also been studied. Finally, beam dynamical analysis has confirmed the possibility to work with a steerer magnet shorter than the electrodes, but which has nevertheless still needs to be positioned in the middle of the structure.

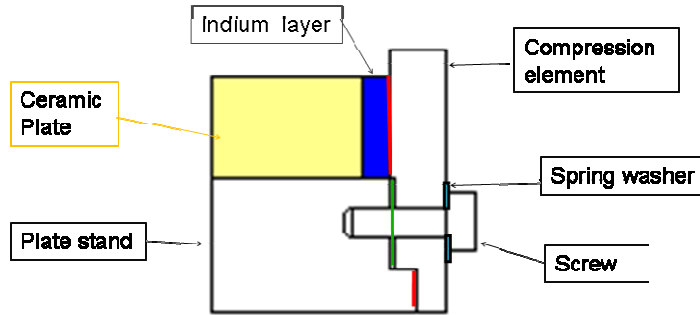


Fig.14: Diagram of the lateral compression scheme proposed for the cooling contacts

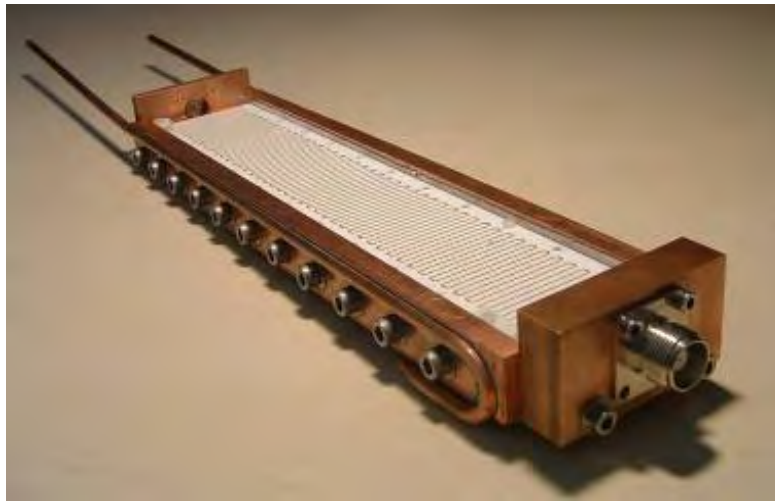


Fig. 15: The ceramic plate with meander-line electrode assembled on the water-cooled support.

7.8 Beam diagnostics

The successful delivery of radioactive beams by the heavy-ion linac will require monitoring of the beam throughout the machine – in particular the profile and intensity. At present, for beam rates below some 10^6 pps, no reliable detector exists which fulfils the requirements imposed by operation in such an environment. The beam diagnostics subtask has thus looked into the development of a new type of beam diagnostics, dedicated to low-intensity radioactive beams.

However, the recent development for high-energy physics applications of relatively large-area, synthetic polycrystalline diamond (produced via chemical vapour deposition – CVD), offers a very promising alternative, with properties matching very closely those needed to fulfil the above requirements. Given the relatively limited knowledge of the response of such detectors to heavy ions, a programme of R&D was undertaken:

- a) to determine the suitability of CVD diamond for detecting heavy ions, and
- b) to fabricate and test prototype double-sided strip detectors capable of providing event-by-event position measurement and timing.

As a first step, two $25 \times 25 \text{ mm}^2$ diamond wafers of 300- and 500- μm thickness, of different quality and surface preparation, were purchased from Diamond Detectors Ltd., UK (a subsidiary of De Beers). Working with these wafers provided us with the necessary experience needed to develop the various processes for fabricating a detector. In the first instance, simple non-segmented detectors were produced. Following testing with an alpha source, the two detectors, along with others supplied by colleagues from GSI-Darmstadt and CEA-Saclay, were tested in beams at GSI (50 MeV/nucleon

^{124}Xe) and GANIL (7–11 MeV/nucleon ^{13}C , ^{58}Ni). The results of the tests undertaken with the detectors based on the Diamond Detectors' wafer confirmed the fast rise-time (typically ~ 5 nsec) and response-time (signal width ~ 15 nsec) of the material. While the observed energy resolution was extremely poor, as expected, the signals were always well clear of the noise, which is intrinsically very low.

In order to fabricate the prototype double-sided strip detectors, a number of preliminary studies were undertaken to master the production of the masks and evaporation procedures.

The strips used were of 0.9 mm pitch with an inter-strip gap of 0.1 mm. Four prototype detectors of slightly varying sizes (16×16 to 20×20 mm² active areas), thicknesses (240–575 μm) and different grade wafers were produced (figure 16). Once again, preliminary tests were carried out using an alpha source prior to in-beam tests at GANIL (4–14 MeV/nucleon ^{16}O , ^{36}S , ^{70}Zn).

These tests broadly confirmed the results obtained for the non-segmented detectors. Owing to the lower capacitance of the individual strips as compared to the non-segmented detectors, the rise times observed were shorter (typically ~ 3 nsec). The effects of cross-talk between strips were also observed and investigated. Given the opposite polarity and small amplitude of the signal induced on the neighbouring strips, this effect can be easily eliminated. A comparison of the responses of the detectors fabricated using the two different grades of wafers supplied by Diamond Detectors demonstrated the superior characteristics of the “premium” grade material (produced by reducing a 1 mm thick wafer to the desired thickness). Moreover, we concluded that the detectors should be as thin as possible (i.e. – given current wafer production techniques – around 300 μm), in order to reduce to acceptable levels any possible bulk polarisation effects when the range of the incident ions is small compared to the thickness.

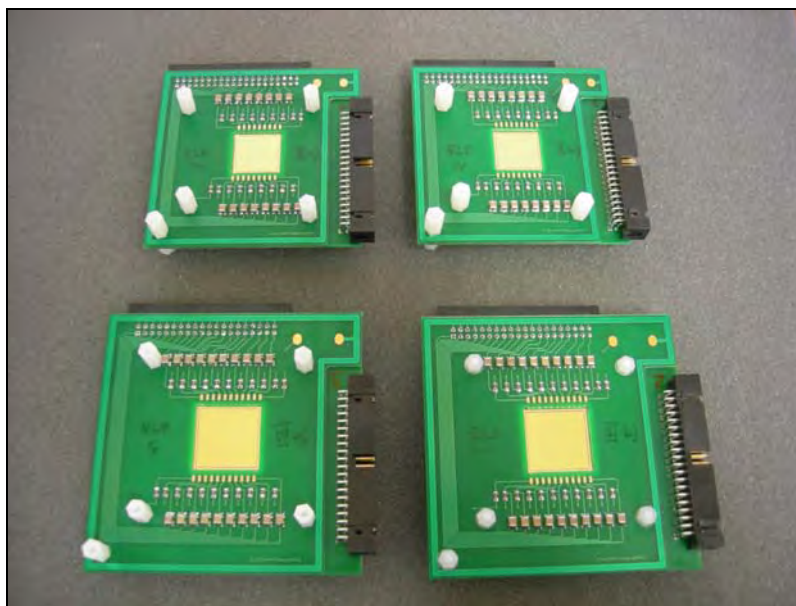


Fig. 16: The four prototype double-sided strip detectors.

In summary, it has been demonstrated that CVD polycrystalline-diamond-based, double-sided strip detectors are well suited to the requirements for a beam profiler for characterising low-intensity radioactive beams in the heavy-ion linac ($<10^6$ pps). The further characterisation of such detectors and the engineering of the readout electronics and other associated elements of a fully fledged profiler are expected to be carried beyond the present design study in the context of intermediate projects, such as SPIRAL2, and beam tracking for experiments at the RIBF-RIKEN that will simulate high-energy applications at EURISOL.

The detailed presentation of this development is described in a report [14], available on the EURISOL DS web-site.

7.9 Input for safety & radioprotection studies

The Safety & Radioprotection group needed input about geometry, material and beam dynamics results, especially beam losses, in order to make the shielding calculations for the post-accelerator. Simulations and some extrapolations from existing accelerators like those at GANIL and from projects like SPIRAL2 have been done, to give an order of magnitude of the losses in the different parts of the accelerator. A summarised scheme of the various inputs is given in reference [10], available on the EURISOL DS web-site.

7.10 Conclusions

The Heavy-Ion Accelerator group completed all of its initial objectives, with the exception of in-beam tests of the high-frequency chopper at SPIRAL2 (which is unfortunately still in the construction phase). The design for the whole post-accelerator is now very solid, in the sense that it is based on existing type of cavities and accelerators. Various beam tests performed have confirmed the assumptions made, in particular where charge-breeder emittances are concerned. Beam dynamical calculations for the whole linac show that the proposed accelerator is very safe (i.e. with minimal beam losses), even if multi-charge transport still needs some software development to permit proper studies.

Beam tests with the two types of RFQ have been satisfactory as well: the normal-conducting (NC) IH-RFQ is undergoing further tests in Frankfurt, and more precise measurements are being made. However, the final choice for the NC-RFQ solution favours a 4-rod type RFQ, because it has some advantages. Where the superconducting (SC) RFQ is concerned, an example has been in operation for more than 2 years at LNL, Legnaro, and the results are very encouraging.

Therefore, at this stage of development, both RFQ solutions appear equally feasible, with the following provisos:

- The reliability of high-power operation of a 4-rod NC-RFQ has only been tested at SARAF during short periods: longer-term operation is needed to declare this solution fully acceptable.
- Proof of the operation of superconducting resonators on a 30-kV platform (SC-RFQ solution) should be demonstrated before the solution can be declared to be fully feasible;

The final choice will therefore have to be made nearer to construction time, depending on the long-term operation reliability of the NC-RFQ, and the technical proposed solution proposed for the SC-RFQ on a high-voltage platform.

For RIB diagnostics, the development of CVD polycrystalline-diamond-based, double-sided strip detectors has proved to be very interesting. The first results are really promising, and their development will continue in the frame of intermediate projects like SPIRAL2 and HIE-ISOLDE.

The fast chopper still requires some more development before it can be and tested with SPIRAL2 beam, when this becomes available. This is certainly a very important device, and its development will be pursued in the frame of SPIRAL2 project. The tests of the whole system have still to be completed under vacuum, and the last step will be to test it with the SPIRAL2 beam in future.

The final item of concern is safety and radioprotection: very low beam losses were taken into account for the evaluation of shielding wall thickness, etc., but nevertheless the importance of contamination remains an open question, and should probably be investigated in more detail in the near future. Intermediate projects like SPIRAL2 or HIE-ISOLDE will help to give more precise information about this problem, and will indicate where robot manipulators may be necessary for maintenance during post-accelerator operation.

References

1. N. Orr, “*Experimental Requirements - Beam and Machine Characteristics - Final Version*”, EURISOL DS report 06-25-2009-0011.
2. A. Bechtold et al., “*The MAFF IH-RFQ Test Stand at the IAP Frankfurt*”, EPAC06.
3. A. Bechtold & H. Zimmermann, “*Beam measurements with NC MAFF RFQ*”, EURISOL DS report 06-25-2009-0016.
4. A. Bechtold, “*The normal conducting RFQ for EURISOL post-accelerator*”, EURISOL DS report 06-25-2009-013.
5. G. Bisoffi, P.A. Posocco, A. Palmieri & A. Pisent, “*Beam tests with the LNL Superconducting RFQ*”, EURISOL DS report 06-25-2009-014.
6. G. Bisoffi, P.A. Posocco, A. Palmieri & A. Pisent, “*SC RFQ engineering design revised*”, EURISOL DS report 06-25-2009-015.
7. G. Bisoffi, “*Comparison of NC and SC RFQs*”, EURISOL report 06-25-2009-0023.
8. A. Facco, F. Scarpa, “*The triple harmonic buncher for the PIAVE project*”, LNL Annual Report 1996.
9. P. Delahaye et al., “*Review of the different options for the velocity matching section issue*”, <https://edms.cern.ch/document/887375/1>.
10. G. Normand, “*Beam Dynamics Simulations*”, EURISOL DS report 06-25-2009-014.
11. G. Le Dem, M. Di Giacomo, “*A Single Bunch Selector for the Next Low- β Continuous-Wave Heavy Ion Beam*”, [Proc. PAC07](#), Albuquerque, New Mexico, IEEE (2007).
12. G. Le Dem, “*High Frequency Chopper of the Heavy-Ion Accelerators - Annual Status Report*”, EURISOL DS report 06-25-2009-0008.
13. M. Di Giacomo, “*EURISOL fast chopper: cooling and connecting proposal*”, EURISOL DS report 06-25-2009-0019.
14. M. Parlog, N. Orr, “*Diamond detector R&D for low intensity heavy-ion beam profilers*”, EURISOL report 06-25-2009-0021.

Chapter 8: Superconducting Cavity Development

8.1 Introduction

The main objective of the Superconducting Cavity Development group of the EURISOL Design Study was to study, design, fabricate and test superconducting cavities and all their associated components (cold tuning system, power coupler and RF sources), following the recommendations of the Proton Accelerator group about the most relevant accelerating structures to be designed. These developments were meant to conclude with a test of one cavity type in a configuration as close as possible to a real accelerator configuration, i.e. in a cryomodule with all the ancillaries, at the nominal operating temperature and nominal RF power.

The EURISOL driver linac is based on several different superconducting structures: half-wave resonators, spoke cavities and elliptical cavities, each of them of two different β (with $\beta = v/c$, the reduced particle velocity). The driver accelerator group of the Design Study prompted us to focus our work on the superconducting accelerating structures for the intermediate energy part of the driver (between ~ 10 MeV to ~ 140 MeV). The obvious reason for this choice is that, at the start of the project, these structures were in a less advanced stage of development compared to the high-energy accelerating cavities already developed and operated in other projects (SNS for instance).

Development of a suitable, reliable accelerating structure does not rely only on the optimization of an accelerating cavity but also on the careful design of all the cavity ancillary systems such as the cold tuning system (CTS) for an in-situ control of the cavity resonant frequency, and the power coupler (supplying the RF power to the cavity from the external RF source). We addressed all these issues for two different superconducting cavity types: half-wave resonators and spoke resonators. For each of them, prototypes were designed, fabricated and tested, as well as their associated cold tuning system and power coupler. For the spoke superconducting structure, a test cryomodule was also designed and fabricated, and a final test of a fully equipped spoke cavity in this cryomodule was performed.

The task was divided into several sub-tasks:

- Half-wave resonators prototyping and test, including CTS
- Spoke resonators prototyping and test, including CTS
- 352 MHz solid-state RF amplifier development
- RF power coupler prototyping and test
- Spoke test-cryomodule design and test.

This document reports on the major achievements on all these sub-tasks. The participating laboratories to the task are mainly INFN/LNL (Italy) and CNRS/IN2P3/IPN Orsay (France), and, to a less extent, GANIL (France).

8.2 Half-wave resonator developments

Half-wave resonators (HWRs) are particularly efficient in a beam velocity range of $0.06 < \beta < 0.4$ and a frequency between 150 MHz and 350 MHz. They can efficiently accelerate high-power hadron beams just after the RFQ, at the same frequency. HWRs are the preferred technology for the EURISOL beam acceleration between the RFQ exit and ~ 60 MeV/u.

8.2.1 Half-wave resonator prototypes at 352 MHz

The first development was performed on HWR at 352 MHz, taking experience from previous design work for the SPES project. The design of the two cavities at different beta (0.31 and 0.17) is shown in figure 1. Two different shapes for the inner conductor were used (flattened and cylindrical). They are characterized by a double-wall coaxial structure with an integrated helium vessel (figure 2). The beam

port aperture is 30 mm, and they are equipped with a $1\frac{5}{8}$ " port for a coaxial RF coupler. Two more 16-mm diameter ports are available for RF pick-up.

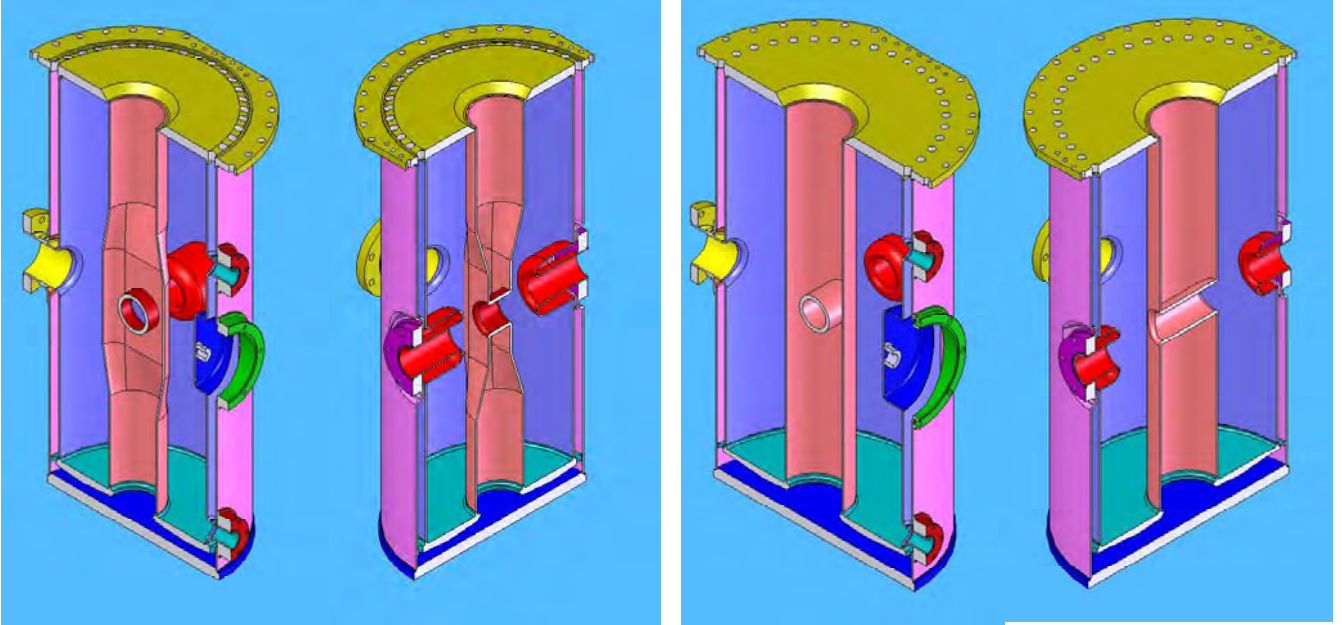


Fig. 1: Geometry of the $\beta = 0.17$ (left) and $\beta = 0.31$ (right) 352-MHz half-wave resonators.

The outer niobium wall (helium jacket) is made of reactor-grade niobium. The $\beta = 0.17$ cavity top and bottom plate is made of titanium and welded to the resonator, while for the $\beta = 0.31$ prototype, these plates were made of stainless steel connected to the cavity by means of an indium seal. All RF parameters are given in the table of figure 2.



β_0	0.17	0.31	
U/E_a^2	0.067	0.086	$J/(MV/m)^2$
B_p/E_a	12	10.4	$mT/(MV/m)$
E_p/E_a	5.8	3.9	
R_{sh}/Q_0	1230	1180	Ω/m
$R_s \times Q_0$	55	66	Ω
Tuning df/dh	~ 70	~ 107	kHz/mm
Active length L	180	224	mm
Maximum Length L_{re}	232	286	mm
Aperture a	30	30	mm
Design E_a	5	6	MV/m

Fig. 2: The main RF parameters of the two 352-MHz HWR prototypes shown at left.

Both prototypes have been tested at 4.2K at LNL, Legnaro in a vertical cryostat. The results are shown in figures 3 and 4. Very good results were obtained with a maximum accelerating field of 6.8 MV/m for the low-beta cavity, and 7.9 MV/m for the high-beta cavity. We should mention that these good performances were obtained despite the lack of a standard cavity preparation (e.g. no high-pressure rinsing).

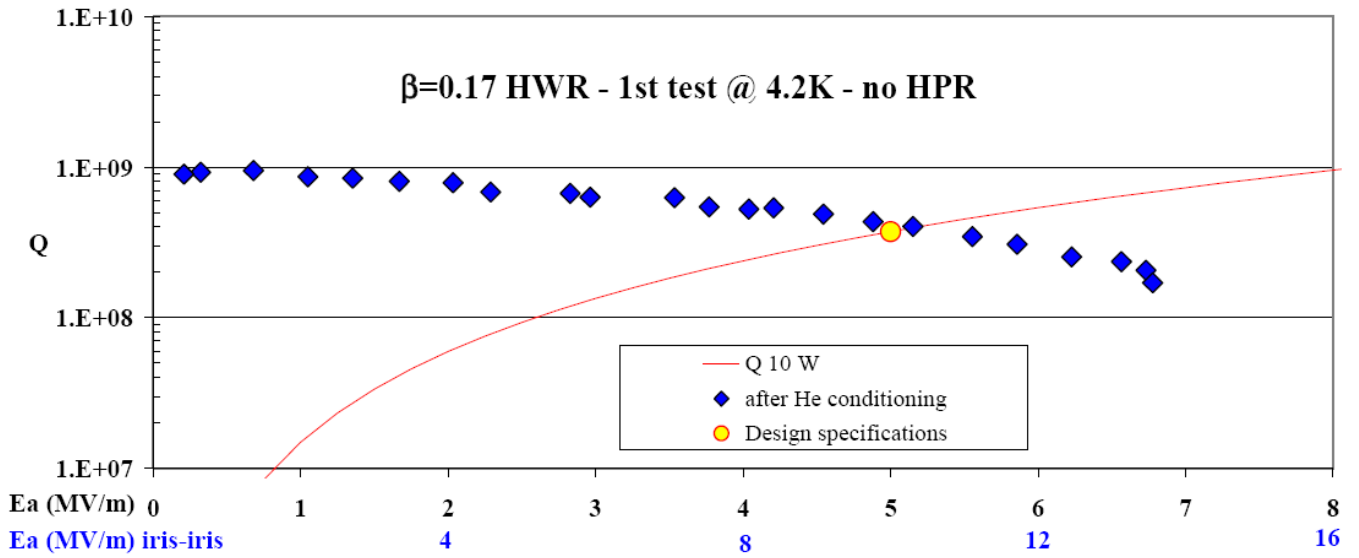


Fig. 3: Test results at 4.2K of the $\beta = 0.17$ half-wave resonator.

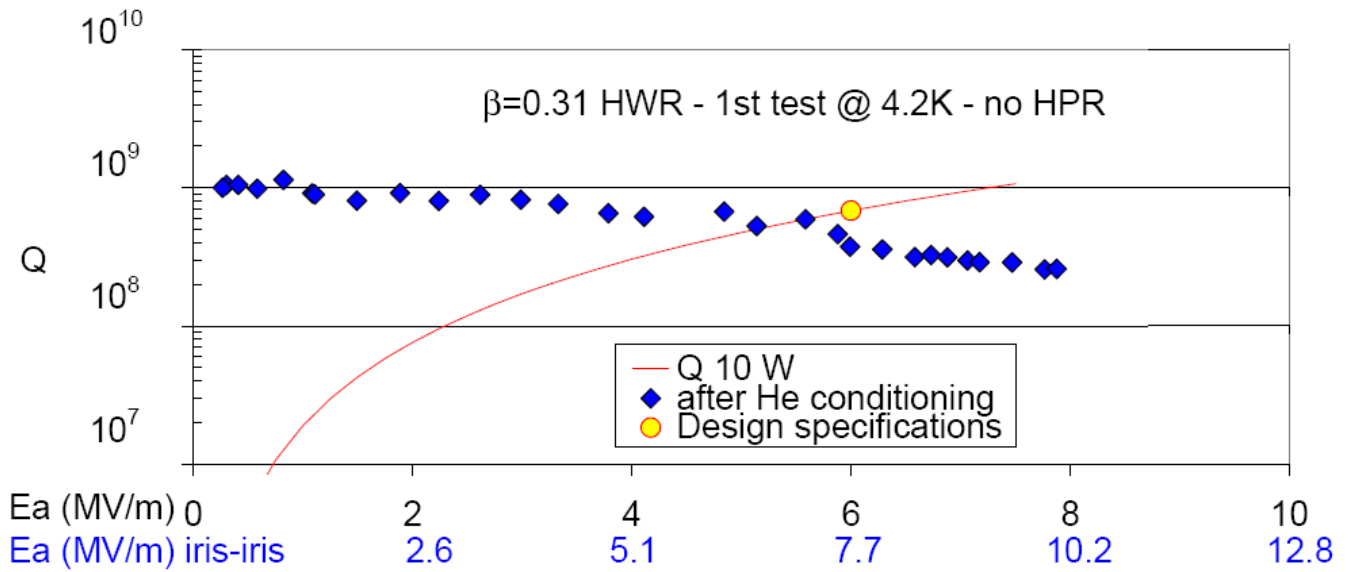


Fig. 4: Test results at 4.2K of the $\beta = 0.31$ half-wave resonator.

8.2.2 Half-wave resonators designed for 176 MHz

The previous HWR design at 352 MHz was adapted at 176 MHz to take into account the evolution of the EURISOL driver reference layout. Two different beta values ($\beta = 0.09$ and $\beta = 0.16$) were also studied and optimized (see figure 5). The RF parameters are given in the table shown in figure 6.

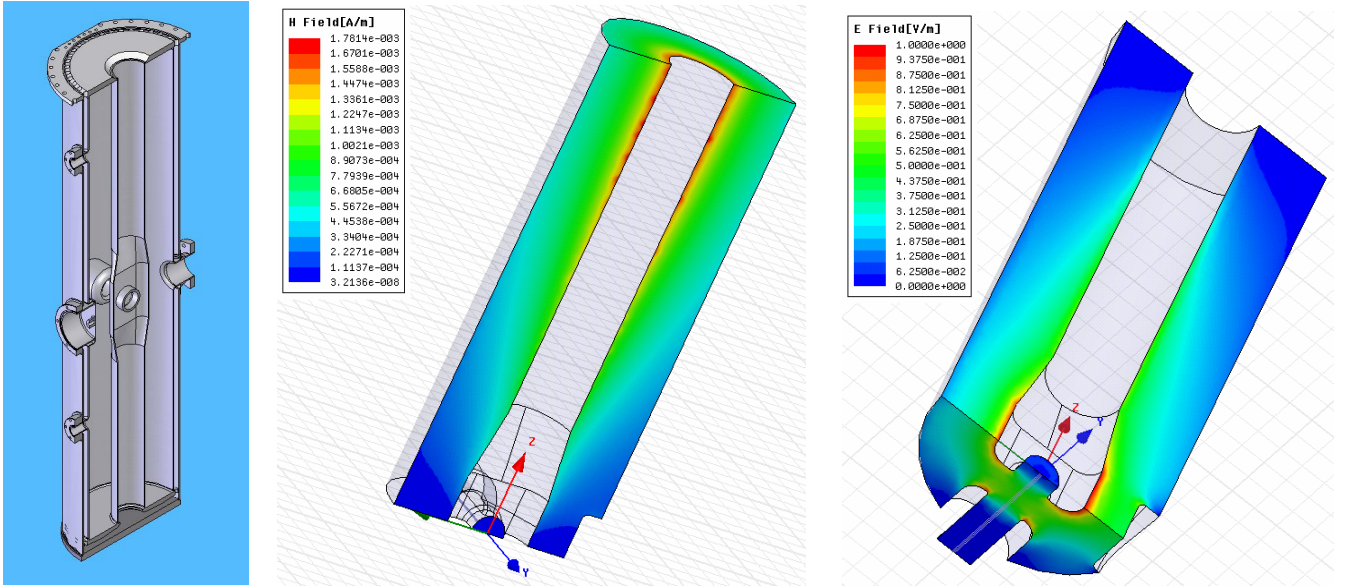


Fig. 5: 176-MHz, $\beta = 0.09$ half-wave resonator (left) and RF field distribution (centre: magnetic field; right: electric field).

Resonator type:	HWR1	HWR2	Units
β	0.085	0.155	
U/E_a^2	0.134	0.173	$\text{J}/(\text{MV}/\text{m})^2$
B_p/E_a	12.4	11.7	$\text{mT}/(\text{MV}/\text{m})$
E_p/E_a	5.8	4.2	
R'_{sh}/Q_0 ($E_a^2 \cdot L/(Q_0 P)$)	1215	1181	Ω/m
$R_s \times Q_0$	31.9	38.2	Ω
Active length L	180	224	mm
Maximum length L_{re}	232	286	mm
Aperture diameter a	30	30	mm
Design E_a	5	6	MV/m
He pressure detuning	1	3.7	Hz/mbar
Lorentz force detuning	-3.6	-1	$\text{Hz}/(\text{MV}/\text{m})^2$

Fig. 6: Main RF parameters of the two 176-MHz half-wave resonators.

8.2.3 Cold tuning system (CTS) for half-wave resonators

A cold tuning system (CTS) is a mandatory ancillary system for a resonant accelerating structure in order to be able to tune a cavity inside the module. The high efficiency (quality factor) of a superconducting cavity leads to a quite narrow frequency bandwidth, putting strong requirements on the CTS in terms of resolution and adjusting frequency range. For the HWR, the proposed solution for the CTS is the following (see figure 7): a 1.25-mm thick niobium membrane closes a port located on the cavity at the opposite side of the power coupler port. A mechanical system composed of a stepping motor, a screw-nut system and an L-shaped lever can push or pull on the niobium membrane, deforming it and changing the inner cavity volume, thus resulting in a cavity frequency change.

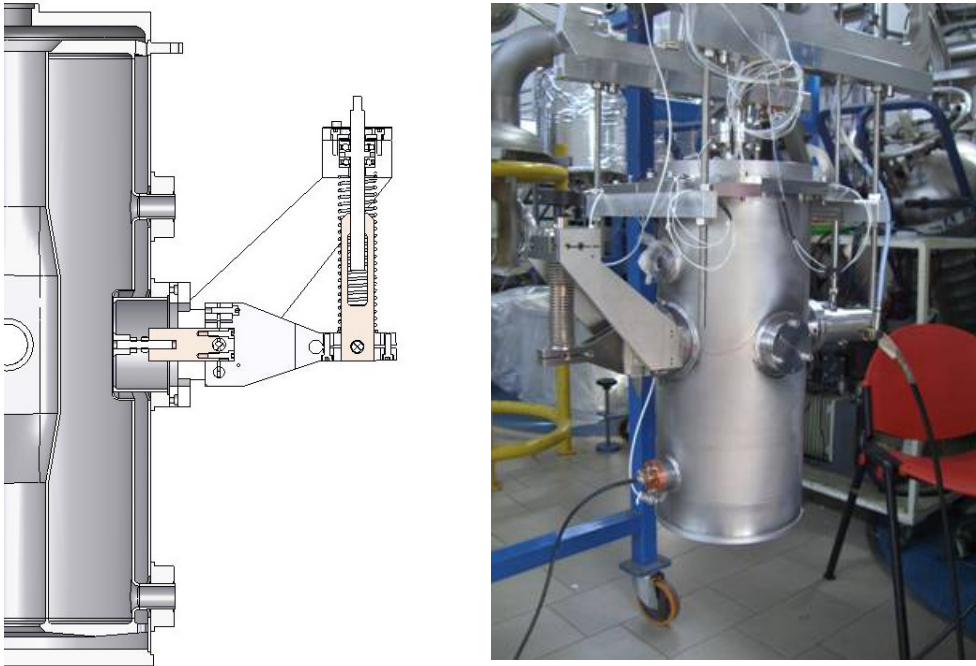


Fig. 7: Sketch and picture on the cold tuning system mounted on the HWR.

The CTS for the half-wave resonator has been successfully tested at cold temperature in a vertical cryostat. The system could provide a 100-kHz tuning range, with a 10-nm mechanical resolution giving about 1 Hz of frequency resolution.

8.3 Spoke cavity developments

Spoke cavities are superconducting accelerating structures which are very promising for accelerating hadrons beams up to 150 MeV/u (and even more). Their main advantages are the natural stiffness, the capability to deliver high accelerating gradients, and the possibility to have multi-cell structures, leading to a high real-estate gradient. For the energy range between 60- and 140-MeV/u, triple-spoke cavities are the most promising solution to achieve an efficient acceleration of protons, deuterons and $^3\text{He}^{++}$ ions. Important prototyping work on this accelerating structure has been performed as part of the EURISOL Design Study. At first, single-spoke resonators cavities were studied, fabricated and tested before we began designing a triple-spoke cavity with the required parameters to fit the final EURISOL driver specification.

8.3.1 Spoke cavity development at 352 MHz

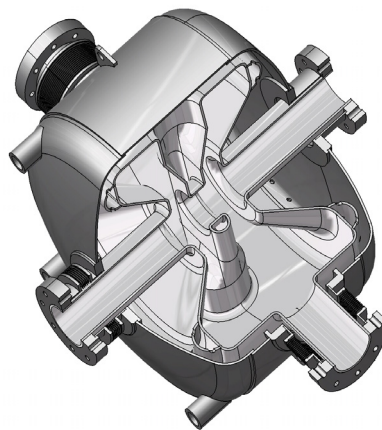


Fig. 8: Cut-away view of the $\beta = 0.15$ single-spoke resonator.

Two single-spoke resonators have been developed at two different beta: 0.35 and 0.15. The high-beta cavity was only optimized in terms of RF performances: the mechanical behaviour was not studied at that time. The low-beta spoke cavity is a more “complete” prototype (fig. 8), including optimized stiffening half-tubes and its helium tank. The spoke bar has a complex shape (racetrack) in order to lower the peak surface fields and to optimize the peak fields over the accelerating field ratio.

Pictures of the two single-spoke prototypes are show in figure 9. On the low beta cavity, the helium tank was welded in a second time, after having tested at cold temperature the “naked” cavity. The beam port diameter for both cavities is 56 mm. The power coupler port location and diameter was modified between the high- and low-beta prototype in order to lower the losses (changing from a 45° angle between the port and spoke bar to 90°) and to increase the power coupler RF capabilities (increasing the diameter from 30 mm to 56 mm). The RF parameters are given in the table of figure 10.



Fig. 9: The two prototype single-spoke superconducting cavities, with $\beta = 0.15$ (left), $\beta = 0.35$ (right)

Parameter	Unit	Single spoke		
		$\beta=0.35$	$\beta=0.15$	Comment
Design frequency	MHz	352.2	352.2	
Number of accelerating gaps		2	2	
β (optimum)		0.36	0.2	
L_{acc}	m	0.297	0.17	$L_{acc} = N_{gap} \cdot \beta \cdot \lambda / 2$
Q_o (4.2 K)		1.9 E+9	1.3 E+9	with $R_{res} = 10 \text{ n}\Omega$
Q_o (2K)		8.8 E+9	6.2 E+9	with $R_{res} = 10 \text{ n}\Omega$
r/Q	Ω	220	88	
G	Ω	101	67	
E_{pk}/E_{acc}		4.56	6.74	with $L_{acc} = N_{gap} \cdot \beta \cdot \lambda / 2$
B_{pk}/E_{acc}	mT/MV/m	12.33	14.48	with $L_{acc} = N_{gap} \cdot \beta \cdot \lambda / 2$
Voltage gain	MV	1.96	0.63	at $E_{pk} = 30 \text{ MV/m}$

Fig. 10: RF parameters for the two single-spoke cavities

The cavities have been tested in the IPN Orsay vertical cryostat after a careful preparation: buffered chemical polishing to remove 120 μm , followed by high pressure rinsing and assembly in a clean room. The test results are shown in figures 11 and 12. The high-beta cavity reached a high accelerating field and the performance of low-beta one was acceptable but a little bit disappointing compared to the first cavity. We suspect the presence of a defect in the niobium surface, limiting the maximum accelerating field.

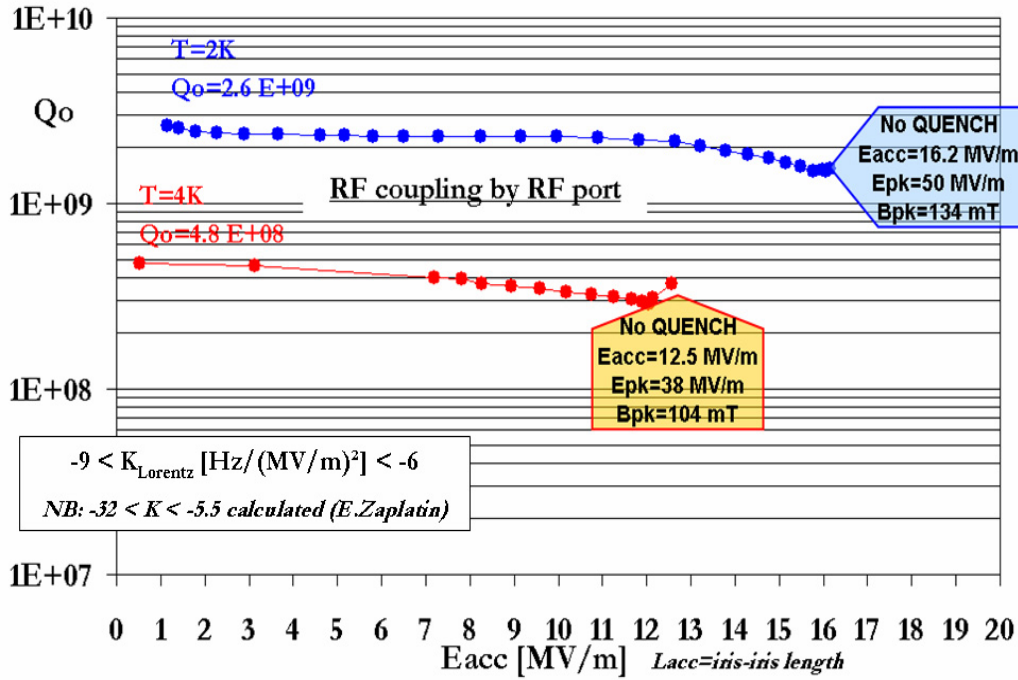


Fig. 11: Cold test results of the $\beta = 0.35$ spoke cavity

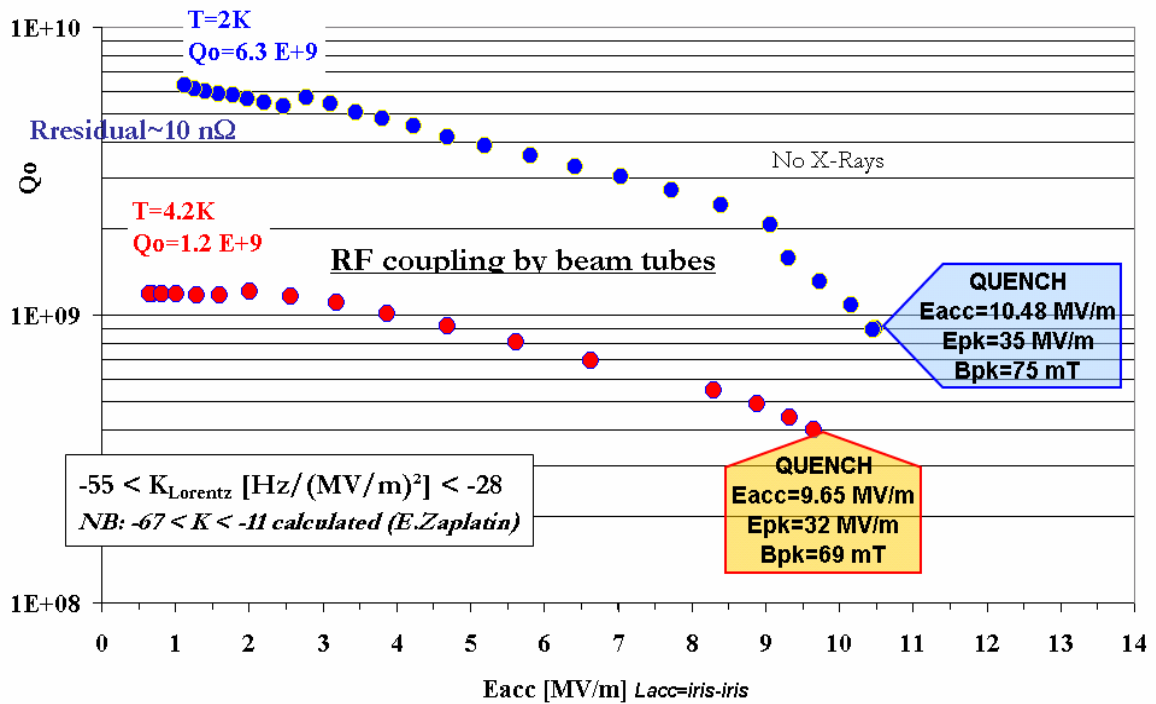


Fig. 12: Cold test results of the $\beta = 0.15$ spoke cavity.

8.3.2 Triple-spoke cavity design at 352 MHz

In order to fit the evolution of the EURISOL driver reference layout, we decided to develop a new spoke cavity prototype with 4 accelerating gaps (3 spoke bars). A cutaway view of the cavity is shown in figure 13. The design was adapted from the first two single-spoke prototypes, but a full optimization was performed in order to achieve the best possible RF geometry. The cavity was modelled using the CST Microwave studio RF code: a full 3D model was used and 13 main parameters were scanned, representing more than 300 computed cavities, to reach the optimum values of the ratio of peak field to accelerating field. The final result is $E_{pk}/E_{acc} = 4.1$ and $B_{pk}/E_{pk} = 9.0$ mT/MV/m. The niobium for the cavity fabrication was received and the cavity fabrication completed.

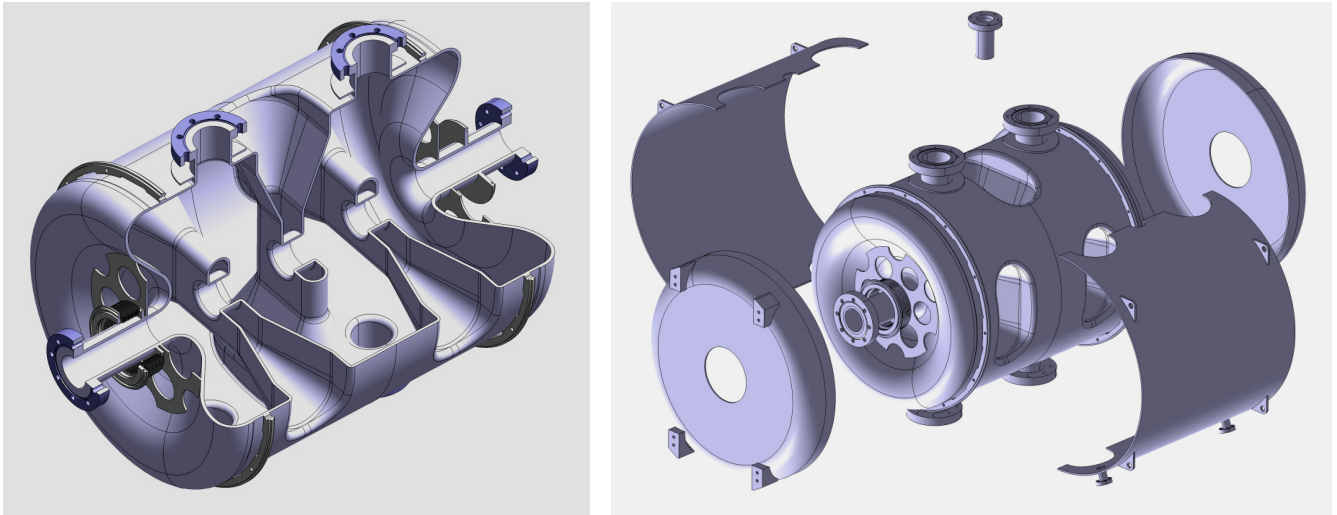


Fig. 13: Cutaway view of the final geometry of the triple spoke (left) and helium tank assembly (right)

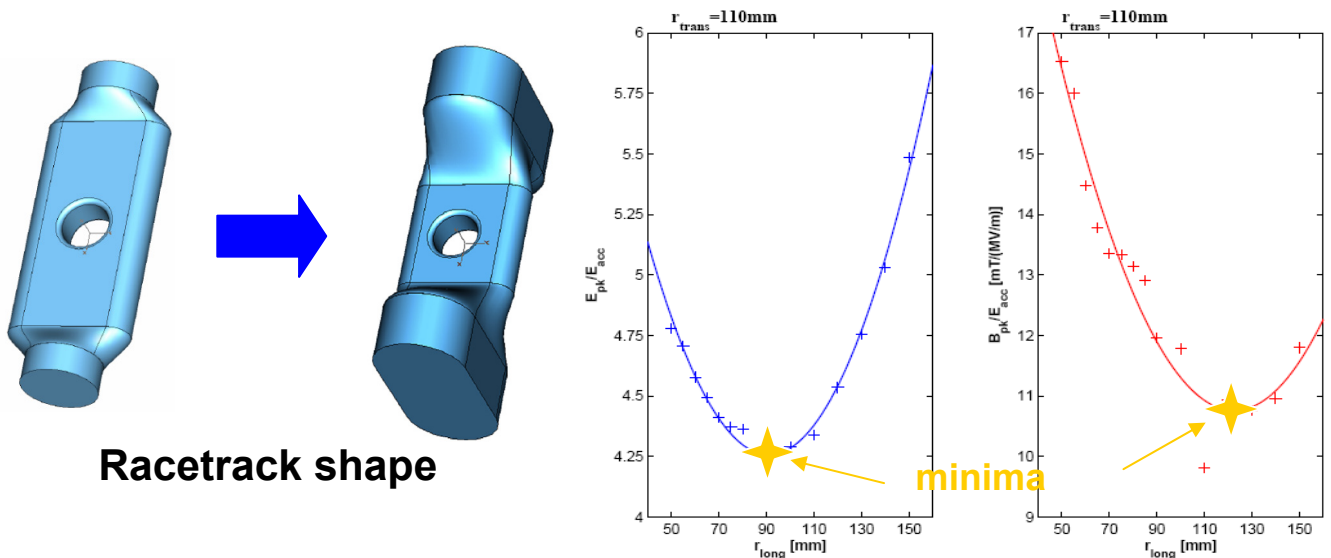


Fig. 14: Optimization of the spoke cavity's bar geometry and the effects on the peak fields.

8.3.3 Cold tuning system (CTS) for spoke resonators

The spoke cavities CTS is an adaptation of the CTS we have developed for the elliptical 700-MHz, 5-cell cavities. Its design is based on the system developed by the CEA for cavities used at SOLEIL. The CTS consists of a mechanical system (figure 15) driven by a cold stepping motor operating in vacuum

and a motoreductor. The motor drives a ball-screw, linked to a double lever-arm mechanism which can act on four rods attached to the cavity. The design was optimized to obtain high rigidity, lowest possible weight and cost. The system also offers the possibility of using piezoelectric actuators for the fast compensation of frequency shifts.

The theoretical resolution of the system is 1 nm per micro-step, giving a frequency resolution of 1 Hz. Another important requirement is the CTS mechanical rigidity that should be much higher than the cavity rigidity, in order to keep all the longitudinal displacement available for the cavity deformation. The $\beta = 0.15$ spoke cavity axial rigidity was estimated at 6 kN/mm. Calculations performed with CATIA give a CTS rigidity estimation of 162 kN/mm. This high value allows 96% of the CTS longitudinal displacement to be effectively seen by the cavity.

The cold tuning system was tested at room temperature and then at 4.2K in the spoke cryomodule. The results are presented in section 8.6.

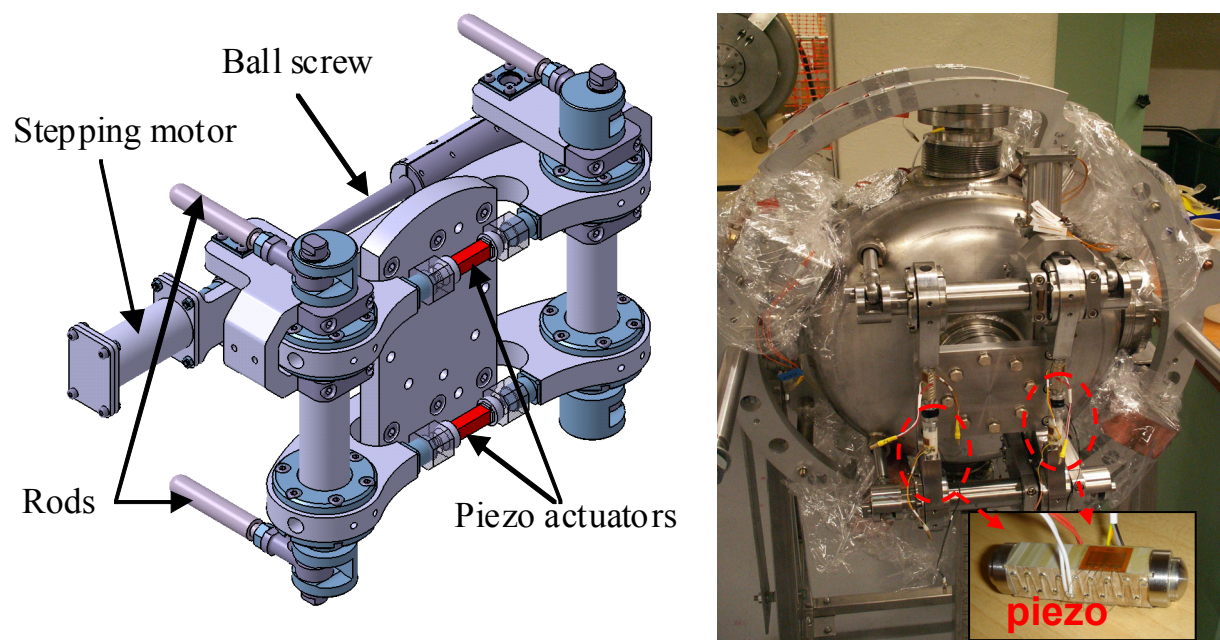


Fig. 15: Cold tuning system developed for spoke resonators.

8.4 Solid-state RF power amplifier developments at 352 MHz

In order to perform the cavity and coupler test at the nominal RF power, RF power amplifiers have been developed by INFN/LNL. Several units were constructed: one of 5 kW, and two of 10 kW. The main purpose of this study was to develop and test an unconditionally stable RF amplifier based on transistors (MOSFET) which is very compact and cost effective. The amplifier uses 300-W solid-state modules, designed at LNL, assembled by means of 8-way RF combiners and splitters and a high-power 4-way combiner (figure 16).

The module is based on a Semelab DMD1029A MOSFET, a 300-W circulator and a power termination in order to manage the reflected power during transients when there is no beam loading in the superconducting cavities. The 10-kW amplifier is housed in a 0.6-m wide, 1-m deep and 2-m tall rack cabinet. The amplifier integrates the power supplies and the necessary cooling channels and plates to limit the transistors temperature increase. The amplifier can be operated from a computer touch-panel located in the front panel, or from a remote computer connected through an Ethernet link.

Pictures of the 5-kW and 10-kW units are shown in figure 17.

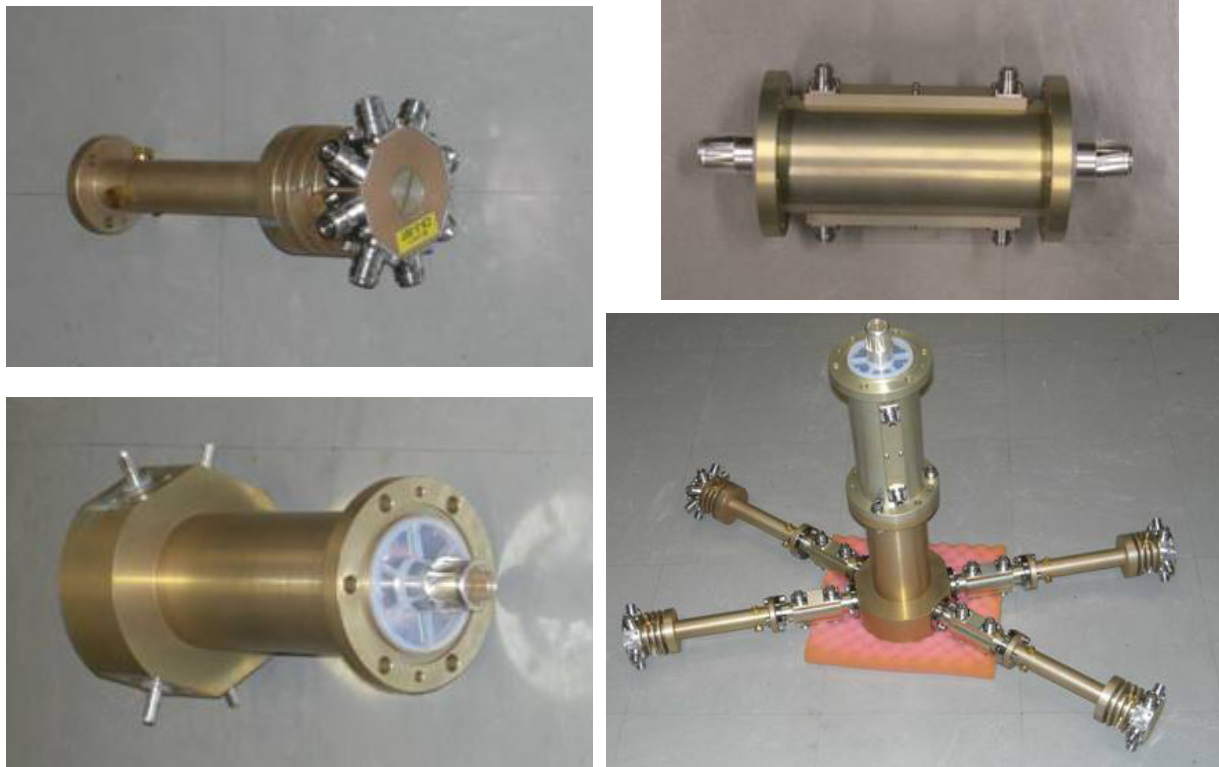


Fig. 16: RF components of the amplifier: a 2.5-kW, 8-way combiner (top left), a 10-kW, 4-way combiner (bottom left), a high-power directional coupler (top right) and a high-power output stage (bottom right).

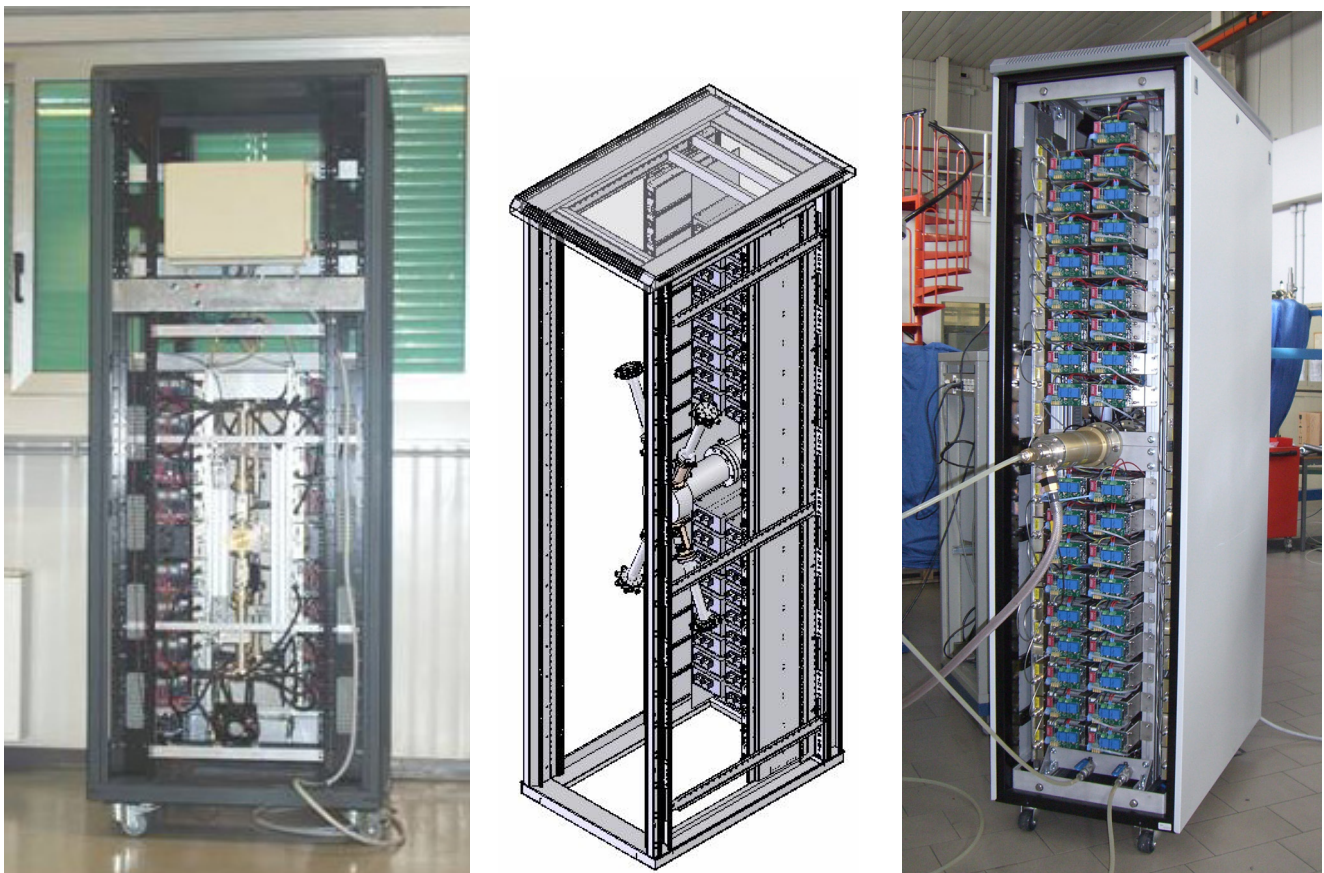


Fig. 17: Solid-state RF amplifiers operating at 352 MHz: the 5-kW unit (left), a sketch of the 10-kW unit (centre) and a rear view one of the 10-kW units (right).

All modules have been individually tested and tuned by a joint LNL/IPN team before assembly in the racks. A intense test campaign was performed, first on the 5-kW unit and then the 10-kW unit, in order to characterized the amplifier fully, and also to check the amplifier's stability (with long test runs) and capability to operate under any condition (with or without reflected power). The power level of 10 kW has been reached with a moderate gain drop of about 3 dB (see figure 18). Long test runs allowed us to define a safe operation point at 8.8 kW.

LNL 10 kW Amplifier

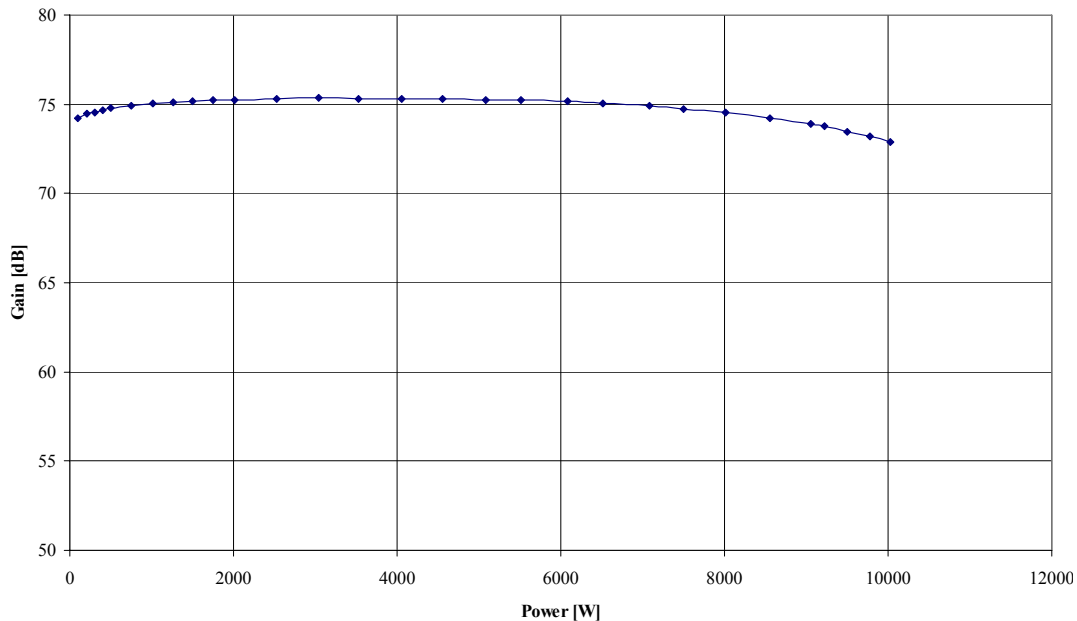


Fig. 18: Measurement of the 10-kW RF amplifier gain as a function of the output power.

In order to have the possibility to reach 20 kW of RF power for future tests, a high-power combiner was developed. It allows one to combine the two 10-kW RF units in a very efficient way. Calculations performed with CST Microwave Studio showed that the combiner's S_{11} parameter (reflected power coefficient) is only -60 dB.

One 10-kW RF unit was sent to IPN Orsay to be used in the power RF bench, to condition the power coupler and to perform the spoke cavity RF power test in the cryomodule.

8.5 Power coupler developments for 352-MHz superconducting cavity

A 352-MHz capacitive power coupler has been developed for the 2-gap spoke cavities to be mounted on the 56-mm diameter port. The same coupler is also suitable for the 352-MHz half-wave resonator, providing that a specific RF transition is used to manage the differences in the cavity's power coupler port diameter.

The coupler geometry is coaxial, at 50 Ω using a warm disk ceramic window. The coupler is designed to be able to transfer 20 kW of RF power to the cavity. Two pipes located on the window outer diameter offer the possibility of water-cooling the ceramic.

Several window geometries were studied: a cylindrical, disk (with and without chokes), and a travelling wave. For each geometry, the HFSS software was used to calculate the RF parameters, the surface field on the ceramics, the bandwidth, and the RF losses. Finally, the design based on a disk ceramic without choke was chosen because it was the best compromise between good RF performance and simplicity, leading to a reliable and cost-effective design. The computed S_{11} parameter is shown in figure 19: a value of -57 dB is obtained at the nominal frequency. The coupler exhibits a very large bandwidth, allowing standard fabrication tolerances to be used.

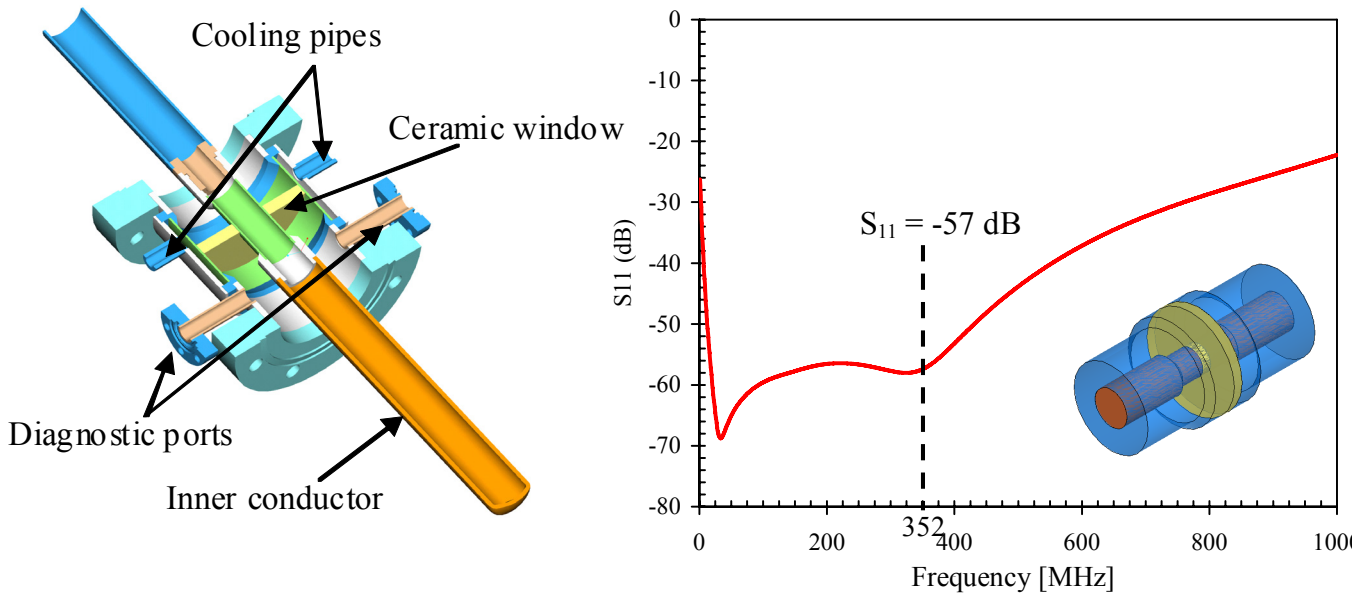


Fig. 19: Assembly drawing of the 352-MHz power coupler (left), and computed S_{11} parameter (right).

Two ceramic windows prototypes were ordered from the SCT Company. They have been characterized at low power (measurement of RF parameters) before the antenna welding. After delivery of the two complete power coupler prototypes, the conditioning test bench was set up, after careful cleaning and final assembly of the important parts (RF ceramic windows, the coaxial part between the cavity and window, and the conditioning cavity) in the IPN Orsay clean room (figure 20).

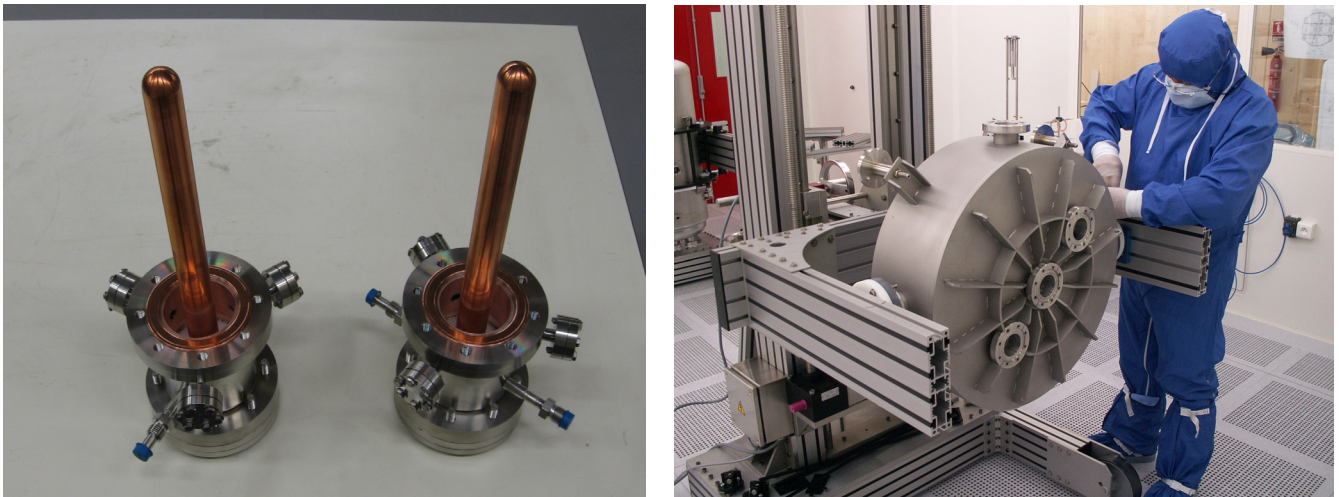


Fig. 20: The two power coupler prototypes (left) and the conditioning cavity assembly in the clean room.

The conditioning of the power coupler has since been carried out on the warm test bench (shown in figure 21). This important stage involved feeding the two power couplers mounted in series with increasing RF power, from 0 to 10 kW, step by step. The aim is to condition the RF surface to get rid of any electron emission or multipacting in the coupler. After a few hours, the couplers succeeded in transmitting the 10 kW of RF power, and a stable operational point was reached.

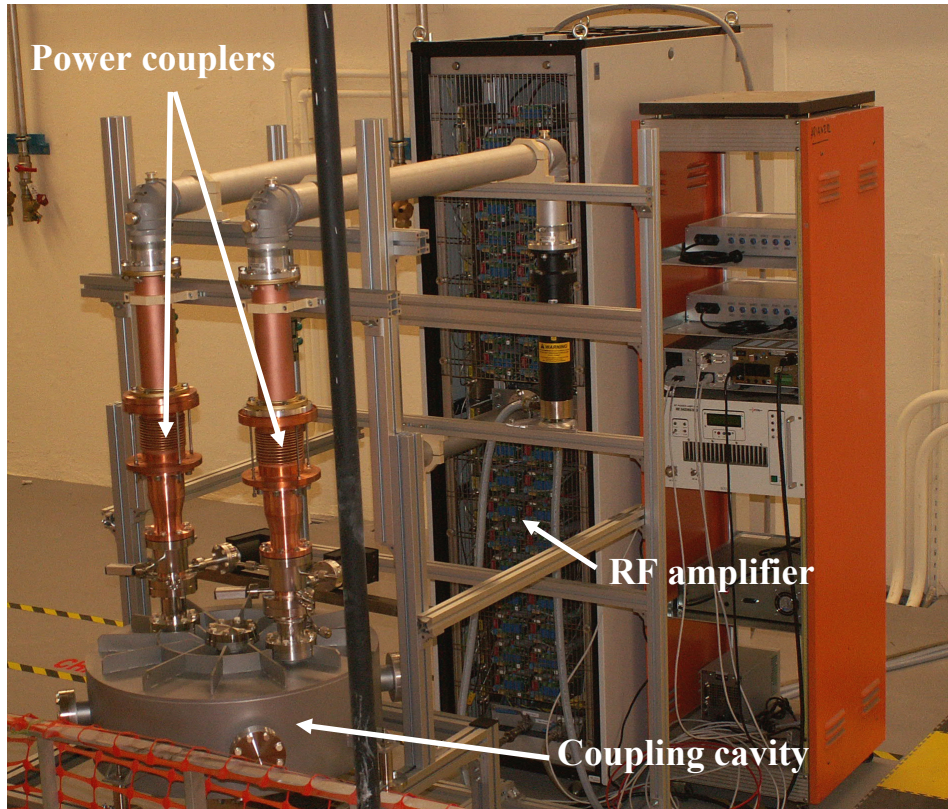


Fig. 21: Power coupler conditioning bench during operation at 10 kW.

8.6 Cryomodule design and test of fully-equipped spoke cavities

To assess that spoke cavities are capable of efficiently accelerating particles with the designed performances, one key test consists of a cold test of a superconducting spoke cavity fully-equipped with all its ancillaries systems: helium tank, power coupler, and cold tuning system. Such a test allows one to address almost all potential difficulties in the operation of a superconducting cavity in a real accelerator. The mechanical, thermal, and RF behaviour of the full system is tested in a cavity configuration close to the final one in the accelerator.

The spoke cryomodule is composed of two main components (see figure 22):

- the vacuum tank, which contains the cavity and its ancillaries, a helium Dewar, the cryogenic piping and instrumentation;
- the “cold box”, external to the cryomodule, which provides the module with the cryogenic fluids (liquid, gas).

The module was designed to be a laboratory test stand to test several types of spoke cavity under several configurations. The main requirements were the following:

- The cryomodule was conceived to have dimensions long and wide enough to hold a fully-equipped spoke cavity, low or medium β .
- The temperature operation point is 4.2K but both module and cold box have the possibility to operate using a depressed helium bath to perform cavity tests at lower temperature (typically 2K).
- The power coupler could be mounted in 2 different configurations: a vertical position (better for mechanical reasons), or with a 45° inclination with respect to the vertical (potentially better for the spoke bar cooling by liquid helium).

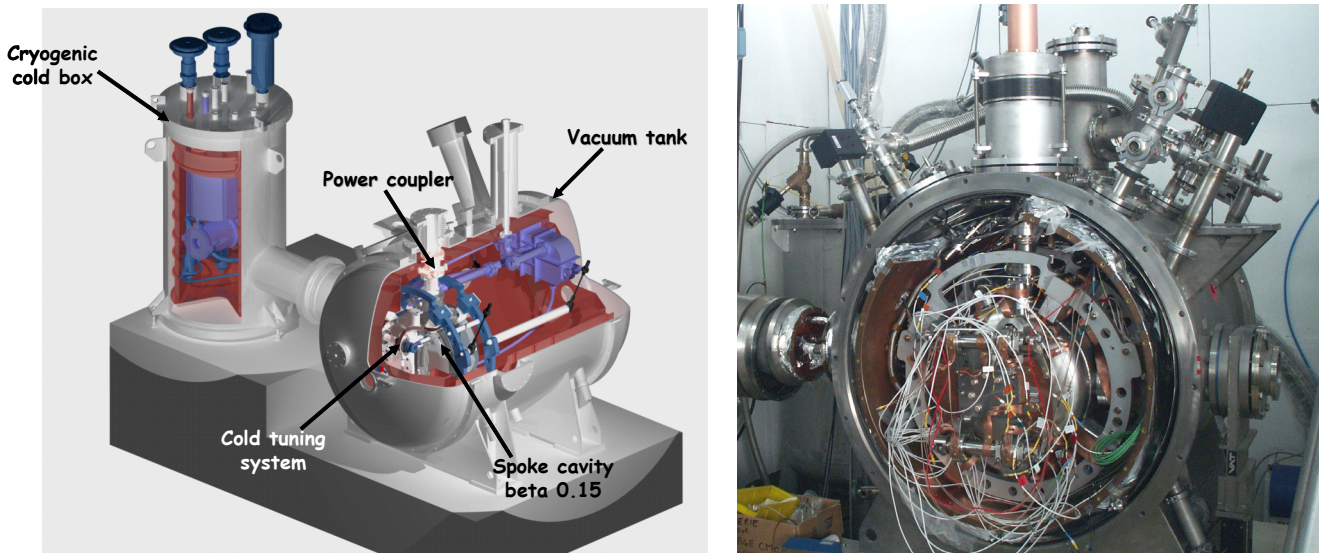


Fig. 22: Sketch and photograph of the spoke-cavity's test cryomodule and its associated cold box

At IPN Orsay, the last preparatory steps for this final test have been done in the Supratech infrastructure. In a Class 10 clean room, the $\beta = 0.15$ spoke cavity was prepared for assembly. The cavity was removed from the cryomodule and subjected to high-pressure water rinsing at 100 bar, with ultra-pure water (resistivity of $18.2 \text{ M}\Omega\cdot\text{cm}^{-1}$). The power coupler was dismantled from the conditioning cavity under the clean room laminar flow and mounted on the spoke cavity. The cavity/coupler assembly was pumped out and a final leak check was performed, in order to assess the vacuum tightness of the assembly. The final module assembly was then completed, and the cavity/coupler assembly was inserted into the module vacuum tank. The coupler external coaxial conductor and the bellows were mounted. The cavity tuner and all the instrumentations were then installed (figure 23). The complete assembly was then installed on the cryogenic test stand.

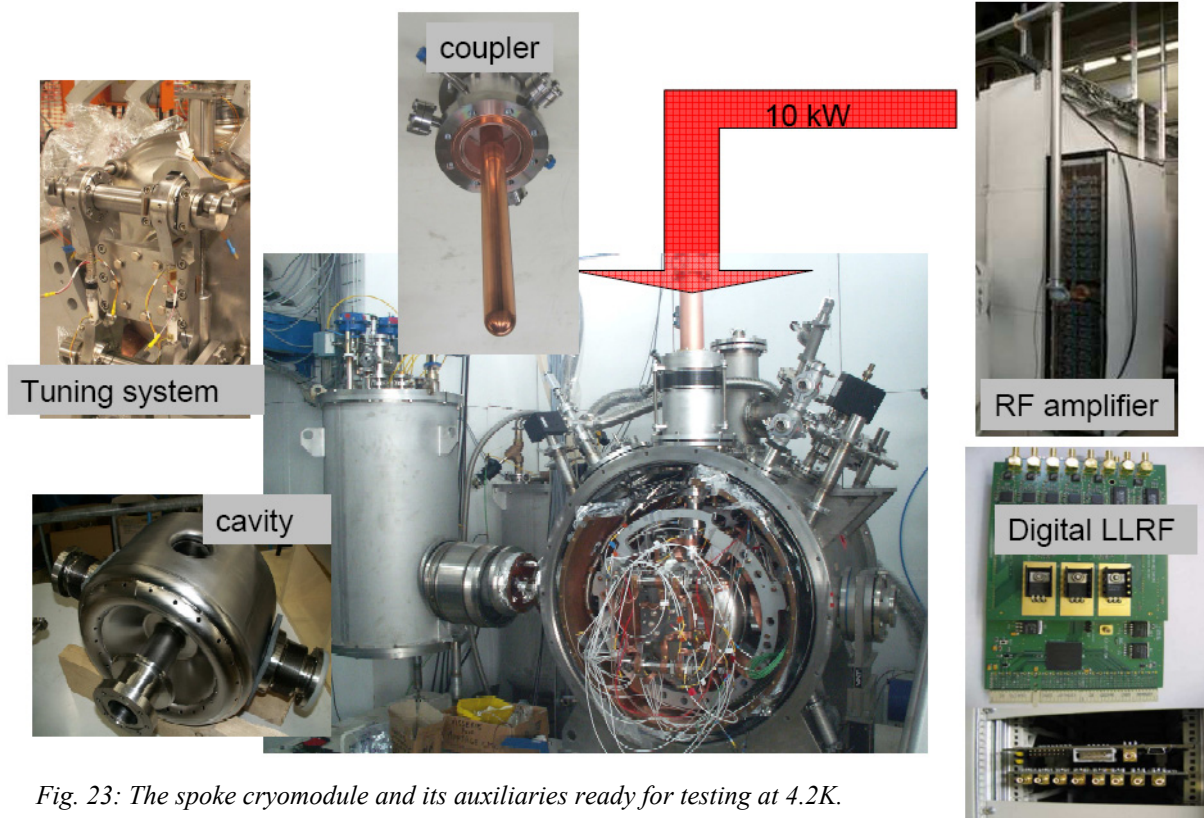


Fig. 23: The spoke cryomodule and its auxiliaries ready for testing at 4.2K.

The INFN/LNL 10-kW power amplifier was then connected to the module by means of a standard rigid coaxial RF line, and the cold box connected to the module cryo-fluids inputs and outputs. The 352-MHz low-level digital RF controller – developed by IPN Orsay and LPNHE laboratories – was used to control the RF excitation of the cavity.

For this experiment, we have set the parameters to simulate a coupler and cavity operation, e.g. the cavity being set to accelerate a beam (i.e. operation with beam loading). The coupling factor of the antenna to the cavity was set to 1×10^6 . In this configuration, but without beam, most of the incident RF power is reflected into the RF line, and the maximum achievable field in the cavity is about 1 MV/m. The main objective was to test the whole RF line and the coupler up to the cavity flange at nominal RF power.

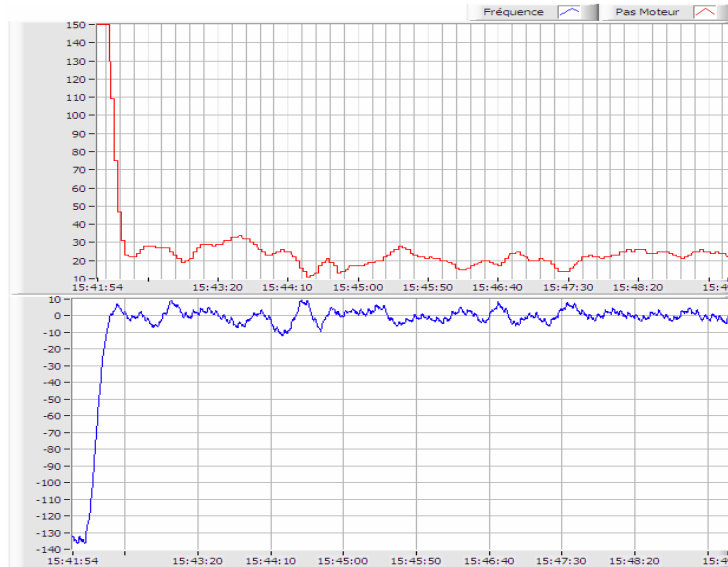


Fig. 25: Experimental curves showing the frequency regulation obtained with the spoke CTS during the cryomodule test at 4.2K. The upper curve is the motor displacement (stepping-motor steps) as a function of time and the lower curve is the frequency error in Hz with the same horizontal time scale – here only a few minutes.

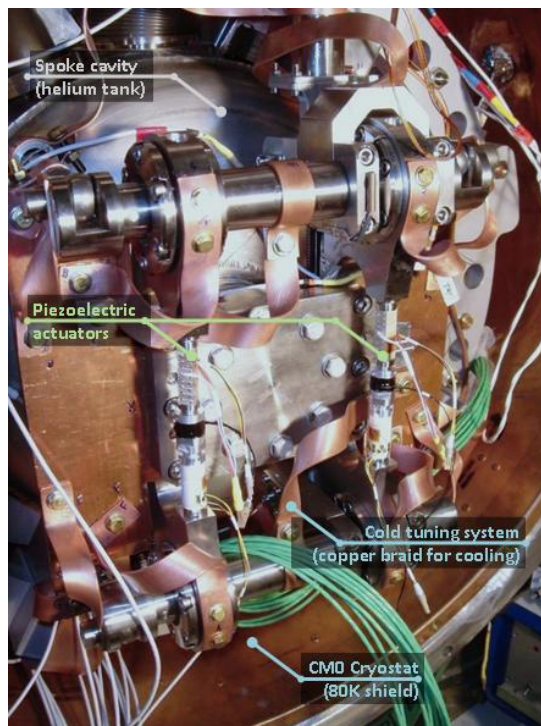


Fig. 26: The spoke CTS with its piezo-actuators.

The main results of this final experiment were the following:

- The cryogenic operation of the cryomodule was successful: modifications performed after a first cryogenic test allowed us to cool the entire system efficiently, including the cold tuning system (CTS), without having any major temperature differences between the cavity and the CTS.
- The coupler was easily conditioned in-situ in less than 2 hours: 5.5 kW of RF power was transported through the whole RF line, through the ceramic window up to the cavity flange in a detuned mode (out of the cavity resonance). The heating of the ceramic window was not an issue.
- The estimated Q_0 (a precise measurement is impossible with a high RF coupling) showed that the magnetic shielding was efficient and that the power coupler has no influence on the cavity dissipation at low accelerating fields.
- The CTS operation was successful: the system operated perfectly, without any mechanical problem and only a minor hysteresis. A frequency regulation was performed, and a ± 10 -Hz regulation was obtained over several hours.
- A cryogenic test at 2K was also performed, just to check the overall capability of the whole system to operate with a depressed helium bath. This configuration might be an alternative to 4K operation because increased performance could be obtained on the spoke resonators (see the 2K results in figures 11 and 12) at a rather low cost, because in the EURISOL driver linac layout the next accelerating section is operating at 2K (elliptical cavities).

This final experiment, with a spoke cavity fully equipped with its helium tank, power coupler and cold tuning system, showed the efficiency of the full accelerating system design (cavity, tuner and power coupler). This experiment is an important and decisive step towards the final proof that spoke cavities are an efficient solution to accelerate intense protons beams.

An experiment had been envisaged within the EURISOL Design Study program to use the low-current beam of the IPN Orsay tandem accelerator to “feed” the spoke cryomodule, and then to test a spoke cavity with beam for the first time.

Unfortunately, due to the recent important development of the ALTO facility at the tandem, insufficient time and space were available to develop this complex experiment.

8.7 Conclusion

Our aim, within the EURISOL Design Study was the design, construction and testing of several key component of the EURISOL accelerators. Important prototyping work was performed on half-wave resonators and spoke resonators in order to assess their capabilities for efficiently accelerating intense hadrons beams. The performance obtained with both these accelerating structures, together with their ancillary systems, proved that this technology is now in an advanced stage, and that that these systems could be considered as a viable part of the reference solution for the EURISOL accelerators.

Chapter 9: Calculated Yields of Exotic Ions

9.1 Outline of the task

The purpose of the proposed ISOL-based secondary-beam facility is to deliver beams of radioactive nuclei with the highest intensities possible and with the most widespread neutron-to-proton ratio possible, for experiments which aim to improve our knowledge of nuclear properties far from the valley of beta stability, reaching areas on the chart of nuclides close to the so-called “drip-lines”. At the start of the EURISOL Design Study, knowledge of attainable beam intensities in ISOL-based secondary-beam facilities driven by protons of about 1 GeV relied mostly on the long-term experience in facilities such as ISOLDE at CERN. However, it is not easy to disentangle the formation cross sections, which are determined simply by physics, and the release, ionization and transport efficiencies, which are subject to progress in technology. Systematic data on spallation cross sections with protons around 1 GeV only became available a few years ago for selected systems, based on innovative inverse-kinematics experiments at GSI. Nuclide cross sections from spallation or heavy-ion induced reactions at lower energies were still scarce.

Clearly, the estimation of the available secondary-beam intensities and, in particular, of the limitations in their neutron-to-proton ratio is of prime importance for the proposed facility. Moreover, these estimations, performed for different possible technical solutions, will help in making decisions on the preferences given to the different technical options in the design phase.

The work has been divided in several sub-tasks:

- 1) Benefit of heavy-ion capabilities of the driver accelerator.
- 2) Fragmentation of post-accelerated ISOL beams.
- 3) Fission models.
- 4) Spallation and fragmentation reactions.
- 5) Neutron- and proton-induced reactions up to Fermi-energy.
- 6) Heavy-ion reactions in the Fermi-energy domain.
- 7) Aspects of secondary reactions in single and double-stage targets.
- 8) Predictions of secondary-beam intensities.

In the following sections, the major results obtained in these different fields are described.

9.2 Benefit of heavy-ion capabilities of the driver accelerator

The secondary-beam production in the EURISOL baseline option (1-GeV proton beam of 3–4 MW on a converter target and also 100 kW onto a direct target) allows for producing a large number of isotopes of many elements using different target materials. However, it was thought that extending the capabilities of the driver accelerator in order to provide additional beam species and more complex technical approaches might result in a benefit for producing nuclides in certain regions of the chart of the nuclides. This question was therefore investigated in a systematic way. To this end, the possible benefits of extended capabilities of the driver accelerator were considered, with a quantitative discussion of nuclear-reaction aspects and the technical limitations of the ISOL method. From this study, the following results have been obtained:

With respect to the standard baseline driver option, the following cases do indeed provide substantial benefits:

- A 2-GeV $^3\text{He}^{2+}$ beam would fill the gaps in nuclide production given by the limited choice of ISOL target materials. This would lead to gains of up to a factor of 4, in particular for the production of neutron-deficient isotopes of many elements.
- A 2-GeV $^3\text{He}^{2+}$ beam would also increase the production of neutron-rich isotopes of light to medium-heavy elements ($Z < 30$) by about a factor of 2.

- The deuteron-converter option with a primary-beam energy between 40 MeV and 100 MeV would provide fission-fragment nuclide distributions with appreciably higher fission yields (normalized to the total number of fission events in the target) for elements between technetium ($Z = 43$) and indium ($Z = 49$), below germanium ($Z = 32$), and above neodymium ($Z = 60$) compared to the standard EURISOL high-power-target option. However, only part of this advantage can be realised in practice, since many of the enhanced elements are poorly released (or not released at all) from ISOL-type targets.
- Fragmentation of heavy-ion projectiles provides higher in-target yields for some neutron-deficient isotopes of light elements and presumably higher overall ISOL efficiencies for short-lived isotopes. It can also be useful to overcome limitations in the choice of the target material in the standard proton option, and to divide production target and catcher. The gain factors depend strongly on the beam energy.
- Due to nucleon-exchange between projectile and target, heavy-ion reactions in the Fermi-energy regime (around $20\text{--}30 \cdot A$ MeV) provide a substantial benefit for the production of neutron-rich isotopes of elements outside the main fission region.

The quantitative conclusions presented here depend on assumptions on the values of some key parameters, e.g. maximum beam intensities or limits on the target heat load. Investigations on these parameters were the subject of intense research and development in other task groups of the EURISOL Design Study. Based on this work, an improved layout of the driver accelerator was proposed. Several capabilities, alternative to the 1-GeV proton beam, such as a ^3He beam at 2 GeV, a 250-MeV deuteron beam and beams with $A/Q=2$ at $125 \cdot A$ MeV, were consequently included in the final driver accelerator design. A final report [1] is available on the EURISOL DS Web-site.

9.3 Fragmentation of post-accelerated ISOL beams

The possibility of using multiple-step reactions in specifically designed complex scenarios was investigated, in order to produce radioactive nuclides with extreme neutron-to-proton ratio, which are not accessible by a “standard” ISOL method. The proposed option is to produce a neutron-rich secondary beam based on fission in a standard ISOL procedure, and then to fragment it after acceleration. For this option, the optimum energy of the post-accelerator was discussed.

The high-power target at the future EURISOL facility will take advantage of an extremely high fission rate for producing medium-mass neutron-rich nuclei – with the exception of the refractory elements. In order to overcome this limitation, a two-step reaction scheme has been proposed. This method also has the advantage of producing even more neutron-rich nuclei than those produced by fission.

According to this idea, intense beams of neutron-rich nuclei could be produced by re-accelerating non-refractory fission residues, e.g. ^{132}Sn , produced in an ISOL facility. These neutron-rich projectiles could then be fragmented to produce more neutron-rich nuclei covering the refractory gaps. This scheme has been tested at the fragment separator (FRS) at GSI, and the measured data has been analysed and compared with different model calculations. In figure 1 (below), the measured isotopic distributions of the production cross sections of residual nuclei produced by the fragmentation of ^{132}Sn in beryllium target are plotted.

As can be seen, very neutron-rich isotopes of In, Cd, Ag, Pd, Rh and Ru with cross sections as low as $10 \mu\text{b}$ were produced, thus covering the gap of refractory elements in this region of the chart of the nuclides. In the case of In, Cd and Ag, the most neutron-rich nuclei that can be produced in the fragmentation of ^{132}Sn – corresponding to the one-proton (^{131}In), two-proton (^{130}Cs) and three-proton (^{129}Ag) removal channels – have been reached. Error bars are dominated by statistical uncertainties.

The good quality of the data obtained in this work has made it possible to benchmark different reaction codes describing the production cross sections of fragmentation residual nuclei. In particular, the semi-empirical formula EPAX and a simplified version of the abrasion-ablation model, i.e. the COFRA code [2], have been tested and the results are shown in figure 1.

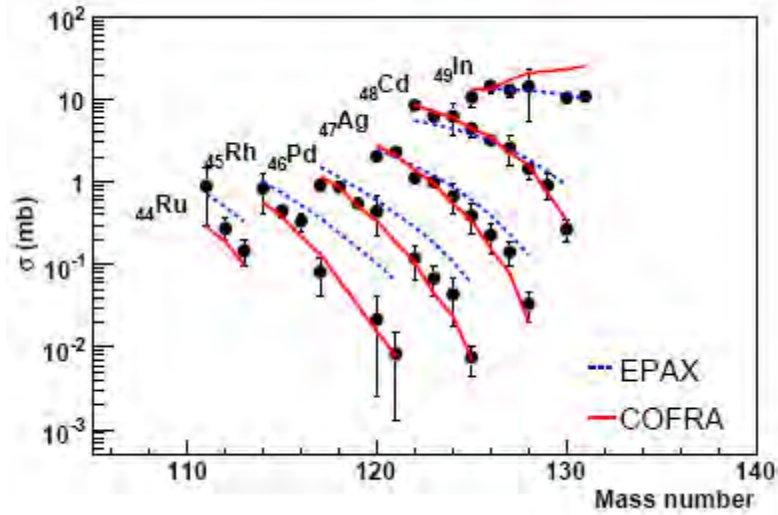


Fig. 1: Isotopic distributions of the production cross sections of residual nuclei produced by fragmentation of ^{132}Sn projectiles in beryllium.

Estimated production at EURISOL

The measured cross sections from this work have been used to estimate the expected production yields in a two-step scenario at EURISOL. To do this, the following assumptions on the productions in the primary target have been made: a total fission rate of 10^{16} s^{-1} in the high-power target, leading to an in-target production of ^{132}Sn of about 10^{14} s^{-1} . This production will be reduced by the target release, ionisation and acceleration efficiencies to about 10%, giving an expected intensity of re-accelerated ^{132}Sn of 10^{13} s^{-1} . For a beam energy of $150 \cdot A \text{ MeV}$, the optimum thickness for the beryllium fragmentation target would be 400 mg/cm^2 . The expected intensities obtained by fragmentation of the re-accelerated ^{132}Sn are depicted in figure 2. The cross sections were calculated with the COFRA and ABRABLA07 codes.

As can be seen in the figure, the fragmentation of intense beams of ^{132}Sn not only covers the region of refractory elements unreachable by ISOL facilities, but also makes it possible to extend the present limits of the chart of the nuclides considerably.

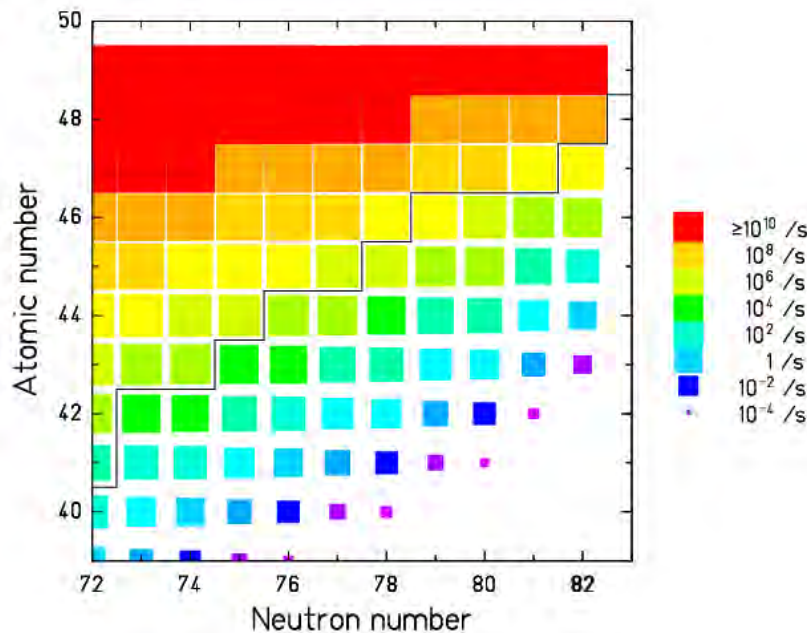


Fig. 2: Intensities obtainable at EURISOL by fragmentation of a ^{132}Sn beam, calculated with the COFRA and the ABRABLA07 codes. The ^{132}Sn is assumed to have an energy of $150 \cdot A \text{ MeV}$ and an intensity of 10^{13} s^{-1} . The stair function denotes the limit of known nuclides.

For example, at present at ISOLDE the maximum available intensities of ^{131}In and ^{130}Cd beams are 5×10^5 ions/ μC and 1×10^4 ions/ μC , respectively. If one assumes a 100- μA proton beam (which would be available at EURISOL), one could make an estimate of 5×10^7 ions/s and 1×10^6 ions/s for ^{131}In and ^{130}Cd beams, respectively, in a direct target configuration. On the other hand, the two-step option would result in an enhancement in intensities of these two beams of about factor of 100. This technique can also be applied with other fission residues having large extraction efficiencies from the ISOL target. The combination of few selected fission residues as fragmentation projectiles will make possible the production of a large variety of medium-mass neutron-rich nuclei.

Optimum energy of the post-accelerator

Different aspects such as reaction mechanism, charge-state distribution and target thickness have to be considered in order to decide on the optimal energy of the post-accelerator. Up to now, there were no data available on the nuclide production by fragmentation of extremely neutron-rich fission fragments, and therefore the benefit of this approach could have only been estimated by model calculations. These data were therefore measured with projectile energies above $100 \cdot A$ MeV and also $\sim 30 \cdot A$ MeV, and have been used as a basis for a quantitative estimate of the fragmentation of a post-accelerated ^{132}Sn beam and the optimal energy of the post-accelerator. This should be the most favourable case for this approach, because it populates neutron-rich isotopes of the refractive elements between Zr and Pd, which cannot be extracted from an ISOL target at all with present technology.

The results of the work above $100 \cdot A$ MeV have clearly shown a non-negligible enhancement of the final cross sections of neutron-deficient residual nuclei close in mass number to the projectile, for the lowest energies ($\sim 200 \cdot A$ MeV). This enhancement of the cross sections has been explained as being due to charge-exchange reaction channels having a larger probability at lower energies. The production of neutron-rich nuclei seems not to be affected by this reaction channel. Therefore one can confirm that the production of neutron-rich nuclei is similar down to energies around $200 \cdot A$ MeV, while one can expect a higher production of neutron-deficient nuclei close in mass to the projectile at these lower energies.

The results around $30 \cdot A$ MeV suggest that the Fermi energy domain can be competitive for production of very neutron-rich nuclei around the $N=50$ and $N=82$ shell closures. Of course, to realize this method in practice, specific technical solutions are mandatory, including ion-optical devices with angular acceptances of up to 10 degrees, such as superconducting solenoids, and an effective event-by-event tagging procedure for an in-flight scenario or a highly effective gas cell for production of high-purity secondary beams.

Another factor influencing optimum energy of the post-accelerator is the charge-state distribution. The evolution of the ionic charge-state distribution as a function of the beam energy is shown in figure 3 for $Z = 50$. The purity of the secondary beam after magnetic selection is disturbed by contaminants of different ionic charge states.

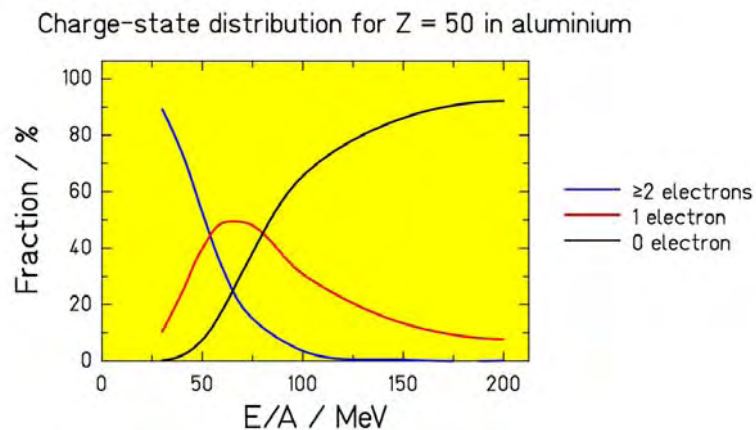


Fig. 3: Charge-state probabilities of tin projectiles after penetrating a thick aluminium layer as a function of the energy.

In particular, when fragmentation products on the neutron-rich tail of the production are considered, less neutron-rich products, which are much more abundantly produced, also pass through the separator. It will depend on the requirements of the specific experiment, how much these contaminants may disturb the experimental conditions. In view of the beam purity, an energy of at least $150 \cdot A$ MeV would be desirable.

All these considerations lead to the conclusion that the optimum beam energy (i.e. the best compromise between the physics goals and cost of the post-accelerator) is about $150 \cdot A$ MeV.

9.4 Fission models

Neutron-rich nuclei in the mid-mass region are the most effectively produced by fission of a heavy neutron-rich nucleus like ^{238}U . The fission characteristics depend sensitively on the entrance channel, e.g. on the kind of projectile and its energy. Fission is such a complex process that calculations of the nuclide production in fission must at least partly rely on empirical information. Semi-empirical models, however, have only a limited predictive power, especially far from regions covered by experiment. Therefore the benchmarking of fission models against available data and their improvement was a major task. For this, two fission models were used: the FIPRODY model developed by JYU and the PROFI model developed by GSI.

The Jyväskylä fission model

The Jyväskylä fission model FIPRODY is a generalized model for the description of the prompt fission neutron spectra and multiplicities at neutron and proton energies up to about 100 MeV. The three main emission mechanisms considered are (a) pre-compound emission, (b) pre-scission particle evaporation before the saddle point and at descent to the scission point, and (c) emission from excited fission fragments. The two-component exciton model is used for the description of the pre-equilibrium stage of the reaction. The time-dependent statistical model with inclusion of nuclear friction effects describes particle evaporation starting just after the pre-compound emission stage and lasting for the duration of the evolution of the compound nucleus toward scission. The fragment mass distribution and fission fragment kinetic and excitation energies are determined from the properties of the composite system at the scission point. The particle spectra from the fission fragments are calculated within the statistical approach. These spectra are then transformed into the laboratory rest frame using the calculated fragment kinetic energies and are averaged over the calculated fragment mass distributions. Details of the model are given in reference [3]. In figures 4 and 5 are shown two examples of the FIPRODY model predictions.

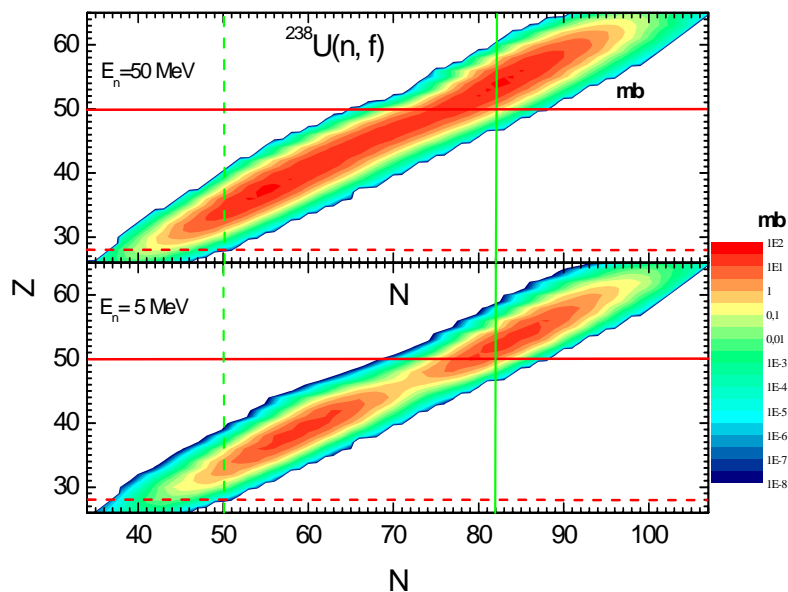


Fig. 4: Calculated fission product formation cross sections in the neutron-induced fission of ^{238}U at $E_n=5$ MeV and 50 MeV, as indicated.

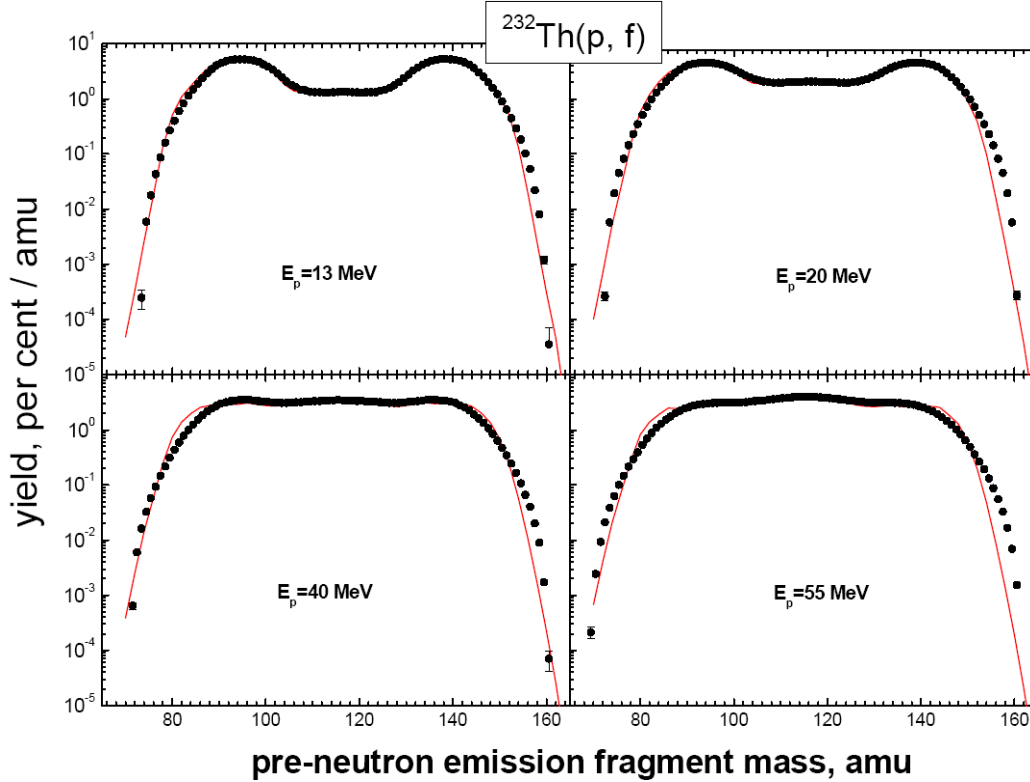


Fig. 5: Calculated and measured mass distributions in the proton-induced fission of ^{232}Th .

The GSI evaporation-fission model

The GSI evaporation-fission ABLA-PROFI code [4] system has been extended to include the production of intermediate-mass fragments with $Z \geq 3$ from binary reactions (extremely asymmetric fission). This reaction mechanism has been used very successfully for the production of very neutron-rich isotopes of elements below $Z = 20$ in uranium targets at ISOLDE. The particle emission during the dynamical descent from saddle to scission has been modelled on the basis of three-dimensional Langevin calculations. The role of transient effects on the fission probabilities and on the mass distributions of fission fragments was analysed from experimental data obtained in spallation-fission experiments. Output from the code gives nuclide production cross-sections and velocities of IMFs, fission residues, evaporation residues, pre-saddle, saddle-to-scission and post-scission multiplicities and kinetic-energy spectra of neutrons and light charged particles ($Z \leq 2$), and isotopic, isobaric and isotonic distributions of fission residues (both before and after particle emission).

Apart from these improvements, the following ingredients are now also considered in the ABLA07 code: simultaneous emission of intermediate-mass fragments in the break-up process, thermal expansion of the source, change of the angular momentum due to particle emission, influence of initial conditions (e.g. deformation) on the time-dependent fission width, double-humped structure in fission barriers and influence of symmetry classes in low-energy fission. All these features have direct or indirect influence on the nuclide production by fission in spallation reactions.

PROFI, the semi-empirical fission model for the prediction of the nuclide distribution in fission, is embedded in the de-excitation code ABLA07. When the system passes the fission barrier and proceeds to fission, it is characterised by mass and atomic number, excitation energy and angular momentum. In the model, probabilities of evaporating neutrons and light charged particles on the descent from saddle to scission are calculated, and the probability that the system ends up in one of the many possible configurations characterized by two fission fragments with atomic numbers $Z_{1,2}$, mass numbers $A_{1,2}$, kinetic energies $E_{1,2}^{kin}$ and excitation energies $E_{1,2}^{exc}$ is predicted.

After the two fission fragments are formed, their de-excitation is followed until their excitation energies fall below the lowest particle-emission threshold.

The most salient features of the PROFi model are formulated as a rather peculiar application of the macroscopic-microscopic approach to nuclear properties. In the consideration of the properties of the fissioning system at the saddle configuration, one attributes the macroscopic properties of the nuclear potential-energy surface to the strongly deformed fissioning system, while the microscopic properties are attributed to the qualitative features of the shell structure in the nascent fragments. In this way, the macroscopic and the microscopic properties are strongly separated, and the number of free parameters is independent of the number of systems considered. This makes extrapolations in experimentally unexplored regions more reliable. With one and the same set of the model parameters we are able to reproduce a large variety of experimental data on mass, nuclear-charge, TKE and neutron-multiplicity distributions in low-energy fission (figure 6) and also in high-energy fission (figure 7).

More details on the latest improvement in the ABLA07-PROFi code system can be found in references [4–6].

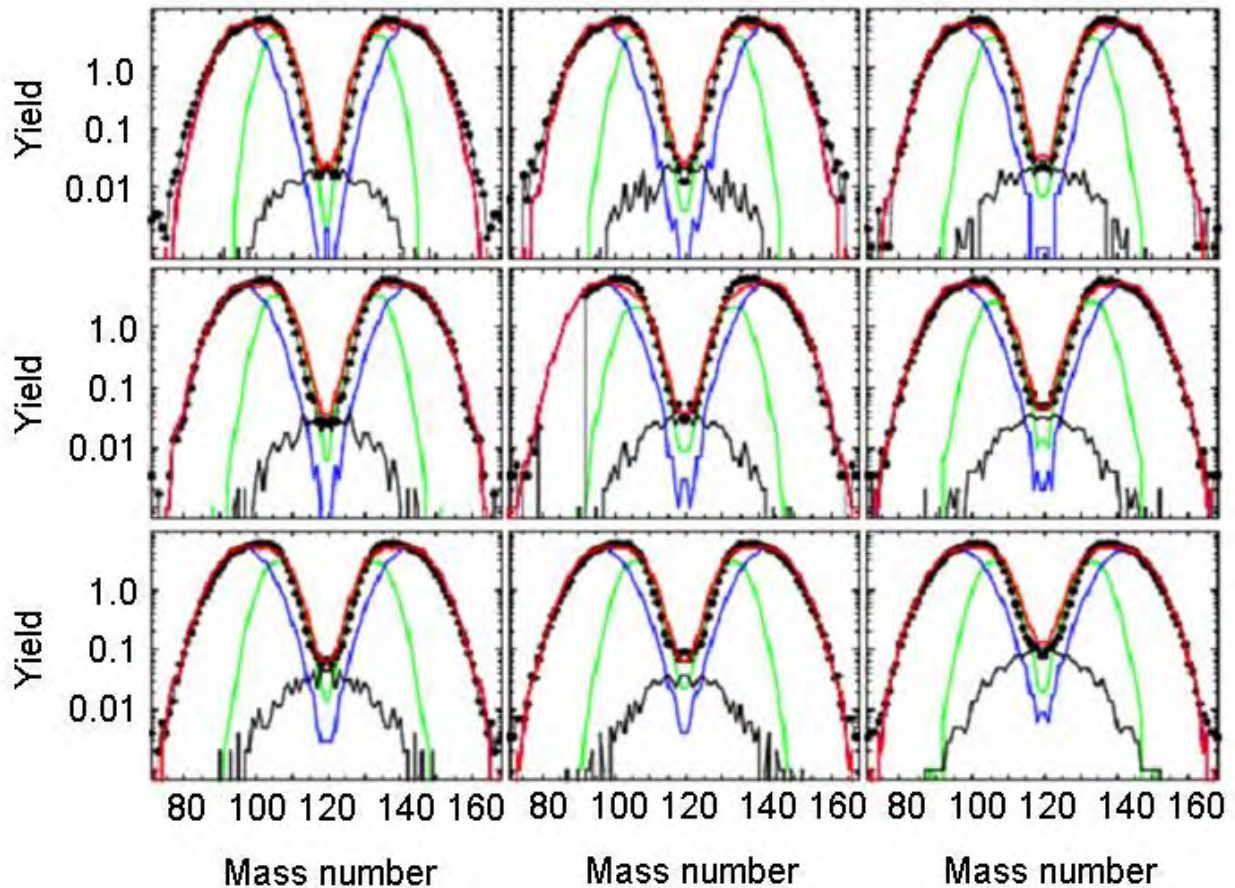


Fig. 6: Mass distributions measured in the neutron-induced fission of ^{238}U for neutron energies ranging from 1.2 to 5.8 MeV, together with the prediction of the ABLA07 code. The red line represents the calculated total mass distribution, while the black, green and blue lines show the contributions from the super-long, standard I and standard II modes, respectively.

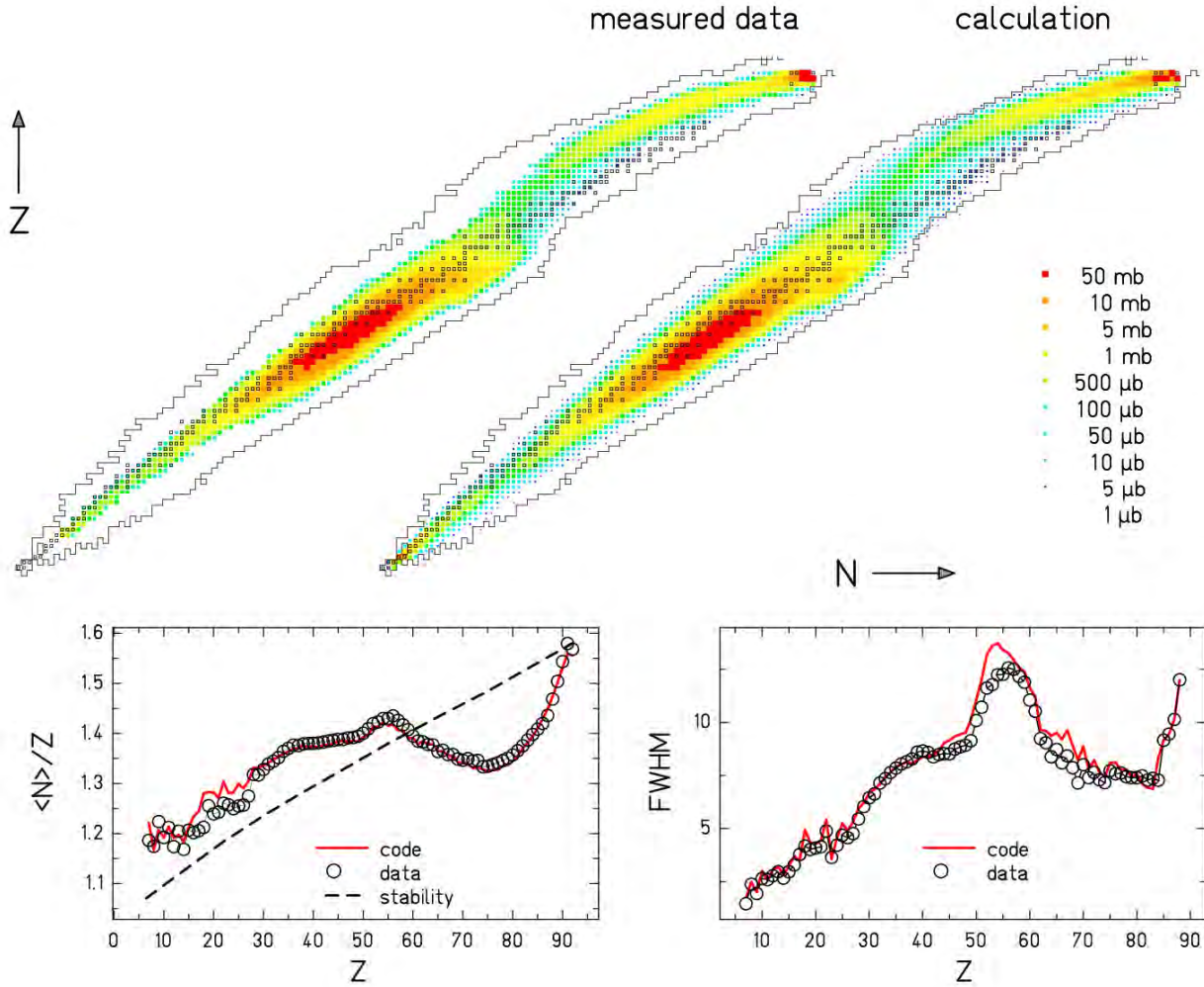


Fig. 7 (Top-left): Chart of nuclides with measured cross sections for nuclei produced by 1-GeV protons on ^{238}U . (Top-right): The prediction of ABRABLA0. (Bottom left): Mean neutron-to-proton ratio of isotopic distributions as a function of atomic number, compared with the stability line (dashed line) and to the ABRABLA07 prediction (red line). (Bottom right): FWHM of the isotopic distributions compared to the prediction of ABRABLA07 (red line).

9.5 Spallation and fragmentation reactions

Fragmentation reactions have been systematically investigated in reactions induced by $^{129,136}\text{Xe}$ beams at $1000\text{-}A$ MeV, $500\text{-}A$ MeV and $200\text{-}A$ MeV, on different target materials. The isotopic composition and production cross section of the residual nuclei obtained with the FRS fragment separator at GSI made it possible to investigate the role of the projectile energy and isospin but also the nature of the target in the production of final residual nuclei.

Beams of ^{238}U , ^{208}Pb and ^{136}Xe impinging on beryllium targets at $1000\text{-}A$ MeV were also used specifically to investigate the production of neutron-rich nuclei approaching the r-process waiting points at $N=126$ and $N=82$ which are important in nucleosynthesis. These data are compared to previous measurements and model calculations in order to determine the optimum reaction mechanism to extend the present limits of the chart of the nuclides.

As an example, isotopic distributions of several elements measured in reactions of ^{136}Xe projectiles at $1000\text{-}A$ MeV with different target nuclei (viz. lead, titanium, beryllium and hydrogen) are shown in figure 8.

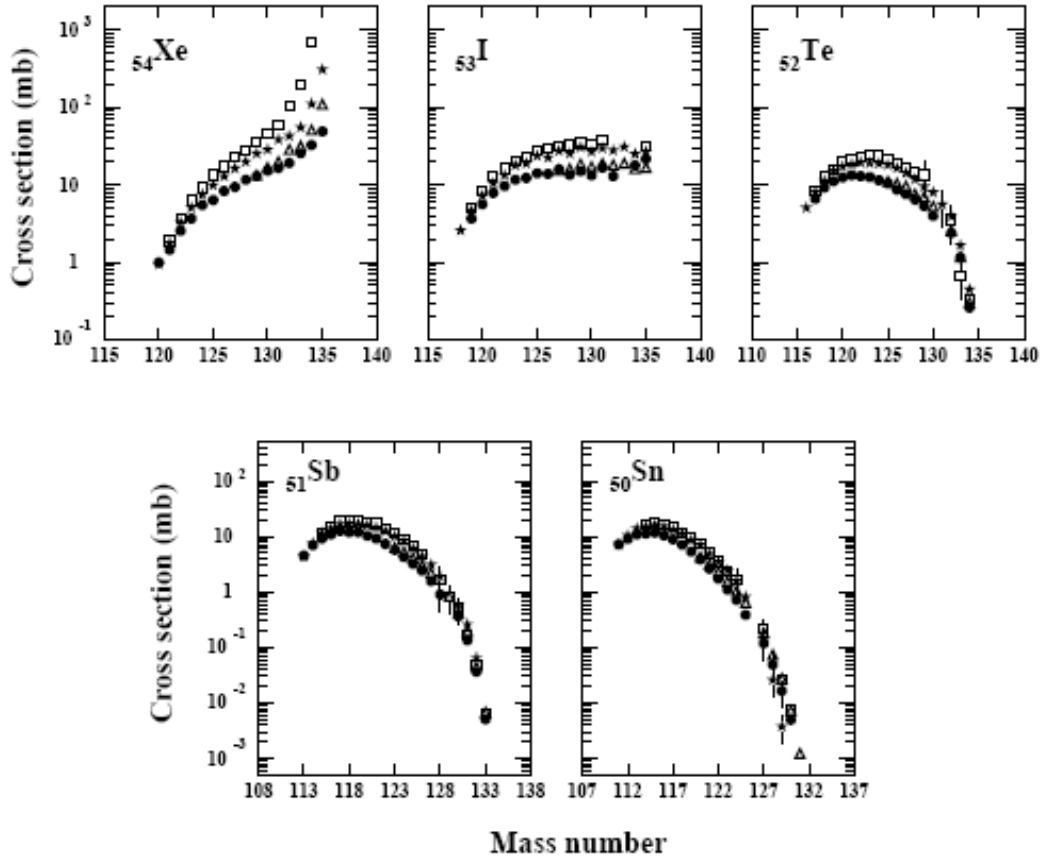


Fig. 8: Isotopic distributions of several projectile fragments formed in reactions of ^{136}Xe beam at 1000-A MeV with targets of lead (open squares), titanium (stars), beryllium (open triangles) and hydrogen (circles).

The figure shows a clear increase in the production of final residues with target mass number. This effect is especially evident for residual nuclei differing by only a few nucleons from the incoming beam, and is caused by different total interaction cross sections. Moreover, in the case of a lead target, for residual nuclei produced in few-neutron removal channels, the strong influence of the Coulomb excitation process additionally enhances the final production cross sections.

In figure 9 are shown the isotopic distributions of several elements produced in the reactions of 1000-A MeV ^{124}Xe on Be, 750-A MeV ^{129}Xe on Al and 1000-A MeV ^{136}Xe on Be. One can clearly observe a difference in the width of the isotopic distributions of the projectile residues, as well as a shift of the maximum of the distributions. Reactions induced by projectile with a smaller neutron excess result in an enhanced production of neutron-deficient residues. The same data are also compared with the results of a reaction model ABRABLA; the agreement between measured and calculated data is more than satisfactory.

9.6 Neutron- and proton-induced reactions up to Fermi energy

This sub-task concerned measurements of data on production yields and cross sections on neutron-rich nuclei in (p,f) (d,f) and (n,f) reactions at IGISOL-JYFLTRAP, and in the (d,pf) reaction at HENDEN in order to simulate (n,f) reactions. These data were then used to benchmark the Jyväskylä Monte-Carlo version of a pre-equilibrium model for neutron/proton-induced fission reactions.

The $^{232}\text{Th}(p,f)$ reaction was studied in the JYFL accelerator laboratory at energies between 13 and 55 MeV. The fission fragment mass distributions, neutron spectra and multiplicities, gamma-ray spectra and multiplicities were measured [8-10].

In another experiment carried out in LNS, Catania, the $^{238}\text{U}(d,pf)$ reaction at 124 MeV was used as surrogate method for neutron-induced fission.

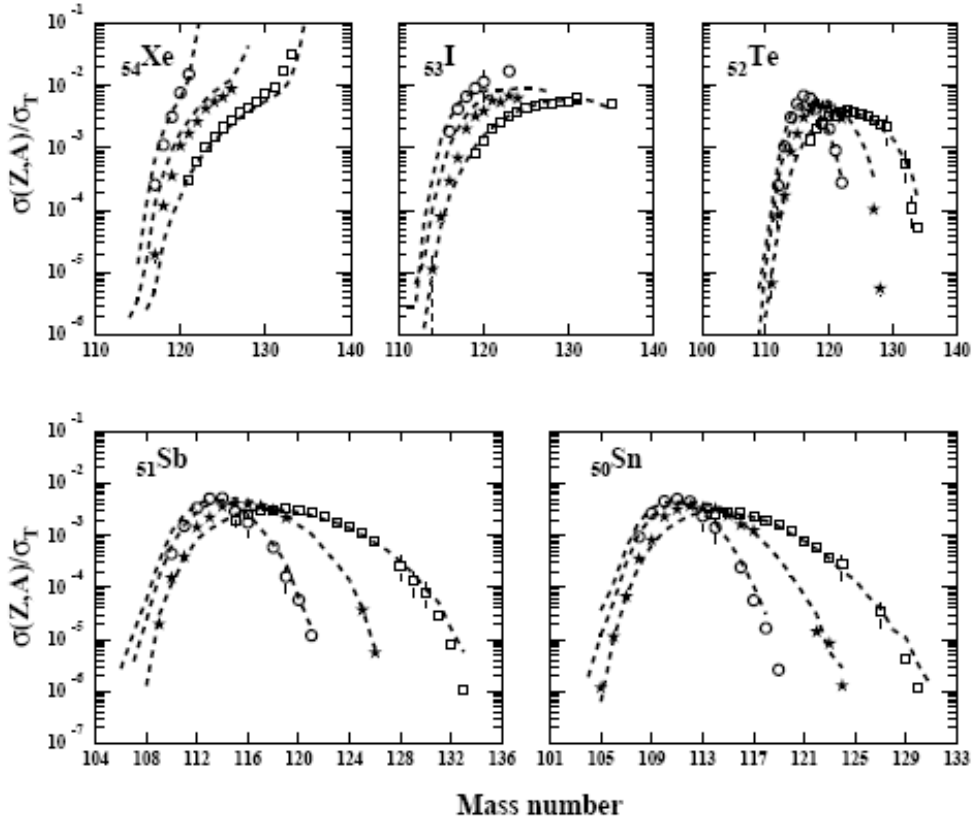


Fig. 9: Isotopic distributions of several residual nuclei produced in projectile fragmentation of ^{124}Xe (1000-A MeV)+Be (circles), ^{129}Xe (750-A MeV)+Al (stars) and ^{136}Xe (1000-A MeV)+Be (squares). Dashed lines correspond to the predictions of the ABRABLA reaction model.

A novel method to determine independent fission product yields in particle-induced fission employing the ion-guide technique and ion counting after a Penning trap was also developed [11,12]. The method takes advantage of the fact that a Penning trap can be used as a precision mass filter, which allows an unambiguous identification of the fission fragments. The method was tested with 25-MeV and 50-MeV proton-induced fission of ^{238}U . The data is internally reproducible and the results for Rb and Cs yields in 50-MeV proton-induced fission agree with previous measurements. In addition to proton-induced fission, yields for 25-MeV deuteron-induced fission of ^{238}U were measured for selected elements [13].

9.7 Heavy-ion reactions at the Fermi energy

Possibilities for production of exotic nuclei in the Fermi energy domain were explored, where only very limited and inconsistent sets of experimental data existed prior to this project.

To supplement the previous high-resolution measurements at 25-A MeV and to study the beam-energy dependence of production rates, an experiment at the Cyclotron Institute of Texas A&M University was carried out during the Design Study. The production rates of neutron-rich nuclei were measured with the MARS recoil spectrometer at 4- and 7-degree angles in the following reactions:

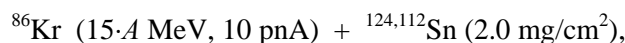
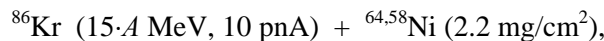


Figure 10 shows the resulting isotopic distributions for the experimentally investigated reaction $^{86}\text{Kr}+^{64}\text{Ni}$ at 15-A MeV, with a spectrometer at 4 degrees from the beam. The products with $Z=29-24$

seem to be reproduced reasonably well by the PE+DIT/ICF+SMM simulation (pre-equilibrium emission followed by either deep-inelastic transfer or incomplete fusion followed by de-excitation using statistical model of multi-fragmentation).

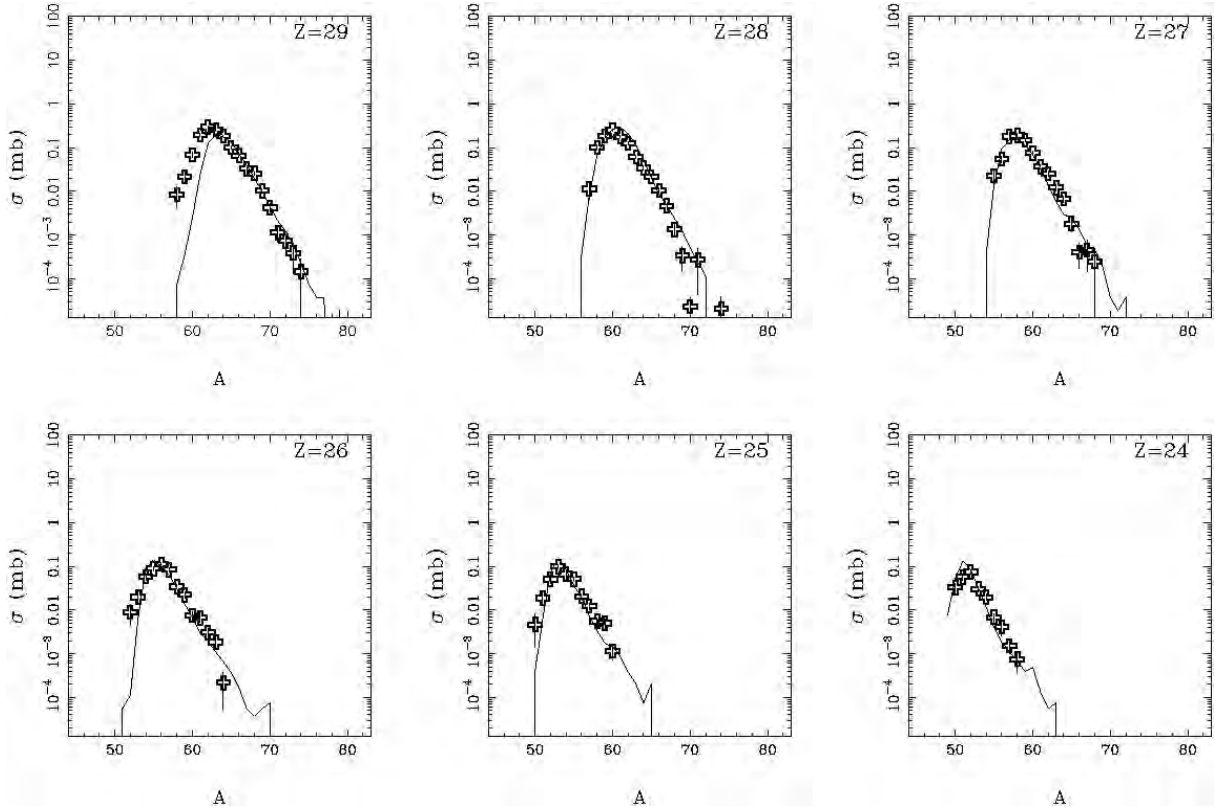


Fig. 10: Mass yield curves from the reaction $^{86}\text{Kr}+^{64}\text{Ni}$ at $15\cdot A$ MeV at 4 degrees. Symbols are measured data. Lines are PE+DIT/ICF+SMM calculation filtered by the spectrometer angular, azimuthal and momentum acceptance.

Calculated PE+DIT/ICF+SMM total mass yield curves from the reaction $^{86}\text{Kr}+^{64}\text{Ni}$ (see figure 11) at $25\cdot A$ MeV (solid line) and $15\cdot A$ MeV (dashed line), which were validated using experimental data, show that the projectile energies around $15\cdot A$ MeV may be close to optimal, specifically for production of the neutron-rich nuclei.

The available experimental data from nucleus-nucleus collisions, at beam energies from the Coulomb barrier up to $70\cdot A$ MeV and various projectile-target asymmetries, were investigated and are listed in a final report [14]. The scenario involving pre-equilibrium emission in the early stage, followed by deep-inelastic transfer or incomplete fusion, leads to consistent agreement in most of the cases. The participant-spectator scenario starts to play a role at energies around $50\cdot A$ MeV for very asymmetric projectile-target combinations. At beam energies around and above $50\cdot A$ MeV there are signals of the mechanism of neutron loss (dynamical emission) preceding the thermal equilibration of the massive projectile-like fragment. At beam energies below $10\cdot A$ MeV, deep-inelastic transfer appears to be the dominant reaction mechanism, with some contribution from the possible extended evolution of nuclear profile in the window (neck) region, mostly in the case of heavy target nuclei.

The achieved level of understanding of the reaction mechanism provides a suitable starting point to consider production of secondary beams in the Fermi energy domain. The comparison with other reaction domains, such as spallation and fragmentation, suggests that this option can be competitive for production of very neutron-rich nuclei around the $N=50$ and $N=82$ shell closures. Thus, the Fermi energy domain would also represent an option for the post-accelerator energy. (Refer also to the results of the work on fragmentation reported in section 9.3).

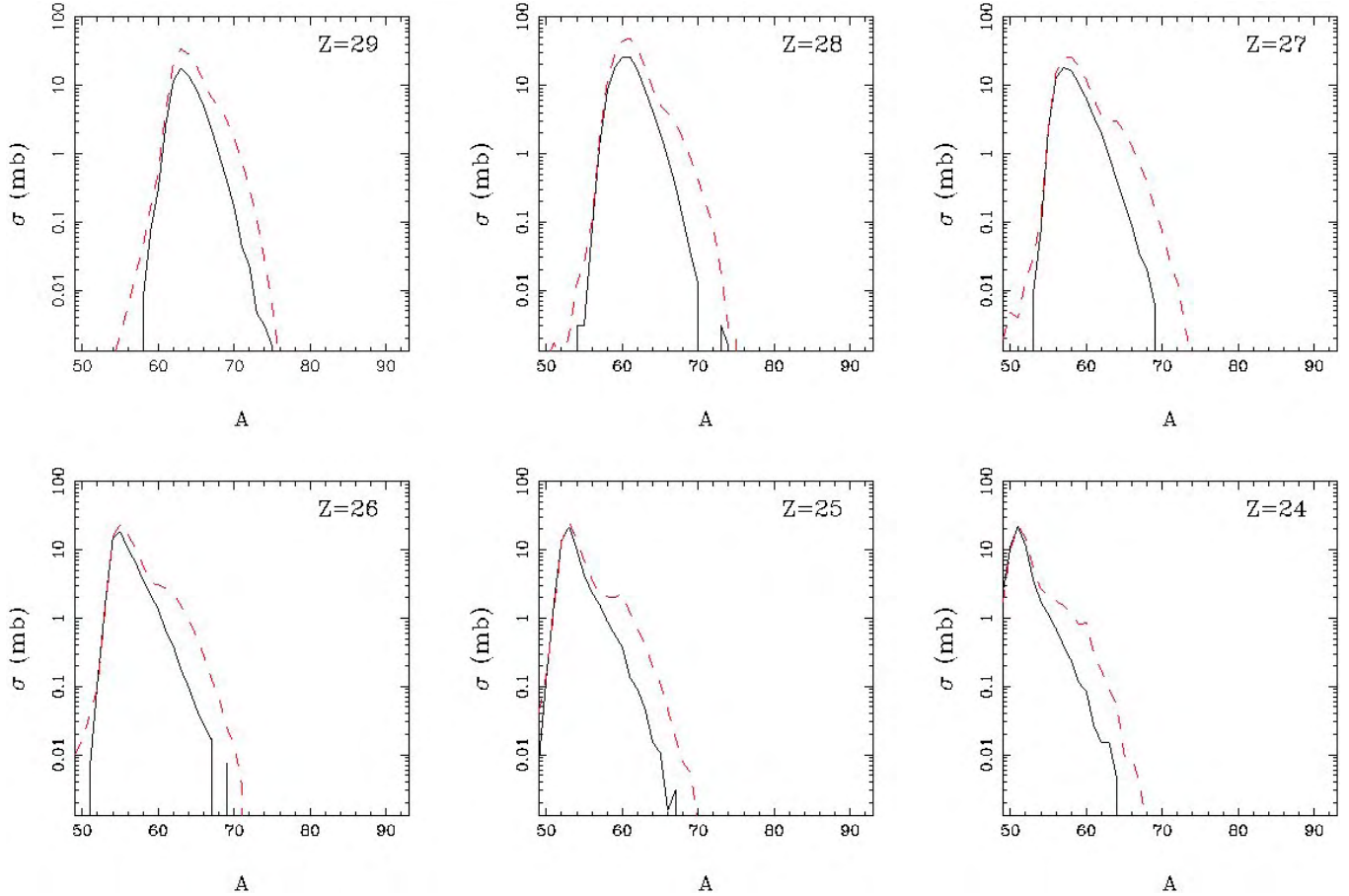


Fig. 11: Calculated PE+DIT/ICF+SMM total mass yield curves (validated using experimental data) from the reaction $^{86}\text{Kr}+^{64}\text{Ni}$ at 25-A MeV (solid line) and 15-A MeV (dashed line).

9.8 Aspects of secondary reactions in single- and double-stage targets

Thick-target reaction environments were modelled in realistic experimental scenarios using transport codes. Optimization of the geometry of target assemblies was also addressed. After code validation, the in-target production rates for single-stage targets and double-stage targets were studied.

Code validation

Two types of experimental data have been used to validate different codes. In the case of direct (single-stage) targets, where the nuclei of interest are produced via spallation reactions, residue production had to be benchmarked. On the other hand, for the fission-target case (double-stage targets) nuclei are produced by neutron-induced fission, where the neutrons are created in the liquid-metal converter via spallation-evaporation reactions. In this case neutron production was benchmarked. For benchmarking purposes MCNPX2.5.0 was used, as it offers the possibility to use 10 combinations of different intra-nuclear cascade models plus de-excitation models.

The results of the benchmarking on residue and neutron production from both thin and thick targets have shown that the most suitable code combinations are ISABEL+ABLA or INCL4+ABLA. In the case of neutron production, CEM2k could be used where needed, to save on computing time.

Production rates for single-stage targets

In order to estimate the in-target RIB production rates in direct targets, 320 different configurations of cylindrical targets were studied. More details of the different target configurations can be found in reference [15]. Four types of material were studied: oxides (Al_2O_3), carbides (SiC, UCx), molten metals (Pb) and refractory metals (Ta). During the design study, energy values ranging from 0.5 to 2 GeV were selected. Finally, the power which the targets have to withstand was fixed at 100 kW.

In attempting to optimize single-stage targets (i.e. to choose the target configuration with the highest production rate for a given nucleus), according to the elements or isotopes studied, one starts by plotting mass and nuclear-charge distributions for all targets and the two extreme energies.

To simplify this work, the radii (18 mm) and masses (2 kg) of the targets were fixed. This allowed us to reduce the number of files to be analysed, since we obtained information on which material should be used for a given isotope of interest. Thereafter, investigation of the production rate per energy unit resulted in the optimal energy.

Since the power was fixed at 100 kW, and with the assumption that energy costs more than intensity, where similar results existed we preferred those obtained with low-energy protons. In the next step, two-dimensional graphs – target length versus target radius – were used in order to get optimal lengths and radii.

In the table below, optimal configurations and the estimated production rates for some isotopes are summarized. This information is then used as the input for calculating the RIB intensity after taking into account different efficiencies (e.g. ionization, release, etc.) – see section 9.9 below.

Table 7.1 In-target production rates for some isotopes with direct targets using INCL4/Abla

Isotope	Target material	Length (cm)	Beam energy (GeV)	In-target production rate (atoms/s)
¹¹ Li	Al ₂ O ₃	~75	1	1.8×10^9
⁷ Be	SiC	~48	0.5	1.0×10^{13}
¹¹ Be	Al ₂ O ₃	~50–75	1	1.2×10^{11}
¹² Be	Al ₂ O ₃	~50–75	1	3.0×10^{10}
¹⁸ Ne	SiC	~48–64	1	8.3×10^{10}
²⁵ Ne	SiC	~32–48	1	3.2×10^9
²⁰ Mg	SiC	~64	1	2.4×10^{10}
⁷² Ni	UC ₃	~40	0.5	7.6×10^{10}
⁸¹ Ga	UC ₃	~40	0.5	1.9×10^{10}
⁹² Kr	UC ₃	~40	0.5	8.9×10^{11}
¹³² Sn	UC ₃	~40	0.5	2.9×10^{11}
²⁰⁶ Hg	Pb	~18	0.5	2.9×10^{11}
¹⁸⁰ Hg	Pb	~27	1	1.5×10^{10}
²⁰⁵ Fr	UC ₃	~(40–60)	1	1.8×10^9

Production rates for two-stage targets

The production rates in case of two-stage targets have been calculated in two steps. In the first step, the fission rate in the spallation neutron field has been calculated, while in the second step, the fission yields have been obtained. Six elements of interest recommended by NuPECC were analysed in this work: Ni, Ga, Kr, Ag, Sn, and Xe.

In the analysis, six different target assembly configurations were used, i.e. five cases based on uranium compounds with ²³⁵U fractions of 100%, 20%, 3%, 0.72% (natural uranium) and 0.02% (depleted uranium) as well as ²³²Th. The geometry model of the target set-up used for Monte-Carlo calculations

was supplied by INFN and represents the latest design variant of a MAFF-like target able to accommodate a 30-kW load heat. As an example, distributions for Kr ($Z = 36$) and Sn ($Z = 50$) isotopes for the six target configurations studied are shown in figure 12 below.

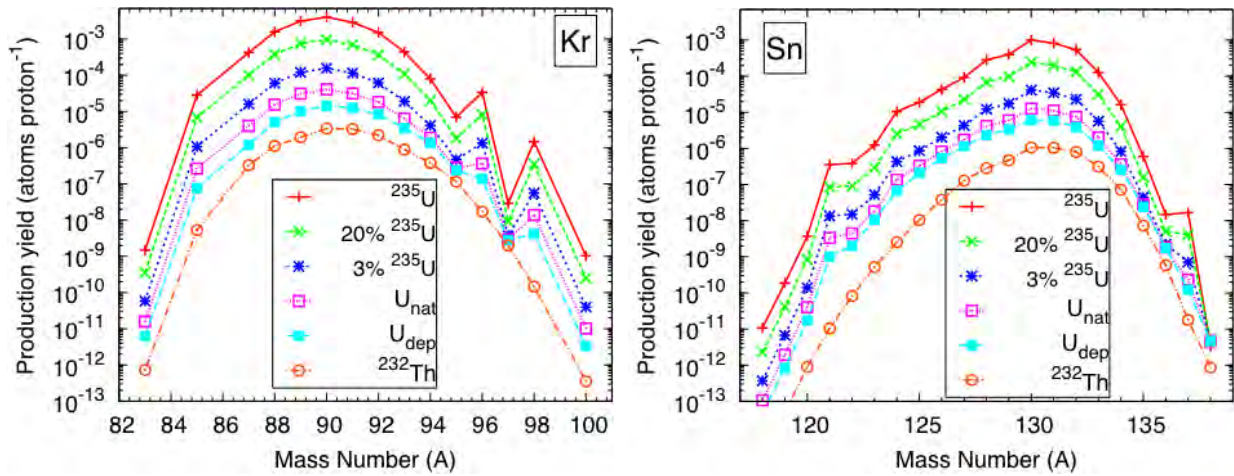


Fig. 12: Fission-yield isotopic distributions for two selected products: Kr (left) and Sn (right).

The present study provides quantitative estimates of the fission yields for a variety of isotopic distributions for different target systems. Examples of some results are given in table 2. The results obtained represent the input information needed for calculating the beam intensities predicted for the future EURISOL facility.

Table 2: In-target production rates for some isotopes with fission targets (normalized to a 1-mA proton beam)

Target:	100% ^{235}U	20% ^{235}U	3% ^{235}U	Natural U	Depleted U	^{232}Th
^{72}Ni	6.59E+07	1.95E+07	7.85E+06	6.23E+06	5.85E+06	1.42E+07
^{81}Ga	4.75E+10	1.17E+10	2.14E+09	7.92E+08	4.82E+08	6.98E+08
^{92}Kr	9.53E+12	2.31E+12	3.87E+11	1.15E+11	5.23E+10	1.39E+10
^{132}Sn	3.38E+12	8.25E+11	1.43E+11	4.67E+10	2.45E+10	5.00E+09

9.9 Predictions of secondary-beam intensities

In order to predict secondary-beam intensities, apart from measured and calculated production cross sections and predicted in-target production rates, the most demanding goal is to collect the available information on efficiencies for release, ionisation, transport and post acceleration. These aspects have been studied in detail during the EURISOL Design Study, and are reported in references [16,17].

Detailed studies of attainable secondary-beam intensities with EURISOL have been done and are described in reference [18]. Three methods for their production were considered: a single-stage target configuration, a double-stage target configuration and the two-step method. As a summary, the calculated intensities are shown in figure 13 for several nuclei considered, viz. Be, Ar, Ni, Ga, Kr, Sn and Fr (elements of interest suggested by NUPECC) and also Li, Mg and Hg which could play a pre-eminent role in the experiments planned within the EURISOL collaboration. Intensities were also obtained for several additional elements (most of them refractory) from Zr to In, all produced in the

two-step option. These were on the list of elements considered important for EURISOL, which was drawn up by the Physics and Instrumentation Group within the design study.

More details, as well as tabulated values of secondary-beam intensities, are available in reference [18].

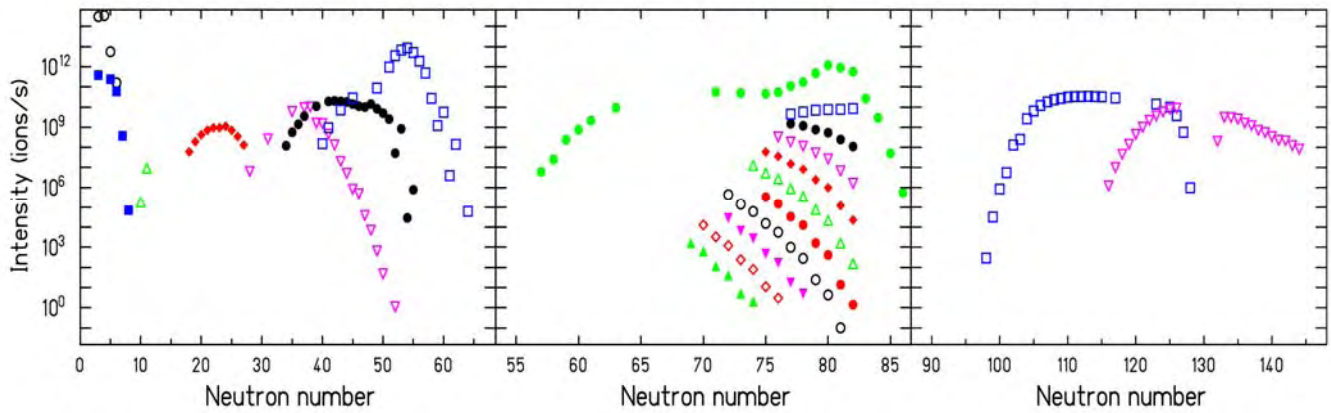


Fig. 13: Predicted EURISOL intensities of several nuclides:

- | | | |
|---|---|--|
| <p>Left: Be (black open dots),
 Li (blue filled squares),
 Mg (open green triangles),
 Ar (red filled rhomboids),
 Ni (magenta open triangles),
 Ga (black filled dots),
 Kr (open blue squares);</p> | <p>Centre: Zr (filled green triangles),
 Nb (open red diamonds),
 Mo (magenta filled triangles),
 Tc (black open dots),
 Ru (red filled dots)
 Rh (green open triangles),
 Pd (red filled diamonds)
 Ag (magenta open triangles)
 Cd (filled black dots),
 In (open blue squares),
 Sn (green filled dots);</p> | <p>Right: Hg (squares)
 Fr (triangles)</p> |
|---|---|--|

References

1. K-H. Schmidt et al., “*Studies on the benefit of extended capabilities of the Driver Accelerator for EURISOL*”, Phys. Rev. ST Accel. Beams **10** (2007) 014701
2. The COFRA code is available at: www.usc.es/genp/cofra.
3. V.A. Rubchenya, “*Prompt fission neutron emission in neutron and proton induced reactions at intermediate energies*”, Phys. Rev. **C75** (2007) 054601.
4. The code is available on request from A. Kelić.
5. A. Kelić, M.V. Ricciardi and K-H. Schmidt, “*ABLA07 – Towards a complete description of the decay channels of a nuclear system from spontaneous fission to multifragmentation*”, Proc. Joint ICTP-IAEA Advanced Workshop on Model Codes for Spallation Reactions, ICTP Trieste, Italy, 4–8 February 2008, eds. D. Filges et al., IAEA INDC(NDS)-530 (Vienna, August 2008) p. 181; arXiv_nucl-th/0906.4193v1
6. K-H. Schmidt, A. Kelić, M. V. Ricciardi, “*Experimental evidence for the separability of compound-nucleus and fragment properties in fission*”, Europhys. Lett. **83** (2008) 32001.
7. A. Kelić, M. V. Ricciardi and K-H. Schmidt, to be published.
8. I.V. Ryzov, et al., in preparation.
9. A.A. Bogachev et al., “*Yields of correlated fragment pairs and average gamma-ray multiplicities and energies in $^{208}\text{Pb}(^{18}\text{O},F)$* ”, Proc. Internat. Conf. on Dynamical Aspects of Nuclear Fission. 2–6 October 2006, Smolenice Castle, Slovak Republic, World Scientific, Singapore, eds. J. Kliman, L. Krupa and S. Gmuca, 2007.
10. A.A. Bogachev et al., in preparation.
11. H. Penttilä et al., “*Independent fission yields with JYFLTRAP*”, Eur. Phys. J. Special Topics **150** (2007) 317.
12. H. Penttilä et al., in preparation.
13. H. Penttilä et al., “*Fission Yield Measurements at the IGISOL Facility with JYFLTRAP*”, Proc. Fourth Internat. Conf. on Fission and Properties of Neutron-Rich Nuclei, Sanibel Island, Florida, 11–17 November 2007, eds. J.H. Hamilton, A.V. Ramayya & H.K. Carter, (World Scientific, Singapore, 2008) p. 410.
14. M. Veselsky and G.A. Souliotis, “*Production of exotic nuclides in nucleus-nucleus collisions in the Fermi-energy domain*”, EURISOL DS technical note: 11-25-2009-0018.
15. S. Chabod et al., “*In-target radioactive nuclei production rates with EURISOL single-stage target configuration*”, EURISOL DS technical note: 11-25-2009-0022; and also S. Chabod et al., “*Optimization of in-target yields for RIB production: Part I: direct targets*”, EURISOL DS technical note: 11-25-2008-0011.
16. S. Lukić et al., “*Systematic comparison of ISOLDE-SC yields with calculated in-target production rates*”, Nucl. Instrum. & Meth. **A 565** (2006) 784.
17. J. Cornell (editor) “*The EURISOL Report*”, Appendix C, published by GANIL, 2003 <http://pro.ganil-spiral2.eu/eurisol/feasibility-study-reports/feasibility-study-appendix-c>
18. A Kelić et al., “*Beam intensities with EURISOL*”, EURISOL DS technical note: 11-25-2009-0025.

Chapter 10: Physics & Instrumentation

10.1 Overview of the task

The EURISOL radioactive ion beam facility is an ambitious leap beyond the capabilities of any current ISOL facility in the world. EURISOL is intended to produce and accelerate isotopes spanning the broadest possible range of isospin and mass. It promises to open up an entirely new vista for nuclear physics and have a significant bearing on many other fields of science, including condensed matter, atomic, particle and astrophysics.

As a major project like EURISOL has to be driven by science, an integral part of the Design Study was the “Physics and Instrumentation” task. The aim of this task group was to build upon the conclusions of the report published within the feasibility study for EURISOL, funded within the European Commission’s 5th Framework Programme, to select a few key scientific goals and identify the required experimental methods using novel detector technologies.

The physics and instrumentation task group has proposed a limited number of original experiments spanning different fields in which major scientific breakthroughs are expected from EURISOL. Through detailed simulations, the innovative instruments necessary to perform these experiments were defined, and these influence the layout of the EURISOL experimental areas. During several meetings, feedback was given to the more technical task groups, in order to promote compatibility between the beam characteristics and the scientific goals. The aim of this task has also been to ensure continued interest and involvement of the broader user and scientific community, including theoreticians, in the Design Study. This has been achieved by the organisation of a dedicated workshop during which various aspects of the user needs were discussed, especially in terms of the required parameters for the post-accelerated beams, the priority ion beam species and their required intensities, and the modes of operation needed for experimental programmes, including parallel operation. In the latter half of the Design Study, there was close collaboration with the User Group to organise sessions and meetings.

10.2 Physics with low-energy beams

The ideas that emerged from the Trento workshop were distilled into a selection of 25 experiments to provide a snapshot of the possible science programme at EURISOL. One idea that has strong synergies with the ion source design is in-source laser spectroscopy, the feasibility of which has recently been demonstrated at ISOLDE. This technique offers the prospect not only of the rapid release of short-lived species as pure beams, but also of selecting nuclei in a specific isomeric state. These isomer beams are of considerable interest for a range of different nuclear physics experiments, as well as in nuclear astrophysics, for instance in determining the destruction rate of $^{26\text{m}}\text{Al}$ in stellar environments.

Many experiments will require the use of isotopically-pure beams directly from the beam preparation stages, without further post-acceleration. For example, collinear laser spectroscopy measurements to determine nuclear charge radii, isotope shifts and hyperfine structure of ions will exploit recent advances in beam cooling and bunching prior to laser spectroscopy that have led to significant improvements in sensitivity. Combined with the higher yields for nuclei far from stability expected from EURISOL, this should allow the technique to be applied to many currently inaccessible nuclei.

Atomic mass measurements have also advanced rapidly in recent years, with the development of fast, precise and sensitive measurement techniques. For example, high-precision measurements using ISOL beams have been obtained for a wide range of nuclei with Penning traps. In addition to being of interest in their own right, mass measurements allow Q -values to be deduced that are of vital importance for nuclear astrophysics and super-allowed β -decay studies, where such measurements will be combined with precise half-life and branching-ratio measurements to deduce the ft values for the super-allowed pure Fermi β -decays of heavy $N=Z$ nuclei. From these the vector coupling constant can be determined, in turn allowing the V_{ud} matrix element of the CKM quark mixing matrix to be extracted. The determination of ft values can be extended to transitions between $T=1/2$ isospin

doublets, which provide an additional sensitive set for such studies. Furthermore, in-trap correlation measurements, like those between β -particles and recoiling nuclei, are very sensitive tools to investigate the presence of exotic (i.e. scalar or tensor type) weak interaction components, search for right-handed charged weak currents and new sources of time reversal violation. Such correlation measurements enable the Gamow-Teller/Fermi mixing ratios in mirror decays to be extracted, which are necessary to determine the vector coupling from these transitions. All of these experiments will benefit from the higher intensities and the range of ion species available at EURISOL.

10.3 Nuclear astrophysics

An understanding of nucleosynthesis and energy production in stellar environments requires knowledge of the properties of unstable nuclei. For example, the rp-process is a complex network of proton capture reactions and decays involving unstable proton-rich nuclei and EURISOL offers the possibility of measuring some key reaction rates directly using beams of radioactive nuclei accelerated to energies of astrophysical interest, as well as studying the structure of the nuclei involved through indirect measurements. The cross sections for many of these reactions are expected to be very low at energies around the Gamow window, so experiments lasting several weeks are envisaged. This, combined with the special requirements for beams at low energies, led to the decision to construct a dedicated accelerator for such nuclear astrophysics studies.

Investigating the r-process path between the $N=50$ and $N=82$ shells at EURISOL will require a systematic study of basic nuclear structure properties of neutron-rich isotopes of elements from Fe to Sn, covering all “waiting-point” nuclei. A range of complementary experiments will be required, including measurements of masses, half-lives, β -delayed neutron emission probabilities, ground-state deformations, neutron capture cross sections and the excitation energies, spins and parities of excited states.

The neutron capture cross sections of radioactive nuclei can be measured using pure samples of radioactive nuclei produced by EURISOL and implanted into thin carbon foils. The advent of high-flux neutron sources will allow for precision measurements on such minute samples, which will be an important contribution to understanding the production of many nuclei in astrophysical environments.

10.4 Physics at Coulomb-barrier energies

Accelerating the radioactive ions to higher energies will open up many new possibilities. At Coulomb-barrier energies, the γ -ray spectrometer AGATA will be used at EURISOL to study high-spin states in nuclei up to the fission limit using compound nucleus reactions. Neutron-rich nuclei that are inaccessible using stable beams could be studied and symmetric reactions to generate the maximum angular momentum could be exploited to search for the predicted phenomenon of hyperdeformation in nuclei.

The availability of neutron-rich beam species at Coulomb-barrier energies will also provide new avenues for exploring the properties of heavy elements, since new compound nuclei can be populated. This will allow the synthesis and decay of heavy elements to be studied, for example in the region around the end of the decay chains of the superheavy nuclei produced in Dubna. In-beam spectroscopy of heavy elements will also be possible through the combination of an efficient recoil separator with a γ -ray and conversion electron spectrometer around the target position to detect prompt radiation emitted in the decay of high-spin states in heavy nuclei. Highly-selective tagging techniques will be used to identify the prompt radiation of interest from the background due to fission.

Optical spectroscopy of the heaviest elements will also be performed using a buffer gas cell placed at the focal plane of the recoil separator to stop reaction products, where they will be selectively ionized with a collection of high-power lasers.

As well as elucidating ground-state properties of heavy nuclei, these experiments will probe the interplay of relativistic effects and the QED effects of self-energy and vacuum polarization in heavy systems. The expected low cross sections for producing such heavy nuclei means that the experiments will require long periods of beam time and hence a separate accelerator for energies up to 5 MeV per nucleon is needed for EURISOL.

10.5 Nuclear structure from reaction studies

Determining single-particle energies using transfer reactions in order to understand the evolution of shell gaps and changing level ordering in nuclei increasingly far from stability will be a major physics goal of EURISOL. One nucleon transfer reactions such as (p,d) and (d,p) provide a direct measurement of single-particle energies as long as a large fraction of the spectroscopic strength is observed. The experiments will be performed in inverse kinematics and require the simultaneous detection of the light charged particle and γ -rays, together with the scattered projectile-like nucleus for channel selection. Transfer reactions will also be used to probe the isospin dependence of correlations by measuring how the spectroscopic factors and occupancy of the $3s_{1/2}$ proton orbital change in the heavy neutron-rich Pb isotopes. One-nucleon transfer reactions such as (p,d) or (d, ^3He) in inverse kinematics will be studied with incident exotic beam energies of 5–30 A MeV, complemented by one-nucleon removal reactions with higher incident exotic beam energies of 50–150 A MeV.

Break-up reactions will be used to study the interior part of wave functions of nucleons and clusters to check the limits of validity of mean field and single-particle concepts. We will investigate whether spectroscopic factors just represent asymptotic properties of wave functions and probe the limits of validity of the mean field concept, since the long-range and short-range correlations can vary as a consequence of the isospin dependence of the nucleon-nucleon interaction. The experimental tool will be experiments with heavy exotic projectiles and heavy targets, using quasi-elastic reactions in which the projectile core can be excited below particle threshold while the target excitation will be measured by neutron multiplicity or gamma-ray measurements.

Structure beyond the neutron drip-line can be explored using intense beams of neutron-rich nuclei and proton knock-out reactions. The character and structure of the very neutron-rich isotopes of oxygen, $^{26,28}\text{O}$ for example, have been long-standing issues in nuclear structure. Indeed, ^{28}O is arguably the only doubly-magic system that remains to be observed. In order to probe the low-lying structure of these nuclei, as well as 2-neutron and 4-neutron correlations, high-energy beams of $^{28-30}\text{Ne}$ will bombard a thick target. The unbound $^{26-28}\text{O}$ will be populated via two-proton removal reactions and their relative-energy spectra will be reconstructed from the measured momenta of the ^{24}O fragments and coincident neutrons.

10.6 Producing nuclei using secondary beam fragmentation

Cross section measurements performed as part of the Design Study have shown that higher yields of nuclei at the outermost limits can be achieved through fragmentation of reaccelerated radioactive beams of species such as ^{132}Sn than by the fragmentation of a stable primary beam. This opens up possibilities for exploring the highly exotic nuclei produced in this way and gaining new insights into nuclear properties. For example, β -delayed two-neutron emission is a potentially important probe of nuclear correlations, which could yield valuable information about the pairing of nucleons inside the atomic nucleus, which is not accessible otherwise. In particular, two-neutron emission has the decisive advantage over two-proton emission that the Coulomb barrier does not affect the neutrons and a possible correlation should be observable outside the nucleus. Beyond their interest for correlation studies, the decay characteristics of these nuclei are also of interest for the modelling of the astrophysical rapid neutron capture process. The decays will be studied by implanting the β -delayed two-neutron emitters into an active stopper, which is surrounded by a high-efficiency, high-granularity neutron detection system. Similar detector setups can be applied to study the decay properties of other highly exotic nuclei, such as two-proton emitters. In addition, magnetic moments of isomeric states populated in fragmentation reactions can be measured from time-differential perturbed angular distributions using a dipole magnet coupled with an array of germanium γ -ray detectors.

10.7 Phase transitions, nuclear reactions and dynamics

Isoscalar giant resonances in exotic nuclei are not only of intrinsic interest, but the study of the Giant Monopole Resonance is especially important because it is related to the nuclear matter incompressibility K_∞ , which is of fundamental importance in describing nuclear matter, as well as a basic parameter in calculations describing neutron stars and supernova explosions. Studying the breathing mode in nuclei far from stability is expected to characterise the asymmetry energy term of

the effective force. The experiments will measure inelastically scattered deuterons or α -particles at very low energies and over a large angular range using an active target, such as the time and charge projection chamber MAYA.

The density dependence of the symmetry energy will be explored through the study of selected isospin observables in mid-peripheral collisions of exotic nuclei. Although the symmetry energy cannot be directly accessed from data, the different energy functionals can be implemented in transport equations and converted to transport observables. In order to focus on the isovector properties and minimize the theoretical as well as experimental uncertainties, systems of similar size and widely varying N/Z ratios from ~ 1 to ~ 1.7 will be compared. To produce and detect low-density matter, reaction mechanisms leading to the formation of a neck need to be used and 4π -detection is essential for impact parameter selection. The experiments will therefore exploit FAZIA to provide 4π -coverage, a low threshold and complete A and Z identification for intermediate mass fragments; a large acceptance spectrometer for mass identification of the heavy remnant; and high angular resolution ($\Delta\theta < 0.5^\circ$) light charged-particle and neutron detector arrays for correlation measurements.

The neutron–proton effective mass splitting will also be probed in experiments exploiting FAZIA combined with a 4π neutron detector. These experiments will focus on the isovector part of the energy functional of asymmetric nuclear matter, which is still very poorly known. The difference in the effective mass of protons and neutrons differs widely in different theoretical approaches, even at normal density. Experimental constraints on this quantity are essential for nuclear structure, as well as for the structure of neutron star crusts.

Nuclear matter is known to have at least two major phase transitions: a transition to the quark-gluon plasma at high energy density and a transition to a nucleonic vapour phase at a temperature of a few MeV. The isospin dependence of the fragmentation phase transition will be explored at EURISOL to determine quantitatively the low temperature phase diagram of nuclear matter and the characteristics of the expected liquid-gas phase transition. Although multi-fragmentation experiments in recent years have established approximate values for the temperature, energy and density of this phase change, its nature and order are still largely unknown, as is its isospin dependence. This physics case has strong interdisciplinary connections with atomic, molecular, and cluster physics, as well as important consequences for modelling the supernova explosion process and the cooling dynamics of proto-neutron stars.

Isospin fractionation and isoscaling will also be investigated at EURISOL. Fractionation is a generic feature of phase separation in multi-component systems and in nuclear physics it implies a different isotopic composition of coexisting phases for isospin asymmetric systems. Since an increased fractionation is expected if fragmentation occurs out of equilibrium, a quantitative study of fractionation will elucidate the mechanism of fragment production in excited and correlated quantum media. Moreover, if fractionation is associated with finite temperature, the first moments of the isotopic distributions give a direct measure of the temperature dependence of the symmetry energy in correlated matter at sub-saturation density with important consequences for the dynamical evolution of massive stars and the supernova explosion mechanisms. In particular, the electron capture rate on nuclei and/or free protons in pre-supernova explosions is especially sensitive to the symmetry energy at finite temperatures.

10.8 Low-energy beta-beams

In addition to the possibilities of experiments with high-energy β -beams at EURISOL, there are also opportunities for important measurements with β -beams at lower energies. Low-energy β -beams are neutrino beams in the 100 MeV energy range, which could be produced by the decay of boosted radioactive ions circulating in a storage ring. Such beams could be used to carry out a test of the CVC hypothesis and a measurement of the Weinberg angle at low momentum transfer, as well as nuclear structure studies. This would require the scattering of neutrinos on electrons, protons or oxygen nuclei at $Q^2 = 10^{-4} \text{ GeV}^2$ in a 1-kton water Cerenkov detector.

A precise knowledge of the nuclear isospin and spin-isospin excitations is crucial for our understanding of weak processes such as beta decay, muon capture, neutrino-nucleus interactions and

neutrinoless double β -decay. Besides their intrinsic interest, gaining a precise description of such states constitutes a crucial step to progress on open issues in astrophysics, like understanding the nucleosynthesis of heavy elements during the r-process, or in high-energy physics, for the search of new physics, like the Dirac or Majorana nature of neutrinos. So far, the best-studied cases are the isobaric analogue state (IAS) and the Gamow-Teller (GT) giant resonance. Information on these states is obtained in particular through beta-decay and charge-exchange measurements. A good description of these excitations is nowadays achieved, although the “quenching problem” still remains unresolved. Little is known for the states of higher multipolarity, such as the spin-dipole or the other multipoles, that might well be similarly affected, or require modifications of the effective interactions. An important further step could be obtained using neutrino beams produced with low-energy β -beams. The (anti)neutrinos impinging on a 1-kton water Čerenkov detector will interact mainly with the protons and with the oxygen nuclei. The neutrino-oxygen events can be selected by doping with gadolinium. Systematic studies on other nuclei can be performed by replacing the Čerenkov detector by detectors based on other nuclei, such as iron and lead.

10.9 Instrumentation for EURISOL

This diverse and exciting physics programme envisaged for EURISOL requires an associated suite of instruments for its delivery. While some of these might be considered to be well-established devices and techniques that will exploit the new species available at EURISOL, there are others that still require significant research and development effort before they can be exploited. For some of these latter cases, the necessary work was being undertaken either by existing long-term collaborations (e.g., AGATA and FAZIA) or within Joint Research Activities within the 6th Framework contract EURONS (e.g., TRAPSPEC, LASPEC, and ACTAR). However, some instruments were identified that fell outside of these areas and were selected for further investigation within the EURISOL Design Study. These were the design of detector arrays for the detection of fast neutrons; an array for the simultaneous detection of light charged particles and γ -rays in direct reaction experiments; a conceptual design for a recoil separator for heavy element studies; and simulations of the low-energy β -beam experiments. The outcomes of this work are summarised below.

10.10 Neutron detector simulations

Some of the most demanding experiments will be those requiring neutron detection to investigate the structure of systems beyond the neutron drip-line through nucleon knock-out (mainly proton) and fragmentation-type reactions. For these experiments, such as the proposed study of $^{26,28}\text{O}$ described in section 10.5, it is necessary to detect “fast” neutrons over a range of energies ($1 \text{ MeV} < E_n < \sim 200 \text{ MeV}$), with high efficiency and good energy and angular resolution. In addition, the ability to detect multiple neutrons and discriminate between neutron and γ -ray events is essential. To design a detector array optimised for these and other experiments with similar requirements, a Monte-Carlo simulation was developed, employing the GEANT4 package as a starting point. These simulations model in particular the distribution of the neutrons resulting from the in-flight decay of the unbound nuclei and the scattering of the neutrons inside the scintillation material. Using these simulations, realistic estimates of the efficiency and resolution for a given detector array geometry may be obtained.

It was found during this study that the neutron scattering models available in the GEANT4 package did not properly reproduce the measured detection efficiencies for existing detectors. In addition, the angular distributions of the neutrons after scattering in a detector were found to be incorrect, which resulted in inaccurate predictions of the probability of cross-talk between detectors. For these reasons, a revised neutron scattering model “MENATE_R” was developed to be used in place of the existing GEANT4 neutron scattering models.

In order to validate this model, the results of Monte-Carlo simulations were benchmarked against experimental data obtained using elements of the modular liquid scintillator array DEMON. The simulations were used to compute both the intrinsic neutron detection efficiency of a module and the cross-talk probability between two modules, where neutrons scatter from one detector to another. Improvements to the neutron scattering model were implemented and good overall agreement was obtained, to within $\sim 5\%$ (see figure 1).

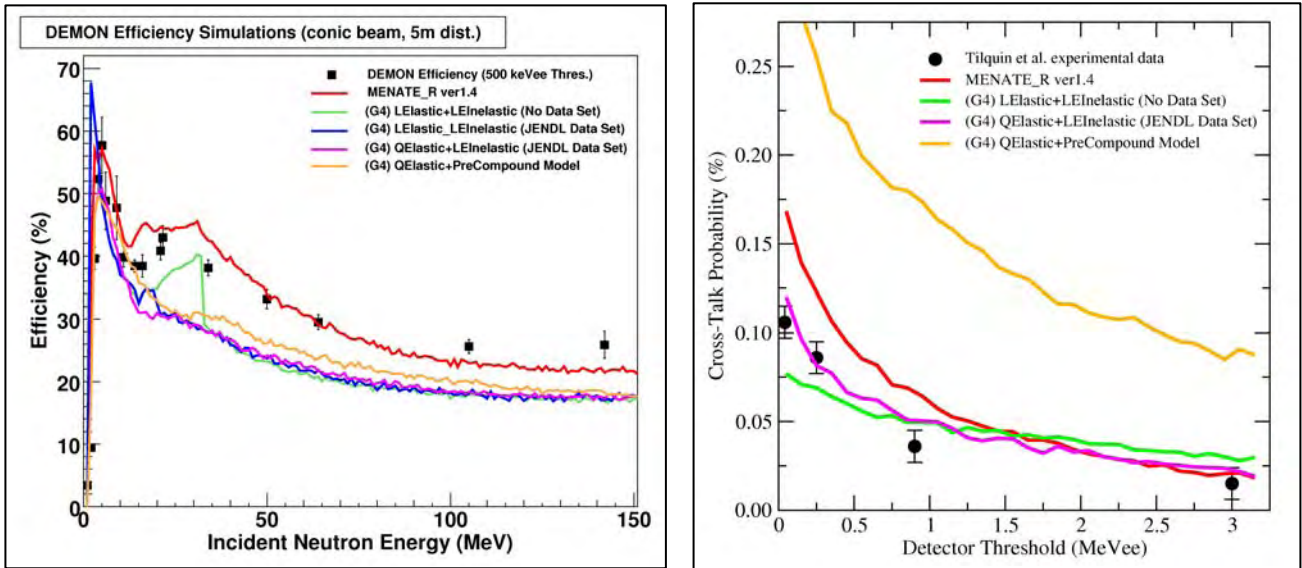


Fig. 1: Comparison of the efficiency (left) and cross-talk probability (right) simulated using different neutron scattering models within GEANT4, compared with measured data for the DEMON array.

This model was then used to simulate the performance of a DEMON-like modular neutron detector array and a “wall-type” array over a range of energies (35-150 MeV/nucleon) (see figure 2). Based on these simulations, two neutron detector array designs, one of each type, were proposed and costed. A detailed report on the modified neutron scattering model, its implementation within GEANT4 and the simulations of the two different array types is in preparation.

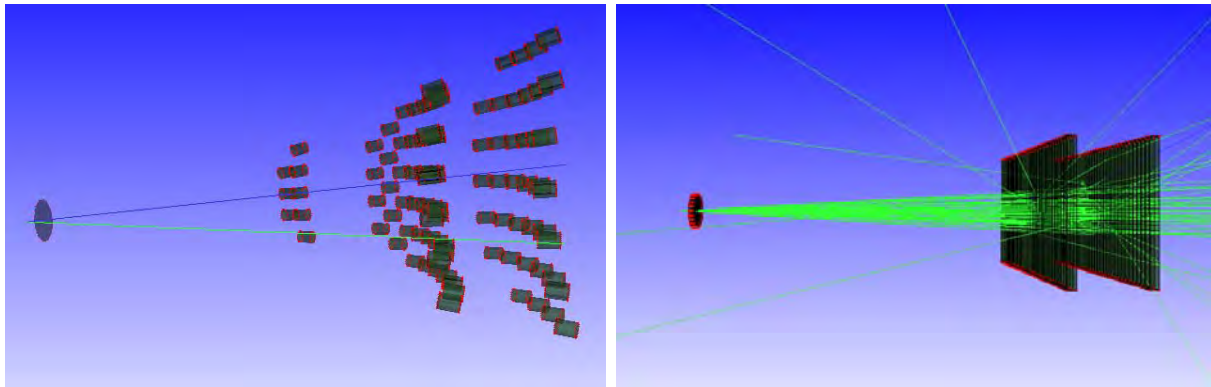


Fig. 2: Visualisation of a “modular” neutron detector array (left) and a “wall-type” array within GEANT4.

10.11 Simultaneous charged-particle and gamma-ray detection

A campaign of experiments using a combined detection system of silicon and germanium arrays for simultaneous detection of light charged particles and γ -rays was carried out at SPIRAL/GANIL in autumn 2007. This gave an opportunity to validate the simulation tools developed using the GEANT4 package for such experimental scenarios. The experimental setup comprised the MUST2 silicon array at forward angles (0° – 30°) coupled to the TIARA barrel and the Hyball at angles of 35° – 180° . This composite array covered a large fraction of the 4π solid angle for the charged particles. The EXOGAM germanium array was placed at 5 cm from the target to enhance the γ -ray detection efficiency. In addition the large acceptance spectrometer VAMOS was used to select the beam-like particles providing a full kinematic identification of the reaction channel.

Two experiments were carried out using ^{20}O and ^{26}Ne SPIRAL beams aimed at studying the shell structure of exotic nuclei at the $N=16$ shell gap. The experimental conditions in terms of beam intensity were slightly different, allowing the simulations to be tested further. While the ^{20}O beam was provided by the SPIRAL facility with an intensity of 10^4 pps, the ^{26}Ne beam was an order of magnitude weaker, requiring the use of a deuterated polyethylene target that was twice as thick to compensate partially for the lower beam intensity.

The complete silicon and germanium detector system was implemented in the GEANT4 simulation toolkit (see figure 3). It was found that the simulations accurately reproduced the response of arrays and gave an insight into the main parameters that contribute to performance. This validation of the simulations should therefore allow both the optimization of future experiments using this hybrid array and the design of an integrated charged particle and γ -ray spectrometer for EURISOL.

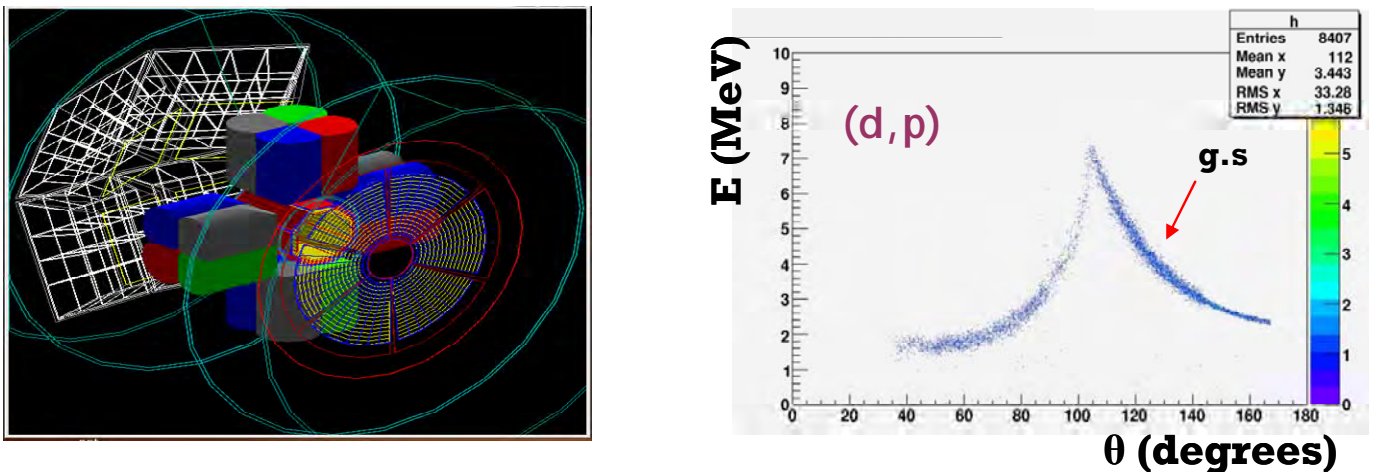


Fig. 3: Visualisation of TIARA + MUST2 + EXOGAM within GEANT4 (left) and the simulated energy-angle correlation matrix obtained in TIARA (right).

10.12 Conceptual recoil separator design

The study of the heaviest elements at EURISOL will require a highly efficient recoil separator with a beam suppression factor of at least 10^{12} . It is anticipated that such a device should also be suitable for a wide range of other experiments involving fusion-evaporation reactions. While many recoil separator devices are in operation at nuclear physics laboratories around the world, none has been specifically designed for dealing with the very high intensities of radioactive beams that are envisaged for EURISOL. In general they have been designed for use with stable beams with the key performance criteria of high transport efficiency and high beam suppression factor. Many separators also have the capability to separate recoiling ions according to the ratio of their mass (A) and charge state (q), and for these separators the resolution in A/q is also an important design criterion. What is generally less important is where the unreacted primary beam is deposited, because once stopped the stable beam ions do not cause experimental difficulties.

Clearly this will not be the case in experiments with EURISOL that require radioactive beam intensities of up to 10^{12} particles per second. Typical beam species that are proposed for these experiments include ^{132}Sn and ^{92}Kr . The decay chains of both of these nuclides involve 4 β -decays to reach a stable nuclide, with half-lives ranging from 1.8 s for ^{92}Kr to 76 h for ^{132}Te . This leads to the additional design criterion for a recoil separator for heavy element studies with EURISOL that the primary beam should be deposited in a controlled fashion. The location where the beam is stopped can be in a heavily shielded cave to prevent the radioactivity from causing high background levels in the experimental apparatus and to allow user access to the equipment on shorter timescales after the beam is switched off. Another, more elaborate, possibility could be to recycle the radioactive beam, although the feasibility of this remains to be demonstrated.

The conceptual solution proposed to meet the design criteria involves transporting the beam straight through a Wien filter that will form the first stage of the recoil separator (see figure 4). The beam can then be dealt with as appropriate. The reaction products that are of interest for the physics experiments will be deviated by the Wien filter. The remainder of the recoil separator, which could comprise one or several deflecting elements plus focusing elements, will be used to collect these ions and transport them with the highest possible efficiency to the focal plane detector system, while at the same time maximally suppressing scattered beam particles.

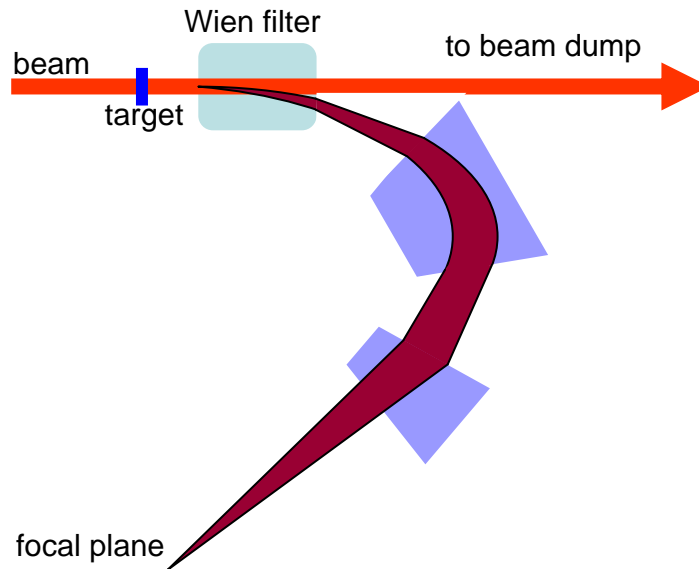


Fig. 4: Schematic diagram of the recoil-separator concept.

An in-beam test to validate the proposed design concept was made using VAMOS, which is a versatile recoil-separator device that has a Wien filter as its first separation element. Beam optics simulations indicated that this mode should not affect the transmission compared with the standard mode of Wien filter operation and that a better degree of beam suppression should be achievable. Three different reactions were used in the tests. In the reaction $^{22}\text{Ne} + ^{197}\text{Au}$ at a bombarding energy of 114.5 MeV, the α -decays of $^{213,214}\text{Ac}$ were observed in the silicon detector system at the VAMOS focal plane. This demonstrated that it is possible to collect the evaporation residues of interest with high transport efficiency when the Wien filter is set to transmit the beam straight through. It should be noted that for the experimental programme at EURISOL employing more symmetric reactions it will be necessary to construct a Wien filter capable of providing greater field strengths than are possible with VAMOS.

10.13 Low-energy beta-beam concept

In order to develop the ideas proposed for low-energy β -beams, calculations were performed using the QRPA approach for both the total cross sections as a function of neutrino energy and the flux-averaged cross sections associated to either conventional sources (muon decay at rest) or low-energy β -beams. A detailed analysis of the states of different multipolarity (allowed and forbidden) contributing to the cross sections was performed as a function of the Lorentz ion boosts, to explore whether information on the various multipoles can be extracted by combining different neutrino ion accelerations. It was concluded that by varying the boost factor, the role of the spin-dipole states becomes as important as the Isobaric Analogue and Gamow-Teller states, allowing nuclear structure studies of the forbidden states to be undertaken. Combining neutrino-nucleus interaction measurements with different boost factors would make it possible to disentangle the information from a core-collapse supernova neutrino signal.

Detailed calculations were also made to investigate the possibility of measuring the weak magnetism term of the weak currents. The proposed method exploits anti-neutrino capture by protons in a water Čerenkov detector. Due to the increasing importance of the weak magnetism contribution with the impinging neutrino energy, working at higher gamma values turns out to be advantageous for such an application. Furthermore, the calculations demonstrate that the angular distribution is a much better

signature than the total number of events when the systematic errors are taken into account. It has been shown that the weak magnetism form factor can be determined within an accuracy of several percent. This way of probing the weak magnetism form factor at low momentum constitutes a new test of the Conserved Vector Current (CVC) hypothesis. A possible measurement of the Weinberg angle at low momentum transfer has also been investigated. Such a measurement exploits neutrino-electron scattering. By combining measurements with different ion boosts one can determine the Weinberg angle with a precision of about 10% and therefore improve the present precision in this range by about a factor of 2.

Calculations of neutrino-nucleus reactions rates were performed for a range of different experimental scenarios. It was found that with two off-axis detectors located near a standard β -beam decay ring (see figure 5) one can obtain sizable low-energy neutrino fluxes to perform various experiments, after suitable subtractions. Interestingly, the energy spectrum of the neutrinos is pushed to lower energies than for the low-energy β -beam (see figure 6). Thus the option of two off-axis detectors at a standard β -beam facility might be a suitable alternative to having a dedicated storage ring for the realization of low-energy neutrino experiments.

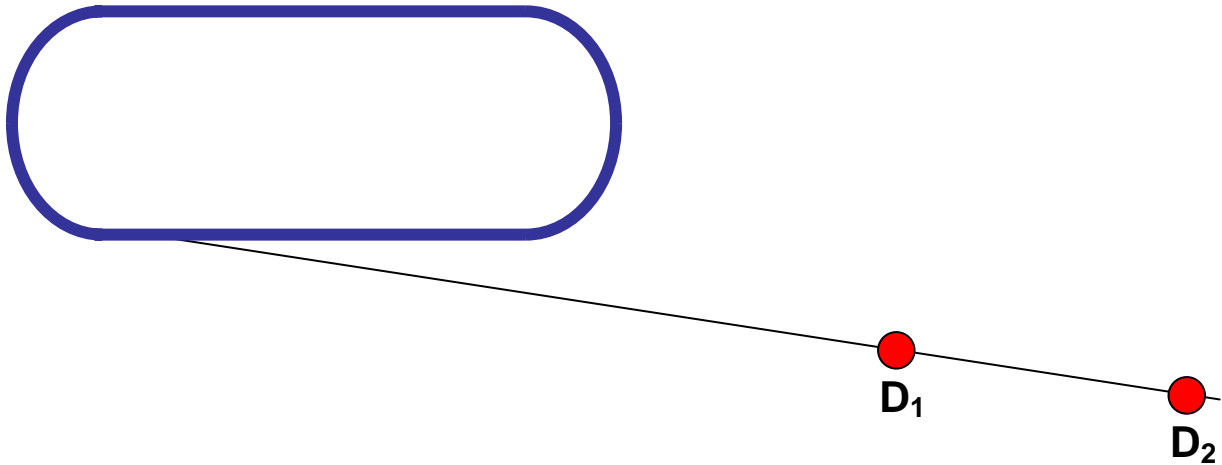


Fig. 5: Schematic diagram showing two off-axis detectors located near a standard beta-beam decay ring.

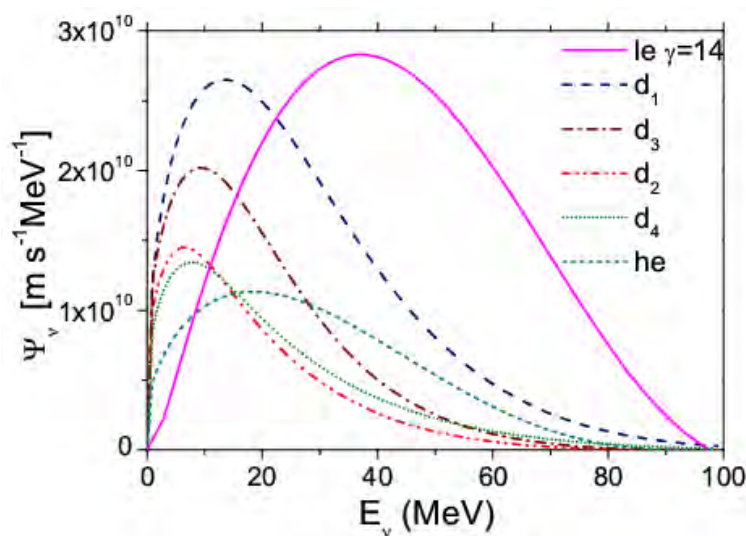


Fig. 6: Comparison of the different low-energy neutrino fluxes obtained with a standard beta-beam, exploiting two off-axis detectors. The different curves correspond to four different detector geometries, namely the cylinder-sausage (d_1), the cylinder-normal (d_2), the cylinder-disc (d_3) and the spherical (d_4). For comparison, the flux from a low-energy beta-beam (le), and for a single off-axis detector d_2 (he) are also given.

10.14 Conclusion

It is clear that experimental techniques, theoretical models and the physics case for EURISOL will continue to evolve in the coming years. One legacy of the 'Physics and Instrumentation' task is the formation of the EURISOL User Group, which is charged with the responsibility of continually updating the physics case and engaging the EURISOL user community. The EURISOL User Group has already organized one workshop in January 2008 at the Galileo Galilei Institute in Florence as part of its remit, and further meetings are planned.

Chapter 11: Radiation Safety

11.1 Introduction

The Safety and Radioprotection task of the EURISOL design study has aimed at providing a quantitative evaluation of the major safety-related questions arising during the design study.

Originating from the main objective of EURISOL of increasing the radioactive ion beam (RIB) intensities by several orders of magnitude, the radioactive inventory and corresponding radioprotection issues will reach levels never before obtained in any ISOL facility. The multi-megawatt target station is the central issue and a lot of effort has been devoted to this. Nevertheless, this ambitious facility also needs careful studies of the other areas, in order to provide all safety constraints and to give the range of realistic options.

In order to achieve these goals, the task addressed a number of identified issues. The first of these was radioprotection throughout the facility, with radiation and activation estimates and shielding guidelines. The second was radioactivity control (restricted to the beam areas), avoiding dispersion in air and transport in ground water. The third was decommissioning, since any technical problems expected after the facility shutdown must already be taken into account in the design phase, to avoid unexpected costs in future. Fourthly, conformity to legislation was researched, since the EURISOL facility will be close to a research reactor as far as safety issues are concerned, and different potential host countries may have different legal frameworks. Finally, risk assessment is the last section of this report. A quantitative risk analysis should be made during the next phase of the EURISOL project – the full engineering study, and all knowledge acquired during this design study will be of utmost importance.

Under the leadership of the CEA in Saclay in France, seven institutes participated in this Safety and Radioprotection task: FZJ and LMU in Germany, CERN in Switzerland, GANIL in France, FI in Lithuania, NIPNE IFIN-HH in Romania and the University of Warsaw in Poland. Thus around forty people in Europe worked on the safety aspects of the EURISOL facility, while laboratories like ITN in Portugal helped as contributors and other North-American and Asian institutes (TRIUMF, ORNL, ANL, JAERI, and KAERI) shared their expertise during various working meetings.

11.2 Radiation, activation, shielding and doses

Simulation codes and models are needed to estimate radioactivity and doses and to design radioprotection shielding properties. The two main transport codes which were used for this were FLUKA and MCNPX2.5.0, but also PHITS for the heavy-ion cases. The first step was to benchmark them for EURISOL calculations. Then a compilation of experimental data was set up in order to test their validities according to projectile type, energy range, target material and observables.

The beam energy proposed for the proton driver of EURISOL is about 1 GeV: consequently data around this energy have been selected for the benchmark calculations. Residue, neutron and light-charged-particle (lcp) production was examined with eleven spallation models (ten in MCNPX2.5.0 and one in FLUKA). While neutron spectra are quite well described by all models, lcp production can be improved, especially the tritium production, and finally the residues showed that only four models are reliable: INCL4-Abla, Isabel-Abla, CEM2k in MCNPX2.5.0 and FLUKA. Before doing shielding assessment for the post-accelerator, the PHITS and MCNPX2.6.e codes were benchmarked on neutron double-differential cross sections from reactions induced by ^{40}Ar at two incident energies, i.e. 95 and 560 MeV per nucleon and by ^{132}Sn (150.4 MeV) incident on a copper target. Both codes gave good results and PHITS was chosen because it conservatively overestimates experimental data at low neutron energies. Finally neutron and photon attenuation was also tested with MCNPX for concrete and iron, the two main shielding materials. Except for the photon flux in iron, which is overestimated, the other results gave good confidence. The CINDER'90 evolution code, also used for safety calculations, was compared to fission yield tables generated by the EURISOL "Yield Calculations" task group: details can be found in the reference [1]. Radiation estimates and shielding guidelines are given below for each part of the facility.

Proton driver

The proton beam energy envisaged for EURISOL to bombard targets is 1 GeV, with intensities such that 100 kW and 4 MW will be delivered to the direct targets and to the multi-MW target, respectively. The proton linear accelerator will be built using superconducting radiofrequency technology, demanding a low level of beam losses in order to preserve the superconducting state. Therefore, beam losses along the length of the proton accelerator have been analysed with the help of a beam dynamics code (see Chapter 2). Over most of the accelerator's length the linear loss power density is well below 1 W/m, except close to the source and at the end of the accelerator.

The method used to estimate the shielding is the so-called line-of-sight model, which is a quick alternative to Monte-Carlo codes for the case of energy varying with the length coordinate of the accelerator. The first step gives the source term for an emission under 90 degrees and in the second step radiation attenuation is calculated in arbitrarily thick walls using dose rate limits as constraint. Doing this with the given estimates for uncontrolled beam loss suggests that the EURISOL proton driver could be built in a shallow trench with a roof shielded with 2 metres of concrete or, alternatively, a combination of concrete and an equivalent thickness of earth. However, the high-energy end of the driver linac will require local shielding, since any beam losses will be much more important in this section.

Direct target

The direct targets will be targets bombarded by 1-GeV protons with a maximum beam current of 100 μ A. The power of the particle beam is therefore 100 kW. Minimum dimensions of the shielding are given below, since the purpose was to provide a guide and not the definitive shielding, which can only be done once a definitive layout becomes available. The layout of the target stations is described in Chapter 3, so below we give only the part used to determine the shielding.

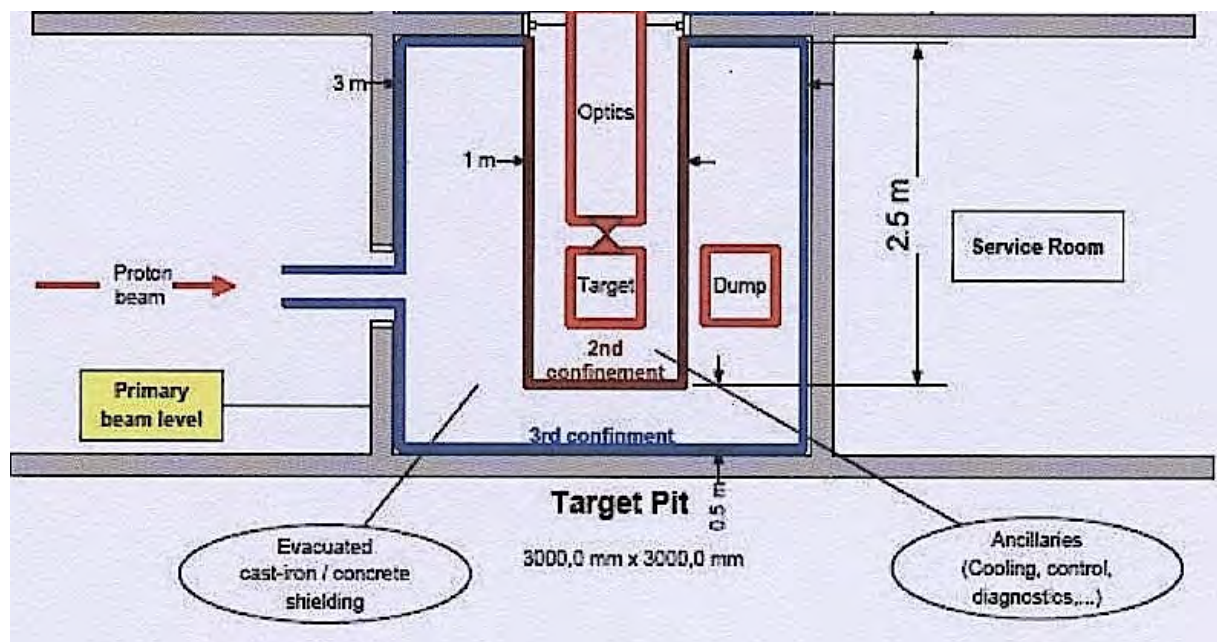


Fig. 1: Conceptual lay-out of a 100-kW EURISOL target station with a vertical arrangement. Here only the target level is shown. On the floor above, the target handling level, a hot-cell and its operator's room (from where the manipulators are controlled) are envisaged.

As usual, constraints are required to define the thicknesses needed for the walls. We have assumed that access for routine work can be granted once the ambient dose rate in the respective area is less than 10 μ Sv h^{-1} . Exceptional access can be given to areas where dose rates are not higher than a value between 0.01 and 1.0 mSv h^{-1} , depending on the duration of the access. The code used for these calculations was FLUKA and the dimensions obtained are shown in figure 2 below.

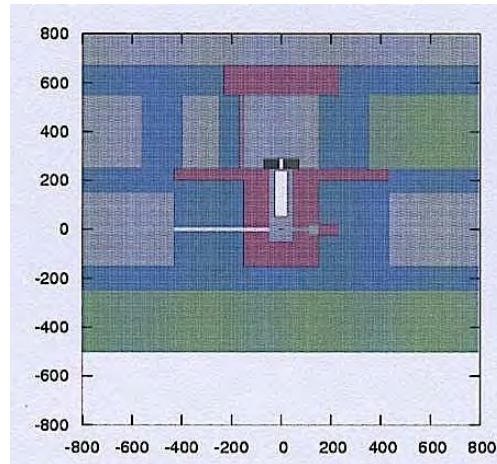


Fig. 2: Shielding dimensions for a 100-kW target. Red=stainless steel. Blue=concrete. Grey=air. Green=soil.

MMW fission target

Irrespective of the details of the fission target (30 kg of depleted uranium or 6×15 g of highly enriched ^{235}U), the shielding requirements for the multi-megawatt target are driven by the need to absorb the secondary radiation from the neutron spallation source. For the original design, shielding was estimated in a simplified geometry from radiation attenuation calculations with the FLUKA Monte-Carlo code. The results could be described in a simple exponential attenuation model, which can be extrapolated to arbitrary penetration depths, where Monte-Carlo calculations become tedious because of numerical fluctuations. For deep penetration, an exponential attenuation term in concrete has been evaluated. A total shielding thickness of 600 cm is necessary to reach an ambient dose equivalent rate of $1 \mu\text{Sv/h}$.

Another calculation, assuming a fission target configuration with small ^{235}U targets, arrives at the identical conclusion that 600 cm of shielding concrete are required to attenuate radiation sufficiently in the beam handling area (see figure 3 below).

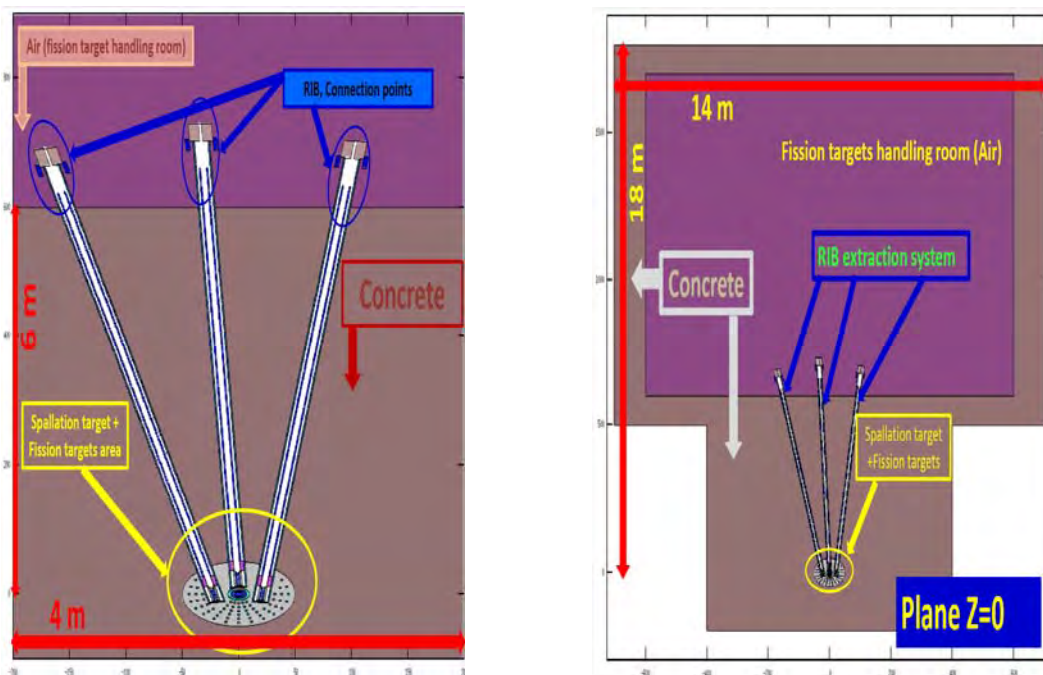


Fig. 3 (Left): The spallation target and fission target geometry including the RIB extraction tubes and connection points, in the $z=0$ plane, perpendicular to the proton beam. (Right): Same plane, but also showing the spallation target shielding area and the fission target-handling room.

In addition to the shielding of the area, the layout of the target handling area has been estimated. This area must be a high building with massive concrete walls (1 metre thick), in which huge activities of alpha-emitting actinides can be handled safely.

Calculated dose rates showed that the mercury “converter” target will be even a stronger source of radiation than the fission targets (see figure 4 below – normalized to 1 MW). However, the fission target container, which is one of the most critical regions in the extraction tubes, is subject to very high neutron fluxes, and therefore its material has to be very resistant from a thermo-mechanical point of view. Molybdenum and tantalum have high melting points, but the activity obtained with tantalum is even higher than the fission target activity and could rule it out as the choice for the fission target container.

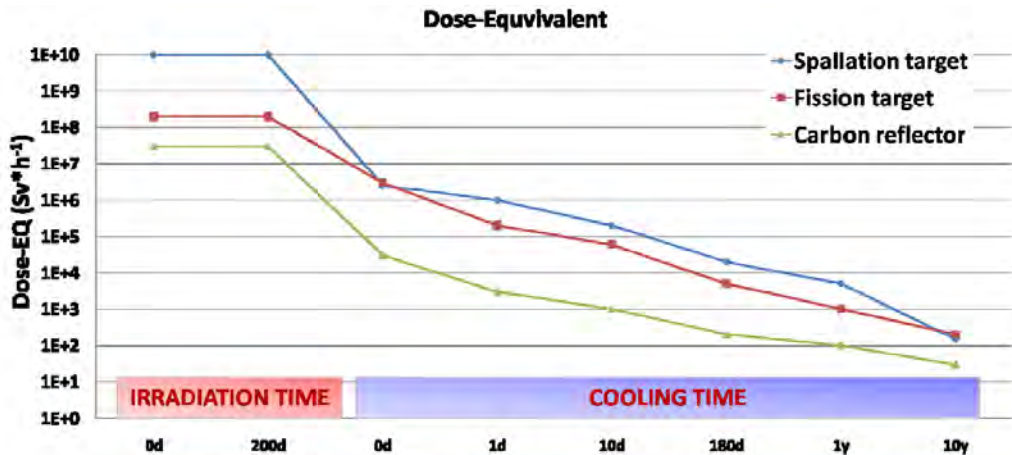


Fig. 4: Calculated dose rates for a mercury spallation target and fission targets, normalised to 1 MW.

Post-accelerator and experimental area

The post-accelerator of EURISOL is supposed to deliver secondary beams of 10^{13} pps at energies up to 150 MeV/u, thus exceeding by at least a factor 100 the ion yields delivered by existing facilities or those under construction. This part of the facility, like the target stations, is challenging in several different fields and especially so with respect to the shielding requirements. The procedure followed was the same, however, in that the dose rate constraints had to be defined, and then a penalising case was chosen and calculations performed.

The constraints are taken from ICRP60, e.g. 0.1 μ Sv/h for public areas and 10 μ Sv/h for controlled areas. A beam loss of 10^{-4} m^{-1} ($\times 10$ for point loss) was assumed, which is also adequate for accidents (full beam loss), if the linac cut-off time is less than 1s. Calculations were done with a beam of ^{132}Sn and the transport code was PHITS version 1.94, coupled with the DCHAIN-SP2001 code for activation analysis. Two options have been studied, with and without a stripper. The shielding obtained in both cases is shown in figure 5 below. The use of a stripper would reduce the shielding volume by a factor 2, partly due to a reduction in the linac length.

A shielding for the beam dump has also been studied based on geometry used for a beam dump at GSI. Preliminary calculations show that the graphite block would reach ignition temperature in air, so this should be in a vacuum or an inert gas, while a kicker/wobbler magnet could also be advantageous in order to avoid hot spots. With this taken into account, the thicknesses of the shielding walls around the beam dump were estimated to be about 5 m of concrete. A specific study of the beam dump geometry should be performed during the next phase of the project.

Concerning the experimental halls a penalising case was selected with members of the Physics and Instrumentation task group; however the results obtained for the activity levels were such that it was impossible to extrapolate to other experiments. The conclusion is that a specific study has to be performed according to each type of experiments planned.

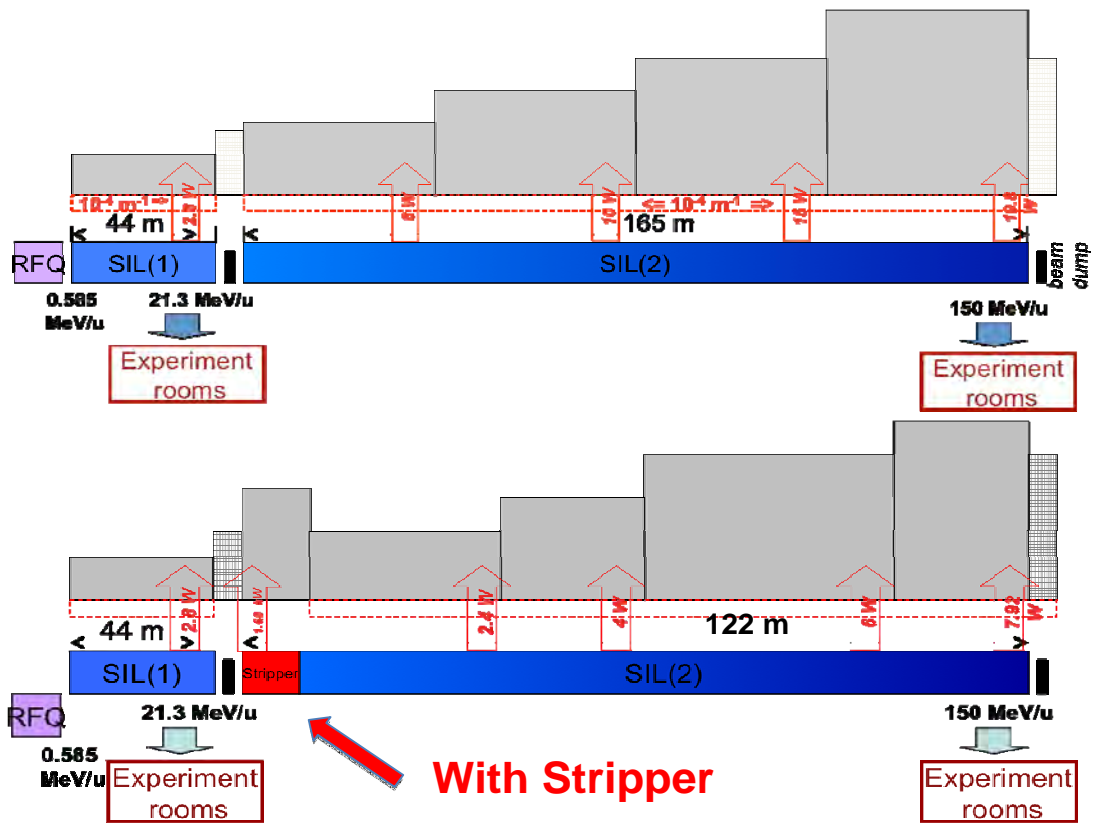


Fig. 5: Shielding thicknesses calculated for the post-accelerator. (Lengths not to scale).

11.3 Radioactivity Control, safety and risk

Dispersion of radioactivity

The extraordinary high radioactivity inventory expected for the EURISOL facility has caused the project’s scientific management to seek advice in an environment where consolidated expertise on comparable activity levels is available, i.e. in the physics and engineering of the nuclear power industry. In this context, the team at NIPNE investigated ways and means of transferring relevant knowledge and data, as well as adapting and developing appropriate methods and tools to assist the management of safety and radioprotection at RIB facilities. The result is a software package named EDAT (EURISOL Desktop Assistant Toolkit), consisting of computer-based knowledge and data libraries and presented in the form of a distributable CD.

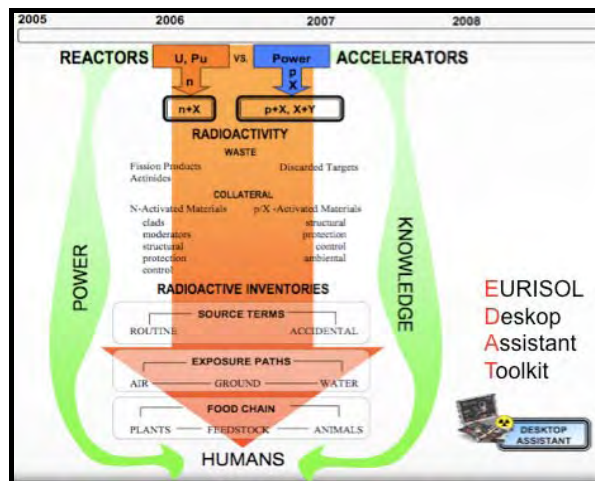


Fig. 6: The EURISOL Desktop Assistant Toolkit CD.

Test of purification system

In radioactive ion beam facilities like EURISOL, where the exotic beam species are produced via a uranium fission target, the vacuum system must be treated as being contaminated. Thus characterization tests of a filter system for vacuum exhaust gases were carried out.

This system is based on a cryotrap, cryopumps and an aerosol filter. The cryotrap localizes the volatile radioactivity close to the fission source, while the cryopumps assist in the freeze-out of unwanted volatile radioactivity as well as in the avoidance of maintenance interventions in contaminated areas; the exhaust gases are stored in decay tanks, and once the activity level as reached a suitable limit the gases are released via an efficient aerosol filter system.

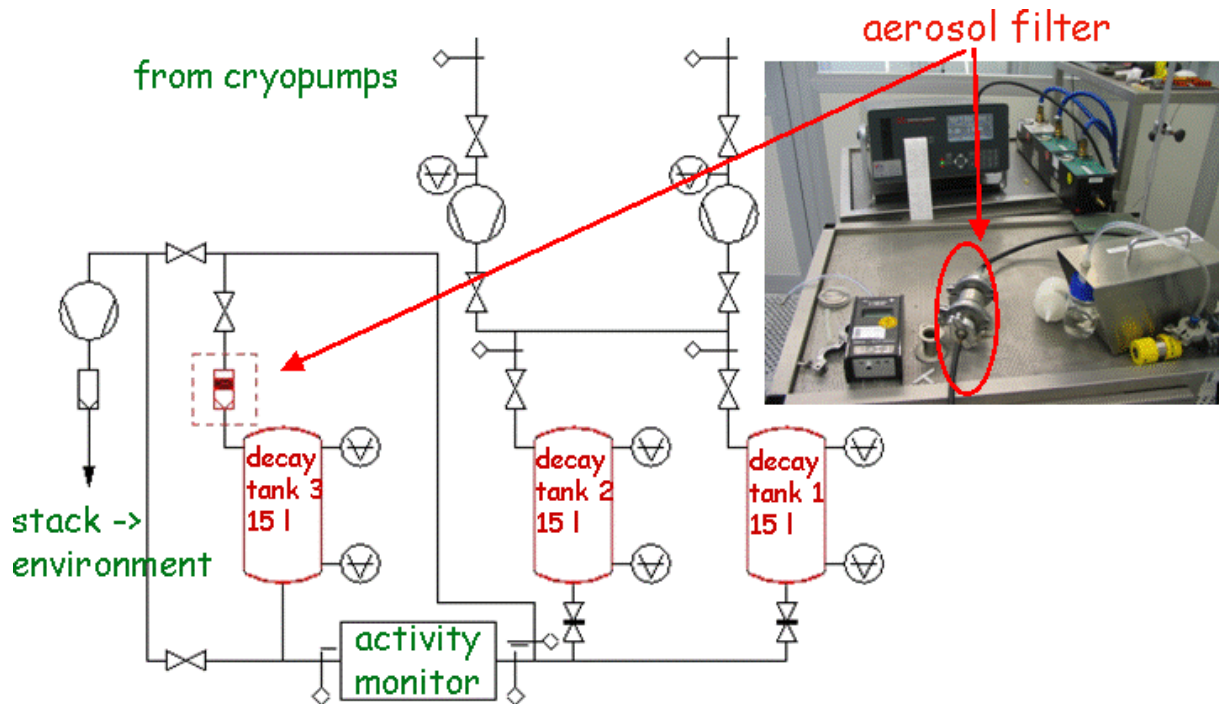


Fig. 7: The purification system layout, with aerosol filter (inset).

The vacuum system gas treatment scheme was successfully verified using “clean room” areas and aerosol production and detection technology. As a key element of the gas purification system, an all-metal nickel membrane filter was characterized, resulting in a measured filtration efficiency of better than 10^{-12} for aerosol particle sizes between 0.1 and 0.2 μm .

Containment of radioactivity

A cryotrap system could also be characterized. Since in EURISOL the radioactivity will reach that of a nuclear research reactor, it was obvious to use the concept developed in the framework of the Munich Accelerator for Fission Fragments (MAFF) project at the FRM2 research reactor in Garching. The basic idea is to localize unwanted volatile radioactivity on the cold surface of a cryotrap close to the fission source and wait for the radioactive decay to transform volatile to non-volatile species.

A test-bench setup was realized that allowed us to quantify the localization capability of the cryotrap as a function of the gas load introduced by a test leak, the gas species and its operational temperature. Agreement with the activity distribution simulations could be demonstrated, resulting in an overall localization factor of 99.98% for a cryotrap system consisting of two panels (see figure 8) surrounding the fission source in a distance of about 1 m at either side of the beam tube, operated at an average temperature of 15K.

Thus cryotrapping of volatile radioisotopes is an efficient tool to minimize the migration of unwanted radioactivity into the beamline system of a radioactive ion beam facility.



Fig. 8: Photographs of the various cryotrap prototypes.

Activity transport in ground water

From what has been outlined before, radioprotective shielding is necessary as well as filters and cryotrap to contain radioactivity. Moreover, one has to prove that the installation workers, the environment and the public are sufficiently protected against any danger of radiation escaping the facility. Thus a reliable method for the calculation of the potential radioactive burden outside the facility fence is required. A complete calculation of all nuclide activation and transport processes in soil and ground water is a complex and time-consuming procedure. Consequently a simplified but fast-to-apply model was developed, based on transport calculations performed within the EURONS-SAFERIB project of FP6, where the input parameters have been generated within EURISOL-DS.

Since the composition of soil and ground water play an important role, two typical sites, CERN and Jülich, were chosen in order to determine the potential activation in the environment and to prove that the effective dose resulting from drinking water at the boundary of the supervised area remains below the legal limit of 1 mSv/y defined by the EURATOM directive 96/29.

An example of partition coefficients K_D for the most relevant nuclides according to their half-lives is given below as a matrix of the most relevant radionuclides identified for the soil composition taken for the site of FZ Jülich, originating below 0.8 m of concrete shielding of the accelerator and assuming a beam loss of 1 W/m. Their saturation concentration is listed together with the corresponding partition coefficient K_D

Isotope:	P-32	Ca-45	H-3	Cl-36	Partition Coefficient K_D ↓
Half-life:	14.26 d	163 d	12.3 y	300000 y	
Saturation concentration:	5 cm ³ /g	5 cm ³ /g	0 cm ³ /g	0 cm ³ /g	
Partition coeff. K_D :	6E-8 Bq/cm ³	1E-8 Bq/cm ³	35 Bq/cm ³	1.3E-5 Bq/cm ³	
Isotope:	Co-55	S-35	Co-60	C-14	
Half-life:	17.5 h	87.5 d	5.27 y	5730 y	
Saturation concentration:	30 cm ³ /g	14 cm ³ /g	30 cm ³ /g	7 cm ³ /g	
Partition coeff. K_D :	9.5E-13 Bq/cm ³	1.2E-7 Bq/cm ³	2.7E-12 Bq/cm ³	3.3E-6 Bq/cm ³	
Isotope:	Na-24	Co-57	Mn-54	Si-32	
Half-life:	14.96 h	14.26 d	312 d	172 y	
Saturation concentration:	76 cm ³ /g	30 cm ³ /g	50 cm ³ /g	35 cm ³ /g	
Partition coeff. K_D :	7E-8 Bq/cm ³	3.5E-12 Bq/cm ³	2.4E-12 Bq/cm ³	1.4E-10 Bq/cm ³	

Half -life →

Fig. 9: Partition coefficients K_D for the most relevant nuclides according to their half-lives, shown for the relevant radionuclides identified in soil from the site of FZ Jülich.

11.4 Decommissioning issues

A significantly activated and contaminated facility like EURISOL requires careful investigations on decommissioning, dismantling and disposal procedures. The volume of materials involved at EURISOL will be large and several innovative components have never before been decommissioned and will require specific treatment. The latter holds particularly for the liquid-metal target. Candidates for this are mercury and a liquid Pb-Bi eutectic. Since the eutectic is solid at room temperature, all model work during the design study was done with mercury, and only this material was considered for the decommissioning exercise.

Accordingly, the study of decommissioning a EURISOL facility was separated into 3 parts:

- (i) de-commissioning and disposal of a possible mercury target, including R&D on the solidification of proton-irradiated mercury;
- (ii) a collection of other wastes to be expected on decommissioning and its treatment; and
- (iii) a rough estimate of the EURISOL decommissioning costs.

Mercury target

About 15000 kg (1.1 m³) of mercury would be irradiated in the EURISOL target for about 30 years. Ten years after shutdown the mercury would still contain an activity of about 6×10^6 GBq. Several of the relevant nuclides produced also play an important role in fission reactor disposal procedures and thus some knowledge is already available concerning their treatment. Volatile nuclides are already separated from the target after the end of operation. Except for tritium they are short-lived and do not require any special attention during decommissioning. However, proton-irradiated mercury contains a major amount of ¹⁹⁴Hg, a nuclide with a half-life of 512 years, which decays to the short-lived ¹⁹⁴Au, a strong γ -emitter. ¹⁹⁴Hg cannot be separated from the target mercury (in contrast to most other nuclides formed during the spallation process), and the whole mercury volume would have to be solidified prior to its disposal, since no radioactive waste repository in Europe allows liquids with high activities to be disposed of.

One important requirement for a mercury compound suitable for waste disposal is a low solubility in water, because a water-ingress accident in a repository has to be considered as the dominating accident. Several ionic inorganic compounds and metal alloys were studied, first on the base of their solubility. It turned out that HgS and HgSe for ionic inorganic compounds and silver amalgam for metal alloys were the best solutions.

Stability in aqueous environments also in the presence of γ -irradiation is another important selection criterion. The γ -irradiation may enhance dissolution by radiolytic reactions, forming highly reactive species in the aqueous solution. Irradiation experiments were conducted on solid mercury compounds, some embedded in a cement matrix, to study their dissolution behaviour. The main conclusion from measurements without the matrix is that the stability of amalgams during accidents in a repository is less compared to that of chalcogenides. Despite its even better dissolution behaviour, mercury selenide (HgSe) was not considered for detailed studies: high costs and biotoxicity of selenium (Se) are major disadvantages and HgS was chosen as solid compound for final disposal. Results on a specimen embedded in a cement matrix show that retention is improved compared to pure Hg compounds. Nevertheless, due to the large density differences between mercury compounds and cement, a homogeneous Hg distribution in cement was difficult to achieve.

Another possibility, a polysiloxane matrix, was also investigated. Unfortunately we were not able to perform leaching experiments on polysiloxane-embedded HgS under γ -irradiation conditions, because the Jülich research reactor was shut down and a transfer of the irradiation equipment to another irradiation site was found to be too time-consuming. Nevertheless the conclusion is that polysiloxane is a promising candidate as matrix material for HgS if a layered polysiloxane waste package is used. Future work must investigate the leaching behaviour under γ -irradiation.

Finally a chemical engineering study on the formation of HgS from irradiated mercury was carried out. The process chosen from literature was the “wet” process, i.e. with dissolution and precipitation.

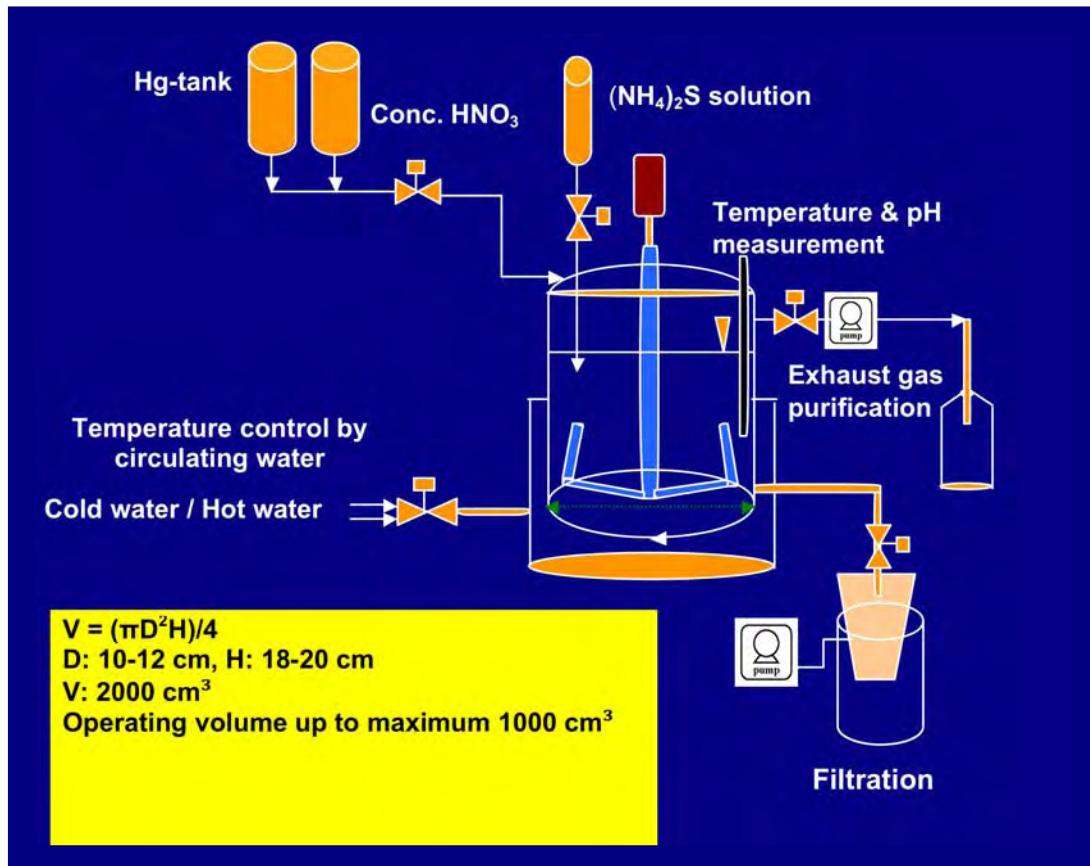


Fig. 10: Schematic diagram showing the method for formation of HgS from irradiated mercury.

A laboratory-scale apparatus for process studies on the formation of HgS was constructed and operated in the chemical hot cells of FZJ (shown schematically in the figure above). The whole process was straightforward, as it is required in a hot cell. This procedure allows a complete conversion of liquid Hg to solid HgS. The work on mercury solidification and disposal outlined here is a first step in the development of a complete disposal strategy for a mercury target. It may however be regarded as an indication that the disposal of proton-irradiated mercury is possible, even within the strict limitations of European regulations. However, because of the required solidification, which as a chemical process resembles a small-scale nuclear reprocessing step, the effort is very large compared to target materials which do not require a solidification process.

Waste atlas

The total amount of waste has to be estimated before such a facility can be constructed, in order to avoid surprisingly high costs once decommissioning begins. Another task is to classify the different types of wastes whenever possible. For example, a classification of the multi-MW target shielding wastes has been proposed. This study has been based on the clearance index concept [2] and the wastes were divided in 3 types. The results show clearly the need of such a study, since 80% of the concrete was declassified (non-active waste), i.e. more than 8000 tons! 17% will have to be sent to an interim storage and finally only 3% (~300 tons) requires disposal as permanent radioactive waste.

For the case of a multi-megawatt target based on mercury, it should be noted firstly that, after solidification, 100 m³ of waste (HgS + concrete) would need to be stored in an underground repository, and secondly, that around 5.5 kg of irradiated ²³⁵U would then be expected, if only highly-enriched uranium (HEU) targets are used, and total amount of waste could be multiplied by a factor of 50 for low-enriched uranium (LEU) targets.

The volume of concrete and soil used as shielding for the proton driver accelerator would be around 5000–7000 m³ and 30000 m³ respectively. For the post-accelerator about one half of these values has to be taken into account.

Cost

A rough estimate of decommissioning costs for EURISOL is possible on basis of benchmarking with related facilities: the SNS at Oak Ridge, Tennessee in the US and the European Spallation Source ESS which is currently in a preparatory phase for construction.

While the high-power target and the accelerator of EURISOL are comparable to the two above-mentioned facilities where decommissioning is concerned, there are major differences in other components (fission targets, post accelerator etc.). However, preliminary cost estimates revealed that the dominant contributor to decommissioning costs (>75 %) will be the mercury target. Based on the SNS facility, the ESS team have estimated decommissioning costs (for a 5-MW facility) of about 395 M€ in 2008 values. Considering the additional targets and the additional post-accelerators in the EURISOL facility, a decommissioning cost of the whole EURISOL system is assumed to be about 20% higher than that of the ESS, leading to a value of some 470 M€

It should be noted that the mercury decommissioning as required for EURISOL, SNS and ESS will most probably leads to substantially higher decommissioning costs than for alternative high-power target systems without mercury, such as the Pb-Bi eutectic target tested at PSI in the MEGAPIE project.

It remains also to be noted that cost estimates for accelerator decommissioning other than those of the SNS and ESS lead to substantial higher values (PSI, GSI, DESY) of up to 50 to 100% of the accelerator construction costs, which for high-power proton drivers amounts to some hundred M€. This difference remains to be examined. For this reason, cost estimate for decommissioning EURISOL should be used with some caution. The contribution of the EURISOL accelerators to the total decommissioning costs should also be regarded as a lower limit.

11.5 Conformity to Legislation

In dealing with a project like EURISOL, a study of the relevant legislation is needed at least for three reasons:

- i) Such a facility has never before been built in Europe.
- ii) With a liquid-metal target one will have to manage conventional and radiological toxicity.
- iii) The site for the EURISOL facility is not yet decided and legislation can vary according to the final host country.

A comparative study concerning six European countries (France, Germany, Italy, Poland, Romania and Switzerland) was carried out and the following subjects were discussed:

- nuclear safety administration;
- nuclear facility classification (criteria of different classifications);
- instruction procedures (most important steps to obtain the authorization of the construction and exploitation);
- limits of exposures and releases;
- safety constraints and quality insurance for the conception and the construction;
- nuclear waste management and decommissioning policy.

Details can be found in a report [3] of the Safety & Radioprotection task on the EURISOL web-site.

The EU safety considerations are based on 3 categories (with probabilities of occurrence in any year):

- Normal operation and frequent abnormal events or “incidents” ($>10^{-2} \text{ y}^{-1}$)
- Design Basis Accidents (DBA) (10^{-2} y^{-1} to $5 \times 10^{-6} \text{ y}^{-1}$)
- Design Extension Accidents (DEA) “hypothetical” events ($<5 \times 10^{-6} \text{ y}^{-1}$).

For normal operation, regulations in all countries are based on the EURATOM directive 96/29. However, some differences exist in radiological dose estimates for DBA and DEA. Concerning conventional toxicity and mercury chemical plants, safety guidelines have to be applied and are different according to the country. In this case an EU directive applies for the toxicity of inactive Hg

(the Seveso-II Directive [4]) but only for a mass above 50 tons, while the EURISOL mercury target mass will be around 15 tons. (Note: Since 2007 regulations in Europe concerning the use of mercury are becoming ever more stringent.)

Finally the licensing/authorization process is not completely established in Europe for such a multi-megawatt target and proposers of possible sites should examine whether detailed legislation exists in their respective candidate countries.

11.6 Risk assessment

One objective of the safety task was to address the risk concept. At this stage of the EURISOL project, i.e. the design study, only qualitative assessments could be done. These qualitative assessments will be the starting point for a next phase, the engineering study, which will carry out the quantitative estimate of risks.

Minimizing potential risks motivates all of the studies described in the previous sections and here is a summary of the main points:

- Code validation: To use the best models and to know their validity.
- Shielding: To prevent radiation, but with optimisation to take into account cost and waste.
- Dose rate: To classify the different areas.
- Cryopump: To simplify maintenance.
- Cryopanel: To avoid radioactivity in the vacuum system, with study of thermal stress.
- Filter: To purify the beam.
- Model/Toolkit: To model dispersion of radioactivity (air and ground water).
- Decommissioning: To estimate costs, means and solutions before building the facility.

However, the Safety & Radioprotection task had to focus on some specific and critical innovative subjects, whereas risks exist in all parts of the facility. For this reason every task leader within EURISOL-DS were asked to fill in a ‘risk register’, in order to identify and rank the risk inherent to the installation, operation, maintenance, dismantling and disposal of each item of the facility and to propose the mitigation methods. The example below illustrates the risks identified for the co-axial flow target vessel of the liquid-metal, multi-MW target station .

EURISOL-DS RISK REGISTER

Equipment			Operational phase and Risk			RP [mSv/h] and intervention		Risk assessment before mitigation			Mitigation of Risk	Risk assessment after mitigation		
Owner	Name and location	Acronym	Action type	Description of failure	Associated risk	Dose rate	Job duration	Prob.	Impact	Score	Comments - Actions needed	Prob.	Impact	Score
T2	CGS target vessel	CGS-TV	Installation	Faulty mechanical connection	Leak of Hg			1	2	2	Helium test before filling loop to ensure leak-proof connection and containment of HG leak by safety hull	1	1	1
				Misalignment of the target against the beam	Window rupture due to beam off centered			1	2	2	Beam Diagnostic device and interlocks	1	1	1
					Vanes rupture due to beam off centered			1	1	1	Instrumentation to control target integrity	1	1	1
			Commissioning	Excessive vibration of target at pump start-up	Breakage and Hg leak			2	3	6	Containment of Hg (safety hull)	2	1	2
				Rupture of the vanes	Flow disturbed and vibration			1	2	2	Instrumentation to control target integrity	1	1	1
					Windows rupture due to impact			1	3	3	Instrumentation to control target integrity	1	1	1
			Pitting by impact				1	3	3	Instrumentation to control target integrity	1	1	1	
			Operation	Rupture of the vanes	Loss of Hg flow, flow blockage and cavitation			2	2	4	Instrumentation to control Hg flowrates	2	1	2
					Explosion by Hg boiling			1	5	5	Containment of Hg (safety hull)	1	1	1
					Overheating of the window			3	3	9	Instrumentation to control Window temperature	3	1	3
				Window rupture	Partial melting of the window			1	5	5	Containment of Hg (safety hull)	1	1	1
					Hg leak			3	5	15	Containment of Hg (safety hull)	3	1	3
				Beam focusing	Hg leak			2	5	10	Containment of Hg (safety hull)	2		
Excessive vibration of the target	Cracks in the shell			2	2	4	Vibration control of the target	2	1	2				

Fig. 11: An example of the risk analysis tabulation: part of the much larger table for the multi-MW target.

For the multi-MW target the main risk concerns the liquid-metal (e.g. mercury) target. An example of failure is shown above with the rupture of the vanes, but we can see that the risk can be mitigated.

Two major risks with the fission target are the breaking of the target container and a target fire. In both cases the main consequence is dissemination of radioactivity. Methods of mitigating the risk for a target fire is proposed.

The main risks for the direct 100-kW targets are associated with the frequent target change – once every 3 weeks – and with beam misalignment. The consequence might be dispersion of radiological contaminants and fire.

Identified risks were taken into account in the design of each component. Further explanations and details are given in an Appendix in the CD.

11.7 Conclusion

The envisaged increase by several orders of magnitude of the radioactive ion beam (RIB) intensity within EURISOL means a drastic increase of the radioactive inventory and corresponding radioprotection related issues. The goal of this task within the Design Study was to provide a quantitative evaluation of the major safety and radioprotection issues. Calculations of the expected levels of radiation production and activation have been performed and have shown that the high-power (4 MW) target station should be considered as a research reactor. Methods for shielding against prompt radiation have been given. The containment of activity was also studied, and both cryotrap and aerosol filter devices were developed and tested with very good results. Methods and software (EDAT) were developed to manage activity transport in soil and groundwater and the dispersion of radioactivity. Decommissioning of the facility, and in particular the disposal of spent targets, was analysed and an innovative strategy were developed. Costs related to decommissioning will be high, and should be taken into careful consideration. Finally, when any site is proposed, one should examine whether detailed legal regulations exists in each candidate country, and whether the proposed facility conforms to such legislation.

From the safety point of view the mercury target is a crucial point. Much work has been done to determine how to manage this liquid-metal target and mitigate the risks. Some solutions have been found for the decommissioning, but the studies must be continued. Nevertheless, other options exist. For a liquid-metal target, a Pb-Bi eutectic can be used. This target needs heating to become liquid, and becomes solid again when the heating is removed, so decommissioning should be easier. In fact, such a target has been irradiated for 4 months in 2006 during the MEGAPIE project at PSI, Villigen, using a 575-MeV proton beam current of around 1 mA. This experiment was successful as regards the neutron flux obtained, and the main problem studied concerning safety was gas production and release. A post-irradiation experiment [5] will provide the nuclides produced in the target and not released. This will indicate what decontamination issues could be encountered for the Pb-Bi eutectic target.

Thus, while a mercury target is quite promising, a Pb-Bi target remains an interesting alternative.

References

1. “Yields for double-stage targets”, EURISOL Design Study technical note: [11-25-2009-0022](#).
2. IAEA Safety Guide SS - N°11-G1 (1994).
3. “Conformity to legislation”, EURISL Design Study technical note: [05-25-2008-0026](#).
4. Seveso-II Directive: “European Council Directive 96/82/EC on the control of major-accident hazards”, 9 December 1996 and the amendment: [Directive 2003/105/EC of the European Parliament and of the Council of 16 December 2003](#).
5. L. Zanini, J-C. David, A.Y. Konobeyev, S. Panebianco and N. Thiollière, “Neutronic and Nuclear Post-Test Analysis of MEGAPIE”, PSI Bericht Nr. 08-04, December 2008, ISSN 1019-0643.

Chapter 12: Layout of the Facility

In planning the possible layout of the EURISOL facility, we have to bear in mind that the final layout will depend very much on the chosen site, its size, shape and contours. However, without these constraints, which are not known at present, we have planned the facility to be as functional as possible. The major components which must be incorporated are the following:

- an injector building for the driver accelerator, with ion sources for protons, deuterons and ^3He ions,
- the driver accelerator building or tunnel,
- a power-supply building alongside the length of the driver accelerator,
- a building to hold the cryogenic plant (liquid-helium and liquid nitrogen supplies),
- beamlines to the ISOL target stations, incorporating several beam-splitting devices,
- a multi-MW target station and its target-handling facilities,
- six fission-target stations, with target-handling facilities,
- three 100-kW target stations, with RIB ion sources and target-handling facilities,
- a beam-preparation area, equipped with
 - ◆ a beam-merging station for 6 RIB beamlines from the fission targets,
 - ◆ high-resolution mass-spectrometer(s),
 - ◆ beam coolers,
 - ◆ EBIS and ECRIS charge breeders,
 - ◆ beam switchyards;
- a low-energy experimental area equipped with traps, etc.,
- an astrophysics area with its own very low-energy post-accelerator,
- a low-energy post-accelerator,
- a high-energy post-accelerator, with intermediate-energy tapping-off beamlines,
- experimental areas fed by both the low- and medium-energy beamlines,
- a large fragment separator,
- high-energy experimental areas.

In addition, there should of course be ancillary buildings, such as a control room, data-acquisition rooms, offices and laboratories, workshops, air-handling system and nuclear ventilation systems, pump-rooms, cooling towers, electricity supply lines and a transformer yard, etc. (figures 1–4).

We have attempted to design a facility which incorporates all the above items. It was decided that the driver accelerator should be underground, since this means that earth shielding can be used instead of metres of concrete. Such a tunnel could have a circular cross-section, if it is a bored tunnel, or a square cross-section if it is a so-called “cut-and-cover” tunnel (see figure 3). In many respects the EURISOL facility would resemble the SNS in Oak Ridge, Tennessee, which has a similar driver accelerator. We note that the injector end of the SNS driver tunnel is located at ground level, by exploiting a natural change in the ground level, making access to the driver-accelerator tunnel easier.

The 1-GeV proton beam from the EURISOL driver is split, using small-angle deviations, into at least 4 beamlines, one leading to the multi-MW target station, and the others to three 100-kW target stations (figure 5 & 6). Each of these will require a large amount of concrete shielding around it, and is also placed below ground to reduce the volume of concrete needed.

Above each 100-kW target station will be a target-handling level, and operator areas, as well as a pre-separator magnet, to remove unwanted ions from the RIBs produced. From each pre-separator, the RIB will ascend into the beam-preparation area for further purification and treatment.

The multi-MW liquid-metal target must be provided with a maintenance bay into which it can be retracted and serviced, using remote-handling equipment. This maintenance bay will be of similar size to that at the SNS or at JPARC.

Six fission targets will be arranged above or alongside the multi-MW liquid-metal spallation-neutron target. These targets and their associated ion sources have to be lifted out of the 6-metre concrete shielding above the multi-MW target, and thus require a high-bay handling room equipped with a special crane and remote-handling equipment, and provision has to be made for mounting and dismounting the target/ion-sources, and for handling and storage of these highly radioactive components. The fission-target handling building is thus located above the level of the liquid-metal target and its maintenance bay.

The fission targets will each be equipped with a laser-ioniser system, so that a laser laboratory will be located adjacent to the target-handling area. The RIBs from the 6 fission targets must then be merged together into one beam in a specially-designed ECR ion source, the ARC-ECRIS. This high-intensity beam must then be purified in a high-resolution mass-separator. Since the beam energy is low, the mass-separator is relatively small, and we therefore propose to provide a second one for use with the 100-kW beams. Operation of the 100-kW station is envisaged to have only one beam in use at any one time, while another target station is cooling down and the third target/ion-source assembly is being prepared for the next beam required by the users. However, two 100-kW target stations could indeed be used simultaneously during maintenance periods of the multi-MW target, for example.

Ion-beam coolers and both ECR and EBIS charge-breeders are also envisaged, together with several switchyards which enable beams from any two of the target stations to be directed to any of the user areas or post-accelerators (figures 7 & 8). Thus two independent RIBs can be in use at any one time.

Although a number of instruments have been selected for possible use in the future EURISOL facility, we have not attempted to show them in the various experimental areas, as the requirements will undoubtedly change in future. (See figures 9 & 10.)

Various views of the 3-dimensional layout drawings are presented below. The relative orientation of the driver and post-accelerator linacs is not absolute, and will depend on the chosen site. We have not folded the 240-m driver linac in half to reduce the space required, but this remains a possible option, depending on site limitations. Note that the thickness of shielding walls is not accurately represented around the accelerators or experimental areas, and will also depend on local conditions such as soil composition, water-table level, etc. Shielding roof-beams have also been omitted from these areas, for clarity.

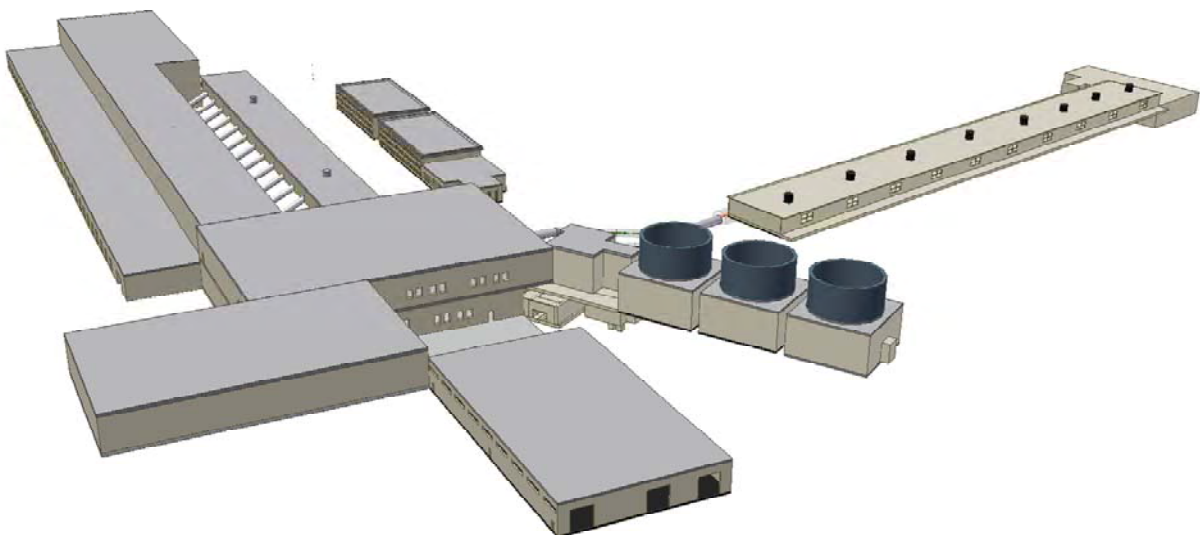


Fig. 1: A general view of the facility, with the driver accelerator at right, target areas in the centre, and the post-accelerators and experimental areas on the left. The accelerators and target rooms are below ground level to reduce the amount of concrete shielding needed.



Fig. 2: Proposed layout on a “green-field” site. The driver accelerator (240 m long) is located beneath the red discs.

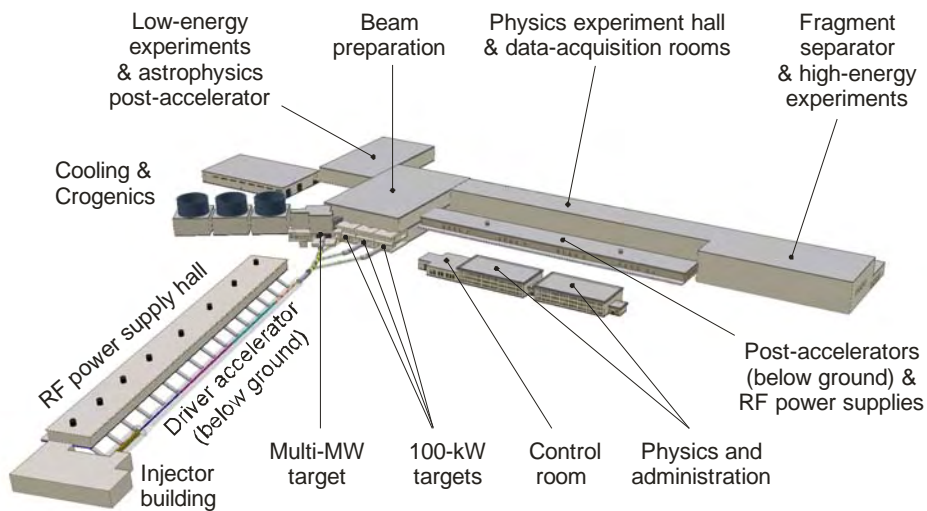


Fig. 3: Key to the figure above.

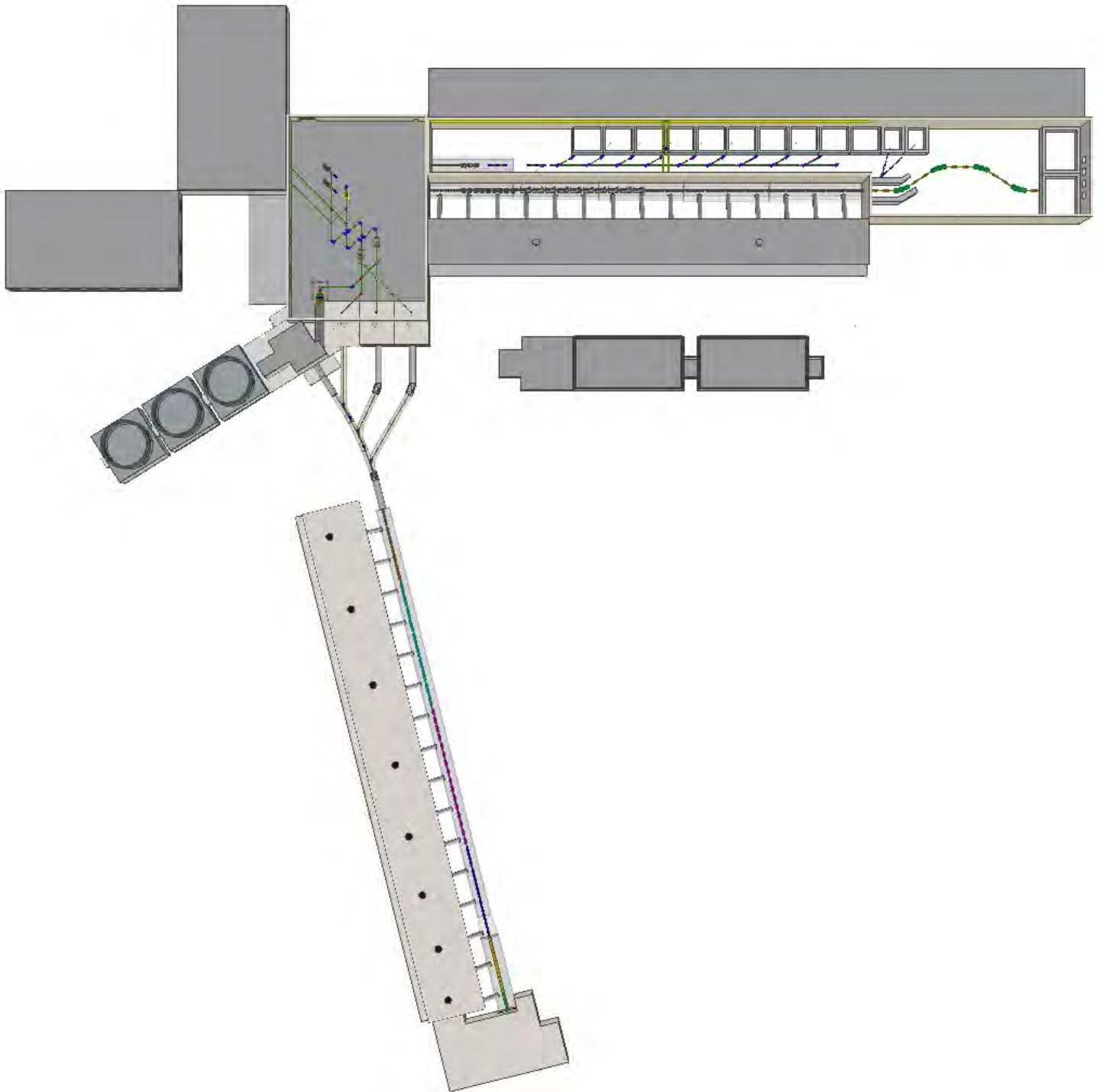


Fig. 4: Plan view, showing interior detail of drive accelerator (bottom), beam preparation area (top left), post-accelerators and experimental areas (top right). The driver is 240m long and the post-accelerator linac is 207 m long.

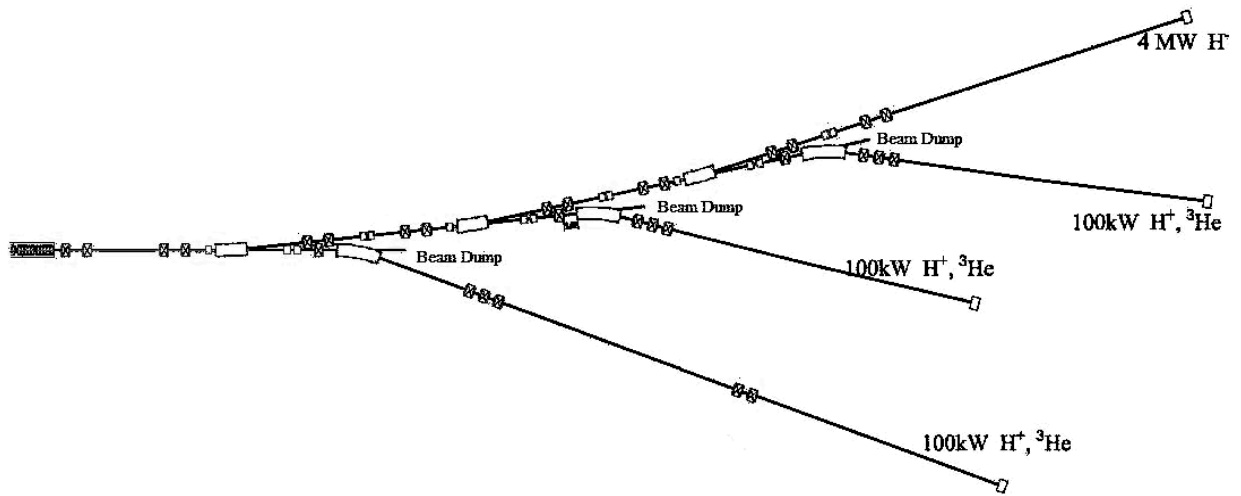


Fig. 5: Layout of the system proposed for splitting the driver beam (from the left) into three 100-kW beams and one 4-MW beam. The fraction of each deviated beam is smoothly variable from zero upwards.

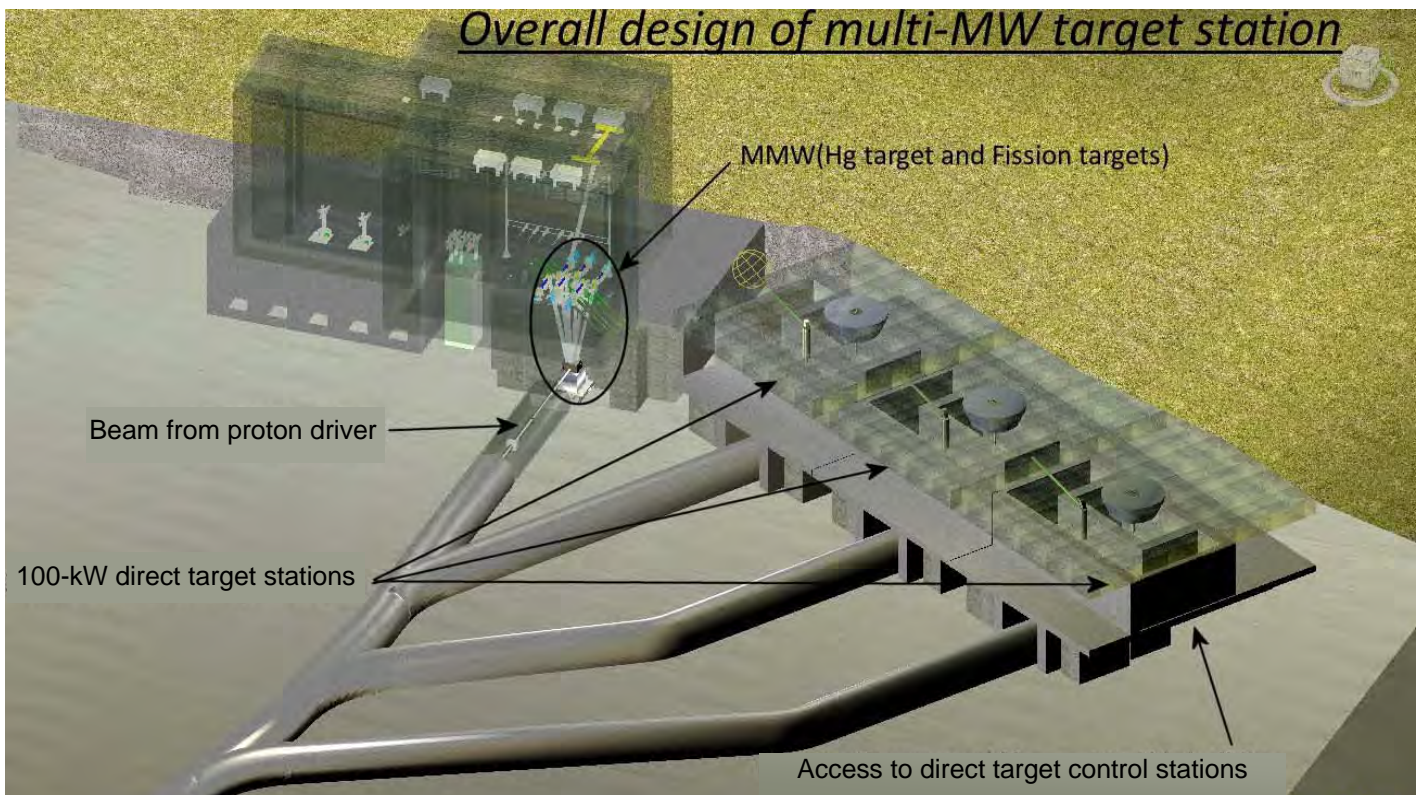


Fig. 6: Drawing showing the multi-MW target area and three 100-kW target vaults.

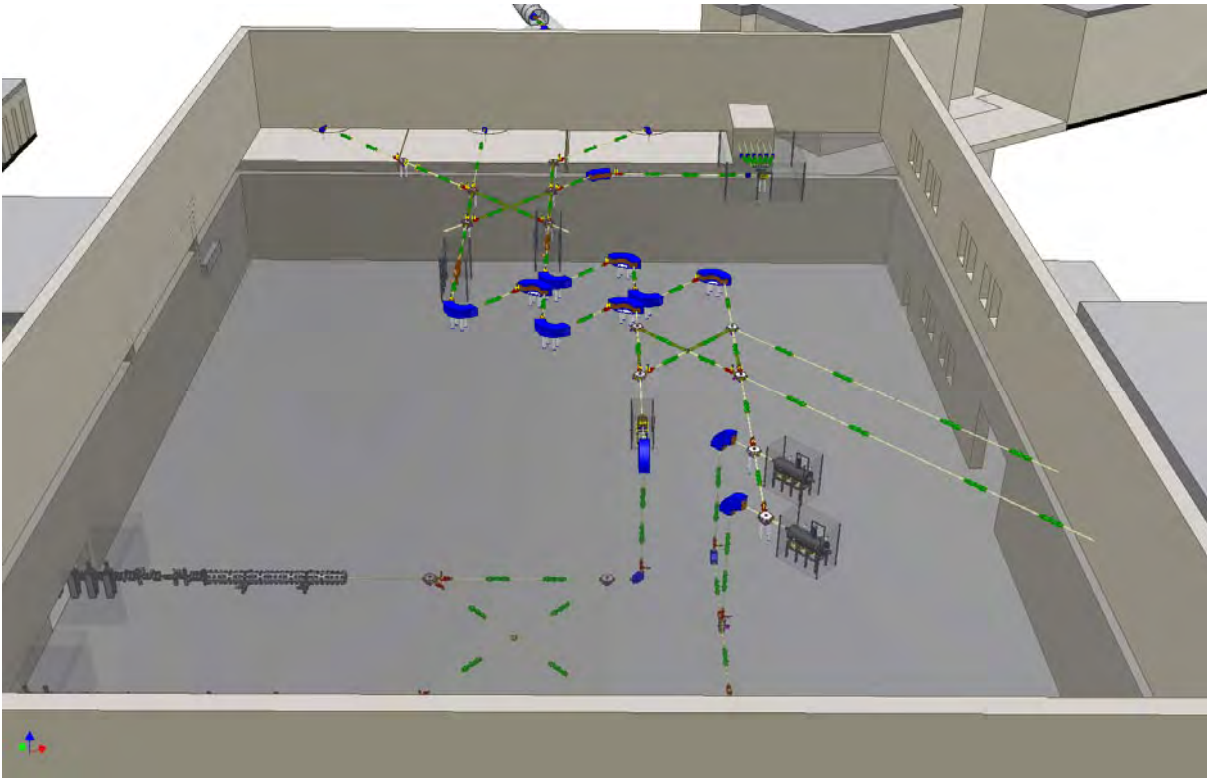


Fig. 7: Beam preparation area: this is on two levels, with beams entering (in upper part of picture) from the target/ion-source units below, and finally descending to the post-accelerators below ground level. The floor of the upper level is shown here as semi-transparent.

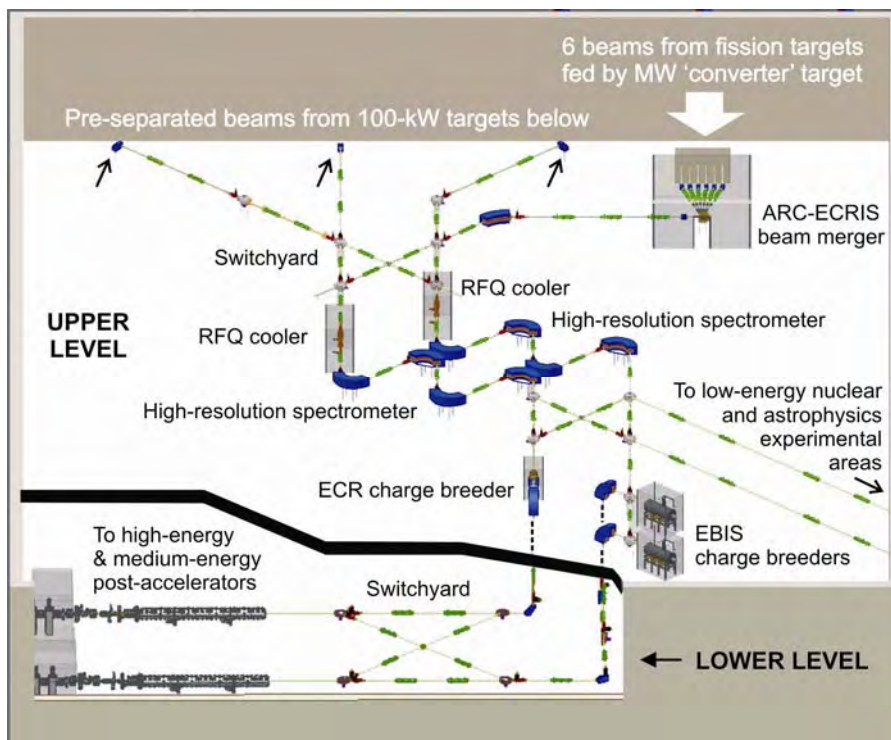


Fig. 8: Key to the figure above.

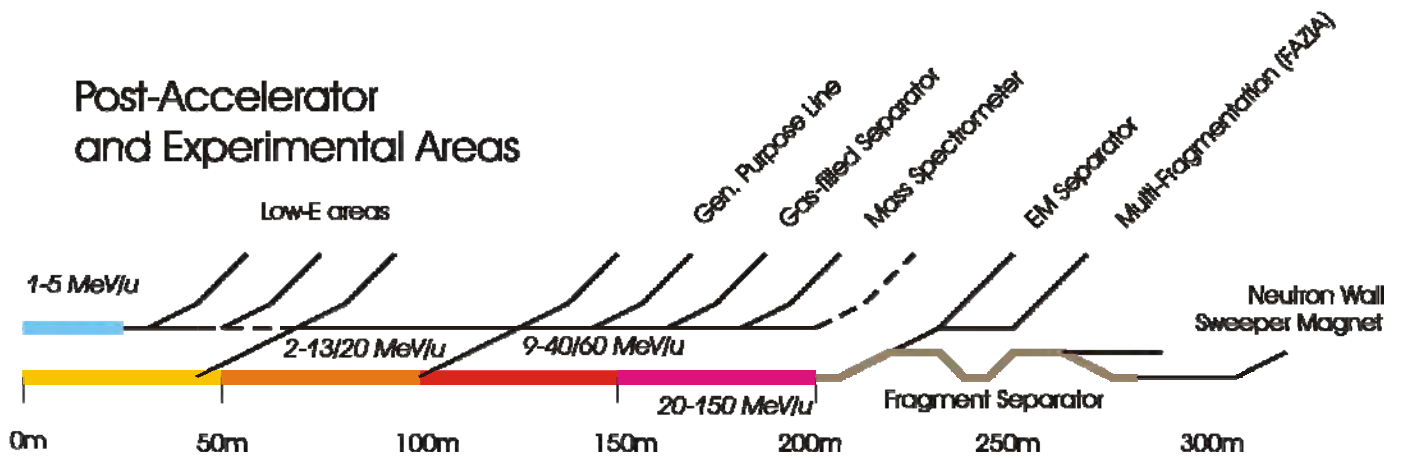


Fig. 9: Schematic layout of beamlines from the proposed two post-accelerators (at left). The various energy regimes covered by the RIBs are indicated.

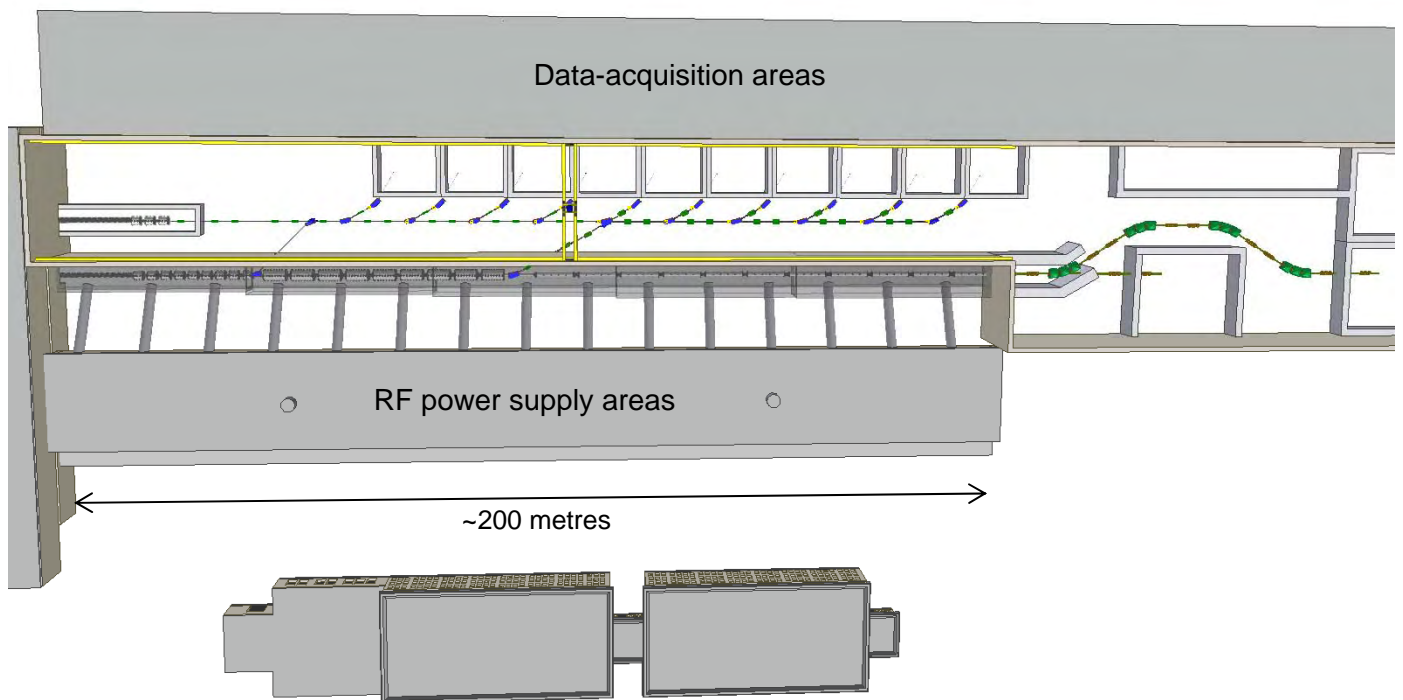


Fig. 10: A possible layout of the experimental areas meeting the physics user requirements. The low-energy post-accelerator (centre left) is a clone of the first section of the main post-accelerator, but allows coulomb-barrier experiments to continue for long periods without monopolising the high-energy post-accelerator (centre). Instruments for physics are not shown, and are not included in the cost of the facility. The fragment separator shown here is only a generic schematic representation.

Chapter 13: The Site Investigation Panel Report

13.1 Introduction

Included in the EURISOL Design Study is the requirement for some preliminary consideration to be given to the siting of the facility in Europe. At present these considerations can be only of a very general nature, but should nevertheless provide a basis to encourage the community to formulate the final site selection process. The Management Board of the Design Study set up a Site Investigation Panel, tasked with looking at general site issues and compiling a report [1].

Membership of the panel comprised the following people: Giacomo Cuttone (INFN-LNS, Italy), Don Geesaman (Argonne, USA), Alex Mueller (IN2P3, France), Steve Myers (CERN, Switzerland) under the chairmanship of Alan Shotter (TRIUMF, Canada and Edinburgh, UK).

There are three generic types of sites that could host EURISOL: existing international accelerator-based laboratories, national accelerator-based laboratories, and green-field sites. An important task for the panel was to select a subset of present European laboratories – purely as examples – and to consider in a very general way how they currently satisfy or could in the future satisfy the general criteria for siting EURISOL.

The conclusion of the panel was that some of the laboratories chosen as examples currently satisfy the vital criteria better than others, but all, given time, resources and commitment, could host EURISOL. By necessity the investigative scope of the panel was limited, but nevertheless the panel takes the view that there are other possibilities in addition to the examples investigated – including green field sites – that successfully could host EURISOL.

It is worth repeating that the sites studied are EXAMPLES ONLY, and do not reflect any pre-selection of possible sites.

We quote from the Site Investigation Panel's report in the following sections:

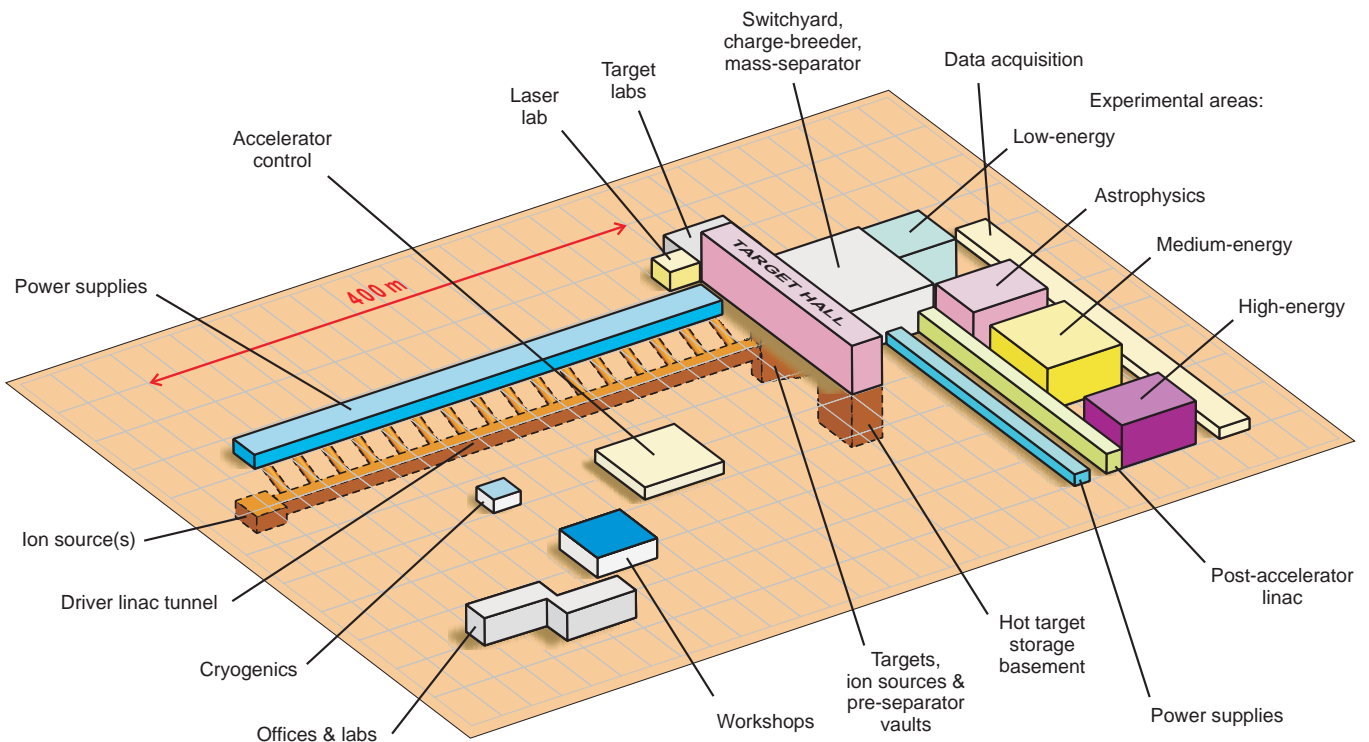


Fig. 1: Schematic layout of the EURISOL facility used in assessing examples of sites.

13.2 Types of sites

The panel considered three types of generic sites that could host EURISOL. Each type will have a different foundation from which EURISOL could evolve, which will also influence the overall cost of EURISOL. The type of site could also influence the extent to which EURISOL becomes a facility with an extensive pan-European involvement in establishing financing and exploitation.

(a) An international accelerator-based laboratory

Within Europe there are laboratories with accelerator facilities that serve a wide scientific user base. There are laboratories providing high energy beams for particle physics, laboratories providing intense neutron beams, and laboratories providing synchrotron radiation beams. Some of these laboratories are governed by international treaties. The staffs that run these accelerator facilities will have considerable experience in accelerator technologies, and in some cases experience of using high-powered targets. Depending on the land availability, and the international will, siting EURISOL at one of these international laboratories is a distinct possibility.

(b) A national accelerator-based laboratory

If a country has a national laboratory which has major acceleration facilities, then such a laboratory could be a potential site for EURISOL, provided it meets the requirements listed the report, such as sufficient additional land which could accommodate this new facility. Such a laboratory would be expected to have staff already experienced in running accelerator facilities, dealing with national nuclear facility regulations, and interacting with users. Such a laboratory currently may or may not provide facilities for nuclear physics users.

(c) A “green-field” site

In this scenario the site would be tailor-made to meet the requirements of EURISOL. All the criteria set out in the panel’s report would have to be considered in some depth for this type of site. In addition, considerations of transport would need to be undertaken, both for the construction stage and the operation stage for users accessing the site. A local airport, or rapid rail service linking to a major airport, would be an essential requirement. This type of site could be located in a European area that has no large multinational facilities; such a siting could be a boost to the local economy and provide a technical infrastructure to drive forward the development of a local high-tech industry. Such a scenario could attract targeted EU funding. A potential advantage is that from the outset all contributing partners would be considered on equal basis since a common fund would have to be set up to establish the infrastructure as well as building and operating the facility. The downside of this type of site is that it probably would be the most expensive since there will be no established infrastructure or manpower.

13.3 Examples of possible sites

The Management Board requested the panel to consider examples of different generic site types, to help identify the issues involved in a site selection, specifically identifying CERN(Switzerland/France), GANIL(France), LNL (Italy), Rutherford Appleton Laboratory (United Kingdom) and a generic green field site as examples. To this end, the panel constructed a brief questionnaire which was sent to the Directors of various ‘example’ laboratories with the aim of establishing the potential viability of constructing EURISOL on such a laboratory site. The panel made clear to the Directors that responding to the questionnaire in no way implied any future commitment. An overview of the comparison of each of these facilities with the criteria indentified in the report is included in the report.

The primary conclusion is that Europe has several sites that are extremely well-suited for hosting EURISOL and have a great deal of existing value in facilities, equipment, expertise and experience. CERN and GANIL appear to meet all the criteria put forward at present. Significant additions at LNL, and a clear commitment by the Rutherford Appleton Laboratory management would likely bring these candidate sites to a similar level. With appropriate partnering scenarios, a new green-field site could also make EURISOL a success, though likely to be at a cost of a longer time-scale to operation, a greater overall price tag and higher project risk than one of the more established examples.

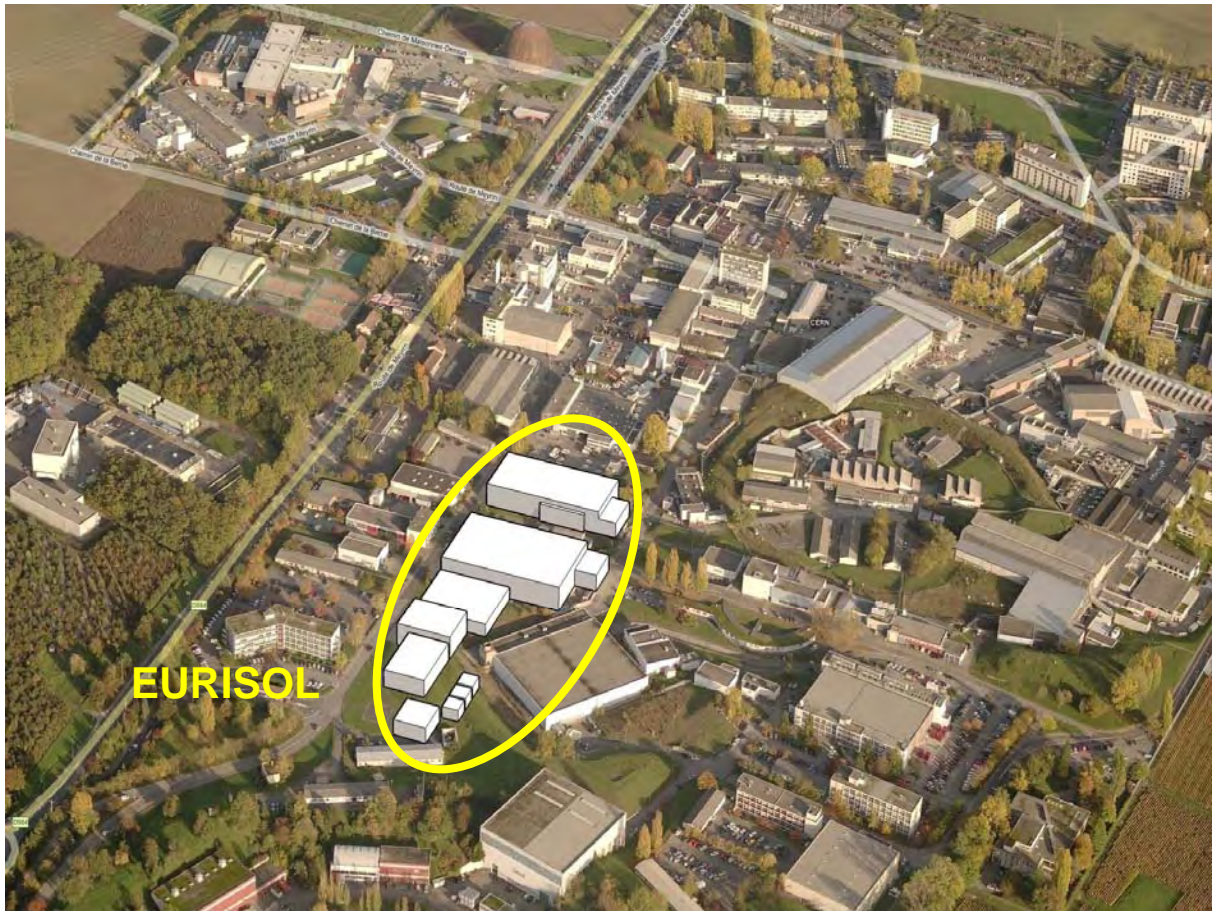


Fig. 2: Possible location of EURISOL at CERN.

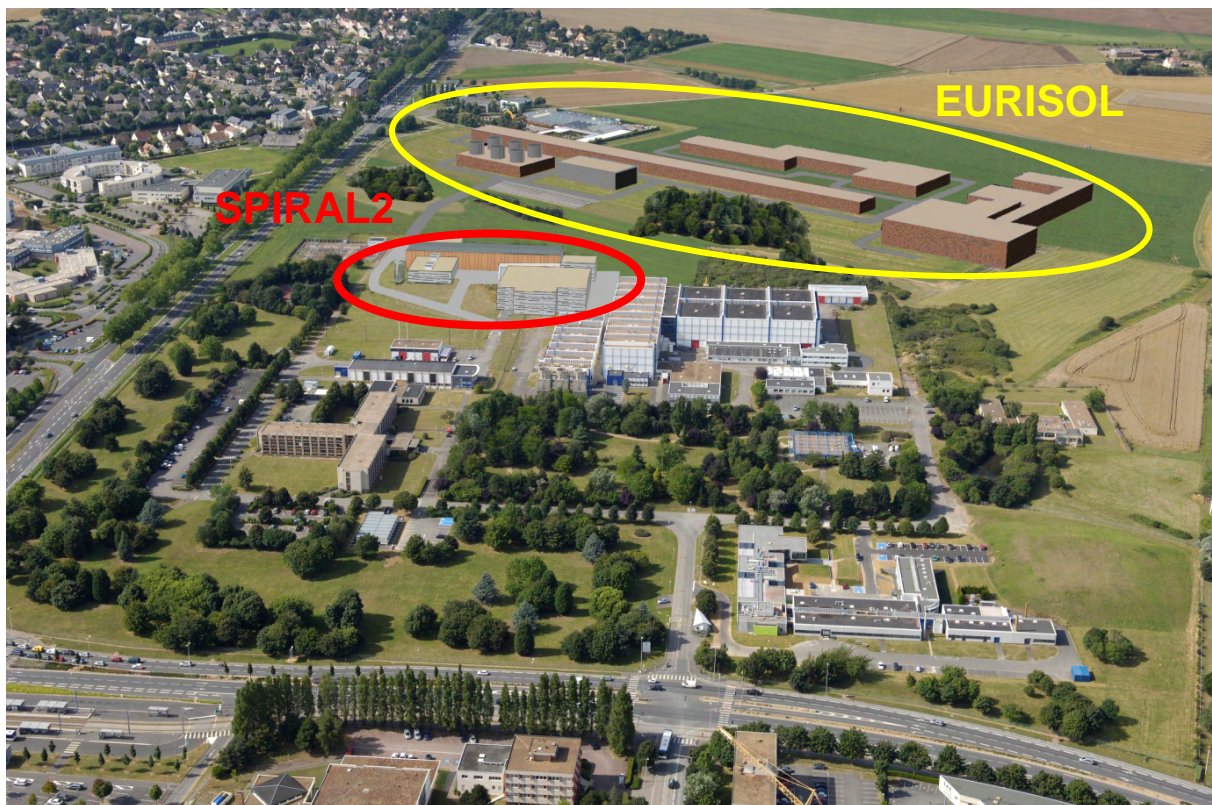


Fig. 3: Possible location of EURISOL at GANIL.



Fig. 4: Possible location of EURISOL at LNL, Legnaro.

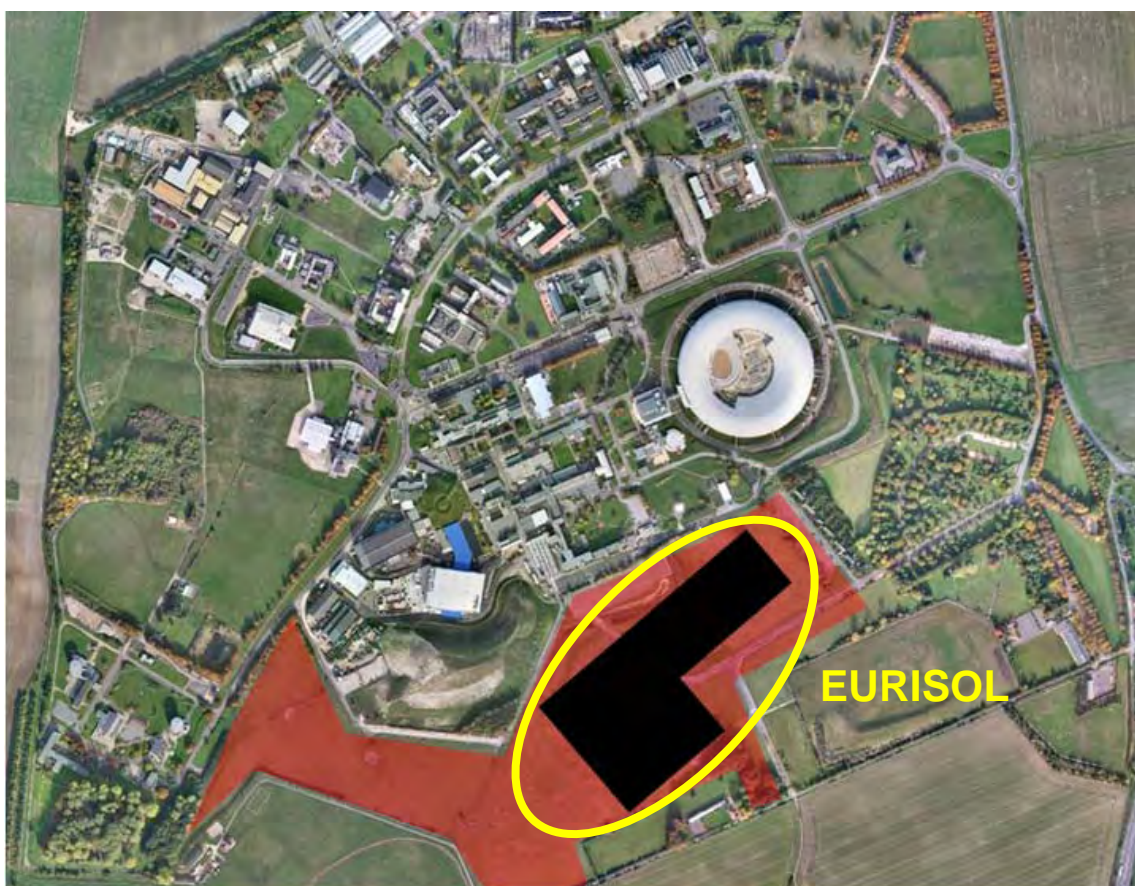


Fig. 5: Possible location of EURISOL at the Rutherford Appleton Laboratory.



Fig. 6: Possible layout of EURISOL on a “green-field” site.

We must emphasise once again that the sites discussed and pictured above are EXAMPLES ONLY, and there is no intention to imply that they are all candidate sites, nor that they would be the only sites considered in future for siting of the proposed EURISOL facility.

Reference

1. G. Cuttone et al., “*EURISOL Site Investigation Panel Report*”, EURISOL DS technical report: 01-25-2009-0013.

Chapter 14: Beta-Beam Aspects

15.1 Introduction

The beta-beam project is a concept of large-scale facility that aims at providing pure electronic neutrino and antineutrino beams for the measurement of $\nu_e \rightarrow \nu_\mu$ oscillations, with unprecedented sensitivity for detection of the θ_{13} mixing angle and CP-violating phase. In the scenario presented in different publications [1–3], a beta-beam facility could be advantageously placed at CERN making use of the PS and SPS for accelerating the beta-decaying, neutrino-emitting beams to a Lorentz gamma value of 100. Intense beams of ${}^6\text{He}$ and ${}^{18}\text{Ne}$ would be produced using the so-called “isotope-separation-on-line” (ISOL) method in a facility of the scale of EURISOL. The synergy between the two projects was pointed out in reference [4]. The beta-beam task of the EURISOL Design Study has aimed at producing a conceptual design report for the accelerator chain of a EURISOL/CERN-baseline beta-beam facility (figure 1). This document summarizes the achievements made during the time of the Design Study. This task was led by CERN.

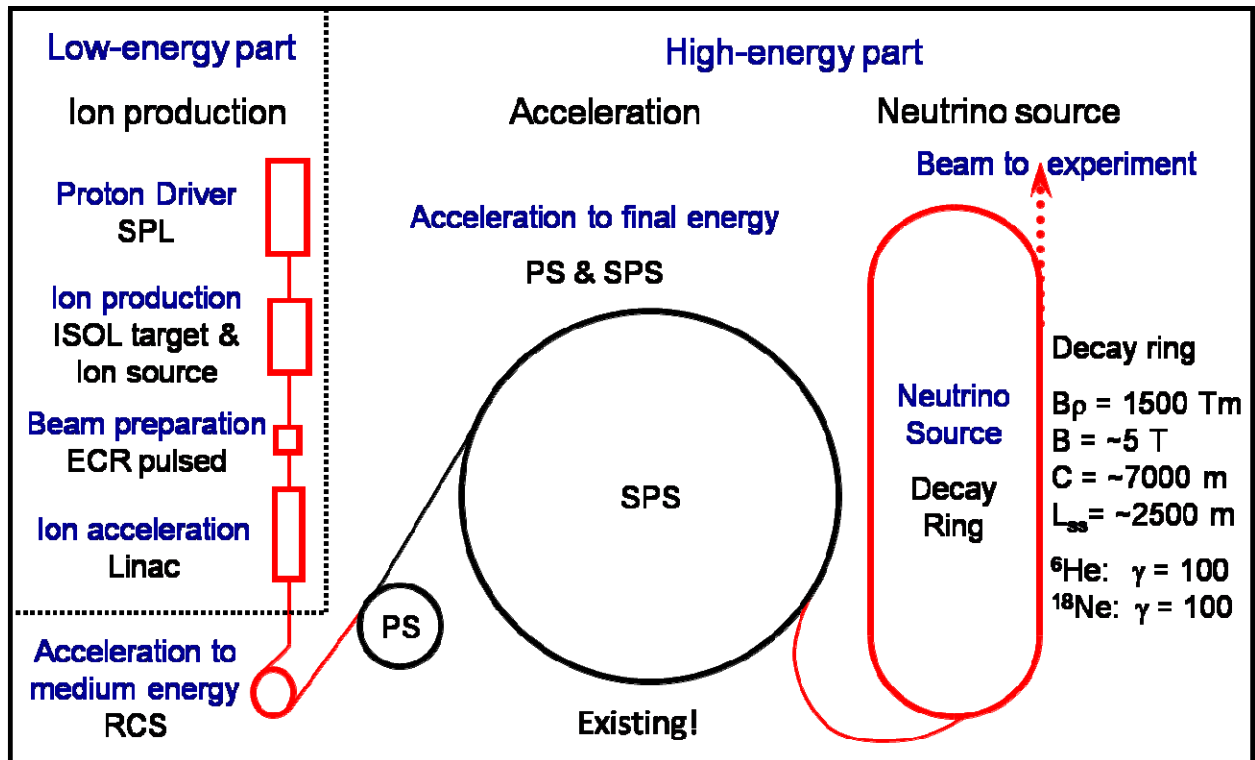


Fig.1: Overview of the CERN baseline beta-beam facility. SPL = superconducting proton linac, PS = proton synchrotron, SPS = superconducting proton synchrotron, RCS = rapid-cycling synchrotron.

Comments on the ${}^6\text{He}$ and ${}^{18}\text{Ne}$ production and ionization method

For an optimal sensitivity of the beta-beam facility to the θ_{13} angle and CP-violating phase, a total throughput of 1.1×10^{19} neutrinos and 2.9×10^{19} antineutrinos was generally assumed over a running period of 10 years. In turn, a top-down approach results in the need for production of about 3.3×10^{13} radioactive ${}^6\text{He}$ atoms and 2.1×10^{13} ${}^{18}\text{Ne}$ atoms per second, with efficiencies along the accelerator chain as quoted in the next section. While the ${}^6\text{He}$ production rate appeared to be possible from a fairly standard 200-kW EURISOL target [5], the ${}^{18}\text{Ne}$ production was found to be more problematic. A team at the cyclotron laboratory in Louvain-la-Neuve have conducted some promising tests for using the reaction ${}^{16}\text{O}({}^3\text{He}, n){}^{18}\text{Ne}$ on large oxide targets. The production rates do not seem out of reach, and the envisaged production methods are briefly summarized in table 1.

Table 1: Envisaged production methods for ${}^6\text{He}$ and ${}^{18}\text{Ne}$.

Isotope	Primary beam and target	Reaction	Yields
${}^6\text{He}$	2-GeV (200-kW) p on a neutron converter surrounding a BeO target [5]	${}^9\text{Be}(n,\alpha){}^6\text{He}$	$2\times 10^{13}/\text{s}$
${}^{18}\text{Ne}$	60-cm diameter MgO target, 2-MW ${}^3\text{He}$ beam (14.8 MeV, 130 mA)	${}^{16}\text{O}({}^3\text{He},n){}^{18}\text{Ne}$	$10^{13}/\text{s}$

A 60-GHz ECRIS is under study for the multi-ionization and bunching of the ${}^6\text{He}$ and ${}^{18}\text{Ne}$ ions into 10-Hz, 50- μs pulses. A first design was done within the EURISOL ‘Beam Preparation’ task, and a prototype should be built and tested at LPSC Grenoble within the 7th Framework Programme [6]. Alternative neutrino emitters, viz. ${}^8\text{B}$ and ${}^8\text{Li}$, have been proposed that could possibly be produced in copious amounts using the concept of an ionization cooling ring [7].

Comments on the post-accelerating linac

It was originally believed that the design of the EURISOL post-accelerator could be replicated for the injector into the rapid-cycling synchrotron of the beta-beam facility. It turned out in the middle of the study that the superconducting linac of EURISOL would not be suited to the post-acceleration of the intense pulses of ${}^6\text{He}$ and ${}^{18}\text{Ne}$. For this reason, a separate study was done by IAP Frankfurt for delivering specifications of a normal-conducting linac that would fulfil the beta-beam requirements. The results of this study are shown in reference [8].

Comments on the possibility of using an accumulation ring

The possibility of using an accumulation ring using electron cooling between the linac and the RCS was studied as an option by the Manne-Siegbahn Lab, and a cost estimate was made [8].

15.2 The beta-beam database

The flux out of the beta-beam facility [12] is determined by the number of ions that can be produced, by the number remaining after acceleration and by the total accumulated in the decay ring. A ‘‘bottom-up’’ analysis of the ion intensities along the accelerator chain and of the neutrino and antineutrino flux out of the decay ring was realized by CERN, starting with the rate at which atoms are transported out of the target. We recall here the main arguments which were used in the compilation of the database. A full description of the beta-beam project can be found in references [1] and [3]. Figure 1 represents the beta-beam facility as described in these articles. The original version of the database [8] was revised a first time to take into account more recent simulations of the stacking of ${}^{18}\text{Ne}$ ions in the decay ring and beneficial trends [10] in output flux as functions of certain machine parameters. In the course of the study, the RCS ejection energy was upgraded to overcome potential space charge difficulties, which resulted in a second update of the database [11].

Production

In the beta-beam baseline design it is assumed that we can produce and transport 2×10^{13} ${}^6\text{He}$ atoms/s and 8×10^{11} ${}^{18}\text{Ne}$ atoms/s out of the target, with a proton driver beam current of 100 μA impinging on the target at 2.2 GeV. These numbers are based on an evaluation of suitable isotopes and their production rates at ISOL facilities and have been presented as part of the beta-beam contribution to NuFact02. The full write-up of this presentation could not be published as part of the proceedings, but it exists as a CERN internal note [1].

ECR source

Efficient bunching and stripping of the high-intensity beam are achieved using a high-frequency ECR source [13]. We assume the efficiency of such a source to be 100% for ${}^6\text{He}$, with all ions being extracted in the 2+ charge state, but only 30% for ${}^{18}\text{Ne}$ ions due to only one of several charge states (i.e. 6+) being extracted. We further assume that the ECR operates at 10 Hz with an accumulation time of 97.5 ms, that the source is at a potential of 50 kV relative to the linac, and that the ions are ejected in 50 μs long bunches with a physical transverse emittance of about 50π mm.mrad.

Linac and rapid-cycling synchrotron

The linac accelerates the ions to 100 MeV/nucleon, after which they are multi-turn injected into a rapid-cycling synchrotron (RCS). We assume an injection efficiency of 50%. Both ion species are accelerated to a magnetic rigidity of 14.47 T·m in a time dictated by the 10 Hz repetition rate of the ECR source. Each cycle provides a single bunch.

PS and SPS acceleration to high energy

The PS waits for 20 shots from the RCS then accelerates the 20 bunches to reach a magnetic rigidity of 86.7 T·m. Then they are transferred to the SPS and accelerated to $\gamma=100$ and ejected off-momentum into the decay ring for stacking. The cycle time of the SPS is a multiple of the 1.2-s basic period of the CERN machines. The extra acceleration required for the ${}^6\text{He}$ results in a 6-s cycle, compared with only 3.6 s for ${}^{18}\text{Ne}$.

Decay ring

The 20 incoming bunches are combined with the 20 circulating ones of the stack by an asymmetric merging process in the decay ring (see later decay ring section). The number of times this process can be repeated is constrained by the 1 eV·s longitudinal emittance of each bunch delivered by the SPS. Simulations for ${}^6\text{He}$ show that such bunches can be stacked up to 15 times. At any given relativistic γ -value, the aperture of the decay ring defines a longitudinal acceptance limit, which scales with ion momentum. Consequently, the more advantageous charge-to-mass ratio of ${}^{18}\text{Ne}$ ions should allow the number of merging steps needed to fill the decay ring to be increased by something approaching a factor of 3 with respect to the stacking procedure established for ${}^6\text{He}$ involving 15 merges. However, the sensitivity of the process to phase errors between the two rf components employed in the merging puts an upper limit of about 20 on the number of merges that can realistically be achieved. We therefore assume that the extra acceptance available for ${}^{18}\text{Ne}$ in the upstream PS and SPS is exploited to stabilize the beam and consider 2 eV·s per bunch (cf. 1 eV·s for ${}^6\text{He}$) injected into the decay ring, giving 40 eV·s in the stack.

The resultant relative momentum spread of the stack is $\pm 2.5 \times 10^{-3}$ at the start of merging for both ion species and, applying the full 20+20 MV of the 40+80-MHz rf systems in the decay ring, the duration of each bunch is 5.2 and 4.5 ns for ${}^6\text{He}$ and ${}^{18}\text{Ne}$, respectively. The annual integrated flux of potentially useful neutrinos and antineutrinos emanating from the decay ring is linearly dependent on the relative length of the straight section that points towards the detector. This is taken to be 36% of the decay ring circumference [14].

Transverse emittance and tune shift

The transverse emittance and tune shift evaluations were reported in references [10] and [11].

Results

The up-to-date parameters given in reference [11] result in the numbers of ions listed in table 2 at each stage of the CERN beta-beam facility. The decay losses are properly accounted for, but the transfer efficiencies between the different machines are assumed to be 100% except for the multi-turn injection into the RCS. The source rate is given (in atoms/s) at the entrance to the ECR, while the decay ring figure is the maximum number of stored ions immediately after injection from the SPS.

Table 2: Ion intensities in the EURISOL baseline scenario.

Position	${}^6\text{He}$	${}^{18}\text{Ne}$
RCS injected	8.5×10^{11}	2.6×10^{11}
PS injected	1.7×10^{13}	5.2×10^{12}
PS accumulated	1.1×10^{13}	4.5×10^{12}
SPS injected	9.5×10^{12}	4.3×10^{12}
Decay injected	1.8×10^{14}	8.5×10^{13}
Decay accumulated	9.7×10^{13}	7.4×10^{13}

15.3 Design of low energy ring(s): the rapid-cycling synchrotron

The RCS is described in detail in [15] (IPNO, CNRS/IN2P3). Its preliminary design was presented in reference [16]. We recall here the main elements of its conceptual design report. A dedicated radioprotection study was performed at CERN, showing no ‘showstopper’ for the RCS. It is reported in reference [8] together with dynamic vacuum studies performed by GSI.

RCS general parameters

The RCS accelerates He and Ne ion beams from 100 MeV/u to a maximum magnetic rigidity of 14.47 T·m (i.e. the rigidity of 3.5-GeV protons) with a repetition rate of 10 Hz. The threefold symmetry lattice proposed is based on FODO cells with missing magnets providing three achromatic arcs and three sufficiently long straight sections for accommodating the injection system, the high energy fast extraction system and the accelerating cavities. Relative to the first design, the number of dipoles has been increased to obtain a transition energy allowing acceleration of protons up to 3.5 GeV. These dipoles have been split into two parts separated by a drift space for inserting absorbers to intercept the decay products. Finally, the physical radius has been adjusted to 40 m in order to facilitate the synchronization between the CERN PS and the RCS and therefore the transfer of bunches from one ring to the other. As a consequence, the ring is composed of 60 short dipoles and 48 quadrupoles. A schematic view of the RCS layout is shown in figure 2 and the main parameters are summarized in table 3.

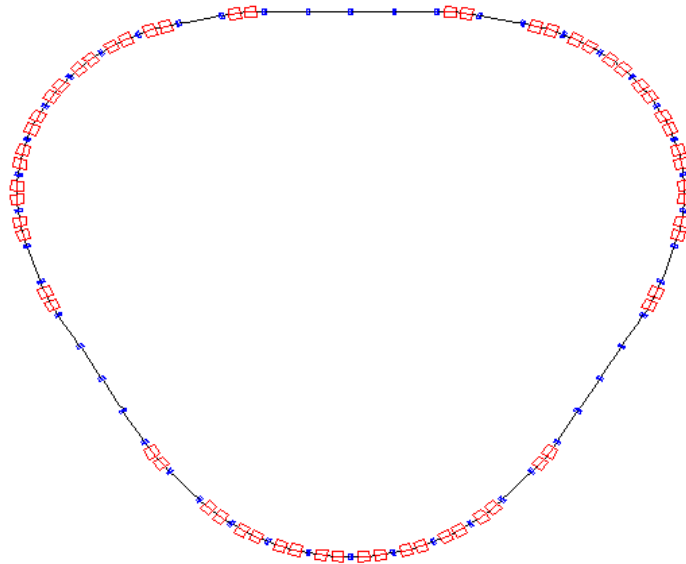


Fig. 2: Schematic layout of the RCS.

Table 3: Main parameters of the ring.

Circumference	251.32 m
Superperiodicity	3
Physical radius	40 m
Injection energy	100 MeV/u
Maximum magnetic rigidity	14.47 T.m
Repetition rate	10 Hz
Number of dipoles	60
Number of quadrupoles	48

Optical design

The RCS is partitioned into 24 FODO cells, 6 in arcs and 2 in a straight section. The betatron phase advance per cell (i.e. quadrupole strength) and the length of the 2 sections without dipoles in the arcs have been adjusted so as to cancel the dispersion function in long straight sections and to obtain, with only two quadrupoles families, a working point located in a region of the tune diagram which is free of systematic resonances up to the fourth order. The lattice functions of one period calculated with BETA [18] are shown in figure 3. Dipoles are only 1.4 m long in order to obtain a maximum magnetic field of 1.08 T and therefore to avoid a large ramping rate for the 10-Hz operation. Quadrupoles have a length of 0.4 m and a maximum gradient of less than 11 T/m. The diluted transverse emittances in the RCS after multi-turn injection are calculated from the emittances required in the PS at the transfer energy with a possible blow-up of 20 %

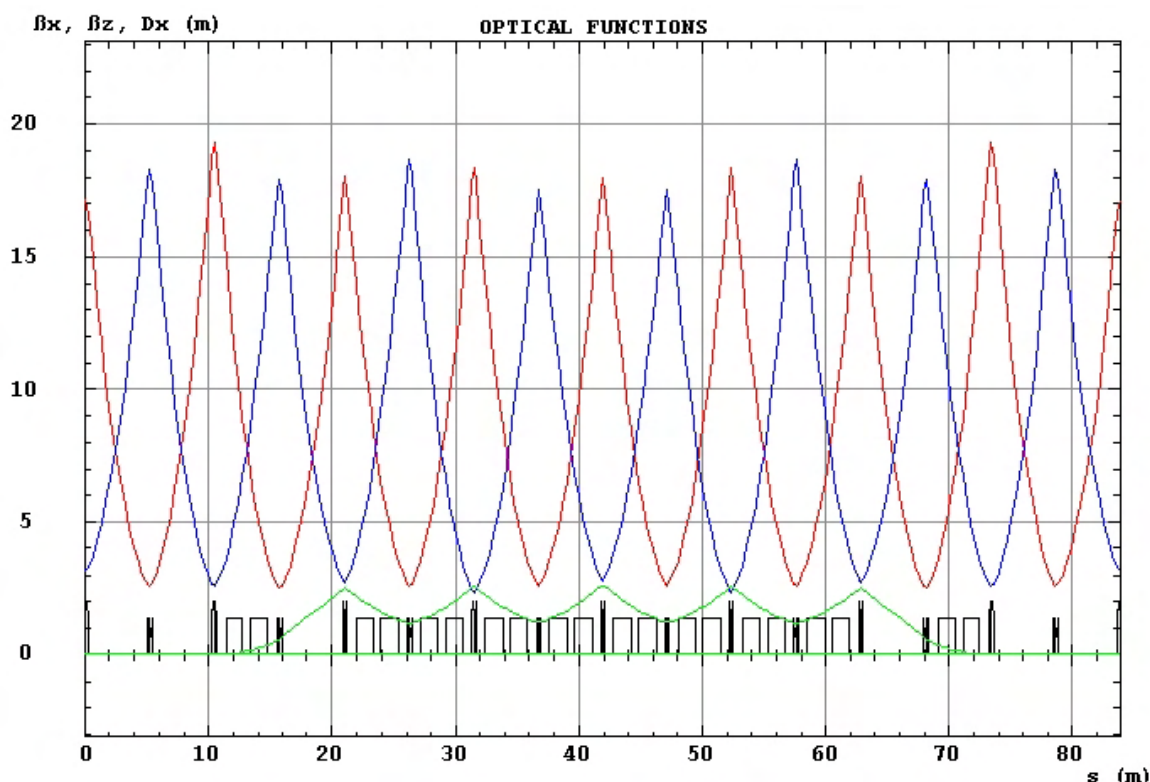


Fig. 3: Optical functions for one superperiod.

Injection

It is assumed that the ion source delivers a beam pulse of 50 μs . The revolution period of ions at 100-A MeV being 1.96 μs , the injection process takes place over several (26) turns in the machine and is therefore referred to as multi-turn injection. Ions are injected into one of the long straight sections by means of an electrostatic septum and at least 2 pulsed kickers, producing a local closed orbit bump which places the distorted orbit near the septum for the first injected turn and which moves it away from the septum on subsequent turns until it has collapsed.

The aim of the injection process is to maximise the number of injected ions within the specified transverse emittance. Optimum filling in the horizontal phase space is achieved when incoming ions are injected with a position and a slope which minimize their Courant and Snyder invariant. In the vertical phase space the dilution is obtained by a betatron function mismatch and a beam position offset. Figure 4 shows the diluted emittances in transverse phase spaces after multi-turn injection, obtained with the WINAGILE code. We obtain an injection efficiency of 80% after optimization.

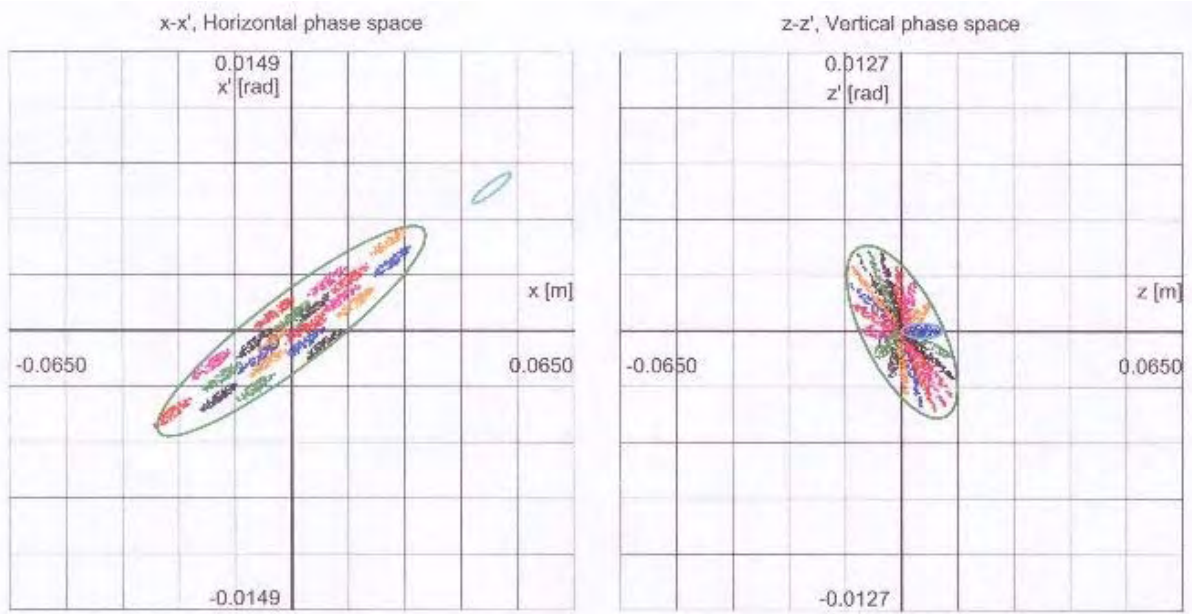


Fig. 4: Phase space distributions of the multi-turn injected beam (left: horizontal plane; right : vertical plane).

Acceleration

The programs for RF voltage and synchronous phase are determined by the following requirements:

- In order to maintain the central trajectory on the reference orbit, the energy gain per turn must be related to the variation of the magnetic field.
- The voltage must provide a sufficient “bucket” area to enclose all the longitudinal emittance.
- The trapping process must be optimized to minimize the beam losses.
- At extraction the bunch must be matched to the bucket of the next machine.

After injection, the circulating beam is continuous and occupies a rectangle in the longitudinal phase space. To capture the injected beam, one stationary bucket is created. During trapping, the magnetic field is clamped at its minimum value for a period of few ms and the synchronous phase is zero. The RF voltage is optimized to obtain a beam rotation of about 90° and a momentum spread as small as possible before the acceleration phase. When the magnetic field starts to ramp, the synchronous phase is shifted and the beam is accelerated. The program of the rise of the RF voltage and the synchronous phase variation are defined to obtain a sufficiently large bucket area and to minimize losses. Finally, at the end of the cycle, the bunch is manipulated so as to be matched to one of the PS RF buckets. The RF cycle has been simulated and optimized with the code ACCSIM developed at TRIUMF [19]. Figure 5 shows the variation of the synchronous phase and voltage during a cycle for He ions.

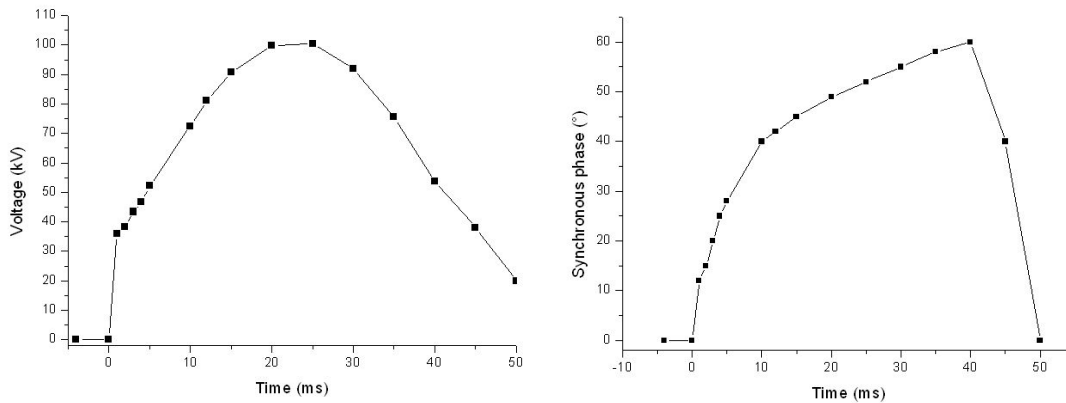


Fig. 5: Synchronous phase and voltage evolution during a cycle for He ions.

Other aspects

Several beam dynamics studies have been investigated in order to assess the feasibility of the RCS, in addition to the results presented here. Unavoidable magnet misalignments and dipole field errors can affect the RCS closed orbit. Distortions to be expected have been statistically estimated assuming standard error tolerances and a correction system has been defined. In fast ramping machines such as the beta-beam RCS, eddy currents induced in metallic vacuum chamber walls by the time varying magnetic field produce various field components acting on the beam. In dipoles vacuum chambers, one important component is a sextupole which modifies the natural chromaticity of the ring. The associated effects have been estimated and it has been shown that they could be compensated for, so that they do not pose problems from the point of view of beam dynamics.

Finally, after injection, ions beams are extracted in a single turn and directed towards the CERN PS. A fast extraction system consisting of fast kickers and septum magnets has been defined to produce the deflection angle required to eject the beam from the ring.

All the beam dynamics studies made on the RCS have shown that there are no ‘showstoppers’ on this ring. It can be realized with the present technology. In addition, radioprotection and beam dynamics studies were realized and show no major problems in the operation of such machine [8].

15.4 Ion acceleration scenarios in PS and SPS

Ion acceleration in the PS and SPS is a routine operation since many years. Different ion types from light ions such as sulphur up to heavy ions such as lead have been accelerated. We summarize here the results of the study realized by CERN within FP6 for the acceleration of the beta-beam nuclides ${}^6\text{He}$ and ${}^{18}\text{Ne}$. Dynamics vacuum studies were in addition performed by GSI. They are reported in reference [8]. An acceleration in the PS2 is being followed at CERN as a non-baseline option. Finally, dedicated studies for protecting the PS magnets against power deposition which is too high – as well as radioprotection studies – were initiated at GSI with the help of CERN [8], and these are reported in reference [20].

PS - RF considerations

Since the beta-decay lifetime at injection in the PS is much longer than the cycle time of the RCS, it pays to operate the PS at the rf harmonic consistent with the 10-MHz upper frequency limit of the accelerating cavities and to transfer the maximum number of batches from the RCS. Thus, the PS harmonic of choice becomes $h=21$ and 20 bunches are accumulated one by one leaving one rf bucket empty to accommodate the extraction kicker rise-time.

Figure 6 shows how beta-decay diminishes the number of helium ions accumulated on the PS injection plateau. Figure 7 shows the corresponding relative intensity along the bunch train. As little as 40% of the first helium bunch remains when the last one arrives.

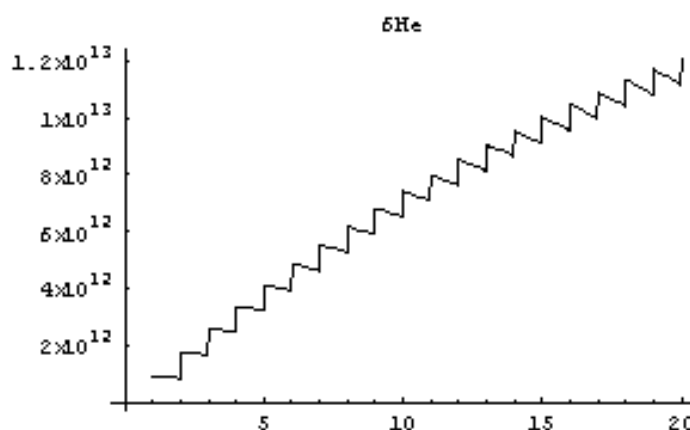


Fig. 6: Number of helium ions accumulated in the PS versus RCS batches.

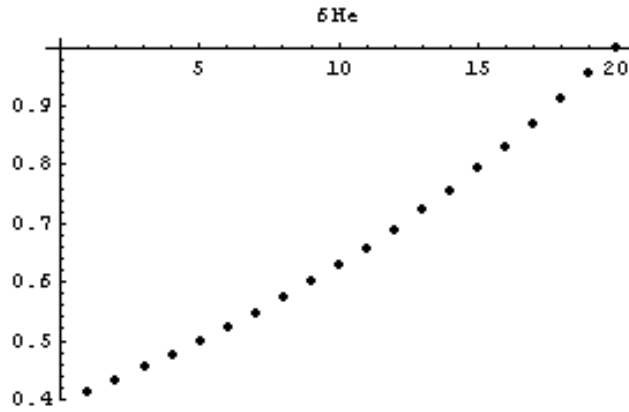


Fig. 7: Relative helium intensity along the bunch train in the PS.

The situation is better in the neon case due to its longer half-life and more advantageous charge-to-mass ratio, but the PS extraction kicker gap must still be established at a different position within the bunch train from batch to batch in order to even out the bunches that are ultimately stored in the decay ring.

The longitudinal emittance that the PS must deliver is 0.80 eV·s in the case of helium ions and 1.8 eV·s for neon. This implies matching voltages of ~30 kV and ~10 kV, respectively, in order to provide the requisite bunch length of 20 ns at ejection. No bunch shortening gymnastics are required due to the addition of a 40-MHz rf system in the receiving SPS (see next section).

SPS - RF simulations

Rather than consider another new machine, the space charge bottleneck at SPS injection has been addressed by adding a “modest” 40-MHz rf system to the existing infrastructure. This would allow much longer bunches to be transferred from the PS, the matching voltage for 20-ns bunches being ~120 kV and ~5 kV for helium and neon, respectively. Then, near transition, when the bunches are short enough, the standard 200-MHz system of the SPS would take over for the bulk of the acceleration. Conceptually this is fine, but the baton must be passed between buckets of very different aspect ratio so mismatching the bunches is unavoidable.

1 MV is at the limit of what might be considered as “modest” at 40 MHz and constrains the maximum ramp rate to around 0.1 T/s in the early part of the cycle. Even so, the ramp rate must be slowed down still further for the re-bucketing, because even a small ramp rate reduces the 200-MHz bucket length and buying this back with voltage is costly in terms of mismatch. Assuming a ramp rate of 0.02 T/s and that the emittance the SPS is supposed to deliver is already established before transition, figure 8 shows how proximity to transition ($\gamma_{tr}=23$) reduces the 200-MHz voltage that is required to accommodate the bunch length accelerated in the proposed new 40-MHz bucket. Performing rf gymnastics close to transition is bound to be a delicate matter, but it incurs no penalty in mismatch because the aspect ratios of the two buckets scale identically with γ .

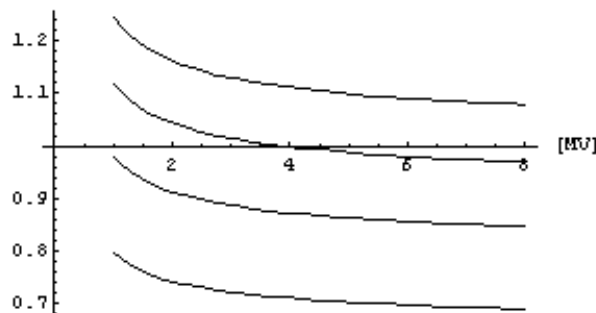


Fig. 8: Ratio of 40-MHz bunch length to 200-MHz bucket length versus 200-MHz voltage for helium ions at $\gamma=19, 20, 21, 22$ (from top to bottom) and a ramp rate of 0.02 T/s in the SPS.

Figures 9 and 10 show ESME simulations of re-bucketing at $\gamma=21.5$ from 1 MV at 40 MHz to 1.75 MV at 200 MHz for helium ions. The bunch is mismatched at 200 MHz, but one quarter of a synchrotron period later (figure 11) it can be re-matched by a step in voltage to 7.9 MV (figure 12). Thereafter, the ramp rate can be increased and acceleration can proceed normally.

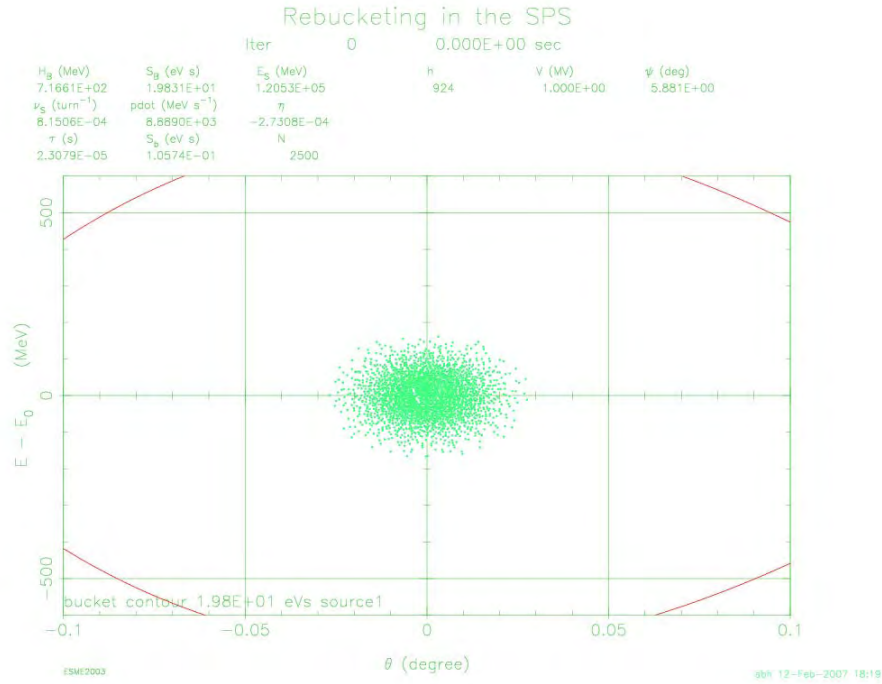


Fig. 9: A 1.0-eV-s bunch of helium ions in a 1-MV, 40-MHz bucket at $\gamma=21.5$ and a ramp rate of 0.02 T/s in the SPS.

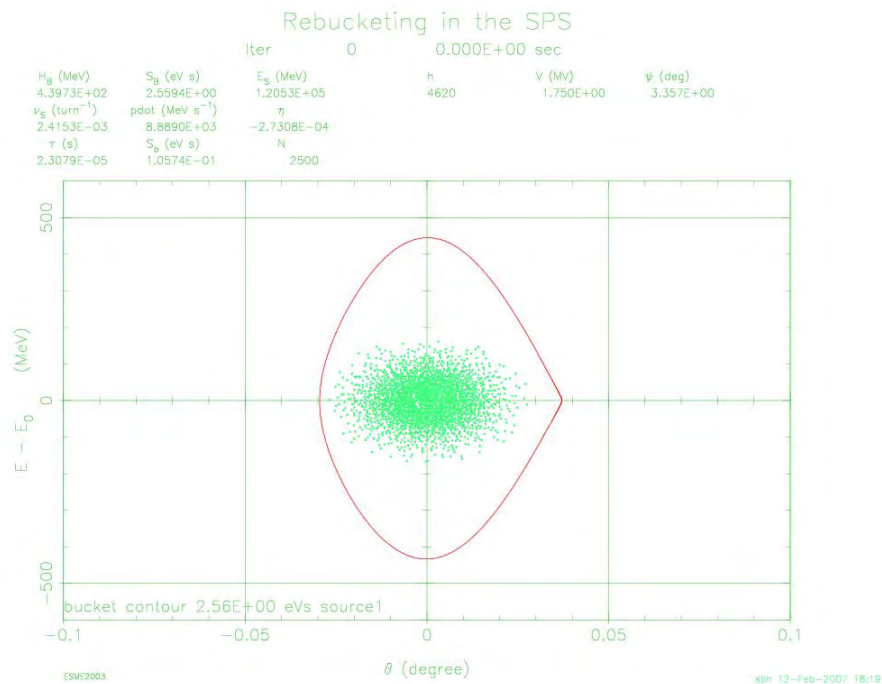


Fig. 10: The bunch of fig. 9 after the 40-MHz bucket is superseded by a 1.75-MV, 200-MHz one.

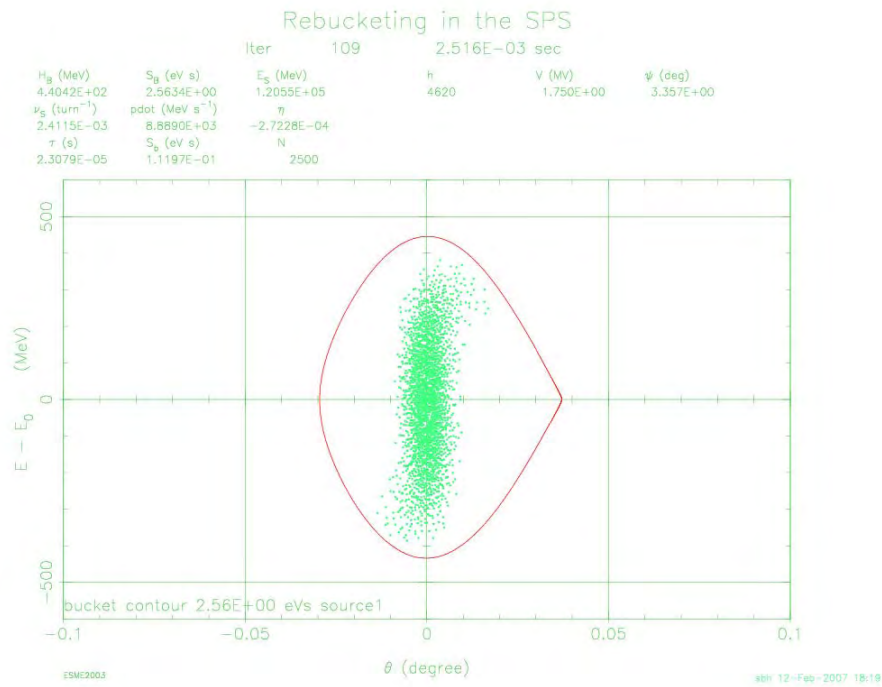


Fig. 11: The bunch of fig. 10 after rotation during one quarter of a synchrotron period.

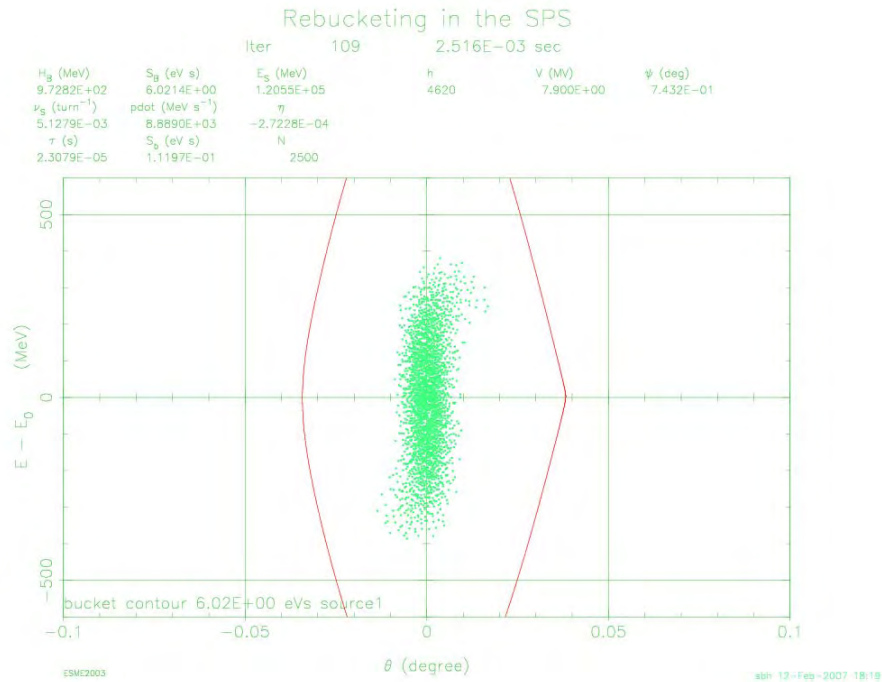


Fig. 12: The bunch of Fig. 11 after a step in 200-MHz voltage to 7.9 MV. A small fraction of the bunch population remains at large amplitude.

Despite a larger emittance, the situation is easier in the neon case due to its advantageous charge-to-mass ratio. Although re-bucketing must still be performed at the same miniscule ramp rate of 0.02 T/s, proximity to transition can be decreased to $\gamma=20$, still having 1 MV at 40 MHz passing the baton to 1.75 MV at 200 MHz. To rematch, 7.8 MV is needed at 200 MHz.

1 MV is very much the minimum 40-MHz voltage required. It also costs cycle time because of the need to slow the ramp rate down to permit re-bucketing. However, since the 40-MHz system sees almost all the frequency swing during acceleration, more voltage would be expensive. Alternatively, one could consider re-bucketing at zero ramp rate as this reduces slightly the problem of matching.

The longitudinal emittance that the SPS must deliver is 1.0 eV·s in the case of helium ions and 2.2 eV·s for neon. These values are derived from the known performance for protons and, allowing an emittance budget of some 25% for blow-up during each acceleration stage, they also fix those in all the upstream machines. The novel injection scheme proposed for the decay ring requires the beam to be delivered off-momentum into the non-linear region of the receiving bucket. Consequently, the bunch is deliberately mismatched before extraction from the SPS by a step down in 200-MHz voltage (see figure 13). This bunch tilting is a first-order attempt to increase the capture efficiency at the end of a quarter of a synchrotron turn in the decay ring. The fine detail of capture will depend on the large-amplitude distribution created in the SPS.

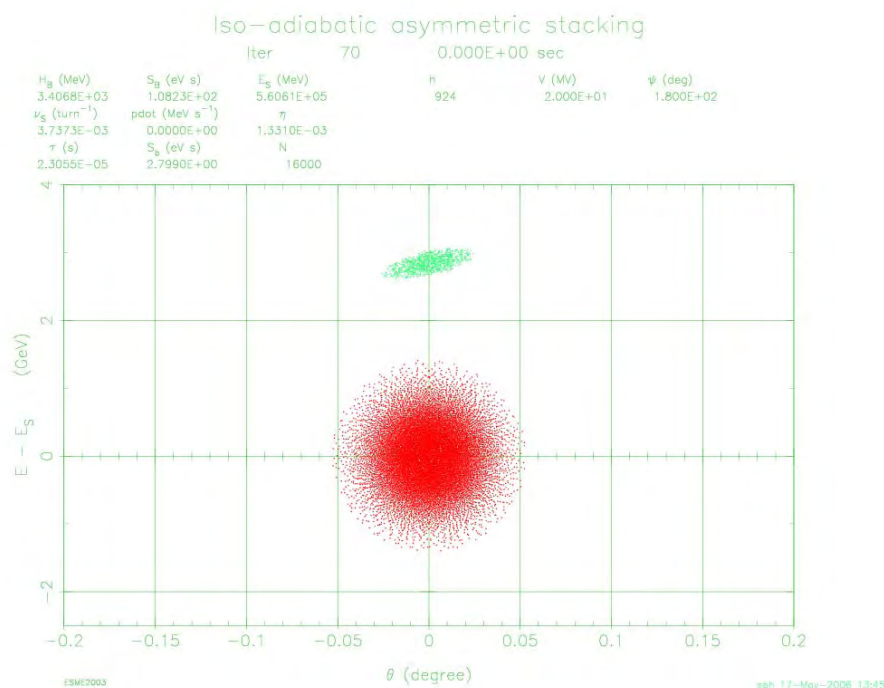


Fig. 13: An SPS bunch of helium ions (green) is delivered tilted (following a step down in rf voltage from 2 to 0.5 MV) and 5% off-momentum with respect to the stack (red) in the decay ring.

Identification of limitations

The budget of decay losses within PS and SPS was estimated and compared to CNGS operation by CERN in reference [21]. From that study, it turns out that the power losses occurring for the beta-beam operation are of the same order of magnitude as occur in CNGS operation, for nominal intensities of ${}^6\text{He}$ and ${}^{18}\text{Ne}$ and are therefore not a showstopper for the project.

15.5 Design of decay ring

The design of the decay ring of the beta-beam facility was performed mainly by CEA Saclay using a stacking mechanism as was originally proposed by CERN [22,23]. CERN has taken part in the design of the collimation section and in a study of the dipoles of the arcs for protecting them from high energy deposition using FLUKA and ACCSIM softwares (see below). The RF was studied by CERN and an original solution was proposed [23].

Optics

The decay ring is a 6911.5-m-long racetrack-shaped ring with two 2468-m straight sections, of which one is directed toward the detector situated in the Fréjus tunnel [24]. The useful section is around 36% of the circumference. The parameters of the beam are given in table 4.

Table 4: Nominal parameters for the decay ring.

Parameter	Units	${}^6\text{He}^{2+}$	${}^{18}\text{Ne}^{10+}$
γ	-	100	100
$B \cdot \rho$	T·m	938	563
B_{dipole}	T	6	3.6
τ at rest	s	0.8	1.67
N_{injected}	ions/batch	9.05×10^{12}	4.26×10^{12}
N_{stored}	ions/batch	9.71×10^{13}	7.40×10^{13}
Bunch number	-	20	20
rms ε_x	π mm.mrad	0.11	0.11
rms ε_y	π mm.mrad	0.06	0.06
$\Delta \nu_x$	-	-0.015	-0.127
$\Delta \nu_y$	-	-0.024	-0.201

A first consequence of storing high-intensity beams is that the tune spread due to the space charge effects may not be negligible. The tune shift was calculated for ${}^6\text{He}^{2+}$ and ${}^{18}\text{Ne}^{10+}$ and is given in table 4. With nominal parameters, the space charge effects can be neglected in ${}^6\text{He}^{2+}$ case, contrary to the ${}^{18}\text{Ne}^{10+}$ case. A solution to decrease the space charge effect would be to increase the rms emittance of the stored beam by injecting a mismatched beam. To have a negligible tune shift for ${}^{18}\text{Ne}^{10+}$ of -0.063 in the horizontal plane and -0.055 in the vertical one, the rms emittance must then be enlarged up to 0.22π mm.mrad in both planes. In the following, we assume this rms emittance for ${}^{18}\text{Ne}^{10+}$ to neglect space charge effects.

The arcs are 2π insertions, the optics of which are given in figure 14. Four functional parts were distinguished in the arcs [25]: a regular FODO lattice in the arc, a matching section between the long straight section and the FODO lattice, which is also used to extract the decay products coming from the long straight section, a low- β , high-dispersion insertion for the injection, and a matching section between the regular FODO lattice and the insertion. Moreover, large betatron functions are needed in the FODO lattices of the long straight sections to maximize the neutrino flux going to the detector.

Losses by β -decay

The decay of the stored ions implies a continuous power loss with a mean value of 10.8 W/m for ${}^6\text{He}^{2+}$ and 11.8 W/m for ${}^{18}\text{Ne}^{10+}$ [26]. The relative rigidity difference between the decay products and the reference one is around -33% for ${}^6\text{He}^{2+}$ and +11% for ${}^{18}\text{Ne}^{10+}$. In turn, the decay products are then lost after a few dipoles. Two principal issues can be underlined. After the long straight sections, the deposition is equal to several tens of kilowatts: a dedicated extraction section at the arc entry is therefore needed. Moreover, the deposition inside the superconducting magnets must be low enough to avoid quenching, for which two solutions were studied. The first consists of inserting absorbers between the magnetic elements. The second consists of using open-mid-plane dipoles, which are dipoles without coils in the horizontal plane. The advantages of this solution is to enable longer dipoles for decreasing their magnetic field (5 T instead of 6 T), to reduce the needed dipole aperture (± 50 mm against ± 80 mm) and to make structural changes simpler if other ions are used.

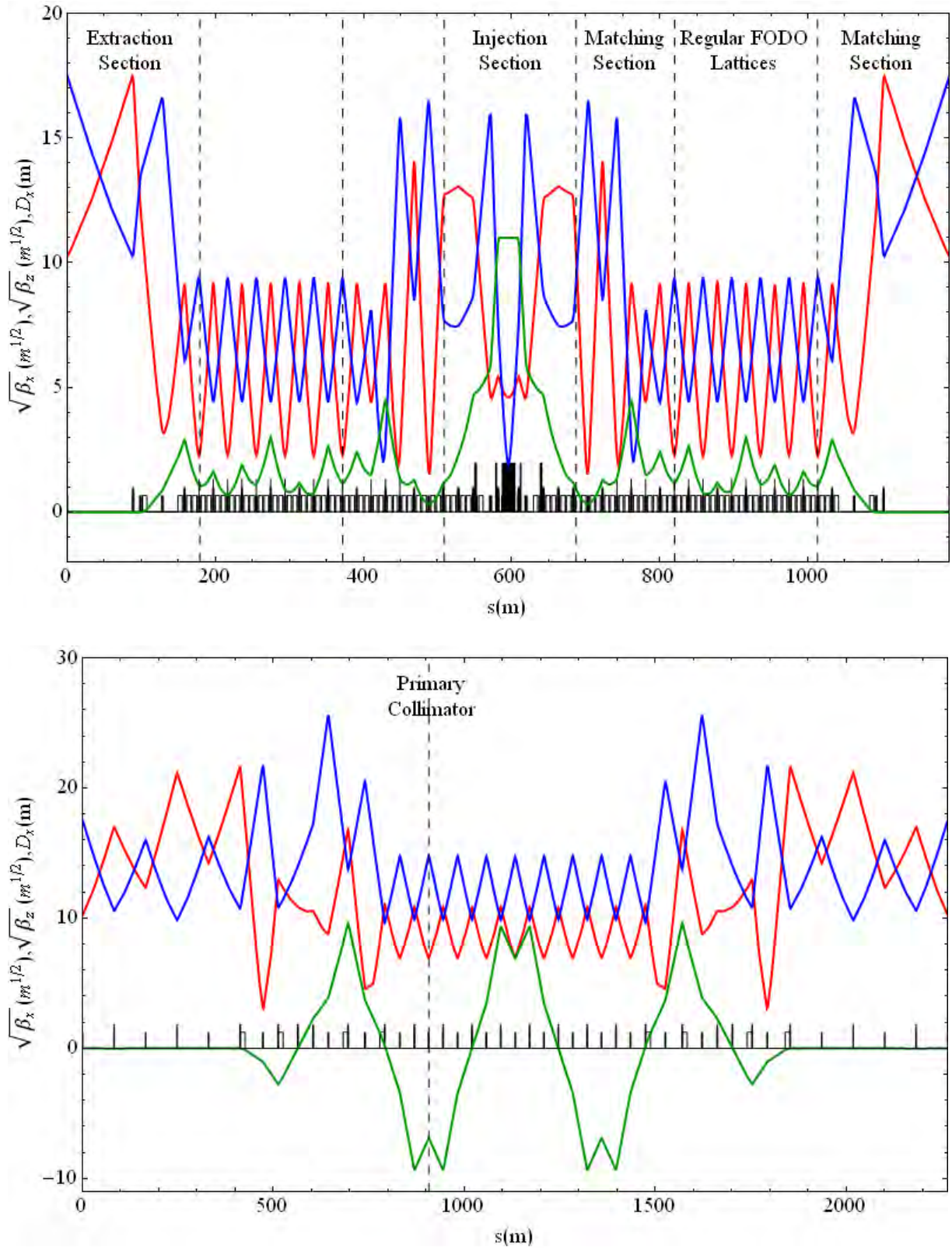


Fig. 14: Optical functions in the arcs (upper graph) and in the energy collimation section (lower graph), showing the horizontal betatron function (red), vertical betatron function (blue) and horizontal dispersion (green).

To evaluate the deposition of the decay products in the chamber, a simple 1D program was implemented in BETA [27]. It does not take into account any interaction with the walls. To improve the model, a 3D simulation with the interactions was run in the case of absorbers [28] using FLUKA together with ACCSIM. In both simulations, the average value deposited in the dipoles is then less than 10 W/m. Unfortunately, peaks exceed the recommended limit: 4.3 mW/cm³ for dipoles. The open mid-planes should significantly improve the situation.

Momentum collimation

The injection system relies on injecting a fresh beam in a dispersive area with an energy different from the reference one. The stored beam and the injected one are then horizontally separated. The injection can be cut in four main steps.

- Firstly, the stored beam is deviated by four kickers.
- Secondly, the entering beam is injected “off momentum” at $\delta = 5 \times 10^{-3}$ on its chromatic orbit.
- Thirdly, the kickers are switched off. The injected beam stays on its chromatic orbit and runs under
- the septum blade.
- Finally, both beams are merged together by a specific RF program using two variable cavity families, of which one is at double frequency [29].

Several injection cycles were simulated, which has identified two loss sources. The first comes from the fresh ions which are not captured at the injection. The second one is due to the blow-up in the space (l, δ) injection after injection. In figure 15, the survival of a beam injected at $t = 0$ is represented as a function of the number of injection cycles. After around 15–20 injections, most ions are not accepted anymore. When the steady state is reached, the loss amount between two injections is compensated by the injection itself. About 50% (helium) and 20% (neon) of the losses which occur between two cycles are due to the β -decay. The mean power to collimate in the ring can then be evaluated as 74 kW for ${}^6\text{He}^{2+}$ and 248 kW for ${}^{18}\text{Ne}^{10+}$. Therefore, a two-step collimation system is needed and this was designed to collimate in energy at $\delta = 2.5 \times 10^{-3}$ (figure 14). It is located in the long straight section which is not directed toward the detector.

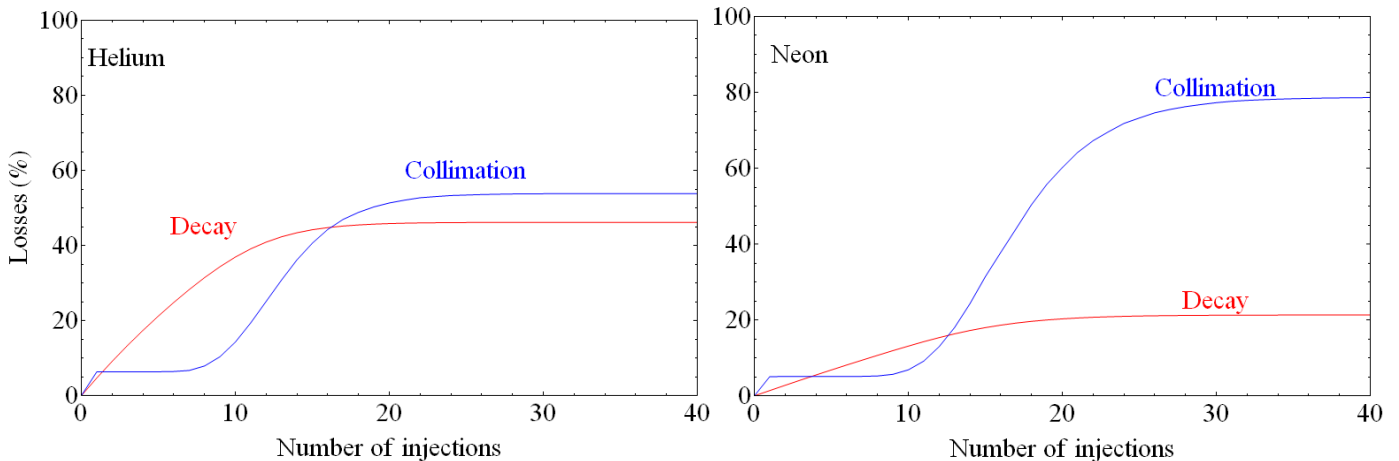


Fig. 15: Loss amount as a function of time for helium (left) and neon (right).

A 3D simulation of the collimation section has been done with FLUKA with losses generated by ACCSIM. The use of graphite absorbers before the warm magnets of the collimation section decreases considerably the power losses in the coils [23]. The preliminary design of the collimation section will be further optimized to reach reasonable orders of magnitude for the energy deposition within the coils and to improve the lifetime of the magnets.

Defects in the magnetic elements

Misalignments of the magnetic elements and errors in the main field must be taken into account. One consequence is a distortion of the closed orbit. The random rms errors in the magnetic field, the rms transverse misalignment and the rotation around the machine axis, are respectively assumed to be 0.5×10^{-3} , 0.5 mm and 1 mrad for the dipoles. The rms error on the gradient in the quadrupoles is assumed to be 1×10^{-3} . Their rms transverse misalignment is 0.4 mm. The beam profile monitors (BPMs) are assumed to be ideal. The order of magnitude of the closed-orbit distortion is then a few centimeters, which makes the closed-orbit correction necessary. 85 horizontal & 85 vertical BPMs were inserted in the structure. After correction, the rms resultant of the closed orbit is then less than 0.4 mm. The maximum rms value for the horizontal dipole correctors is 0.042 mrad and for the vertical ones 0.064 mrad. Since the closed orbit is corrected up to three standard deviations, the integrated field in the dipole correctors must be respectively 0.118 T·m and 0.180 T·m. The natural chromaticity in the decay ring is respectively -1.72 and -2.35 in each plane. Without correction, the injected beam is not accepted.

After correcting the chromaticity with only two sextupole families, we obtain the dynamic aperture of the blue curve in figure 16. The dynamic aperture is quite large but the coupling resonances are not corrected and the beam does not keep an elliptic shape. After minimizing the sextupolar resonances with six sextupole families, we obtain the red curve in figure 16. The dynamic aperture is much larger. However, the obtained dynamic aperture is in the case of ideal dipole magnets. The large aperture of the dipoles implies unavoidable multipole components.

Until now, only systematic multipole components were considered. The assumed systematic multipole components in the dipoles are $b_3 = -1.68 \times 10^{-4}$, $b_5 = 33.02 \times 10^{-4}$, $b_7 = -50.12 \times 10^{-4}$ and $b_9 = 29.58 \times 10^{-4}$ at the reference radius 60 mm [30]. A direct consequence is a reduction of the dynamic aperture. In order to identify the main multipole effects, figure 16 gives the dynamic aperture calculated for each alone multipole component for the same reference structure. The strongest contribution comes from the fifth and the seventh order multipole components. In order to decrease their effects, different working points were considered and an automatic enlargement program of the dynamic aperture was added in BETA, which enabled us to obtain a dynamic aperture of more than 6σ [31].

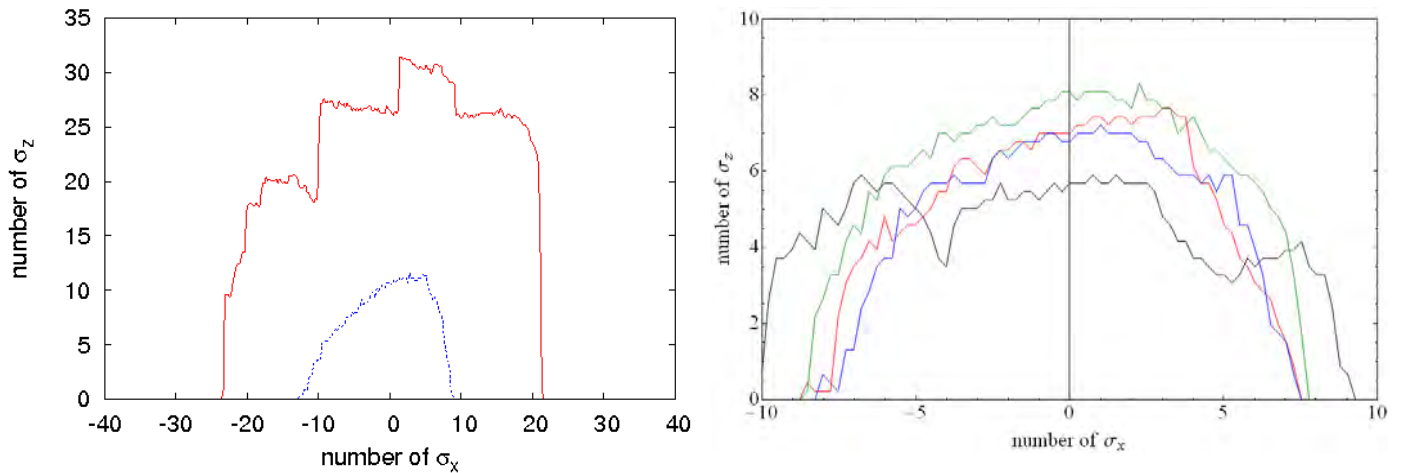


Fig. 16: Dynamic aperture for 1000 turns. On the left, the dipoles are ideal. In blue, 2 sextupole families were used and in red 6 sextupole families. On the right, the multipole defects of the fifth order (red), the seventh order (blue), the ninth order (green) or every multipole component (black) were applied.

15.6 Conclusion

A conceptual design report on a CERN/EURISOL baseline scenario for the beta-beam facility was summarized here. The EURISOL design study has provided insights on the method to produce ${}^6\text{He}$ and ${}^{18}\text{Ne}$ with the required intensities. The accelerator chain includes a rapid-cycling synchrotron (RCS) for injecting the radioactive ions from the linac to the existing PS and SPS. An original stacking

mechanism was proposed in the decay ring for optimizing the throughput of the facility. Both the RCS and decay ring were studied in detail. This study also included aspects concerning the beam losses along the accelerator chain, the momentum collimation in the decay ring, dynamic vacuum and RP studies. A long version of the report is being prepared to be published as a CERN yellow report.

References

1. B. Autin et al., “*The acceleration and storage of radioactive ions for a neutrino factory*”, [CERN/PS 2002-078 \(OP\)](#), Nufact Note 121, J. Phys. **G 29** (2003) 1785 and long internal CERN version, [PS/OP/Note 2002-181](#).
2. M. Mezzetto, “*Physics reach of the beta-beam*”, J. Phys. **G 29** (2003) 1771.
3. J. Bouchez, M. Lindroos and M. Mezzetto, 5th Internat. Workshop on Neutrino Factories and Superbeams (NuFact 03), AIP Conf. Proc., **721** (2004) 37.
4. [Letter of Intent: FP6 Design Study for a beta-beam facility](#), September 2003.
5. N Thollieres et al., EURISOL DS technical note 03-25-2006-0004.
6. <http://www.euronu.org/>.
7. C. Rubbia et al., “*Beam cooling with ionization losses*”, Nucl. Instrum. & Meth. **A 568** (2006) 475–487.
8. CERN Baseline Beta-Beam, in preparation.
9. [Parameter and Intensity Values, Version 1, April 2005](#), EURISOL DS/TASK12/TN-05-01.
10. [Parameter and Intensity Values, Version 2, July 2005](#), EURISOL DS/TASK12/TN-05-03 (revised 13th October 2005, see equation 2 and table 2).
11. [Parameter and Intensity Values, Version 3, July 2007 \(doc-version\)](#), EURISOL DS technical note 12-25-2009-0014.
12. P. Zucchelli, “*A novel concept for a neutrino factory: the beta-beam*”, Phys. Lett. **B 532** (2002) 166.
13. T. Thuillier, “*High frequency ECR source (60 GHz) in pre-glow mode for bunching of beta-beam isotopes*”, Proc. NuFact08, [PoS\(Nufact08\)089](#).
14. A. Chancé and J. Payet, “*Studies of the injection system in the decay ring of a beta-beam neutrino source*”, Proc. Particle Accelerator Conf., Knoxville, Tennessee, USA (2005).
15. A. Lachaize and A. Tkatchenko, EURISOL DS technical note 12-25-2009-0021.
16. A. Tkatchenko, presentation at the first task meeting, EURISOL DS technical note 12-25-2009-0015.
17. A. Lachaize and A. Tkatchenko, EURISOL DS technical note 12-25-2009-0018.
18. J. Payet, *Code BETA*, jpayet@cea.fr.
19. F. Jones, *ACCSIM Code*, Jones@triumph.com.
20. M. Benedikt and S. Hancock, EURISOL DS technical note 12-25-2009-0019.
21. A. Fabich, M. Benedikt, EURISOL DS technical note 12-25-2006-0004.
22. A. Chancé and J. Payet, EURISOL DS technical note 12-25-2006-0001.
23. A. Chancé and J. Payet, EURISOL DS technical note 12-25-2009-0022.
24. M. Benedikt et al., “*Baseline Design for a Beta-Beam Neutrino Facility*”, Proc. EPAC’04.

25. A. Chancé, “*Etude et conception de l’anneau de désintégration d’une usine à neutrinos utilisant les décroissances beta des noyaux Hélium 6 et Néon 18 produits par un faisceau intense de protons frappant diverses cibles*”, Ph.D. thesis, Université Paris Sud, 2007.
26. A. Chancé et al., “*Loss Management in the Beta-Beam Decay Ring*”, Proc. EPAC’06.
27. J. Payet, Code BETA, LNS version.
28. F.W. Jones et al., “*Simulation of Decays and Secondary Ion Losses in a Beta-beam Decay Ring*”, Proc. PAC’07.
29. S. Hancock et al., “*Stacking Simulations in the Beta-Beam Decay Ring*”, Proc. EPAC’06.
30. C. Vollinger et al., private communication, 2006.
31. A. Chancé et al., “*Studies of dipole field quality for the beta-beam decay ring*”, Proc. PAC’07

Chapter 15: Cost Estimation

15.1 Introduction

Cost estimation for a project of this size will generally require professional costing services. However, this was beyond the resources of the Design Study, and the Management Team and Task Leaders have therefore constructed a costing spread-sheet to arrive at a total estimated cost (TEC) for the facility. Actual cost figures are now available for the SNS in the US, which was constructed between 1998 and 2008, although the major expenditure was between 2000 and 2005.

Other figures for a related facility are those for the Isotope Science Facility at MSU, which is now approved, although the proposed facility has been modified since the proposal was made in 2006.

For these US institutions, we have assumed that 1\$US circa 2000 will be equivalent to 1€ in 2009 terms, allowing for inflation and some exchange-rate fluctuations.

Some figures from SPIRAL2 have been used when planned facilities are similar. Costs for FAIR, RIKEN, JPARC and the ESS are less easily obtained, but have been used as a guide where applicable.

15.2 Methodology

The leaders of several Tasks within EURISOL design Study were asked to provide cost estimates of the parts of the facility they were concerned with. These were essentially ‘bottom-up’ estimates, encompassing capital costs only, to which labour costs have since been added. Because of the lack of time and manpower, a “top-down” approach was used for buildings and other conventional facilities. Standard office-type buildings were costed at 2k€/m². Certain other areas were costed at 10k€/m², inclusive of shielding, cabling, ventilation, etc, based on known costs for similar facilities.

However, for the multi-MW target, both “top-down” and “bottom-up” approaches were used, resulting in roughly similar estimates, giving some credence to the methods used.

Where labour costs were not already included in the estimations, these have been calculated simply as an additional 25% of the capital cost of every item. Some allowance for research and development has also been made, where appropriate

Overleaf we show the costing spreadsheet, down to level 3 (and in some cases to level 4).

15.3 Exclusions

No physics instrumentation has been included (apart from the Fragment Separator), since such instrumentation is often provided by users and funded from other sources, or existing equipment may be moved from other facilities.

No provision has been made for “nuclearisation” for the post-accelerator RFQ and stripping stations – i.e. remote-handling of activated components designed specifically for such methods.

No contingency allowance has been included since the total estimated cost is at this stage only likely to be accurate to within 10-20%.

No decommissioning costs have been included. These will depend heavily on the type of liquid metal used for the multi-MW target and the requirements for treating the activated target material.

15.4 Conclusions

Given that the cost estimate for made during the earlier EURISOL Feasibility Study (2000-2003) amounted to 613 M€, excluding Project Management, R&D and Conceptual Design Effort, Environmental Impact Analysis, and installation costs for systems and sub-systems, it is no great surprise that the final total cost is in excess of 1.3 billion euros.

To put this in context, we note that the SNS total project cost was 1.4 billion dollars, although some 65 million of this was for instrument facilities. The SNS has a similar driver accelerator, a similarly

complex liquid-metal target – 2 MW as opposed to 4 MW for EURISOL – plus an accumulator ring, but no ISOL facilities, and no post-accelerators.

Similarly, the ESS project cost is estimated to be 1.55 billion euros (year 2000 costs), including capital and labour and a 15% contingency (202 M€).

Since no architectural or structural engineering studies of the proposed buildings were possible within the ambit of the Design Study, these costs must be regarded as rough estimates only, generally based on costs per square metre appropriate for the respective types of buildings and facilities. It must also be pointed out that this is a preliminary costing exercise, and that much will depend on the site chosen for the facility, particularly with respect to existing infrastructure, where applicable.

We remark that the beta-beam proposal was not included in this cost estimation, since it would depend on the availability of CERN rings, etc. and would therefore have to be considered as a separate project.

Costing Spreadsheet

EURISOL Cost Estimation

WBS	Description	Totals (k€)	Sub-systems (k€)
1	TEC (Total Estimated Cost)	1,326,074	
1.1	Conventional Facilities	383,900	
1.1.1	Site work	20,000	
1.1.2	Driver linac facilities	60,000	
1.1.2.1	Injector building		4,400
1.1.2.2	Driver linac tunnel		5,600
1.1.2.3	RF power supply facilities		20,000
1.1.3	MW Target building	60,000	
1.1.3.1	100-kW Target building (with 3 target areas)	90,000	30,000
1.1.4	Beam preparation facilities with nuclear ventilation system	16,000	
1.1.5	Post-accelerator facilities	25,600	
1.1.5.1	Post-accelerator tunnel		5,600
1.1.5.2	RF power supply facilities		20,000
1.1.6	Low-energy area facilities	8,000	
1.1.7	Medium-energy area facilities	20,000	
1.1.8	High-energy area facilities with nuclear ventilation system	40,000	
1.1.9	Data-taking areas & facilities	6,000	
1.1.10	Services/workshops/control room	12,000	
1.1.11	Cryogenic plant building	6,300	
1.1.12	User buildings (Labs & offices)	20,000	
1.2	Cryogenics	68,000	
1.2.1	Cryogenic plant	60,000	
1.2.3	Distribution	8,000	
1.3	Driver Accelerator	289,000	
1.3.1	Linac front end (ion sources, LEPT, RFQ)	8,000	
1.3.2	HWR linac (60 MeV/q)	22,000	
1.3.3	Spoke linac (140 MeV/q)	27,000	
1.3.4	Elliptical linac (1 GeV/q)	68,000	
1.3.6	Diagnostics	13,000	
1.3.7	RF power supplies	101,000	
1.3.8	Vacuum systems	13,000	
1.3.9	High-energy beam lines & dumps	22,000	
1.3.10	R&D: front end + linac	15,000	
1.4	100 kW targets	29,800	
1.4.1	Target ion-source assemblies (26 units/year for the 3 stations)	1,100	
	Front-Ends (for 3 stations)	1,200	
1.4.2	Remote Handling + Hot Cell area	6,000	
1.4.3	Target service bay	10,000	
1.4.4	Beam dumps	1,500	
1.4.5	R&D	10,000	

[continued]

Cost Estimation

WBS	Description	Totals (k€)	Sub-systems (k€)
1.5	MW target	167,700	
1.5.1	Liquid-metal target assembly	15,300	
	Liquid-metal loop and pumps	23,400	
1.5.2	Liquid-metal target shielding & trolley	4,000	
1.5.3	Target ancillaries	58,000	
1.5.4	Remote Handling	12,000	
1.5.6	Liquid-metal target R&D	55,000	
1.6	Fission targets	55,314	
1.6.1	6 target/ion-source assemblies	5,783	
1.6.2	6 tilted tubes & auto-connect systems	2,858	
1.6.3	Cryopanel systems	3,600	
1.6.4	Graphite block, heat-exchanger & vacuum system	683	
1.6.5	Frame & positioning system for tubes	505	
1.6.6	RIB horizontal transport lines	300	
1.6.7	Testing TIS	1,136	
1.6.8	TIS power supplies	4,632	
1.6.9	Laser systems	10,640	
1.6.10	Cooling pits: mobile flask & crane	3,247	
1.6.11	Hot cell manipulators, TIS rotator, pumps	10,930	
1.6.12	Spent target storage area: robots & crane	1,000	
1.6.13	Fission target R&D	10,000	
1.7	Beam preparation	23,600	
1.7.1	Pre-separators	1,800	
1.7.2	Beam merging ARC-ECRIS	750	
1.7.3	High-resolution mass-separators	4,000	
1.7.4	Charge-breeders	2,500	
1.7.4.1	ECR-source		700
1.7.4.2	EBIS		1800
1.7.5	A/q separator	400	
1.7.6	Beam transport system (mech parts, like	9,050	
1.7.6.1	tubes, supports, bellows, ...)		5000
1.7.6.2	Deflector boxes		300
1.7.6.3	Pump stations		400
1.7.6.4	Diagnostic boxes		750
1.7.6.5	electrostatic quadrupoles		2600
1.7.7	RFQ cooler and buncher	1,100	
1.7.8	Charge-breeder R&D	2,000	
1.7.9	Mass-separator R&D	2,000	
1.8	Post-Accelerator	138,880	
1.8.1	Linac front end (LEBT, RFQ, MEBT)	3,300	
1.8.2	Linac section 1 (2 MeV/u)	5,000	
1.8.3	Linac section 2 (20 MeV/u)	7,000	
1.8.4	Linac section 3 (62 MeV/u)	20,000	
1.8.5	Linac section 4 (150 MeV/u)	36,000	
1.8.6	Warm magnets, power supplies, vacuum, diagnostics, supports	20,000	
1.8.7	Stripping station	1,000	
1.8.8	Robot handling	300	
1.8.9	RF power supplies (RFQs, bunchers, S/C cavities)	10,000	
1.8.10	Cryogenic plant, transfer lines	25,000	
1.8.11	High-energy beamline to beam dump (included)	1,280	
1.8.12	Contamination & safety R&D	10,000	
1.9	Control Systems & Networks	79,600	
1.9.1	Central control system	15,000	
1.9.2	Linac control systems	12,000	
1.9.3	Post-accelerator control system	12,000	
1.9.5	Target control system	18,000	
1.9.6	Safety & personnel control system	10,000	
1.9.7	Central computer system	2,000	
1.9.8	Central RF system	1,000	
1.9.9	Chiller & Cryomodule controls	4,600	
1.9.12	Alignment system	5,000	

[continued]

WBS	Description	Totals (k€)	Sub-systems (k€)
1.10	Post-accelerated Beam Transport	15,980	
	Low energy beam lines (20 Me/A)		
1.10.1	Quadrupoles and power supplies	1,700	
1.10.2	Dipoles and power supplies	420	
1.10.3	Vacuum	100	
1.10.4	Diagnostics	120	
1.10.5	Mechanics and beam tubes	2,660	
	Medium energy beam lines (60 Me/A)		
1.10.7	Quadrupoles and power supplies	2,640	
1.10.8	Dipoles and power supplies	1,560	
1.10.9	Vacuum	120	
1.10.10	Diagnostics	360	
1.10.11	Mechanics and beam tubes	3,000	
	High energy beam lines (150 Me/A)		
1.10.13	Quadrupoles and power supplies	910	
1.10.14	Dipoles and power supplies	640	
1.10.15	Vacuum	60	
1.10.16	Diagnostics	90	
1.10.17	Mechanics and beam tubes	1,600	
1.11	Fragment separator	9,800	
	Target area	4,200	
1.11.1	Magnets & Power supplies	4,000	
1.11.3	Shielding	500	
1.11.4	Remote Handling	100	
1.11.6	R&D for fragment separator	1,000	
1.13	Management & Administration	64,500	
1.13.1	Project Management	50,000	
1.13.2	EDMS	5,000	
1.13.3	Environmental safety & Health	7,000	
1.13.4	Quality Assurance	2,500	

No "nuclearisation" included for post-accelerator RFQs, strippers, etc....

No contingency allowance included.

No decommissioning costs included.

No instruments, detectors, etc. included.

Labour & installation included at 25% of capital cost

Chapter 17: International Advisory Panel Report

Introduction

While the EURISOL Design Study has been fairly successful in achieving its aims, it seems appropriate to quote the remarks made by the International Advisory Panel in their final report to the Steering Committee. This panel was set up to advise the Steering Committee on the progress made during the Design Study, and it has also been invaluable to the Management Board in reviewing the work done during each year, pointing out areas of concern and suggesting items which required more work to be done.

We quote from the IAP's final report:

“The IAP considers that its interaction with the EURISOL Design Study Group and the EURISOL User Community over the full period of the design study has been sufficient to assess the overall progress and results of the EURISOL Design Study. Participation of IAP members in design reviews of the high power fission target, the multi-MW spallation target and the post-accelerator has been very helpful to obtain more detailed insight in the work on these critical components.

The IAP is pleased to observe that the Design Study Group has reacted constructively to the major recommendations in its previous reports.

Organisational aspects

In view of the very limited funding for EURISOL expected from the 7th EU Framework Programme the IAP is concerned about the continuity of the EURISOL collaboration, the preservation of the knowledge and expertise generated in the EURISOL Design Study and the possibilities to keep the science case up-to-date. All three aspects are essential for a successful future continuation of the EURISOL Design Study.

The IAP acknowledges that intermediate projects such as SPIRAL2, HIE-ISOLDE and SPES will provide a strong link between the current EURISOL Design Study and its future successor by exploiting and expanding the technical results of the EURISOL Design Study and by providing the scientific justification for a next stage facility.

The IAP shares the opinion of the management that a strong collaboration in which the intermediate projects and all other interested parties participate and coordinate their research efforts relevant for a future EURISOL facility is mandatory to ensure that the final objectives remain in focus and to pursue the possibilities of worldwide participation. Such collaboration will also facilitate a good integration of the experience gained at the intermediate facilities into the final design of the EURISOL facility.

The IAP remains concerned about the dissemination of the results of the design study, both among the participants and in the scientific community at large. Both the number technical notes of the various task groups on the EURISOL website and the number of papers published so far in peer-reviewed journals are in the opinion of the IAP disappointing. The IAP considers that the quantity and quality of the results of the EURISOL Design Study justifies a significant number of papers. Furthermore, the publication of results either on the EURISOL website or in journals contributes to the transfer of information and expertise to a next stage of the EURISOL Design Study in a few years from now and to on-going projects such as SPIRAL2, HIE-ISOLDE and SPES.

The IAP welcomes the initiative to publish review articles on the different aspects of the EURISOL Design Study in the European Physics Journal A. However, the usefulness of these review articles will be limited if the details of the underlying work are not properly disseminated. The IAP there strongly recommends to the management of the EURISOL Design Study to create a publicly accessible repository of all technical notes written during the design study and to continue its efforts to publish EURISOL results in peer-reviewed journals.

The IAP observes that the communication between the different task groups remains sub-optimal, leading to incompatibilities of specifications at interfaces despite all the efforts by the project

management. This is in particular worrying at the core of the facility, where the biggest challenges exist and where no viable design can be obtained without a strong coordination of the work of the task groups working on production targets, ion sources, beam preparation and radiation safety. Also, a strong coordination between design of the equipment and of the building infrastructure, which so far has not been looked at in detail, is mandatory for this part of the facility. The IAP recommends that in a future EURISOL collaboration the organisational structure be adapted to this need for strong overall coordination of work on the core of the facility.

Science case and user base

The IAP is satisfied with the significantly growing interest in the physics programmes that can be conducted at EURISOL as demonstrated by the many presentations and posters on proposed experiments and experimental equipment. The intense activities for the intermediate facilities, in particular for SPIRAL2 where construction has started now, provide excellent opportunities for the further development of the EURISOL scientific programme and the advanced experimental setups needed for this programme. These facilities will also have an important function in generating the user base for the future EURISOL facility, not only by producing appealing physics results but also by educating the next generation of scientists that will work at EURISOL and are the determining factor for its eventual success.

The creation of the EURISOL User Group has been a crucial step in keeping the community involved. It is crucial that support for the EURISOL User Group is made available during the intermediate period. The IAP was pleased to learn that the next User Group workshop will be held in December 2009 in Catania.

The success of the coordination of the on-going work on both the scientific and the technological front at the intermediate facilities and for EURISOL is in the opinion of the IAP the key factor in generating the long term support needed for EURISOL becoming a reality.

Driver linac

The IAP considers that the design of the driver linac and the beam transport to several production targets simultaneously using Lorentz stripping of H⁻ is well advanced. The study of the effects of tolerances on the beam losses presented at the town meeting gives some confidence in the viability of the very low losses required.

The IAP is confident that solutions will be found for the high losses at a few spots revealed by the calculations.

However, the IAP has serious concerns whether the tracking codes and the modelling of the linac and beam properties are sufficiently accurate to justify the conclusion that the beam losses along the linac will not exceed 1 W/m (0.25 ppm/m @ 1 GeV!) at the confidence level required to decide that hands-on maintenance is feasible.

From the results presented at the current and previous town meetings the IAP concludes that the development programme of the various superconducting cavities for the driver linac has made very significant progress and that no major difficulties are to be expected during the remaining tests.

Multi-MW spallation target

The IAP shares the conclusions of the design review of the multi-MW spallation target in October 2008. In particular the IAP agrees with the recommendation of the review panel that at the current stage the emphasis should be put on the completion of the design of the conventional coaxial mercury target. The IAP feels that collaboration with the European Spallation Source project in Lund offers an excellent opportunity to continue the detailed design of the target after the end of the EURISOL Design Study.

The IAP feels that the expected increase in performance justifies the development of the windowless mercury curtain in a next phase of the EURISOL design study.

Fission target - ion source

The IAP is impressed about the progress made with the development of the MAFF-type fission target and the associated ion sources. The IAP considers that the emphasis of the next stage of the development of the fission targets should be on the technological and radiation safety aspects of the target – ion source system, which are critical for the feasibility of EURISOL, rather than on further optimization of the target material in terms of fission yield and release properties, which obviously have a very significant impact on the performance of EURISOL but not on its fundamental feasibility.

Direct targets

The IAP is positive about the progress in the development of the 100 kW direct targets. The extrapolation from the existing targets developed over many years at ISOLDE and more recently at TRIUMF to the EURISOL objectives is not extreme. The results obtained up to now are promising. Furthermore, the development of these targets fits well with the priorities of ISOLDE and TRIUMF. The IAP therefore considers that the development of the direct targets is on track and does not present a risk for the EURISOL performance.

Beam preparation and ion sources

The IAP is concerned about the progress with the beam preparation task. Progress has been made with the development of high intensity gas-filled RF-coolers, but the overall feasibility of the proposed separation scheme based on small emittance beams and high resolution separators has not been adequately established.

In many cases separation of isobars can not be achieved with the proposed scheme. The IAP considers that the on-going development of element-selective laser ionisation schemes should be significantly expanded to ensure that these ion sources will not be a serious limiting factor for the availability of beams.

The merging of the beams from the different fission targets + ion sources surrounding the multi-MW spallation target into a single charge breeder, which is a critical aspect of the EURISOL project has not been addressed adequately and only an untried concept has been presented up to now.

The IAP observes that the strategy of the beam preparation task to operate the ion sources at a fixed voltage of 60 kV is not compatible with the requirement to inject all different ions with the same velocity (corresponding to 5 keV per nucleon) into the RFQ of the post-accelerator, thus requiring a velocity matching section at the entrance of the post-accelerator. The proposed solutions for this either compromise the overall EURISOL performance or require a significant additional investment.

The IAP is not convinced that the advantages of a fixed source extraction voltage for the operation of the beam preparation section outweigh the inconveniences of the velocity matching section for the operation of the post-accelerator.

Post-accelerator

The IAP agrees with the conclusions of the design review of the post accelerator conducted in October 2008. The superconducting technology adopted for the post-accelerator is a safe extrapolation of that used for the PIAVE and SPIRAL2 linacs. The IAP supports the conclusion of the review panel that there are possibilities for further optimization of the design, resulting in either cost savings or improved performance.

The IAP considers that the results of the study to boost the linac final energy by the use of a stripper and the acceleration of multiple charge states after the stripper are promising and should be further pursued. The safety margin between linac acceptance and beam emittance for this mode of operation seems rather small, in particular when considering that radioactive beams are being accelerated.

The IAP recommends that a beam loss analysis similar to that performed for the driver linac using realistic 4D source emittances be made for all proposed operational modes of the post-accelerator to properly assess the radiation safety issues. Also, the radiation safety consequences of beam tuning procedures should be analysed.

Radiation safety

The IAP is impressed by the progress made in the evaluation of the radiation safety issues of the EURISOL facility and the definition of solutions since the last town meeting. The IAP agrees with the task group that the approaches taken in the evaluation of the radiation and activation levels are rather conservative. This may result in an overestimation of the required shielding and of the need to integrate remote handling into the design of component. In view of the high cost of shielding and remote handling further optimization is needed; the experience gained at in particular SPIRAL2 will be essential for a correct assessment of the needs.

For the post-accelerator more attention should be given to the radiation safety consequences of extended tuning, localized losses and the shielding the beam dumps. The consequences of the exploratory study of the radiation load on the planned AGATA-setup for the design of the experimental setups and the sustainable beam intensities should be assessed and integrated in the design of the relevant equipment as well as in the science case.

The IAP welcomes the initiative presented at the town meeting to establish a risk register for the complete EURISOL facility during the further stages of the design study. The IAP considers that, apart from the legal requirements, such an analysis of the failure modes is also an important tool in the design stage as it enables a quantitative assessment of the risks and associated costs of the different options for a specific piece of equipment. The IAP therefore recommends that a significant effort be made to establish a risk register already at the current stage of the design, where design flaws can still be corrected without too serious consequences. Also, the completion of this analysis will facilitate the continuation of the design study at a later stage because it requires extensive documenting of the design choices made.

Summary of Major Findings and Recommendations

1. *The IAP considers that the dissemination of results from the EURISOL Design Study is up to now rather limited and recommends the development of a policy to ensure that all the results of the EURISOL Design Study will become easily accessible after the end of the present study.*
2. *The IAP recommends completing the risk register and failure analysis for the complete EURISOL design that has been developed in the framework of the current study.*
3. *The IAP strongly supports the efforts to set up a EURISOL collaboration to continue the design of EURISOL. Participation of the intermediate facilities in this collaboration is essential for its success.*
4. *An exciting science case supported by a large and lively user community is an essential factor for the success of any large scale facility. The IAP therefore considers that the efforts of the EURISOL User Group to keep the EURISOL science case exciting and up-to-date and to bring together the future EURISOL users should be strongly supported by a future EURISOL collaboration.*
5. *Considering the limited resources available for continuation of the EURISOL Design Study the IAP suggests to concentrate further studies on a limited number of topic that are critical for the feasibility of the EURISOL concept:*
 - *the coaxial mercury target, preferably in collaboration with ESS. An effort should be made to continue work on the windowless target because of the perspectives for EURISOL performance improvement it holds;*
 - *the MAFF-type fission target in combination with different ion sources, focussing on laser ionisation schemes. The emphasis of this work should be on the technological aspects rather than on the further optimization of the target material;*
 - *system integration of the spallation target and the fission target + ion source;*
 - *beam purification and charge breeding;*
 - *radiation safety of the multi-MW production target and the post-accelerator.”*

We note that several of the areas of concern indicated by the IAP are already earmarked for further research and development proposals at the “intermediate” facilities and elsewhere.

Chapter 18: The Future of EURISOL...

The path towards construction must take into account the technical constraints and the financial and political environments. Europe is currently constructing two major Nuclear Physics facilities: FAIR (at GSI) and SPIRAL2 (at GANIL). In addition two other ISOL facilities are planned, HIE-ISOLDE (at CERN) and SPES (at Legnaro). It has long been recognized that the lessons which will be learnt from the “intermediate generation” ISOL facilities will give essential input to the implementation of EURISOL.

Proposals are also being discussed for possible future development of SPIRAL2 that would enable the intense beams of neutron-rich ions be accelerated to fragmentation energies (100–150·A MeV), which would vastly expand the scientific reach of the facility. At the same time, there are ongoing discussions concerning ISOLDE and the SPL (or the “Light-SPL” version) at CERN: Light SPL will be able to deliver up to 30 kW to the present ISOLDE area at 1.4 GeV. Further improvements would enable up to 150 kW – or even up to 1.6 MW – to be available at CERN, which require a new EURISOL-like target station. Such developments at GANIL and CERN will bring the European ISOL capability closer to EURISOL.

Construction of the ultimate facility will depend on a host country being willing to finance a substantial fraction of the cost of EURISOL, or possibly a consortium of countries to fund the entire project, or alternatively CERN might be a suitable host with an established method of financing new developments.

It is therefore the position of the community represented by NuPECC that construction of EURISOL today would be premature, but that the EURISOL concept must continue to be nurtured and developed with the involvement of the entire community. The Management Board has therefore prepared a path for the future which encompasses several initiatives.

During the Design Study, following a suggestion of the International Advisory Panel, a EURISOL User Group was created. The main objectives of this User Group, according to its charter, are:

- to update and enrich the physics case for EURISOL continuously,
- to contribute to defining the contours and solutions for the EURISOL complex,
- to give a grass-roots input to the European strategy for the development of EURISOL.

A User Group Executive Committee comprising 9 members was elected by the community, and this committee guides the actions of the User Group.

The Management Board of the DS has taken the initiative to create a EURISOL Collaboration to oversee and coordinate the various activities related to EURISOL after the termination of the Design Study. A Memorandum of Understanding is being prepared at the time of writing, and all institutions and laboratories wishing to participate in the future of EURISOL will have the opportunity to sign this MoU. It is envisaged that a Steering Committee – on which all participant institutions should be represented – will pilot the activities of the Collaboration. A project office would take care of the day-to-day management of the Collaboration, with some quite small funding from the participant institutions.

Some actions have already been identified for this Collaboration, namely:

- To apply for a EURISOL networking activity within the ENSAR (European Nuclear Structure and Application Research) integrated initiative in the European Commission’s 7th Framework Program. This network should coordinate Research and Development at the current ISOL facilities with a view towards EURISOL and should promote the development of a coordinated scientific community by organizing Town Meetings and supporting the User Group activities.
- To apply for a EURISOL work package within the TIARA “Preparatory Phase” in the 7th Framework Program. This work package should prepare the R&D platforms which will be

necessary to carry out the R&D work for EURISOL and suggest protocols for their governance.

- To apply for funding for specific EURISOL R&D from the various European funding agencies through the NuPNET network, already established under the 6th Framework Program.

A route to a “Preparatory Phase” funded by the European Commission would only be possible via accession to the list set up by the European Strategy Forum on Research Infrastructures – the so-called “ESFRI List” – and the next update for physics-related projects is scheduled for 2012. At that time the EURISOL concept may be sufficiently mature to be considered as a priority for construction. Application for a Preparatory Phase project could be made, for possible funding through the 8th Framework Program in the period 2014-2017 in which the site would be selected and the legal framework for EURISOL established.

Chapter 18: Conclusion

During the 4½-year period of its existence, the EURISOL Design Study has achieved most of the original aims of the project. A few have not been possible when, for example, unforeseen circumstances led to external facilities envisaged for certain tests being unavailable. The Design Study has provided reports outlining the general layout of the facility and many of the technical solutions for its realization.

Several prototypes of the most challenging elements of EURISOL have been successfully constructed and tested. These include prototypes of possible liquid-metal targets, and one specific coaxial-flow target designed to handle a 4-MW proton beam, and acting as a “converter” target, providing an intense source of spallation neutrons. A feasible system of uranium carbide fission targets surrounding this converter has been proposed, with much detailed design work completed, with provision various types of ion-sources adjacent to the targets including resonant ionization laser sources for selective ionization of nuclei of interest. A method of merging the resulting radioactive ion beams in a novel ARC-ECR ion source has also been proposed, although the efficiency of the merging itself has not been tested. For ions which are not available from neutron induced fission, a number of other combinations of target materials and ion sources have been successfully tested online, based on the use of 100-kW proton beams. A patent application for a nanostructured target material is being processed at the time of writing.

In order to provide these high-intensity beams, a superconducting “driver” accelerator capable of providing a 4-MW beam of H^- ions has been designed, beam dynamics studies have been done and exhaustive Monte-Carlo simulations of beam losses have been made. In order to provide for 100-kW proton beams to be provided at the same time, an innovative magnetic Lorentz-stripping system is proposed, allowing several such beams to be siphoned off in continuously-variable intensities, if desired, without interrupting the main 4-MW beam. This same driver accelerator has been designed to be able to accelerate 100- μ A beams of 2-GeV ^3He ions, as well as 4 mA of 270-MeV deuterons, each of which will be beneficial for the production of certain exotic ion species. Three separate 100-kW target rooms have been suggested, and a multi-level design for their operation has been made.

Beam preparation has also been studied in detail, with proposals for pre-separation of RIBs, followed by a novel design of a high-resolution mass separator. Systems of beam cooling in an RFQ ion-cooler have been tested, which will dramatically improve the emittance and hence the mass-selection process. A switchyard is then proposed leading to a choice of ECRIS or EBIS modules for charge-breeding needed before post-acceleration.

A post-accelerator has been designed, based on a superconducting linac with either a superconducting or a normal-conducting RFQ at the low-energy end. This will be able to accelerate a wide spectrum of ions, and in particular will produce beams of ^{132}Sn at 150-A MeV suitable in particular for fragmentation. A novel fast beam chopper has been developed and prototyped, based on a travelling-wave pulse in a pair of meander strip-line circuits. Several examples of a new type of beam diagnostic device, capable of detecting less than 10^6 pulses per second and based on synthetic polycrystalline diamond, have been prototyped and successfully tested with beams.

Prototypes of superconducting half-wave and spoke-cavity resonators for the linear accelerators have been constructed and tested together with their cold-tuning systems and RF power couplers, and the spoke cavity was tested in a purpose-built cryomodule. A new generation of solid-state RF amplifiers based on MOSFET technology has been developed and tested successfully at 352 MHz in 5-kW and 10-kW modules.

In-target production rates for exotic ions have been predicted, using computer codes which were carefully benchmarked in experiments producing exotic nuclei to verify their cross-sections. Secondary beam intensities have also been calculated, including effects of effusion, diffusion, charge-breeding, etc, with specific reference to fragmentation of the neutron-rich ^{132}Sn ions, which will

produce some very exotic neutron-rich ions. The use of additional driver beams of ^3He or deuterons were studied and their advantages for certain ion species were clearly demonstrated.

Radiation safety at the proposed multi-MW EURISOL facility has been studied, and radiation, activation, shielding and dose-rates have been calculated for the most critical parts of the system. Conformity to legislation in European countries was examined, and aspects such as shielding, dispersion of radioactivity, transport in ground water, nuclear waste and final decommissioning were all studied in detail, and a risk register was drawn up for each part of the facility.

Several key experiments were identified and preliminary designs, simulations and costing of suitable instrumentation for were then carried out, guided in some cases by data from test experiments. A EURISOL User Group was also set up, which will continue to exist beyond the Design Study.

A detailed 3D representation of the EURISOL facility layout was compiled from 3D drawings of the accelerators, target stations and the other sub-systems. Some examples of possible sites were also investigated by an international panel of experts.

A Conceptual Design Report for a beta-beam facility has also been produced, based on the assumption that EURISOL could be constructed at CERN, to use the PS and SPS (or the proposed SPS2) for accelerating ^6He or ^{18}Ne ions to high energy, permitting beta-decay with neutrino or antineutrino emission in the straight sections of an accumulator-type decay ring.

The Design Study provides a firm technical basis for the future construction of a radioactive ion beam facility in Europe, producing vastly improved intensities of exotic ions, and offering unprecedented scientific opportunities to the worldwide Nuclear Physics community.

Publications

Journal articles

1. A. Andrighetto et al., “*On-line Production of Rb and Cs Isotopes from Uranium Carbide Targets*”, Eur. Phys. J. **A23** (2005) 257.
2. A. Andrighetto et al., “*Development of Uranium Carbide Targets for the On-line Production of Neutron-rich Isotopes*”, Nucl. Instrum. Meth. **B 240** (2005) 888.
3. O. Alyakrinskiy et al., “*Absolute Branching Intensity in the Decay of ^{92}Rb to ^{92}Sr* ”, Phys. Rev. **C 74** (2006) 017308.
4. A. Andrighetto et al., “*Combined Target-ion Source Unit for Production of Rare Nuclides*”, Rev. Sci. Instrum. **77** (2006) 705.
5. O. Alyakrinskiy et al., “*Recent Developments and On-line Tests of Uranium Carbide Targets for Production of Nuclides far from Stability*”, Eur. Phys. J. **150** (2007) 297.
6. A.B. Balantekin, J.H. De Jesus, R. Lazauskas, C. Volpe, “A conserved vector current test using low energy beta-beams”, Phys. Rev. **D73** (2006) 073011; [hep-ph/0603078].
7. A.B. Balantekin, J.H. De Jesus and C. Volpe, “Electroweak tests at beta-beams”, Phys. Lett. **B634** (2006) 180 [hep-ph/0512310].
8. M. Benedikt and S. Hancock, “*A novel scheme for injection and stacking of radioactive ions at high energy*”, Nucl. Instrum. & Meth. **A 550** (2005) 1.
9. J. Benlliure et al., “*Production of medium-mass neutron-rich nuclei in reactions induced by ^{136}Xe projectiles at 1 A GeV on a beryllium target*”, Phys. Rev. **C 78** (2008) 054605.
10. Y. Blumenfeld, et al., “*EURISOL Design Study: Toward the Ultimate ISOL Facility for Europe*”, Nucl. Phys. News **19** (2009) No. 1, p22.
11. Y. Blumenfeld and M. Lindroos, “*Physics and Technology for the Next-Generation ISOL Facility: EURISOL*”: Article for the 50th edition of the ‘*Karlsruhe Nuclidkarte*’.
12. Y. Blumenfeld, “*Report on the EURISOL Design Study Week (2007)*”, published in Nucl. Phys. News **17** (2007).
13. S. Chabod et al., “*In-target rare nuclei production rates with EURISOL single-stage configuration*”, submitted to Phys. Rev. ST-Accelerators & Beams.
14. M. Cheikh Mhamed et al., “*Two-dimensional/three-dimensional simulations for the optimization of an electron-beam-generated-plasma-based-type ion source*”, Rev. Sci. Instrum. **79** (2008) 02B911.
15. M. Cheikh Mhamed et al., “*Development of a plasma ion source for next-generation facilities*”, Rev. Sci. Instrum. **77** (2006) 03A702.
16. D. Ene et al., “*Radiation protection aspects of the EURISOL Multi-MW target shielding*”, submitted to Annals in Nuclear Energy.
17. D. Ene et al., “*Characterization of the EURISOL Multi Mega Watt fission target in term of radioprotection and in-target production rates*”, to be published in Eur. Phys. J. A as a Scientific Note.
18. A. Facco et al., “*Low- and intermediate- β 352 MHz superconducting half-wave resonators for high power hadron acceleration*”, Phys. Rev. ST Accel. Beams **9**, 110101 (2006).
19. A. Facco, R. Paparella, D. Berkovits and I. Yamane, “*Splitting of high power, cw proton beams*”, Phys. Rev. ST Accelerators & Beams **10** (2007) 091001.
20. N. Jachowicz, G.C. McLaughlin, C. Volpe, “*Untangling supernova-neutrino oscillations with beta-beam data*”, Phys. Rev. **C 77** (2008) 055501; [arXiv:0804.0360].
21. A. Jokinen et al., “*Precision experiments on exotic nuclei at IGISOL*”, Int. J. Mass Spectrometry **251** (2006) 204.
22. Y. Kadi et al., “*EURISOL High Power Target*”, Nucl. Phys. News, **18** (2008) 19.

23. C. Lau et al., “*Contribution to ion-source developments for SPIRAL-2 and EURISOL*”, Rev. Sci. Instrum. **77** (2006) 03A706.
24. C. Lau et al., “*Status of ionization by radial electron neat adaptation ion source research and development for SPIRAL2 and EURISOL-DS*”, Rev. Sci. Instrum. **79** (2008) 02A903.
25. C. Omet et al., “*Charge change-induced beam losses under dynamic vacuum conditions in ring accelerators*”, New J. of Physics **8** (2006) 284.
26. R. Lazauskas, A.B. Balantekin, J.H. de Jesus and C. Volpe, “*Low-energy neutrinos at off-axis from a standard beta-beam*”, Phys. Rev. **D 76**, 053006 (2007).
27. R. Lazauskas and C. Volpe, “*Neutrino beams as a probe of the nuclear isospin and spin-isospin excitations*”, Nucl. Phys. **A 792** (2007) 219.
28. G. Lhersonneau et al., “*Influence of Radiative Filiation on Measured Release Curves*”, Nucl. Instrum. & Meth. **A566** (2006) 465.
29. S. Lukic et al., “*Systematic comparison of ISOLDE-SC yields with calculated in-target production rates*”, Nucl. Instrum. & Meth. **A 565** (2006) 784.
30. R. Milencović et al., “*Wavelet analysis of experimental results for coupled structural-hydraulic behaviour of the EURISOL target mock-up*”, Nucl. Instrum. & Meth. **A** (in press).
31. R. Milencović et al., “*Structural-hydraulic test of the liquid metal EURISOL target mock-up*”, Nucl. Instrum. & Meth. **A** (in press).
32. R.D. Page, A. Bonaccorso and N.A. Orr, “*Physics Opportunities with EURISOL*”, Nucl. Phys. News **16** (2006) 39.
33. H. Penttilä et al., “*Independent fission yields with JYFLTRAP*”, Eur. Phys. J. Special Topics **150** (2007) 317.
34. V.A. Rubchenya, “*Prompt fission neutron emission in neutron and proton induced reactions at intermediate energies*”, Phys. Rev. **C 75**, 054601 (2007).
35. K-H. Schmidt et al., “*Studies on the benefit of extended capabilities of the driver accelerator for EURISOL*”, Phys. Rev. ST-Accelerators & Beams **10**, 14701.
36. K. Samec et al., “*Design of a compact high-power neutron source – The EURISOL converter target*”, Nucl. Instrum. & Meth. **A 606** (2009) 281.
37. K. Subotic et al., “*ANAMARI simulation code for gas-filled separators and spectrometers*”, Nucl. Instrum. & Meth. **B 266** (2008) 4209.
38. M. Veselsky and G. Souliotis, “*Production of cold fragments in nucleus-nucleus collisions in the Fermi-energy domain*”, Nucl. Phys. **A 781** (2007) 521.
39. C. Volpe, “*Low energy neutrino interactions: from fundamental interaction studies to astrophysics*”, Acta Polonica, in press; [arXiv:0906.1476].
40. C. Volpe, “*Topical review on beta-beams*”, J. Phys. **G34** (2007) R1; [hep-ph/0605033].
41. R. Wilfinger and J. Lettry, “*Feasibility of High Power Refractory Metal-Foil Targets for EURISOL*”, Eur. Phys. J. Special Topics **150** (2007) 379.
42. A. Zukauskaitė et al., “*Modelling of neutron and photon transport in iron and concrete radiation shields by using the Monte-Carlo method*”, Lithuanian J. Phys **47** (2007) 97.

Conference contributions

1. H. Alvarez-Pol et al., “*Expanding the limits of the chart of nuclides using projectile fragmentation reactions*”, Fifth Internat. Conf. on Exotic Nuclei and Atomic Masses (ENAM'08), September 7-13 2008, Ryn, Poland.
2. O. Alyakrinskiy et al., “*Study of Uranium Carbide Targets of a High Density*”, Proc XVth Internat. Conf. on Electromagnetic Isotope Separators and Techniques Related to their Applications (EMIS07), Deauville, France, 24-29 June 2007, Nucl. Instrum. & Meth. **B266** (2008) 4247.

3. O. Alyakrinskiy et al., “**Electron Beam-plasma Ionizing Target for the Production of Neutron-rich Nuclides**”, Proc XVth Internat. Conf. on Electromagnetic Isotope Separators and Techniques Related to their Applications, (EMIS07), Deauville, France, 24-29 June 2007, Nucl. Instrum. & Meth. **B266** (2008) 4294.
4. O. Alyakrinskiy et al., “**Influence of Decay in the Target on the Measurement of Release Times and Release Efficiency**”, Proc XVth Internat. Conf. on Electromagnetic Isotope Separators and Techniques Related to their Applications, (EMIS07), Deauville, France, 24-29 June 2007, Nucl. Instrum. & Meth. **B266** (2008) 4314.
5. O. Alyakrinskiy et al., “**Tests of High-density UC Targets Development at Gatchina for Neutron-rich Radioactive Beam Facilities**”, Proc XVth Internat. Conf. on Electromagnetic Isotope Separators and Techniques Related to their Applications, (EMIS07), Deauville, France, 24-29 June 2007, Nucl. Instrum. & Meth. **B266** (2008) 4326-4329.
6. A. Bechtold et al., “**The MAFF IH-RFQ Test Stand at the IAP Frankfurt**”, Proc. 10th European Particle Accelerator Conf., Edinburgh, 26–30 June 2006 (EPAC06).
7. A. Bechtold and H.Podlech, “**Proposal for a Normal Conducting CW-RFQ for the EURISOL Post-Accelerator and dedicated β -beam Linac Concept**”, Proc. 10th European Particle Accelerator Conf., Edinburgh, 26–30 June 2006 (EPAC06).
8. M. Benedikt et al., “**Estimation of Decay Losses and Dynamic Vacuum for the Beta-beam Accelerator Chain**”, Proc. 10th European Particle Accelerator Conf., Edinburgh, 26–30 June 2006 (EPAC06).
9. J. Benlliure, “**The nuclear landscape seen by the next-generation RIB facilities**”, European Radioactive Ion Beam Conf., Giens, France June 9-13, 2008 (EURORIB08).
10. J. Benlliure et al., “**Production of heavy neutron-rich nuclei ‘south’ of lead**”, Proc. 7th Internat. Conf. on Radioactive Nuclear Beams, July 2-7, 2006 Cortina, Italy, Euro. Phys. J. Special Topics **150** (2007) 309.
11. Y. Blumenfeld et al., “**EURISOL Design Study : Towards an Ultimate ISOL Facility for Europe**”, Invited talk at Franco-Japanese Symposium: New Paradigms in Nuclear Physics. Paris, France, Sept.29 – Oct.2, 2008; EURISOL DS technical note 01-23-2009-0021.
12. Y. Blumenfeld, “**Developments at ISOL facilities: from ISOLDE towards EURISOL**”, Invited talk at Internat. symposium on Exotic Nuclei, EXON 2009, Sochi, Russia, Sept 28-Oct 2, 2009; EURISOL DS technical note 01-22-2009-0064.
13. Y. Blumenfeld, “**Towards New-Generation ISOL Facilities: HIE-ISOLDE and EURISOL**”, Invited talk at SARAF workshop, October 27-29, 2008, Maale Hachamisha (Jerusalem), Israel; EURISOL DS technical note 01-22-2008-0053.
14. Y. Blumenfeld, “**Review of Accelerators for Radioactive Beams**”, Invited talk at European Particle Accelerator Conf., Genoa, Italy, June 23-27, 2008, (EPAC08); EURISOL DS technical note 01-22-2008-0049.
15. Yorick Blumenfeld, “**Radioactive Beam Facilities in Europe: Status and Plans**”, invited talk at 15th Internat. Conf. on Electro-Magnetic Separators and Techniques Related to their Applications (EMIS07), Deauville, France, June 25-29, 2007, Nucl. Instrum & Meth. **B266** (2008) and EURISOL DS technical note 01-23-2007-0015.
16. Y. Blumenfeld et al., “**Nuclear Physics: The EURISOL Project**”, invited talk at Tours Symposium on Nuclear Physics VI, Tours, France, Sept 5-8 2006; EURISOL DS technical note 01-23-2006-0010.
17. Y. Blumenfeld, “**EURISOL : European Collaboration towards the Ultimate ISOL Facility**”, Presentation to the OECD Global Science Forum – Working Group on Nuclear Physics, Rome, Oct 10-11 2006; EURISOL DS technical note 01-25-2006-0005.
18. E. Bouquerel et al., “**TARPIPE: TARget Prototype Irradiations at PSI for EURISOL**”, 7th Internat. Conf. on Radioactive Nuclear Beams (RNB7), Cortina d'Ampezzo, Italy, 3–7 July 2006; EURISOL DS technical note 03-22-2006-0010.
19. E. Bouquerel et al., “**Alkali suppression for pure Radioactive Ion Beam (RIB) production**”, 7th Internat. Conf. on Radioactive Nuclear Beams (RNB7), Cortina d'Ampezzo, Italy, 3–7 July, 2006; EURISOL DS technical note 03-22-2006-0009.
20. P.A. Butler, “**The first steps to EURISOL**”, Zakopane 2006 Conf. on Nuclear Physics, 4–10/10/2006, Zakopane, Poland; Acta Polonica **B38** (2007) 1147; EURISOL DS technical note 01-23-2006-0011.

21. A. Chancé et al., *“The Beta-beam Decay Ring Design”*, Proc. 10th European Particle Accelerator Conf., Edinburgh, 26–30 June 2006 (EPAC06).
22. A. Chancé et al., *“The Loss Management in the Beta-beam Decay Ring”*, Proc. 10th European Particle Accelerator Conf., Edinburgh, 26–30 June 2006 (EPAC06).
23. A. Chancé and J. Payet, *“Studies of the injection system in the decay ring of a Beta-beam neutrino source”*, PAC 2005.
24. S. Chiriki et al., *“Decommissioning and safety issues of liquid-mercury waste generated from high power spallation sources with particle accelerators”*, Joint 11th Internat. Conf. on Radiation Shielding (ICRS-11) and 15th Topical Meeting of the Radiation Protection and Shielding Division (RPSD-2008), 13-18 April 2008, Georgia, USA .
25. P. Delahaye, M. Marie-Jeanne, *“Potentials of the ECR 1+ n+ charge breeding for radioactive ions”*, Proc. 15th Internat. Conf. on Electro-Magnetic Separators and Techniques (EMIS07), Deauville/France, June 24-29, 2007, Nucl. Instrum. & Meth. **B 266** (2008) 4429.
26. M. Eller, J. Lettry, R. Catherall and T. Stora, *“Calculation of Production and Decay of Radioisotopes for Future Irradiation Experiments and Ion Beam Facilities”*, 7th Internat. Conf. on Radioactive Nuclear Beams (RNB7), Cortina d'Ampezzo, Italy, 3–7 July 2006, Eur. Phys. J. Special Topics **150** (2007) 233; EURISOL DS technical note 03-22-2006-0014.
27. D. Ene, et al., *“Preliminary shielding assessment of EURISOL post-accelerator”*, Joint 11th Internat. Conf. on Radiation Shielding (ICRS-11) and 15th Topical Meeting of the Radiation Protection and Shielding Division (RPSD-2008), 13-18 April 2008, Georgia, USA .
28. D. Ene, et al., *“Activation studies of the shielding structures for the EURISOL 4-MW target station in terms of the waste characterization for final disposal”*, First Internat. Workshop on Accelerator Radiation Induced Activation, Paul Scherrer Institute, Switzerland October 13-17, 2008 (ARIA'08).
29. D. Ene, J-C. David, D. Doré and D. Ridikas, *“Lay-out of the EURISOL experimental hall”*, Internat. Topical Meeting on Nuclear Research Applications and Utilization of Accelerators, Vienna, Austria., 4–8 May 2009.
30. D. Ene, J-C. David, D. Doré and D. Ridikas, *“Radiological safety aspects of the design of RNB facilities , 11th Internat. Conf. on Heavy Ion Accelerator Technology, 2009 (HIAT09).*
31. EURISOL Group, *“The EURISOL Beta-Beam Facility”*, Neutrino Oscillation Workshop, Gran Sasso, June 2007.
32. A. Facco et al., *“Low- and intermediate-beta, 352-MHz superconducting half-wave resonators for high-power hadron acceleration”*, Proc. 10th European Particle Accelerator Conf., Edinburgh, 26–30 June 2006 (EPAC06).
33. A. Facco et al., *“Beam dynamics studies on the EURISOL driver accelerator”*, Proc. XXIV Linear Accelerator Conf., Vancouver, Canada, Sep. 29 – Oct 23, 2008 (LINAC08).
34. A. Facco, *“The EURISOL program”*, Proc. High Power Superconducting Ion, Proton, and Multi-Species Linacs Workshop, Northern Illinois U., Naperville, IL, USA, May 22-24, 2005 (HPSL 2005).
35. M. Felcini, *“Dose estimates and shielding design for the EURISOL facility”* Proc. Internat. Workshop on Shielding Aspects of Accelerators, Targets and Irradiation Facilities (SATIF-8), Pohang, South Korea, 22/05/2006 - 24/05/2006.
36. B. Fernández-Domínguez et al., *“Spectroscopy of ²¹O through (d,p) reaction with the TIARA-MUST2-VAMOS-EXOGAM set-up”*, European Radioactive Ion Beam Conf., Giens, France, June 9–13, 2008 (EURORIB08).
37. G. Fortuna et al., *“Status and achievements of the EURISOL DS in the first year of activity”*, 7th Internat. Conf. on Radioactive Nuclear Beams (RNB7), Cortina d' Ampezzo, Italy, 3–7 July 2006; EURISOL DS technical note 01-25-2006-0001.
38. H. Frånberg et al., *“Off-line commissioning of the ISOLDE cooler”*, Proc. 15th Internat. Conf. on Electro-Magnetic Separators and Techniques (EMIS07), Deauville/France, June 24-29, 2007, Nucl. Instrum. & Meth. **B 266** (2008) 4502.
39. O. Gianfrancesco et al., *“A radiofrequency quadrupole cooler for high-intensity beams”*, Proc. 15th Internat. Conf. on Electro-Magnetic Separators and Techniques (EMIS07), Deauville/France, June 24-29, 2007, Nucl. Instrum. & Meth. **B 266** (2008) 4483.

40. S. Hancock et al., “*Stacking Simulations in the Beta-beam Decay Ring*”, Proc. 10th European Particle Accelerator Conf., Edinburgh, 26–30 June 2006 (EPAC06).
41. A. Herrera-Martínez and Y. Kadi, “*Radioactive Ion Beam Production by Fast-Neutron-Induced Fission in Actinide Targets at EURISOL*” Proc. Internat. Workshop on Fast Neutron Detectors and Applications (FNDA06) 3-6 April 2006, Cape Town, South Africa; Proceedings of Science <http://pos.sissa.it/>.
42. A. Herrera-Martínez et al., “*Engineering Design of the EURISOL Multi-MW Spallation Target*”, Proc. High-Power Proton Accelerator Conf., 2007 (HPPA07).
43. A. Källberg, “*A Low Energy Accumulation Stage for a Beta-beam Facility*”, Proc. 10th European Particle Accelerator Conf., Edinburgh, 26–30 June 2006 (EPAC06).
44. A. Kelic et al, “*ABLA07 – Towards a complete description of the decay channels of a nuclear system from spontaneous fission to multifragmentation*”, Proc. Joint ICTP-IAEA Advanced Workshop on Model Codes for Spallation Reactions, February 4-8, 2008, ICTP-Trieste (Italy).
45. A. Kelic et al, “*New Results on Nuclear Fission – Data and Interpretation*”, Proc. Conf. on Compound-Nuclear Reactions and Related Topics, October 22–26, 2007, Tenaya Lodge at Yosemite National Park, Fish Camp, California (USA).
46. C. Kharoua, “*The multi-megawatt target station of EURISOL facility and its performance*”, Ninth Meeting on Shielding Aspects of Accelerators, Targets and Irradiation Facilities (SATIF9) Oak Ridge, TN, USA, 21-23 April 2008.
47. C. Kharoua, “*The multi-megawatt target station of EURISOL: high-power deposition on the spallation and the actinides targets*”, Ninth Meeting on Shielding Aspects of Accelerators, Targets and Irradiation Facilities (SATIF9) Oak Ridge, TN, USA, 21-23 April 2008.
48. C. Kharoua et al., “*The Multi-MW Target Station*”, Proc. 3rd High Power Targetry Workshop, Sept. 10–14, 2007, Bad Zurzach, Switzerland.
49. A. J. Kordyasz and E. Kulczycka, “*Double-sided strip monolithic silicon E-ΔE telescope produced by quasi-selective epitaxy*”, Nucl. Instrum. & Meth. A **596** (2008) 131, Proc. 8th Internat. Conf. on Large Scale Applications and Radiation Hardness of Semiconductor Detectors.
50. G. Le Dem and M. Di Giacomo, “*A Single Bunch Selector for the Next Low Continuous Wave Heavy Ion Beam*”, Proc 22nd Particle Accelerator Conf, Albuquerque, new Mexico, USA, June 25-29, 2007 (PAC07), <http://cern.ch/AccelConf/p07/PAPERS/MOPAN008.PDF>.
51. M. Lindroos et al., “*EURISOL - exploring the limits of the ISOL technology (and stability of nuclear matter)*”, European Radioactive Ion Beam Conf., Giens, France, June 9–13, 2008 (EURORIB08); EURISOL DS technical note 01-22-2008-0047.
52. M. Lindroos, “*Future options for the beta-beam with a focus on production issues*”, Ninth Internat. Workshop on Neutrino Factories, Superbeams and Beta-beams, Okayama, Japan, Aug 6–11, 2007 (NUFACT07).
53. Rainer Moormann, Klaus Bongardt and Suresh Chiriki, “*Safety aspects of high-power targets for European spallation sources*”, Internat. Conf. PHYSOR08, Interlaken, Switzerland, 14-19 September 2008.
54. J. Neuhausen et al., “*Mercury Purification in the Megawatt Liquid-Metal Spallation Target of EURISOL-DS*” Proc. Eighth Internat. Topical Meeting on Nuclear Applications and Utilization of Accelerators (AccApp’07), Pocatello, Idaho, July 29–Aug. 2, 2007, American Nuclear Society, LaGrange Park, Illinois, USA.
55. Juergen Neumayr et al., “*Localization of volatile isotopes on a cryotrap*”, Spring Meeting of the German Physical Society (section for Hadrons and Nuclei), Giessen/Germany, March 2007.
56. E. Noah et al., “*Driver beam-led EURISOL target design constraints*”, Proc. 11th European Particle Accelerator Conf., Genoa, Italy, June 23–27, 2008 (EPAC08); EURISOL DS technical note 03-21-2008-0018.
57. E. Noah et al., “*EURISOL 100-kW target stations operation and implication for its proton driver beam*”, Proc. 10th European Particle Accelerator Conf., Edinburgh, 26–30 June 2006 (EPAC06); EURISOL DS technical note 03-21-2008-0017.
58. M.Pasini, O.Kester, D.Habs and T.Sieber, “*RF Design of the MAFF IH-RFQ*”, Proc. 9th European Particle Accelerator Conf., Lucerne, Switzerland, 5–9 July 2004 (EPAC04) p.1216.

59. M.Pasini, O.Kester, A.Bechtold and A.Schempp, “*Beam Dynamics Studies for the Low Energy Section at MAFF*”, Proc. 9th European Particle Accelerator Conf., Lucerne, Switzerland, 5–9 July 2004 (EPAC04).
60. H. Penttilä et al., “*Fission yield measurements at the IGISOL facility with JYFLTRAP*”, Proc. 4th Internat. Conf. on Fission and Properties of Neutron-Rich Nuclei, Sanibel Island, USA, 11 - 17 November 2007, ed. J.H. Hamilton, A.V.Ramayya and H.K.Carter, World Scientific, Singapore, 2008.
61. D. Perez et al., “*Production of medium-mass neutron-rich nuclei from fragmentation of fission residues around 132Sn*”, Zakopane Conf. on Nuclear Physics, September 1-7, 2008 Zakopane, Poland.
62. P.A. Posocco, G. Bisoffi, A. Palmieri, A. Pisent, “*The superconducting solution for the EURISOL DS post-accelerator injector*”, Proc. 11th European Particle Accelerator Conf., Genoa, Italy, June 23–27, 2008 (EPAC08).
63. N. Prolingheuer et al., “*A simplified method for estimation of groundwater contamination surrounding accelerators and high power targets*”, Joint 11th Internat. Conf. on Radiation Shielding (ICRS-11) and 15th Topical Meeting of the Radiation Protection and Shielding Division (RPSD-2008) of the American Nuclear Society, April 13-18, 2008, Georgia, USA.
64. B. Rapp et al., “*Benchmarking of the modelling tools within the EURISOL DS project*”, Proc. Internat. Workshop on Shielding Aspects of Accelerators, Targets and Irradiation Facilities (SATIF-8), Pohang, South Korea, 22–24/05/2006.
65. M.V. Ricciardi et al., “*Secondary-beam production: protons versus heavy ions*”, Proc. 7th Internat. Conf. on Radioactive Nuclear Beams, July 02-07, 2006 Cortina, Italy; Euro. Phys. J. Special Topics **150** (2007) 321.
66. D. Ridikas et al., “*Safety and Radioprotection issues within the EURISOL DS project*”, Proceedings of the American Nuclear Society’s 14th Biennial Topical Meeting of the Radiation Protection and Shielding Division, Carlsbad New Mexico, USA. April 3-6, 2006.
67. D. Ridikas and A. Herrera-Martínez, “*Radiation Safety with High-Power Operation of EURISOL*”, The Eighth Internat. Topical Meeting on Nuclear Applications and Utilization of Accelerators (AccApp07), July 30–Aug. 2, 2007 in Pocatello, Idaho, USA.
68. Danas Ridikas et al., “*Measurements of Delayed Neutrons Yields and Time Spectra from 1 GeV protons interacting with thick natural Pb targets*”, Proc. Conf. PHYSOR2006, Vancouver, Canada, 10-14 Sept. 2006; ISBN-0-89448-697-7 (2006) B104.
69. D. Ridikas and A. Herrera-Martínez, “*Radiation Safety with High-Power Operation of EURISOL*” Proc. Eighth Internat. Topical Meeting on Nuclear Applications and Utilization of Accelerators (AccApp’07), Pocatello, Idaho, July 29–Aug. 2, 2007, American Nuclear Society, LaGrange Park, Illinois, USA.
70. J. Rodnizki et al., “*Beam dynamics simulations of SARAF accelerator including error propagation and implications for the EURISOL driver*”, Proc. 2006 Linear Accelerator Accelerator Conf., Aug. 20–25, Knoxville, Tennessee, USA. (LINAC06).
71. B.T. Roeder, F. Delaunay, F.M. Marqués and N.A. Orr, “*Next-generation fast neutron detectors for experiments with exotic beams*”, XVth Internat. Conf. on Electromagnetic Isotope Separators and Techniques Related to their Applications, Deauville, France, June 24-29, 2007 (EMIS07).
72. Y. Romanets et al., “*EURISOL-DS multi-MW Hg target: neutron flux and fission rate calculations for the MAFF configuration*” (ICRS11).
73. T. Stora et al., “*First negative halogen beams produced at PSBooster-ISOLDE*”, Presented at the RNB7 conference Cortina d’Ampezzo, Italy, July 3 - 7, 2006, EURISOL DS technical note 03-22-2006-0011.
74. P.G. Thirolf et al., “*Localization of volatile isotopes on a cryotrap*”, Proc. 15th Internat. Conf. on Electro-Magnetic Separators and Techniques (EMIS07), Deauville/France, June 24-29, 2007, Nucl. Instrum. & Meth. **B 266** (2008) 4505.
75. M Veselsky, “*Production of neutron-rich nuclei in the nucleus-nucleus collisions around the Fermi-energy*”, Proc. 9th Internat. Workshop Relativistic Nucl. Phys. from hundreds of MeV to TeV, Modra-Harmonia, Slovakia, May 22-27, 2006; JINR (2006) 282.
76. C. Volpe, “*Low energy neutrino interactions: from fundamental interaction studies to astrophysics*”, 45th Karpacz winter workshop in Theoretical Physics.
77. C. Volpe, “*Neutrino physics*”, European Radioactive Ion Beam Conf., Giens, France June 9-13, 2008 (EURORIB08)

78. C. Volpe, “*Beta-beams*”, Proc. 13th Lomonosov Conf. on Elementary Particle Physics, Moscow, Russia, 23-29 Aug 2007; [arXiv:0802.3352].
79. C. Volpe, “*Physics with a very first low-energy beta-beam*”, 7th International Workshop on Neutrino Factories and Superbeams, Frascati (Rome) June 21 - 26, 2005 (NUFACT05).
80. C. Volpe, “*Physics with a very first low-energy beta-beam*”, Nucl. Phys. Proc. Suppl. **155**, (2006) 97; [hep-ph/0510242].
81. R. Wilfing, J. Lettry, “*Feasibility of High Power Refractory Metal Foil-Targets for EURISOL*”, 7th Internat. Conf. on Radioactive Nuclear Beams (RNB7), Cortina d'Ampezzo, Italy, 3–7 July 2006, Eur. Phys. J. Special Topics, **150** (2007).379; EURISOL DS technical note 03-22-2006-0012.
82. M. Yanyun, A. Facco, F. Scarpa and V. Zvyagintsev, “*Design Optimisation of the EURISOL Driver Low-beta Cavities*”, Proc. 14th Internat. Conf. on Radio-Frequency Superconductivity (SRF 09), Berlin, Germany, 21-25 September 2008.
83. H.Zimmermann et al., “*Beam Tests with the MAFF IH-RFQ at the IAP-Frankfurt*”, Proc. 11th European Particle Accelerator Conf., Genoa, Italy, June 23–27, 2008 (EPAC08).

Technical Notes

Task 1: Management

1. S Brandenburg, W. Nazarewicz and P. Schmor, “*EURISOL Design Study Internat. Advisory Panel report*”.
2. G. Cuttone et al., “*EURISOL Site Investigation Panel Report*”, EURISOL DS technical note 01-25-2009-0013.
3. EURISOL DS Management Board, “*Report on Facility Layout*”, EURISOL DS technical note 01-25-2009-0014.
4. EURISOL DS Management Board, “*Report on Cost Estimation*”, EURISOL DS 01-25-2009-0015.
5. Yorick Blumenfeld, “*EURISOL : Vers une nouvelle génération de faisceaux radioactifs pour l'Europe*”, in “*La lettre de l'IPN Orsay*” (internal laboratory publication); EURISOL DS technical note 01-25-2009-0006.

Task 2: Multi-MW Target

6. A. Herrera-Martinez and Y. Kadi, “*EURISOL Multi-MW Target: Preliminary Study*”, EURISOL DS technical note 02-25-2005-0001.
7. Y. Kadi, “*Multi-MW target station*”, EURISOL DS technical note 02-25-2005-0002.
8. J. Freibergs et al., “*EURISOL Multi-MW Target: Investigation of the hydrodynamics of liquid-metal (Hg) jet*”, EURISOL DS technical note 02-25-2006-0003.
9. T.V. Dury., “*EURISOL Multi-MW Target: First thermal-hydraulic studies for the EURISOL high-power liquid-metal target using Computational Fluid Dynamics*”, EURISOL DS technical note 02-25-2006-0004.
10. A. Herrera-Martínez and Y. Kadi, “*EURISOL-DS Multi-MW Target Neutronic Calculations for the Baseline Configuration of the Multi-MW Target*”, EURISOL DS technical note 02-25-2006-0005.
11. A. Herrera-Martinez and Y. Kadi, “*Multi-MW target station: Neutronic Calculations of the Baseline Design*”, EURISOL DS technical note 02-25-2006-0006.
12. A. Herrera-Martinez and Y. Kadi, “*HIE-ISOLDE: Baseline Design of a Solid Neutron Converter Driven by 160 MeV Protons*”, EURISOL DS technical note 02-25-2006-0007.
13. A.Herrera-Martinez and Y.Kadi, “*Multi-MW target station: Comparative Neutronic Performance of the Baseline Configuration vs. the Hg-Jet Option*”, EURISOL DS technical note 02-25-2006-0008.
14. Q. Prétet, R. Milenkovic and B. Smith, “*Stress Analysis of the EURISOL DS target*”, EURISOL DS technical note 02-25-2006-0009.
15. Y.Kadi and A.Herrera-Martinez , “*HIE-ISOLDE: Baseline Design of a Solid Neutron Converter Driven by 160 MeV Protons*”, EURISOL DS technical note 02-25-2006-0010.

16. Y.Kadi, “*Multi-MW target station: Baseline Parameters*”, EURISOL DS technical note 02-25-2006-0011.
17. Q. Pr  tet, R. Milenkovic and B. Smith, “*Stress Analysis of the target window*”, EURISOL DS technical note 02-25-2006-0012.
18. K. Samec, “*Best-estimate fit for EURISOL Heat Deposition Profile*”, EURISOL DS technical note 02-25-2006-0013.
19. K. Samec, “*Best-estimate fit for EURISOL Heat Deposition Profiles, 24.01.0*”, EURISOL DS technical note 02-25-2007-0014.
20. A.Herrera-Martinez and Y.Kadi, “*Multi-MW target station: Beam Window Issues and Transverse Film Target*”, EURISOL DS technical note 02-25-2007-0015.
21. M. Ashrafi-Nik, “*Thermo-Hydraulic Optimisation of the EURISOL-DS Multi-MW Hg target*”, EURISOL DS technical note 02-25-2007-0016.
22. J. Freibergs et al., “*Engineering design and construction of a function Hg – loop & Contribution of IPUL in windowless Hg-target feasibility studies*”, EURISOL DS technical note 02-25-2007-0017.
23. M. Ashrafi-Nik, “*Beam influence on thermal-hydraulics of EURISOL DS*”, EURISOL DS technical note 02-25-2008-0018.
24. K. Samec, “*Design of the EURISOL converter target*”, EURISOL DS technical note 02-25-2008-0019.
25. Y. Kadi, C. Kharoua and Y. Romanets, “*EURISOL-DS Multi-MW Hg Target: Parameter List*”, EURISOL DS technical note 02-25-2008-0020.
26. Stefan Joray, “*EURISOL-DS METEX: Cooling and Temperature Control of the Mercury Loop*”, EURISOL DS technical note 02-25-2008-0021.
27. V. Geza and R. Milenkovic, “*Hydraulic simulation of the flow condition at the inlet of the beam entrance window of the EURISOL converter target*”, EURISOL DS technical note 02-25-2008-0022.
28. R. Milenkovic et al., “*EURISOL-DS METEX: Post-processing of the experimental data: Test matrix, Pre-calculations, Data Recording and Mining, Statistical and Advance Data Analysis*”, EURISOL DS technical note 02-25-2008-0023.
29. S. Demetjews, “*EURISOL-DS METEX1: Hydraulic mercury test of the target mock-up. Technical requirements on mercury loop*”, EURISOL DS technical note 02-25-2008-0024.
30. E. Platacis et al., “*EURISOL-DS METEX: Operation Manual for the METEX1-Exeriment in IPUL*”, EURISOL DS technical note 02-25-2008-0025.
31. J.Gulley, “*EURISOL-DS METEX: CERN Safety Commission Recommendations*”, EURISOL DS technical note 02-25-2008-0026.
32. J. Lettry et al., “*EURISOL-DS METEX1: LDV measurement to detect cavitations*”, EURISOL DS technical note 02-25-2008-0027.
33. A. Vetter, “*Design of a liquid metal target loop for a high power spallation*”, EURISOL DS technical note 02-25-2008-0028.
34. C. Kharoua et al., “*EURISOL-DS Multi-MW Target Preliminary Study of the Windowless Transverse-Film Liquid-Metal Proton-to-Neutron Converter*”, EURISOL DS technical note 02-25-2008-0029.
35. C. Kharoua and Y. Kadi, “*EURISOL-DS Multi-MW Target Preliminary Study of the Thermal Behaviour of the fission target inspired by the MAFF project*”, EURISOL DS technical note 02-25-2008-0030.

Task 3: 100-kW Direct Target

36. T. Stora et al., “*D5-Comparison of targets*”, EURISOL DS technical note 03-25-2009-0017.
37. S. Fernandes et al., “*On-line tests of a high- power Al₂O₃ EURISOL target prototype*”, EURISOL DS technical note 03-25-2009-0016.
38. T. Stora et al., “*On-line tests of a high-power solid Al₂O₃ EURISOL target prototype*”, EURISOL DS technical note 03-25-2009-0014.
39. E. Noah et al., “*TARPIPE: target prototype irradiations at PSI for EURISOL*”, EURISOL DS technical note 03-25-2009-0015.

40. R. Wilfinger and L. Bruno, “*Considerations on the proton beam shape for refractory metal foil Targets*”, EURISOL DS technical note 03-25-2008-0012.
41. S. Fernandes et al., “*Diffusion studies in prospective polycrystalline silicon carbide target materials for radioactive ion beam production at CERN-ISOLDE*”, EURISOL DS technical note 03-25-2008-0010.
42. E. Bouquerel et al., “*Design and test of a two-body target unit for 100kW solid targets*”, EURISOL DS technical note 03-25-2008-0009.
43. E. Bouquerel et al., “*EURISOL High Power Oxide Target Tests at TRIUMF*”, Project proposal at TRIUMF, EURISOL DS technical note 03-25-2008-0007.
44. E. Noah, “*Engineering aspects for the EURISOL 100-kW liquid-metal targets*”, EURISOL DS technical note 03-25-2008-0006.
45. T. Stora et al., “*Feasibility study for the 100-kW direct targets*”, EURISOL DS technical note 03-25-2008-0005.
46. N. Thiollieres, “*Optimization of ${}^6\text{He}$ production using W or Ta converter surrounded by BeO target assembly*”, EURISOL DS technical note 03-25-2008-0004.
47. T. Stora, E. Bouquerel and J. Lettry, “*W converter - BeO dual target prototype for ${}^6\text{He}$ production - a preliminary note*”, EURISOL DS technical note 03-25-2008-0003.
48. T. Stora et al., “*Baseline parameters 05/2005*”, EURISOL DS technical note 03-25-2008-0002.
49. L. Zanini, “*Radioprotection calculations for the EURISOL-DS direct target irradiation program at PSI*”, EURISOL DS technical note 03-25-2008-0001.

Task 4: Fission Targets

50. O. Alyakrinskiy and L.B. Tecchio, “*In-target Isotope Production at EURISOL*”, EURISOL-DS technical note 04-25-2007-0001.
51. O. Alyakrinskiy, M. Barbui, L.B. Tecchio and M. Tonezzer, “*Preliminary Design of Vacuum System for Fission Target*”, EURISOL DS technical note 04-25-2007-0002.
52. A. Herrera-Martinez and Y. Kadi, “*EURISOL_DS Multi-MW Target: Comparative Neutronic Performance of the Baseline Configuration vs. the Hg-Jet Option*”, EURISOL DS technical note 04-25-2007-0003.
53. A. Herrera-Martinez and Y. Kadi, “*EURISOL_DS Multi-MW Target Issues: Beam Window and Transverse Film Target*”, EURISOL DS technical note 04-25-2007-0004.
54. O. Alyakrinskiy et al., “*Report on the R&D of Uranium Carbide Targets by the PLOG Collaboration at PNPI-Gatchina*”, EURISOL DS technical note 04-25-2007-0005.
55. L. Zanini, “*Neutronic Calculations for the EURISOL-DS Fission target*”, EURISOL DS technical note 04-25-2007-0006.
56. E. Brun, “*Detailed Thermal Stress Analysis of EURISOL Fission Target – First Concept*”, EURISOL DS technical note 04-25-2007-0007.
57. L.B. Tecchio, “*High-Density UC Properties*”, EURISOL DS technical note 04-25-2007-0008.
58. F. Negoita, L. Serbina, L.B. Tecchio and E. Udup, “*Fission Target Design*”, EURISOL DS technical note 04-25-2007-0009.
59. O. Alyakrinskiy et al., “*EURISOL Fission Target Design Adapting MAFF Concept*”, EURISOL DS technical note 04-25-2007-0010.
60. L.B. Tecchio, “*Fission Target – Data Base Parameters*”, EURISOL DS technical note 04-25-2009-011.
61. J. Bermudez et al., “*Fission Target Design and Integration of Neutron Converter*”, EURISOL DS technical note 04-25-2009-0000.
62. F. Olivier, F. Le Blanc and C. Lau, “*Design of 1+ Ion Source Coupling: First Design of the Resonant Ionization Laser Ion Source for the Multi-Megawatt Target Station*”, EURISOL DS technical note 04-25-2009-0013.
63. M. Cheikh Mhamed, S. Essabaa and C. Lau, “*Investigation on Ion Source Parameters*”, EURISOL DS technical note 04-25-2009-0014.

64. O. Alyakrinskiy et al., “*Improving Design of EURISOL Fission Target Design Adapting the MAFF Concept*”, EURISOL DS technical note 04-25-2009-0000.

Task 5: Safety & Radioprotection

65. M. Felcini and A. Ferrari, “*Validation of FLUKA calculated cross-sections for radioisotope production in proton-on-target collisions at proton energies around 1GeV*”, EURISOL DS/Task 5/TN-06-01.
66. A. Plukis, A. Žukauskaite and R. Plukiene, “*Monte-Carlo code validation on accelerator shielding experiments*” EURISOL DS/Task 5/TN-06-02.
67. K. Bongardt, B. Lensing, R. Moormann and H. Schaal, “*Nuclide inventories in Hg-targets*”, EURISOL DS/Task5/TN-06-03.
68. B. Rapp et al., “*Benchmark calculations on particle production within the EURISOL DS project*” EURISOL DS/Task 5/TN-06-04.
69. L. Pienkowski, W. Gawlikowicz and D. Hilscher, “*FLUKA simulation for NESSI experiment*” EURISOL DS/Task5/TN-06-05.
70. D.V. Vamanu et al, “*Dispersion of Radio-elements, Contamination*”, EURISOL DS/Task 5/TN-06-06.
71. Thomas Otto, “*Legal dispositions for transport, storage and use of special fissionable isotopes in Switzerland*”, EURISOL DS/Task 5/TN-06-07.
72. R.Moormann et al. (compilers), “*Licensing aspects for multi-MW spallation sources with an Hg-target: Comparison of different countries*”, EURISOL DS/Task 5/TN-06-08.
73. B. Rapp et al., “*Activation calculation of the EURISOL mercury target*”, EURISOL DS/Task5/TN-06-09.
74. R. Moormann et al, “*The radiotoxic and conventional toxic relevance of Hg-target inventories*”, EURISOL DS/Task5/TN-06-10.
75. R. Moormann (compiler), “*Dose calculations for accidental releases from a mercury target*”, EURISOL DS/Task5/TN-06-11.
76. R. Moormann (compiler), “*Thermochemical studies on the mercury/iodine system*”, EURISOL DS/Task5/TN-06-12.
77. R. Moormann, “*Legal limits for use of U-233 and Pu-239 in Germany*”, EURISOL DS/Task5/TN-06-13.
78. D. Ene, “*High-energy neutron attenuation in iron and concrete: Verification of FLUKA Monte Carlo code by comparison with HIMAC experimental results*”, EURISOL DS/Task5/TN-06-14.
79. T. Otto, “*Fissile Actinides and Alpha-emitters in High-Power Targets*”, EURISOL DS/Task5/TN-06-15.
80. B. Rapp et al., “*Activation Calculations for the EURISOL 4-MW Target Station*”, EURISOL DS/Task5/TN-06-16.
81. A. Prévost et al., “*Importance of the delayed neutrons for the high power liquid spallation targets*”, EURISOL DS/Task5/TN-06-17.
82. B. Schlögl, R. Nabbi and R. Moormann, “*Calculation of the Activity Inventory of Transportable Radionuclides in Soil and Groundwater for Large Neutron Sources*”, EURISOL DS/Task5/TN-07-01.
83. T. Otto, “*Shielding of a 100 kW EURISOL Target Station*”, EURISOL DS/Task5/TN-08-01.
84. P.G. Thirolf et al, “*Confinement of volatile radioactivity from an open fission source in a cryotrap*”, EURISOL DS/Task5/TN-08-02.
85. P.G. Thirolf et al., “*Characterization of a purification system for radioactive vacuum exhaust gases*”, EURISOL DS/Task5/TN-08-03.
86. M. Fadil and B. Rannou, “*Deliverable D4: Conformity to legislation*”, EURISOL DS/Task5/TN-08-04P. Thirolf et al., “*Deliverable D2: Radioactivity control, safety and risk: Final Report*”, EURISOL DS/Task5/TN-08-06.
87. J.B. Neumayr et al., “*Localisation of volatile isotopes on cryotrap*”, Contrib. to Annual Report 2006 of the Maier-Leibnitz-Laboratory, Garching.
88. P.G. Thirolf et al., “*Characterization of a highly-efficient aerosol filtration system*”, Contrib. to Annual Report (2007) of Maier-Leibnitz Laboratory, Garching.

89. T. Otto, “*Screening Approach to the Activation of Soil and Contamination of Groundwater at Linear Proton Accelerator Sites*”, CERN-SC-2008-039-RP-IR, EDMS No. 910 588 v.1 ; EURISOL DS Technical Report 05-25-2009-0028.
90. D. Ene et al., “*Radiation protection aspects of the EURISOL Multi-MW target shielding*”, CEA Saclay Internal report: IRFU-09-15; EURISOL DS Technical Report 05-25-2009-0029.
91. T. Otto, “*Estimation of Radiation Protection Shielding for a EURISOL Linear Proton Accelerator*”, CERN-SC-2009-052-RP-TN, EDMS No. 1 002 239 v.1; EURISOL DS Technical Report 05-25-2009-0030.
92. R. Moormann et al., “*Deliverable D3: decommissioning issues*”, EURISOL DS Technical Report 05-25-2009-0034.
93. Y. Romanets and R. Luís, “*EURISOL Multi MW Target MAFF configuration - Radiological Protection, Radiation Safety and Shielding Aspects*”, CERN/ITN Work Report – June 2009, EURISOL DS Technical Report 05-25-2009-0032.
94. T. Otto et al., “*Deliverable D1: Radiation, Activation, Dose*”, EURISOL DS Technical Report 05-25-2009-0033.
95. R. Moormann, “*Shielding examinations for the European Spallation Source ESS: Update for use by EURISOL*”, EURISOL DS Technical Report 05-25-2009-0035.
96. D. Ene, J. C. David, D. Doré and D. Ridikas, “*Layout of the EURISOL post-accelerator*”, CEA Saclay Internal report: IRFU-09-109 - (2009); EURISOL DS Technical Report 05-25-2009-0036.

Task 6: Heavy-ion Accelerator

97. A. Bechtold, “*Normal conducting injector*”, EURISOL DS technical note 06-25-2006-0002.
98. A. Bechtold, “*The normal conducting RFQ design*”, February 2009, EURISOL DS technical note 06-25-2009-00013.
99. A. Bechtold and H. Zimmermann, “*Beam measurements with NC MAFF RFQ*”, EURISOL DS technical note 06-25-2009-0016
100. P. Bertrand, J-L. Biarrotte, “*A new preliminary conceptual design for EURISOL post-accelerator*”, EURISOL DS technical note 06-25-2006-0001.
101. P. Bertrand, J-L. Biarrotte and G. Normand, “*First evaluation of the steering effect*”, EURISOL DS technical note 06-25-2007-0005.
102. P. Bertrand, J-L. Biarrotte and G. Normand, “*Beam Dynamics with particles from behind the booster*”, EURISOL DS technical note 06-25-2007-0007.
103. P. Bertrand, J-L. Biarrotte and G. Normand, “*Steering effect simulations*”, EURISOL DS technical note 06-25-2007-0009.
104. G. Bisoffi, P.A. Posocco, A. Palmieri and A. Pisent, “*Beam tests with the LNL superconducting RFQ*”, EURISOL DS technical note 06-25-2009-0014.
105. G. Bisoffi, P.A. Posocco, A. Palmieri and A. Pisent, “*SC RFQ engineering design revised*”, EURISOL DS technical note 06-25-2009-0015.
106. G. Bisoffi, “*Comparison between normal conducting and superconducting RFQ options*”, EURISOL DS technical note 06-25-2009-0023.
107. M. Di Giacomo and G. Le Dem, “*Preliminary analysis of the HF chopper solutions*”, EURISOL DS technical note 06-25-2006-0003.
108. M. Di Giacomo and G. Le Dem, “*Fast chopper construction of prototype – Final report*”, EURISOL DS technical note 06-25-2009-0017.
109. M. Di Giacomo, “*Fast chopper prototype tests*”, EURISOL DS technical note 06-25-2009-0018.
110. M. Di Giacomo, “*EURISOL Post Accelerator - High Frequency Chopper – Cooling and connecting proposals*”, EURISOL DS technical note 06-25-2009-0019.
111. M. Di Giacomo, “*Pulse Generator Requirements for the EURISOL High Frequency Chopper*”, EDMS, SPIRAL2 Project, Id I-010809V1.0.
112. G. Le Dem, “*EURISOL Post Accelerator - High Frequency Chopper - Technical design report 2008*”, Internal report, Sept 2008.

113. G. Le Dem, “*High frequency chopper of the heavy ion accelerator*”, EURISOL DS technical note 06-25-2007-0008.
114. G. Le Dem and M. Di Giacomo, “*The EURISOL high frequency chopper: 2006-2008 annual status reports*”, GANIL Internal Note, 2009.
115. G. Le Dem, “*Suppresseur de paquets pour EURISOL – Lignes microruban 100 Ω* ”, EDMS, SPIRAL2 Project, Id I-010678.
116. M-H..Moscatello et al., “*Final report on Task 6 activities*”, EURISOL DS technical note 06-25-2009-0024.
117. G. Normand et al., “*Beam Dynamics simulation for the post-accelerator – Final report*”, EURISOL DS technical note 06-25-2009-010.
118. G. Normand, “*Beam dynamics simulation – Final report*”, EURISOL DS technical note 06-25-2009-0022.
119. N. Orr, “*Experimental requirements – Beams and machine characteristics*”, EURISOL DS technical note 06-25-2006-0004.
120. N.Orr, “*RIB Diagnostics – Design preparation*”, EURISOL DS technical note 06-25-2009-0020.
121. N.Orr and M.Parlog, “*Diamond detector R&D for low intensity heavy ion beam profilers*”, EURISOL DS technical note 06-25-2009-0021.
122. P.A. Posocco, M. Comunian, A. Palmieri and A. Pisent, “*Preliminary study of an 88-MHz bunching RFQ for EURISOL post-accelerator*”, EURISOL DS technical note 06-25-2009-0012.

Task 7: The Driver Accelerator

123. Grigory Belyaev, “*Angular momentum and energy spread measurements by backscattering technique*”, EURISOL DS technical note 07-25-2007-0007.
124. Dan Berkovits, “*An overview of ion beam splitters for the EURISOL driver accelerator*” EURISOL DS technical note 07-25-2007-0010.
125. M. Comunian et al., “*Deliverable D2-RFQ and MEBT*”, EURISOL DS technical note 07-25-2009-0014.
126. R. Duperrier, Jean-Luc Biarrotte and A. Ponton, “*Investigation of different layouts for the EURISOL driver*” EURISOL DS technical note 07-25-2007-0009.
127. R. Duperrier and D Uriot, “*Deliverable D4: High v/c linac*”, EURISOL technical note 07-25-2009-0015.
128. R. Duperrier and D Uriot, “*Deliverable D7: Beam loss calculations*”, EURISOL DS technical note 07-25-2009-0018.
129. A. Facco et al., “*The EURISOL programme*”, EURISOL DS technical note 07-25-2005-0001.
130. A. Facco et al., “*EURISOL driver baseline design*”, EURISOL DS technical note 07-25-2006-0002.
131. A. Facco et al., “*Deliverable D3: Low- and Medium-beta linac*”, EURISOL DS technical note 07-25-2009-0022.
132. A. Facco et al., “*Deliverable D5: Ion Injector*”, EURISOL DS technical note 07-25-2009-0016.
133. A. Facco et al., “*Deliverable D6: High Energy Beam Transport*”, EURISOL DS technical note 07-25-2009-0017.
134. E. Fagotti, “*Deliverable D1: Proton source and LEBT tests*”, EURISOL DS technical note 07-25-2008-0012.
135. S. Halfon et al., “*Hands-on and beam loss criterion at SARAF SC linac*”, EURISOL DS technical note 07-25-2009-0019.
136. J. Rodnizki, D. Berkovits and A. Facco, “*A high acceleration gradient deuteron linac for the EURISOL driver*”, EURISOL DS technical note 07-25-2007-0008.
137. J. Rodnizki, et al., “*Beam dynamics simulations of SARAF accelerator including error propagation and implications for the EURISOL driver*”, EURISOL DS technical note 07-25-2007-0011.

Task 8: Superconducting Cavity Development

138. S. Bousson, “*Eurisol-DS task 8 parameter database*”, EURISOL DS technical note 08-25-2009-0006.

139. S. Bousson et al., “*D1 - Spoke cryostat design and fabrication*”, EURISOL DS technical note 08-25-2009-0010.
140. S. Bousson et al., “*D5 - Spoke cavity cold test*”, EURISOL DS technical note 08-25-2009-0016.
141. S. Bousson et al., “*D1 - Cryostat design and fabrication*”, EURISOL DS technical note 08-25-2009-0017.
142. S. Bousson, “*D3 - Spoke cavity developments*”, EURISOL DS technical note 08-25-2009-0012.
143. S. Bousson et al., “*D6 - Cryomodule assembly and cryogenic test*”, EURISOL DS technical note 08-25-2009-0019.
144. S. Bousson et al., “*D7 - Final report on cryomodule cold test*”, EURISOL DS technical note 08-25-2009-0018.
145. S. Bousson and F. Lutton., “*Spoke Cryomodule overall drawings*”, EURISOL DS technical note 08-25-2009-0009.
146. P. Duthil, “*Spoke cryomodule first cryogenic test - Draft report*”, EURISOL DS technical note 08-25-2009-0008.
147. A. Facco et al., “*D2 - RF source Developments*”, EURISOL DS technical note 08-25-2009-0011.
148. A. Facco et al., “*D4 - Half Wave Resonators developments*”, EURISOL DS technical note 08-25-2009-0013.
149. N. Gandolfo, “*Spoke Cavity Cold Tuning System*”, EURISOL DS technical note 08-25-2009-0003.
150. J. Lesrel, “*Experimental results on the beta 0.35 spoke cavity prototype*”, EURISOL DS technical note 08-25-2009-0007.
151. F. Lutton, “*Spoke cryomodule Preliminary Design Study*”, EURISOL DS technical note 08-25-2009-0001.
152. C. Mielot, “*Study of the ceramic window geometry for HWR and Spoke cavity power coupler*”, EURISOL DS technical note 08-25-2009-0005.
153. H. Saugnac, “*Spoke cryomodule cryogenic scheme*”, EURISOL DS technical note 08-25-2009-0002.
154. F. Scarpa, “*Solid state RF amplifier Manual*”, EURISOL DS technical note 08-25-2009-0004.
155. E. Rampnoux et al., “*D5 - Power coupler conditioning bench*”, EURISOL DS technical note 08-25-2009-0014.
156. E. Rampnoux et al., “*Coupler conditioning bench*”, EURISOL DS technical note 08-25-2009-0015.

Task 9: Beam Preparation

157. J.C. David et al., “*Benchmark calculations on residue production within the EURISOL DS project. Part I: Thin targets*”, Internal report - DAPNIA-07-04.
158. J.C. David et al., “*Benchmark calculations on residue production within the EURISOL DS project. Part II: Thick targets*”, Internal report - DAPNIA-07-59.

Task 10: Physics & Instrumentation

159. N. Orr, “*Experimental Requirements - Beam and Machine Characteristics*”, EURISOL DS technical note 10-25-2007-0001.
160. R.D. Page et al., “*Updated report on design and costing of apparatus*”, EURISOL DS technical note 10-25-2007-0008.
161. R.D. Page et al., “*In-beam validations*”, EURISOL DS technical note 10-25-2007-0006.
162. R.D. Page et al., “*Preliminary design and costing of apparatus*”, EURISOL DS technical note 10-25-2007-0005.
163. R.D. Page et al., “*Selection of key experiments with the associated instrumentation*”, EURISOL DS technical note 10-25-2007-0003.
164. R.D. Page et al., “*Apparatus specification for key experiments*”, EURISOL DS technical note 10-25-2007-0002.

165. R.D. Page, *“Physics and Instrumentation Subtasks and Leaders”*, EURISOL DS technical note 10-25-2007-0000
166. C. Volpe and R. Lazauskas, *“Low-energy Beta Beams”*, EURISOL DS technical note 10-25-2007-0007.

Task 11: Calculated Yields of Exotic Ions

167. J. Benlliure et al, *“Fragmentation of very neutron-rich projectiles around ^{132}Sn ”*, Heavy-ion Laboratory Annual Report 2006, ISSN 1895-6726, p.54, Warsaw 2007, Poland.
168. J. Benlliure, *“Comprehensive investigation of fragmentation reactions”*, EURISOL DS technical note 11-25-2009-0015.
169. J. Benlliure et al., *“Production of medium-mass neutron-rich nuclei in reactions induced by ^{136}Xe projectiles at 1 A GeV on a beryllium target”*, EURISOL DS technical note 11-25-2009-0019.
170. J. Benlliure, A. Kelic, K.-H. Schmidt and M. Veselsky, *“Fragmentation of post accelerator ISOL beams - Report on optimal post-accelerator energy”*, EURISOL DS technical note 11-25-2009-0023.
171. S. Chabod et al., *“Optimization of in-target yields for RIB production: Part I: Direct targets”*, Internal report - IRFU-08-21; EURISOL DS technical note 11-25-2008-0011.
172. J-C. David et al., *“Benchmark calculations on residue production within the EURISOL DS project; Part I: thin targets”*, EURISOL DS technical note 11-25-2009-0006.
173. J-C. David et al., *“Benchmark calculations on residue production within the EURISOL DS project; Part II: thick targets”*, EURISOL DS technical note 11-25-2009-0008.
174. P. Delahaye et al., *“Extrapolation of measured called release-efficiency data”*, EURISOL DS technical note 11-25-2009-0024.
175. D. Ene et al., *“In target yields for RIB production: Part II: two stage target configuration”*, Internal Report IRFU-09-87(2009).
176. D. Ene, S. Chabod, J. C. David, D. Dore and D. Ridikas, *“In-target yields for RIB production: Part II: two-stage target configuration”*, EURISOL DS technical note 11-25-2009-0022.
177. W.Gawlikowicz et al., *“The EURISOL Task 11 database”*, Heavy-ion Laboratory Annul Report 2007, ISSN 1895-6726, p.60, Warsaw 2008, Poland.
178. W. Gawlikowicz, A. Kelic, S. Lukic and K-H. Schmidt, *“Beam-intensity data base”*; link to the database: http://www.gsi.de/eurisol-t11/database/eurisol_database.php.
179. GSI and Jyvaskyla U., *“D3 - Fission models - Validation and improvement of codes report”*, EURISOL DS technical note 11-25-2008-0009.
180. JYFL, Jyvaskyla, *“D5 – Neutron- and proton-induced reactions up to Fermi energy- Report on cross sections”*, EURISOL DS technical note 11-25-2008-0010.
181. A. Kelic et al., *“Beam intensities with EURISOL”*, EURISOL DS technical note 11-25-2009-0025.
182. A. Kelic, M.V. Ricciardi and K.-H. Schmidt, *“GSI fission model results”*, EURISOL DS technical note 11-25-2009-0014.
183. A Kelic et al., *“Aspects of secondary reactions”*, EURISOL DS technical note 11-25-2009-0016.
184. D. Perez-Loureiro et al., *“Production of medium-mass neutron-rich nuclei in ^{238}U fission”*, EURISOL DS technical note 11-25-2009-0017.
185. M.V. Ricciardi, A. Kelic and K.-H. Schmidt, *“Results obtained with ABLA07”*, EURISOL DS technical note 11-25-2009-0020.
186. V. Rubchenya, *“JYFL fission model results”*, EURISOL DS technical note 11-25-2009-0013.
187. V. Rubchenya and K-H. Schmidt, *“The JYFL fission model results”*, EURISOL DS technical note 11-25-2007-0001.
188. V. Rubchenya and K-H. Schmidt, *“Neutron and proton-induced reactions”*, EURISOL DS technical note 11-25-2007-0004.
189. K-H. Schmidt, *“Data and benchmarking of model for ^{238}U ”*, EURISOL DS technical note 11-25-2007-0002.

190. K-H. Schmidt, "*Code validation*", EURISOL DS technical note 11-25-2007-0003.
191. K-H. Schmidt, "*Preparation and execution of the experiment 'fragmentation of ^{132}Sn '*", EURISOL DS technical note 11-25-2007-0005.
192. K-H. Schmidt, "Completion of the ISOLDE yield database", EURISOL DS technical note 11-25-2009-0007.
193. M. Veselsky and G.A. Souliotis, "*Production of exotic nuclides in nucleus-nucleus collisions in the Fermi-energy domain*", EURISOL DS technical note 11-25-2009-0018.

Task 12: Beta-Beam Aspects

194. A. Bechtold et al., "*Conceptual Design Report for a Beta-Beam Facility*", EURISOL-DS Technical Note 12-25-2009-0023.
195. M. Benedikt, S. Hancock, M. Lindroos, "*Parameter and Intensity Values*", EURISOL-DS Technical Note 12-25-2009-0006.
196. M. Benedikt, A. Fabich, S. Hancock and M. Lindroos, "*Parameter and Intensity Values*", EURISOL-DS Technical Note 12-25-2009-0007.
197. M. Benedikt, S. Hancock and M. Lindroos, "*Parameter and Intensity Values, Version 1, April 2005*", EURISOL-DS Technical Note 12-25-2009-0016.
198. M. Benedikt, A. Fabich, S. Hancock and M. Lindroos, "*The EURISOL Beta-beam Facility: Parameter and Intensity Values, Version 2*", EURISOL-DS Technical Note 12-25-2009-0017.
199. M. Benedikt, A. Fabich, S. Hancock and M. Lindroos, "*The EURISOL Beta-beam Facility: Parameter and Intensity Values, Version 3*", EURISOL-DS Technical Note 12-25-2009-0013.
200. M. Benedikt and S. Hancock, "*Ion acceleration in PS and SPS*", EURISOL-DS Technical Note 12-25-2009-0019.
201. A. Chancé et al., "*Decay ring design*", EURISOL-DS Technical Note 12-25-2009-0022.
202. A. Chance and J. Payet, "*First design for the optics of the decay ring of the beta-beams*", EURISOL-DS Technical Note 12-25-2009-0001.
203. A. Chance and J. Payet, "*Simulation of the losses by decay in the decay ring for the beta-beams*", EURISOL-DS Technical Note 12-25-2009-0002.
204. N. Emelianenko, A. Fabich and E. Wildner, "*Database of the Parameter List for the EURISOL Beta-Beam Task*", EURISOL-DS Technical Note 12-25-2009-0005.
205. A. Fabich, M. Benedikt, "*Decay losses along the accelerator chain of the EURISOL Beta-beam baseline design*", EURISOL-DS Technical Note 12-25-2009-0004.
206. M. A. Fraser, "*Monochromatic neutrino beams from the decay of rare earth nuclei*", EURISOL-DS Technical Note 12-25-2009-0010.
207. A. Lachaize, "*Updated RF characteristics of the Beta-beam RCS*", EURISOL-DS Technical Note 12-25-2009-0009.
208. A. Lachaize and A. Tkatchenko, "*Design of low energy ring(s)*", EURISOL-DS Technical Note 12-25-2009-0020.
209. A. Lachaize and A. Tkatchenko, "*Excitation of half-integer resonances by random quadrupole field errors in the BETA-BEAM RCS*", EURISOL-DS Technical Note 12-25-2009-0014.
210. A. Lachaize and A. Tkatchenko, "*Preliminary design of a Rapid Cycling Synchrotron for the EURISOL Beta-Beam Facility*", EURISOL-DS Technical Note 12-25-2009-0018.
211. A. Lachaize and A. Tkatchenko, "*The Rapid Cycling Synchrotron of the EURISOL Beta-Beam facility*", EURISOL-DS Technical Note 12-25-2009-0011.
212. M. Lindroos, "*Possible ways of increasing the number of (anti-) neutrinos from the EURISOL beta-beam facility*", EURISOL-DS Technical Note 12-25-2009-0008.
213. A. Tkatchenko, "*Preliminary considerations on the RCS option*", EURISOL-DS Technical Note 12-25-2009-0015.
214. E. Wildner, Frederick Jones and Francesco Cerutti, "*Beta Beams for neutrino production: Heat deposition from decaying ions in superconducting magnets*", EURISOL-DS Technical Note 12-25-2009-0012.

Final Report of the EURISOL Design Study (2005–2009)